2013

Amphiphilic oligocholate macrocycles: self-assembly, transmembrane nanopore formation, and noncovalent tuning

Lakmini Sandachaya Widanapathirana
Iowa State University

Amphiphilic oligocholate macrocycles: self-assembly, transmembrane nanopore formation, and noncovalent tuning

By

Lakmini Widanapathirana

A dissertation submitted to the graduate faculty

in partial fulfillment of the requirements for the degree of

DOCTOR OF PHILOSOPHY

Major: Organic Chemistry

Program of Study Committee:

Yan Zhao, Major Professor
Mei Hong
Aaron D. Sadow
Javier Vela
Arthur Winter

Iowa State University

Ames, Iowa

2013

TABLE OF CONTENTS

CHAPTER 1. GENERAL INTRODUCTION

Dissertation Organization.

This dissertation is composed of 7 chapters. The first chapter is a review of the application of supramolecular self-assemblies in transmembrane transport. The second chapter was published in the *Journal of the American Chemical Society* in 2011. Macrocyclic oligocholates were synthesized and studied as transmembrane pore-forming agents by leakage assays and fluorescence spectroscopy. The rigid cyclic macrocycles formed nanopores across lipid membranes, assisted by the water molecules within the macrocycles. In this research, Dr. Hongkwan Cho synthesized the (non-labeled) oligocholates and performed the corresponding leakage assays. The third chapter was published in the *Journal of Organic Chemistry* in 2012. The aggregation of macrocyclic oligocholates with introverted hydrophilic groups and aromatic side chains were studied by fluorescence spectroscopy and liposome leakage assays. Smaller, more rigid macrocycles stacked better than larger, more flexible ones. The acceptor−acceptor interactions were more effective than the donor−acceptor interactions in promoting the transmembrane pore formation. The fourth chapter was published in *Organic and Biomolecular Chemistry* in 2012. Three macrocyclic oligocholates containing a carboxyl group, a guanidinium ion, and a Cbz-protected amine, respectively, were studied as membrane transporters for hydrophilic molecules. While small hydrophilic guests were transported via transmembrane nanopores, the macrocycles acted as carriers to shuttle larger guests across the membrane. Hydrogen-bonds among the side chains of the macrocycles strongly affected the transport properties. Dr. X. Li provided the cholate compound with the carboxylate side chain. The fifth chapter was published in *Langmuir* in 2012. A cyclic and a linear tricholate were labeled with a fluorescent dansyl group. The environmentally sensitive fluorophore enabled the aggregation of

the two oligocholates in lipid membranes to be studied by fluorescence spectroscopy, namely environmentally sensitive emission, red-edge excitation shift (REES), and Florescent quenching. The sixth chapter was published in *Langmuir* in 2012. The isotopic labeling of cyclic and linear tricholates allowed the use of solid-state NMR spectroscopy to study the dynamics, aggregation, and depth of insertion of these compounds in lipid membranes. Mr. T. Wang of Prof. M. Hong research group performed the solid state NMR studies. The seventh chapter was published in the *Journal of Organic Chemistry* in 2013. Macrocycles functionalized with 1,4- dicarboxylic acid "side chain" displayed significantly higher transmembrane glucose transport activity than the corresponding methyl ester derivative. Changing the 1,4-substitution of the dicarboxylic acid to 1,3-substitution lowered the activity. Combining the hydrophobic interactions and the hydrogen-bond-based carboxylic acid dimerization was an effective strategy to tune the structure and activity of self-assembled nanopores in lipid membranes.

Literature reviews.

Biological membranes not only serve as a boundary between the cell and the outside environment but also support a wide range of key biochemical processes including respiration and photosynthesis, solute transport, motility, cell–cell recognition, signal transduction, and protein transport. Selective transport of hydrophilic molecules across the lipid membrane mainly occurs with the aid of transmembrane proteins that functions as channels/pores. The transmembrane proteins inhabit an intricate atmosphere with a hydrophilic portion exposed to the aqueous phase on one or both sides of the membrane, interacting with water, small hydrophilic ions and molecules, as well as water-soluble macromolecules. The rest of the surface is mainly hydrophobic and is exposed to the membrane, either at the interfacial region, which forms a layer

approximately15 Å thick on either side of the membrane, or the ~30Å thick hydrophobic core of the membrane.[1]

While it is necessary to understand the transmembrane transport in detail, structural characterization of transport proteins is challenging. The difficulties include crystallizing membrane proteins as well as the requirement of certain lipid compositions and/or other ligands and proteins that is necessary for such pore-formation mechanisms to operate.[1] During the past few decdes, synthetic pore-forming materials have gained much attention as tools useful in understanding the fundamentals of membrane transport mechanisms. While the synthesized transmembrane transport mimics utilize similar covalent and noncovalent forces that biological nanopores possess, they have the advantages of being relatively easy to handle, inexpensive, and less prone to denaturization than their biological equals. Importantly, synthetic pore-forming materials may have a number of practical applications including sensing,[2] drug delivery,[3] DNA sequencing,[4] and catalysis.[5]

The models for channel/pore design comprise of molecules containing a continuous internal void (resembling biological channel forming peptides), stacking of macrocyclic rings, and transmembrane molecular chains that forms a channel.[6] It is known that the self-assembly of organic molecules has given access to a range of complex supramolecular units that functions as transmembrane channels, making use of hydrogen bonding, π-π interactions, electrostatic interactions, and metal-ligand coordination interactions for directing the processes and holding the constituents together.[7] But the creation of nanometer-sized transmembrane pores through such a self-assembly is a difficult task, as the structures created must be able to withstand the external membrane pressure when incorporated into a bilayer. Common ion-channel-forming compounds such as crown ethers and open chain compounds are too flexible for the nanopore formation and

prone to collapse within the bilayer. Therefore, there are only a limited number of synthetic designs available to date that construct transmembrane nanopores through self-assembly.

Over the years, a rich collection of rigid rod β-barrels have been made and studied by Matile and co-workers. Short peptide strands were attached to each phenyl ring of the *p*-oligophenyl stave to create monomers that self-assemble by interdigitation of peptides from adjacent staves through hydrogen bonding and π-π stacking. The β-sheets formed were then rolled to cylindrical β-barrels assisted by the facial amphiphilicity of the sheets and the rigidity of the *p*-oligophenyl rods. The application of these as receptors, ion channels/pores, catalysts, photosystems, and sensors ("artificial tongues") have been reported.[2, 7b, 7d, 7e, 8] Ghadiri *et al* has reported that cyclic peptide structures made up of an even number of alternating D- and L- amino acid residues can adopt a flat-ring conformation and stack under favorable conditions to provide a continuous hydrogen-bonded hollow tubular structures in lipid bilayers forming active ion channels that can transport glucose and glutamic acid.[9,10]

Satake and Kobukes' porphyrin-based nanopores prepared by metal-ligand coordination followed by covalent fixation dimerize in the lipid membrane by hydrogen bonding.[11] The artificial transmembrane water channels based on hydrazide-incorporated pillar[5]arenes shown to function as single-molecular channels to transport water across the lipid membrane at very low concentrations.[12] Recently it was reported that tetraporphyrin metallocycles with Re (I) corners and peripheral carboxylic acid residues are capable of forming nanopores in a lipid membrane by forming a hydrogen bond network which allows the formation of dimers that span the depth of the membrane.[13]

Aromatic oligoamide macrocycles prepared by Gong *et al* were found to self-assemble within the lipid membrane via face-to-face π-π interactions creating a nanopore with high conductance.[14]

Self-assembly of folate dendrimers synthesized by Kato *et al* into π-stacked supramolecular rosettes is shown to produce small, homogeneous, long-lived, ohmic, cation selective ion channels in lipid bilayer membranes.[15] Webb group has shown that a cholate-based ion channel can be gated ‘‘open’’ or ‘‘closed’’ by the addition or removal of palladium(II).[16]

With a cholesterol-like rigid backbone and facial amphiphilicity, cholate derivatives are well suited for membrane related applications including as ion channels[16-17] and molecule or anion-transporters.[18,19] Oligocholate foldamers responsive to solvent polarity[20] and their applications in sensing[21], catalysis[22], molecular recognition[23] and transmembrane transport[24] were reported by the Zhao group. The linear oligomers consist of cholates as facially amphiphilic building blocks fold into a helix in nonpolar solvents containing a small amount of polar solvent. The driving force for folding is the preferential solvation of the cholate hydrophilic faces by the polar solvent that microphase-separates from the bulk solution. The inner cavity of the helix is hydrophilic because of the hydroxyl and amide groups on the cholate backbone pointing inward. The cholate backbone makes the cavity rigid and large enough to contain polar solvents or guests.

In this dissertation, I present an extension of the solvophobic folding of linear oligocholate foldamers in organic solutions to the membrane environment. Cyclic oligocholate derivatives resembling the cross section of a folded hexamer were synthesized and studied for their self-assembly and nanopore formation driven by *hydrophobic interactions*, which are normally stronger in water instead of a hydrophobic environment.

References

(1) Fyfe, P. K.; McAuley, K. E.; Roszak, A. W.; Isaacs, N. W.; Cogdell, R. J.; Jones, M. R. *Trends. Biochem. Sci.* **2001,** *26*, 106-112.

(2) Litvinchuk, S.; Sorde, N.; Matile, S. *J. Am. Chem. Soc.* **2005,** *127*, 9316-9317.

(3) (a) Fyles, T. M. *Chem. Soc. Rev.* **2007,** *36*, 335-347; (b) Davis, J. T.; Okunola, O.; Quesada, R. *Chem. Soc. Rev.* **2010,** *39*, 3843-3862; (c) McNally, B. A.; Leevy, W. M.; Smith, B. D. *Supramol. Chem.* **2007,** *19*, 29-37.

(4) (a) Kasianowicz, J. J.; Brandin, E.; Branton, D.; Deamer, D. W. *Proc. Natl. Acad. Sci. U. S. A.* **1996,** *93*, 13770-13773; (b) Akeson, M.; Branton, D.; Kasianowicz, J. J.; Brandin, E.; Deamer, D. W. *Biophys. J.* **1999,** *77*, 3227-3233; (c) Clarke, J.; Wu, H. C.; Jayasinghe, L.; Patel, A.; Reid, S.; Bayley, H. *Nat. Nanotechnol.* **2009,** *4*, 265-270; (d) Howorka, S.; Cheley, S.; Bayley, H. *Nat. Biotechnol.* **2001,** *19*, 636-639.

(5) Sakai, N.; Sorde, N.; Matile, S. *J. Am. Chem. Soc.* **2003,** *125,* 7776-7777.

(6) (a) Jullien, L.; Lehn, J. M. *Tetrahedron Lett.* **1988,** *29*, 3803-3806; (b) Lehn, J. M.; Mascal, M.; Decian, A.; Fischer, J. *J. Chem. Soc. Chem. Comm.* **1990,** 479-481; (c) Lehn, J. M. *Science* **2002,** *295*, 2400-2403.

(7) (a) Sisson, A. L.; Shah, M. R.; Bhosale, S.; Matile, S. *Chem. Soc.Rev.* **2006,** *35*, 1269-1286; (b) Bhosale, S.; Sisson, A. L.; Sakai, N.; Matile, S. *Org. Biomol. Chem.* **2006,** *4*, 3031-3039; (c) Sakai, N.; Mareda, J.; Matile, S. *Acc. Chem. Res.* **2005,** *38*, 79-87; (d) Bhosale, R.; Bhosale, S.; Bollot, G.; Gorteau, V.; Julliard, M. D.; Litvinchuk, S.; Mareda, J.; Matile, S.; Miyatake, T.; Mora, F.; Perez-Velasco, A.; Sakai, N.; Sisson, A. L.; Tanaka, H.; Tran, D. H. *B Chem. Soc. Jpn.* **2007,** *80,* 1044-1057; (e) Sakai, N.; Mareda, J.; Matile, S. *Acc. Chem.*

Res. **2008,** *41*, 1354-1365; (f) Sakai, N.; Matile, S. *Angew. Chem. Int. Ed.* **2008,** *47,* 9603-9607.

(8) (a) Gorteau, V.; Perret, F.; Bollot, G.; Mareda, J.; Lazar, A. N.; Coleman, A. W.; Tran, D. H.; Sakai, N.; Matile, S. *J. Am. Chem. Soc.* **2004,** *126*, 13592-13593; (b) Sorde, N.; Das, G.; Matile, S. *Proc. Natl. Acad. Sci. U. S. A.* **2003,** *100*, 11964-11969; (c) Litvinchuk, S.; Bollot, G.; Mareda, J.; Som, A.; Ronan, D.; Shah, M. R.; Perrottet, P.; Sakai, N.; Matile, S. *J. Am. Chem. Soc.* **2004,** *126*, 10067-10075; (d) Das, G.; Talukdar, P.; Matile, S. *Science* **2002,** *298*, 1600-1602; (e) Som, A.; Matile, S. *Eur. J. Org. Chem.* **2002,** 3874-3883; (f) Baumeister, B.; Matile, S. *Macromolecules* **2002,** *35*, 1549-1555; (g) Bhosale, S.; Sisson, A. L.; Talukdar, P.; Furstenberg, A.; Banerji, N.; Vauthey, E.; Bollot, G.; Mareda, J.; Roger, C.; Wurthner, F.; Sakai, N.; Matile, S. *Science* **2006,** *313*, 84-86; (h) Tanaka, H.; Litvinchuk, S.; Tran, D. H.; Bollot, G.; Mareda, J.; Sakai, N.; Matile, S. *J. Am. Chem. Soc.* **2006,** *128*, 16000-16001; (i) Matile, S.; Tanaka, H.; Litvinchuk, S. *Top. Curr. Chem.* **2007,** *277*, 219-250; (j) Sakai, N.; Sisson, A. L.; Bhosale, S.; Furstenberg, A.; Banerji, N.; Vauthey, E.; Matile, S. *Org. Biomol. Chem.* **2007,** *5*, 2560-2563; (k) Banerji, N.; Bhosale, R.; Bollot, G.; Butterfield, S. M.; Furstenberg, A.; Gorteau, V.; Hagihara, S.; Hennig, A.; Maity, S.; Mareda, J.; Matile, S.; Mora, F.; Perez-Velasco, A.; Ravikumar, V.; Kishore, R. S. K.; Sakai, N.; Tran, D. H.; Vauthey, E. *Pure. Appl. Chem.* **2008,** *80*, 1873-1882; (l) Tanaka, H.; Matile, S. *Chirality* **2008,** *20*, 307-312; (m) Perez-Velasco, A.; Gorteau, V.; Matile, S. *Angew.Chem. Int. Ed.* **2008,** *47*, 921-923.

(9) (a) Granja, J. R.; Ghadiri, M. R. *J. Am. Chem. Soc.* **1994,** *116*, 10785-10786; (b) Sanchez-Quesada, J.; Kim, H. S.; Ghadiri, M. R. *Angew. Chem. Int. Ed.* **2001,** *40*, 2503-2506.

(10) (a) Ghadiri, M. R.; Granja, J. R.; Milligan, R. A.; Mcree, D. E.; Khazanovich, N. *Nature* **1994,** *372*, 709-709; (b) Ghadiri, M. R.; Granja, J. R.; Buehler, L. K. *Nature* **1994,** *369*, 301-304; (c) Kim, H. S.; Hartgerink, J. D.; Ghadiri, M. R. *J. Am. Chem. Soc.* **1998,** *120*, 4417-4424.

(11) Satake, A.; Yamamura, M.; Oda, M.; Kobuke, Y. *J. Am. Chem. Soc.* **2008,** *130*, 6314-6315.

(12) Hu, C. B.; Chen, Z. X.; Tang, G. F.; Hou, J. L.; Li, Z. T., *J. Am. Chem. Soc.* **2012,** *134*, 8384-8387.

(13) Boccalon, M.; Iengo, E.; Tecilla, P. *J. Am. Chem. Soc.* **2012,** *134*, 20310-3.

(14) Helsel, A. J.; Brown, A. L.; Yamato, K.; Feng, W.; Yuan, L. H.; Clements, A. J.; Harding, S. V.; Szabo, G.; Shao, Z. F.; Gong, B. *J. Am. Chem. Soc.* **2008,** *130*, 15784-15785.

(15) Sakai, N.; Kamikawa, Y.; Nishii, M.; Matsuoka, T.; Kato, T.; Matile, S. *J. Am. Chem. Soc.* **2006,** *128*, 2218-2219.

(16) Wilson, C. P.; Webb, S. J. *Chem. Commun.* **2008,** 4007-4009.

(17) (a) Ma, L.; Melegari, M.; Colombini, M.; Davis, J. T. *J. Am. Chem. Soc.* **2008,** *130*, 2938-2939; (b) Bandyopadhyay, P.; Janout, V.; Zhang, L. H.; Sawko, J. A.; Regen, S. L. *J. Am. Chem. Soc.* **2000,** *122*, 12888-12889; (c) Maulucci, N.; De Riccardis, F.; Botta, C. B.; Casapullo, A.; Cressina, E.; Fregonese, M.; Tecilla, P.; Izzo, I. *Chem. Commun.* **2005,** 1354-1356.

(18) (a) Janout, V.; Di Giorgio, C.; Regen, S. L. *J. Am. Chem. Soc.* **2000,** *122*, 2671-2672; (b) Janout, V.; Staina, I. V.; Bandyopadhyay, P.; Regen, S. L. *J. Am. Chem. Soc.* **2001,** *123*, 9926-9927; (c) Janout, V.; Jing, B. W.; Staina, I. V.; Regen, S. L. *J. Am. Chem. Soc.* **2003,** *125*, 4436-4437; (d) Janout, V.; Regen, S. L. *J. Am. Chem. Soc.* **2005,** *127*, 22-23.

(19) (a) Whitmarsh, S. D.; Redmond, A. P.; Sgarlata, V.; Davis, A. P. *Chem. Commun.* **2008,** 3669-3671; (b) Koulov, A. V.; Lambert, T. N.; Shukla, R.; Jain, M.; Boon, J. M.; Smith, B. D.; Li, H. Y.; Sheppard, D. N.; Joos, J. B.; Clare, J. P.; Davis, A. P. *Angew. Chem. Int. Ed.* **2003,** *42*, 4931-4933.

(20) (a) Zhao, Y.; Zhong, Z. Q. *J. Am. Chem. Soc.* **2005,** *127*, 17894-17901; (b) Zhao, Y.; Zhong, Z. Q.; Ryu, E. H. *J. Am. Chem. Soc.* **2007,** *129*, 218-225; (c) Cho, H.; Zhao, Y. *J. Am. Chem. Soc.* **2010,** *132*, 9890-9899.

(21) (a) Zhao, Y.; Zhong, Z. Q. *J. Am. Chem. Soc.* **2006,** *128*, 9988-9989; (b) Zhong, Z. Q.; Zhao, Y. *Org. Lett.* **2007,** *9*, 2891-2894.

(22) Cho, H. K.; Zhong, Z. Q.; Zhao, Y. *Tetrahedron* **2009,** *65*, 7311-7316.

(23) Zhong, Z. Q.; Li, X. S.; Zhao, Y. *J. Am. Chem. Soc.* **2011,** *133*, 8862-8865.

(24) (a) Zhang, S. Y.; Zhao, Y. *Chem-Eur. J.* **2011,** *17*, 12444-12451; (b) Zhang, S. Y.; Zhao, Y. *Org. Biomol. Chem.* **2012,** *10*, 260-266; (c) Cho, H. K.; Zhao, Y. *Langmuir* **2011,** *27*, 4936-4944.

CHAPTER 2. WATER-TEMPLATED TRANSMEMBRANE NANOPORES FROM SHAPE-PERSISTENT OLIGOCHOLATE MACROCYCLES

A paper published in *Journal of the American Chemical Society* **2011**, *133*, 141-147.

Hongkwan Cho, Lakmini Widanapathirana, Yan Zhao

Abstract

Hydrophobic interactions normally are not considered a major driving force for self-assembling in a hydrophobic environment. When macrocyclic oligocholates were placed within lipid membranes, however, the macrocycles pulled water molecules from the aqueous phase into their hydrophilic internal cavities. These water molecules had strong tendencies to aggregate in a hydrophobic environment and templated the macrocycles to self-assemble into transmembrane nanopores. This counterintuitive hydrophobic effect resulted in some highly unusual transport behavior. Cholesterol normally increases the hydrophobicity of lipid membranes and makes them less permeable to hydrophilic molecules. The permeability of glucose across the oligocholate-containing membranes, however, increased significantly upon the inclusion of cholesterol. Large

hydrophilic molecules tend to have difficulty traversing a hydrophobic barrier. The cyclic cholate tetramer, however, was more effective at permeating maltotriose than glucose.

Introduction

Channels and pores are used in biology to permeate ions and molecules across membranes. In addition to their important roles in signaling, metabolism, and bacterial or viral infection, channels and pores enable design of novel sensors for both small and large molecules.[1] Pore-forming proteins, for example, have shown great promises in the single-molecule detection of RNAs and DNAs.[2]

Although synthetic pores have the advantage of being less expensive and less prone to denaturization than their protein counterparts, development of nanometer-sized synthetic pores has been a difficult challenge.[3] Ghadiri *et al.* prepared cyclic peptides that self-assembled into pores large enough for glucose and glutamic acid to pass through.[4] Matile and co-workers, in a series of seminal work, reported nanometer-sized β-barrel pores through self-assembly of oligo(phenylene) derivatives[5] and demonstrated their applications in sensing[5b] and catalysis.[5c] More recently, Satake and Kobuke prepared nanosized pores based on porphyrin supramolecules.[6] Gong *et al.* described pores ca. 0.8 nm in diameter through the π–π interactions of aromatic heterocycles.[7] In addition, Fyles[8] and Davis[9] used amine–Pd(II) and guanosine quartets, respectively, to construct highly conducting channels consistent with nanometered pore sizes.

A big challenge in creating nanometer-sized pores within the lipid bilayers is to keep the pore from collapsing. For this reason, although chemists have made tremendous progress in the design and synthesis of artificial ion channels,[10] the building blocks involved (e.g., crown ethers and open chain compounds) typically are not amenable to nanopore formation. Despite the advancement made in synthetic nanopores, only limited pore-forming mechanisms exist currently. The majority

of synthetic nanopores reported so far relied on either hydrogen-bonding[4-5,9] or metal–ligand coordination[6,8] for stability.

Herein, we report synthetic nanopores driven by *hydrophobic* interactions—a very different mechanism of pore formation from common biological and synthetic examples. The novelty of the approach lies in the counterintuitive design. Normally, if the environment (i.e., lipid bilayers) is hydrophobic, hydrophobic interactions are not expected to contribute significantly to a supramolecular synthesis. The self-assembled pores displayed highly unusual behavior as a result of the counterintuitive pore-formation. Cholesterol is known to increase the hydrophobic thickness[11] of lipid bilayers and decrease their fluidity.[12] Yet, the enhanced hydrophobicity caused by cholesterol facilitated the pore formation of the oligocholate macrocycles and increased the permeability of glucose across the membranes. Larger hydrophilic molecules normally have difficulty moving across a hydrophobic barrier. The cyclic cholate tetramer, however, was more effective at permeating maltotriose than glucose.

Results and Discussion

Molecular design. With a cholesterol-like backbone and facial amphiphilicity, cholic acid derivatives have been used in membrane-related applications including as ion channels[9,13] and molecule-[14] or anion-transporters.[15] In an effort to prepare conformationally controllable foldamers,[16] we synthesized linear oligomers of facially amphiphilic cholates.[17] In nonpolar solvents (e.g., CCl_4 or hexane/ethyl acetate) containing a small percentage of a polar solvent (e.g., DMSO or MeOH), the oligocholate folds into a helix with a nanometer-sized hydrophilic inner pore. The polar solvent phase-separates from the bulk into the hydrophilic pore and efficiently solvate the introverted polar groups of the oligocholate.

Since the folded helix has three monomer units per turn,[17a] cyclic tricholate **1** essentially represents the cross-section of the folded helix. According to the CPK model, the molecule has a triangular hydrophilic cavity about 1 nm on the side (the N–N distance is ~1.3 nm). Its exterior is completely hydrophobic and fully compatible with lipid membranes. Its rigidity, resulting from both the triangular geometry and the fused steroid backbone, is expected to prevent the inner cavity from collapsing. Note that, although other strategies (e.g., internal charge repulsion)[18] have been used with success, rigidity of the building blocks is a key factor in keeping synthetic nanopores from collapsing.[3-9]

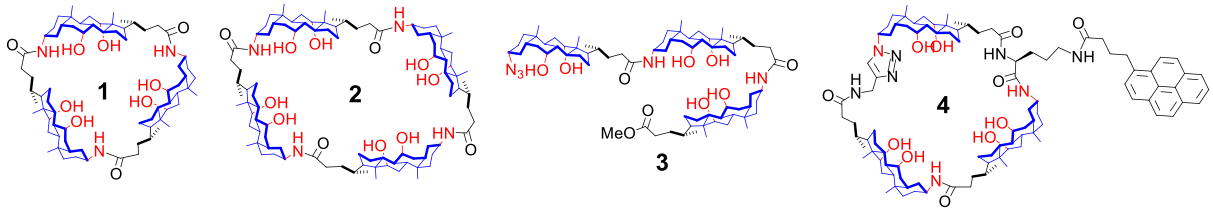

We hypothesized that the same solvophobic driving force in the folding of the linear oligocholates[17] would prompt **1** to stack in the *z*-direction (Scheme 1). In a largely nonpolar solvent mixture, the polar solvent molecules should phase-separate into the middle of the macrocycle and solvate the inward-facing polar groups. Aggregation also allows these polar solvents to move up and down the polar channel—an entropically favorable process.

Scheme 1. Schematic Representation of the Solvophobically Driven Folding of a Linear Oligocholate and Aggregation of **1**.

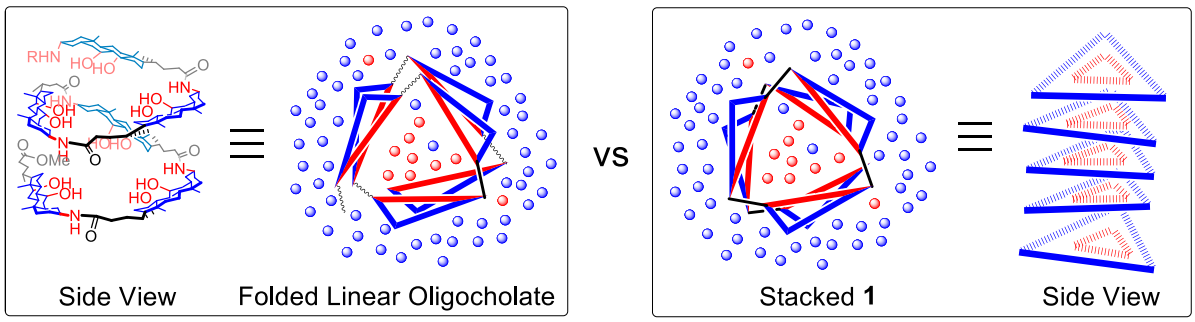

In addition to **1**, cyclic tetramer **2** and linear trimer **3** were prepared as control compounds. Compound **4** has a pyrene group on the side chain, allowing us to use fluorescence to probe the self-assembly. Linear oligocholates such as **3** were synthesized through standard peptide-coupling reactions.[17a] Cyclization of the corresponding amino/carboxyl-terminated oligocholates yielded compounds **1** and **2** (see the Supporting Information for details). For compound **4**, we took advantage of the azide group at the end of the oligocholates and used the click reaction[19] for the cyclization (Scheme 2). The pyrene group was introduced at the side chain of the L-ornithine inserted in between two cholates.

Scheme 2. Synthetic Route for Pyrene-Labeled Macrocycle **4**.

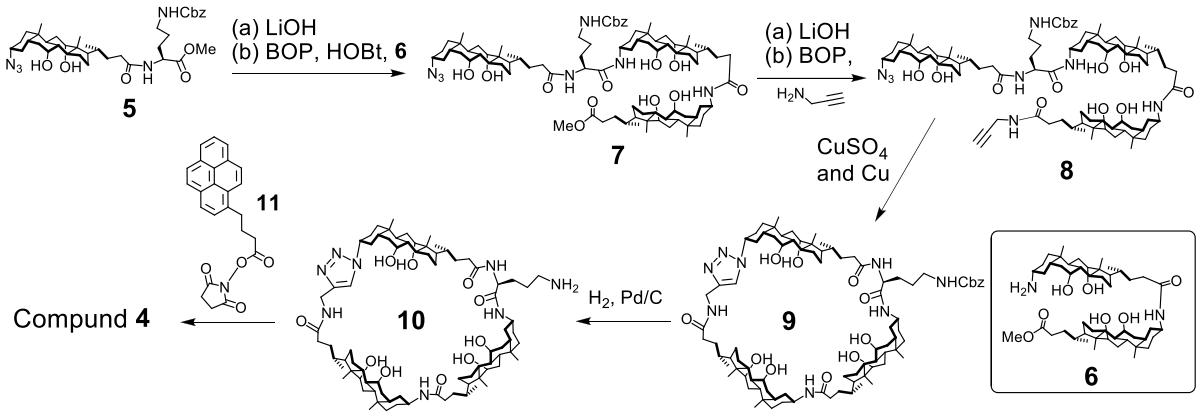

Glucose Leakage from POPC/POPG LUVs. An ideal system to test the stacking is the lipid bilayer. The lipid hydrocarbon tails essentially are the nonpolar solvent in Scheme 1 and the assembly of **1** in the *z*-direction would create a transmembrane nanopore (Figure 1, **C**). Because the nanopore is open to bulk water on both ends, the water molecules inside the pore can readily exchange with bulk water. This is very important if the pore-formation is to occur. Because the entropic cost for trapping a single water molecule can be as high as 2 kcal/mol,[20] any partial pore-formation (as in **A** or **B**) is strongly disfavored.

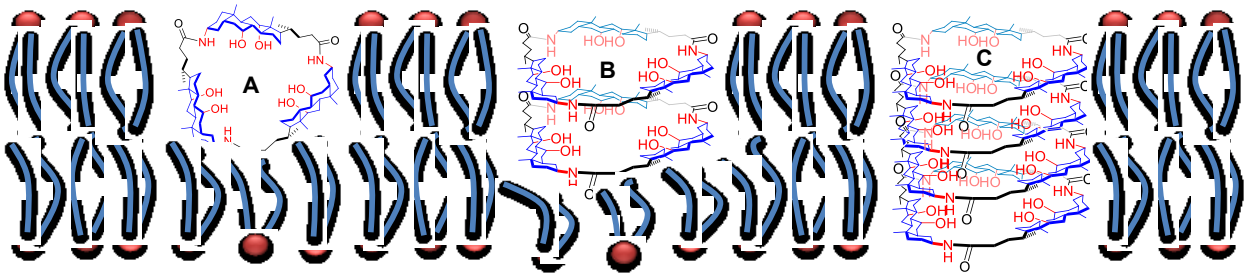

Figure 1. Possible arrangements of cyclic tricholate **1** in a lipid bilayer.

Many macrocycles of bile acids have been reported in the literature.[15b,21] A similar cyclic trimer of a cholate derivative was found to bind monosaccharides.[21a,b] We thus employed the well-established glucose leakage assay to test the pore-formation. Briefly, glucose (300 mM) was first encapsulated within POPC/POPG large unilamellar vesicles (LUVs) and the external glucose was removed by gel filtration. When different amounts of **1** were added to the liposomal solution,[22] the glucose that leaked out was converted by extravesically added hexokinase and ATP to glucose-6-phosphate, which was oxidized by glucose-6-phosphate dehydrogenase while NADP was reduced to NADPH. Because of the fast enzymatic kinetics, the formation of NADPH at 340 nm correlates directly with the rate of glucose efflux.[23]

To our delight, tricholate **1** was highly effective at transporting glucose across lipid membranes (Figure 1S, Supporting Information). The leakage was strongly dependent on its concentration. Glucose efflux was negligible below 0.125 μM of **1**. The leakage showed a noticeable increase at 0.25 μM of the macrocycle, but another two-fold increase in the transporter concentration caused a dramatic increase in leakage—over 90% of glucose leaked out after 60 min.

Because **1** cannot turn its hydrophilic inside out, we did not consider "toroidal pores", in which amphiphilic molecules (typically surfactants or amphipathic peptides) cause local phase changes in the lipids and produce transient openings in the membrane.[3] We performed the lipid mixing

assay and tested the possibility of membrane fusion as a potential cause of leakage,[24] but <10% lipid mixing occurred even at the highest [oligocholate]/[lipid] ratio used in the glucose leakage assay (Figure 1S).[25]

After lipid fusion was excluded as a main cause for leakage, we considered three other possible mechanisms for the glucose efflux, with either the monomer or an aggregate of **1** as the main transporting species. In a carrier- or ferry-based mechanism, a glucose-bound macrocycle (either in the form of **A** or **B** shown in Figure 1) migrates from the inner to the outer leaflet of the bilayer, where the guest is released.[26] In a relay mechanism, the guest still has to be bound by **A** or **B** but the binding is only transient and the guest hops from one station to another before exiting the bilayer. The third possibility is the hypothesized nanopore, represented by (the idealized) **C** in Figure 1.

A carrier-based mechanism typically gives a linear relationship between the leakage rate and the monomer concentration[27] but the strong dependence of leakage on the concentration of **1** suggests that its aggregate was the active transporter (vide infra).[3,27] Either **B** or **C** would fit such a scenario. To distinguish between the latter two mechanisms, we studied cyclic tetramer **2** and linear trimer **3** in the transport. The difference between **1** and **2** is not just in size but, more importantly, in their rigidity. A triangle cannot change its shape as long as the sides are rigid, but a quadrilateral can bend and twist even if the sides are completely rigid. Thus, stacking and transmembrane pore-formation should be more difficult with **2** than with **1**. Linear trimer **3** should be even less competent, as it has to fold before it can stack to form the pore (assuming the same pore-formation mechanism is involved).

Figure 2a shows the glucose leakage of LUVs at 30 min in the presence of the different oligocholates. The topology of the oligocholates impacted the transport strongly. It took 4–5 times

as much **2** as **1**, for example, to leak the same amount of glucose from the LUVs. The general facial amphiphilicity of the cholate clearly was *not* the determining factor, as tetramer **2** contained more cholates than trimer **1** and yet was less effective. The conclusion was further supported by linear trimer **3**, which displayed leakage slightly above the background (6–10%) even at the highest tested concentration. Once the ring structure was removed, the oligocholate completely lost its ability of transport.

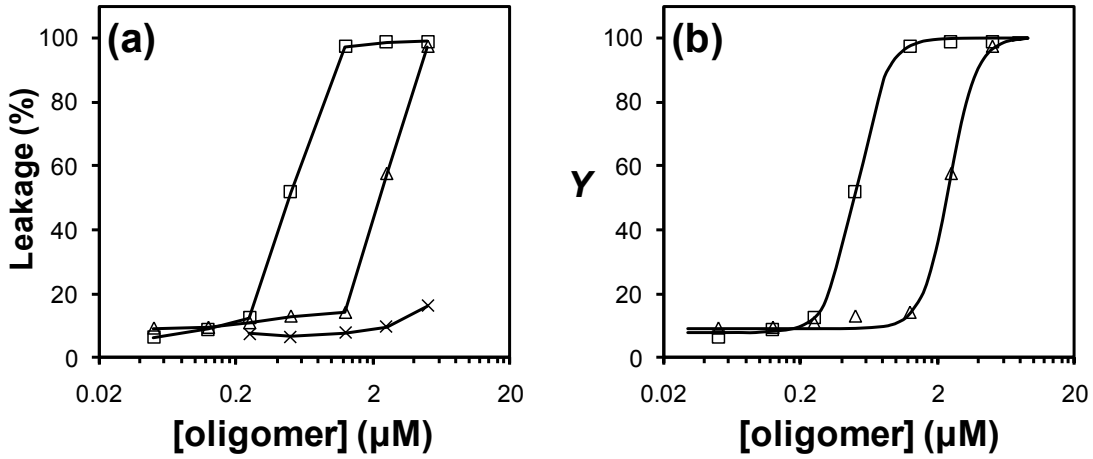

Figure 2. (a) Percent leakage of glucose at 30 min from POPC/POPG LUVs as a function of oligocholate concentration for **1** (□), **2** (△), and **3** (×) at ambient temperature. Total concentration of phospholipids was 107 μM. These leakage experiments were typically done in duplicates and the error within the two <10%. (b) Nonlinear least-squares fitting of the leakage data to the Hill equation for **1** (□) and **2** (△). The fraction activity (Y) is the percent glucose leakage of the LUVs at 30 min after addition of the oligomers.

The leakage data in Figure 2a suggests high cooperativity among the macrocycles.[3] A common way to analyze the cooperativity of a supramolecular system is through the Hill equation, $Y = Y_{low} + (Y_{high} - Y_{low})/[1 + (EC_{50} / c)^n]$, in which the fractional activity (Y) of a supramolecule is related to the monomer concentration (c).[28] EC_{50} is the concentration of the monomer that produces 50%

activity. The Hill coefficient (n) indicates both the stability of the self-assembly and the number of monomers in the supramolecule responsible for the activity. A Hill coefficient of $n > 1$ means that the monomer is the dominant species and yet the supramolecule is responsible for the observed activity.[3b,29]

Significantly, the leakage data fit well to the Hill equation (Figure 2b), yielding a Hill coefficient of $n = 4.0 \pm 0.3$ for cyclic trimer **1** and 4.4 ± 0.5 for tetramer **2**.[30] Thus, for both macrocycles, the active transporting supramolecule seems to consist of four macrocycles. POPC bilayer is about 2.6 nm in the hydrophobic thickness.[11,31] The cholate is about 0.6–0.7 nm on the side. To the extent that the Hill analysis reflects accurately the assembly process, the active transporting species was most likely a transmembrane pore assembled from four macrocycles.

Comparison of the three possible arrangements of the macrocycle in Figure 1 reveals the reasons for the pore-formation.[32] When a cyclic oligocholate enters the membrane, the introverted hydroxyl/amide groups demand the internal cavity to be filled with water/glucose instead of lipid hydrocarbon. If the macrocycle exists as a monomer (Figure 1, **A**), the entrapped water/glucose would face hydrocarbon at least on one end of the cavity or on both ends if the molecule penetrates deep into the bilayer. The unfavorable hydrophilic–hydrophobic contact can be reduced if the molecules stack on top of one another (**B**), but can be eliminated only if a transmembrane pore (**C**) is formed. In the last case, not only is water–hydrocarbon contact eliminated on both ends of the cavity for all the macrocycles involved, but also the water molecules inside the macrocycle are no longer confined in a nanospace. The water molecules within the pore can solvate all the polar groups on the inner wall and yet still exchange with the bulk water rapidly. The exchange of water clearly will be more difficult if one or both ends of the cavity are capped by hydrocarbon, as in **A** or **B**.

Effect of Cholesterol on the Oligocholate-Induced Leakage. To gain additional evidence for the pore-formation, we included 30 mol % of cholesterol in the lipid formulation. Cholesterol is known to increase the hydrophobic thickness[11] of POPC bilayer and decrease its fluidity.[12] Cholesterol-containing bilayers are much less permeable to hydrophilic molecules, including glucose and glycerol.[33]

Notably, glucose leakage became *significantly faster* when the bilayers contained 30 mol % of cholesterol (Figure 3). The data points connected by solid lines represent leakage from the cholesterol-containing LUVs and those by dotted lines are from the cholesterol-free ones. Both the trimer and the tetramer clearly benefited from cholesterol. The concentration of the transporter that causes 50% leakage at 30 min (i.e., EC_{50}) for the trimer went from ~0.5 to ~0.1 μM upon cholesterol inclusion; that for the tetramer decreased from ~2.4 to ~0.5 μM. The cyclic topology remained critical to the transport, as the linear trimer (×) was completely unaffected by the cholesterol added.

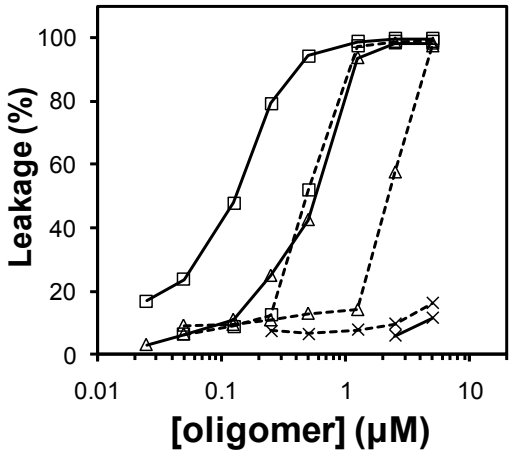

Figure 3. Percent leakage of glucose at 30 min from POPC/POPG LUVs as a function of oligocholate concentration for **1** (□), **2** (△), and **3** (×) at ambient temperature. The data points connected by solid lines are for the LUVs containing 30 mol % of cholesterol, whereas those

connected by dotted lines are for the LUVs without cholesterol, taken from Figure 2. Total concentration of phospholipids was 107 μM.

These results strongly support the pore-formation mechanism. Because cholesterol makes the membrane more hydrophobic,[33b,c] the hydrophobic driving force mentioned above is higher for the stacking of the macrocycles. Cholesterol is able to induce lateral heterogeneity in lipid membranes.[34] If cholesterol-rich and deficient domains exist, pore-formation should be easier if the macrocycle phase-separates into one domain. Given that cholic acid is a metabolite of cholesterol, **1** and **2** are highly likely to fall into cholesterol-rich domains.

Effect of Guest Size on the Oligocholate-Induced Leakage. Different transport mechanisms are expected to respond very differently to an increase in the guest size. Diffusion of the carrier–guest complex in the membrane slows down as its size increases. Because it is more difficult for a larger hydrophilic guest to hop from one station to another in a hydrophobic membrane, relay will become less efficient as well. Leakage through a nanopore, on the other hand, should not be affected very much as long as the cross section of the guest is smaller than the pore diameter.

We thus studied the permeation of maltotriose by the cholate macrocycles (Figure 4). Although the trisaccharide is much longer than glucose, its cross section remains the same. Consistent with the pore-formation mechanism, the increase of the sugar size did not slow down the leakage. The EC_{50} for the trimer (□) was almost the same for maltotriose (~0.6 μM) and glucose (~0.5 μM). Remarkably, tetramer **2** was considerably more effective at leaking the longer sugar; the EC_{50} of the tetramer (△) went from 2.4 μM for glucose to ~0.7 μM for maltotriose.

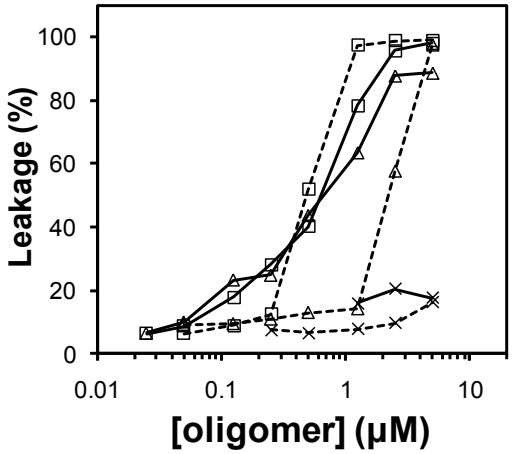

Figure 4. Percent leakage of maltotriose at 30 min from POPC/POPG LUVs as a function of oligocholate concentration for **1** (□), **2** (△), and **3** (×) at ambient temperature. The data points connected by solid lines are for maltotriose, whereas those connected by dotted lines are for glucose, taken from Figure 2. Total concentration of phospholipids was 107 μM.

Why did the tetramer transport a longer sugar better than a shorter one? The result is highly unusual and contrary to what the diffusion of the guest (inside the pore) would predict. As shown by the molecular models (Figure 5), the trisaccharide is too long to fit within one macrocycle. Hence, as the sugar enters the membrane, it will thread through the macrocycles and template the pore formation. If one assumes that a longer sugar diffuses more slowly than a shorter one inside the pore, the fact that **2** benefited more than **1** in the trisaccharide transport suggests that the template effect was stronger in the tetramer. The conclusion is supported by both the rigidity consideration and the earlier glucose leakage data, which suggest that pore-formation is more difficult with the tetramer. In general, an effect is manifested most strongly where it is most needed. Such a trend is frequently observed in physical organic chemistry—the extent of neighboring group participation, for example, increases with an increase of the electron demand at the reactive center.[35]

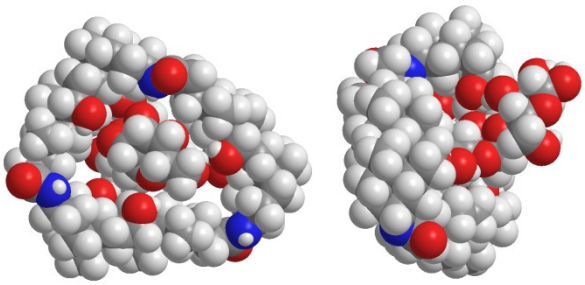

Figure 5. Two views of space-filling molecular models of compound **1** with an included maltotriose. The molecular models were generated by Chem3D and optimized with the MM2 force field.

Another reason why the tetramer benefited more from the template effect than the trimer could be its larger pore size. According to the molecular model (Figure 5), a sugar fits quite snugly within the inner cavity of **1** and forms multiple hydrogen bonds with the inner wall of the pore. As the sugar gets longer, the number of hydrogen bonds involved would increase, making the passage of the guest more difficult. Hence, the template effect of maltotriose was probably offset by the small pore size of the trimer. For the tetramer, the larger gap between the guest and the pore probably geometrically prohibited the formation of some hydrogen bonds, allowing the trisaccharide to go through the pore with less hindrance.

It should be mentioned that the leakage data with the cholesterol-containing LUVs (Figure 3) or with maltotriose as the guest (Figure 4) did not give the high cooperativity shown in Figure 2. The Hill coefficient (n) was only 1–2 in all the cases. The Hill coefficients have been reported to change significantly with minor structural modification of a given system.[29,36] Similar observations were made in biology including in well-established systems such as the hemoglobin–oxygen binding. The reason for the change was not always clear. The Hill equation is known to operate best when extreme positive cooperativity exists between the binding of the first and second molecule.[37] Such a condition may not be met in the glucose transport across the cholesterol-

containing hydrophobic membrane or in the maltotriose transport where a template effect is operating.

Aggregation of Cyclic Oligocholates Studied by Fluorescence. Due to its long fluorescence lifetime, pyrene can form excimers quite readily even at relative low concentrations.[38] Aggregation of **4** within a lipid bilayer brings the pyrene groups within proximity and promotes the excimer formation (emitting at 470 nm). Instead of the membrane extrusion method[39] used to prepare the LUVs for the leakage assay, we incorporated the oligocholates into lipid bilayers for DLPC (dilauroylphosphatidylcholine) and POPC/POPG liposomes by the detergent dialysis method. This procedure is often employed to reconstitute membrane proteins into liposomes[40] and has the benefit of generating the most homogeneously mixed lipids. Because cholesterol was found to interfere with the detergent dialysis (possibly because of its strong interactions with the Bio-Beads used in the procedure), we added **4** to preformed LUVs prepared with the membrane extrusion method.

Figure 6 shows the excimer/monomer ratio for compound **4** as a function of the [**4**]/[lipid] ratio in three different bilayers. Two trends are immediately noticeable. First, the pyrene excimer became stronger as the membrane became more hydrophobic. Among the three bilayers, the C12 DLPC membrane (△) was the least hydrophobic and the cholesterol-containing C16–18 POPC/POPG (◇) the most hydrophobic. With an increase in the membrane hydrophobicity, the inflection point in the excimer/monomer curves, corresponding to the critical aggregation concentration (CAC) of the macrocycle, decreased steadily from 0.02 to 0.01 to 0.007. The trend shows that the formation of pyrene excimer is promoted by membrane hydrophobicity and tracks well with the leakage data. Second, all the excimer/monomer curves were sigmoidal in shape—a hallmark of cooperativity behavior.[41] In fact, when the fluorescence data were fit to the Hill

equation, the Hill coefficient (*n*) was ~1.5 for the DLPC membrane, ~3 for POPC/POPG, and ~4 for the cholesterol-containing POPC/POPG. The results showed that the number of the macrocycles in the aggregates correlate with the membrane thickness. The result is in full agreement with our pore-forming mechanism and the leakage data. Because the aggregation is driven by hydrophobic interactions and the pore needs to span the bilayer (to allow water molecules inside the pore to exchange with bulk water), the pore length should not exceed the hydrophobic thickness of the membrane.

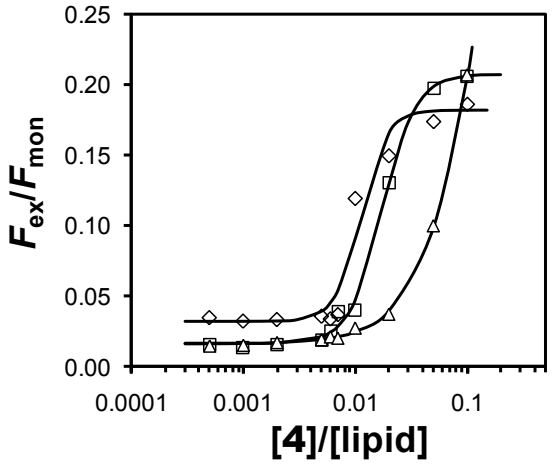

Figure 6. The excimer/monomer ratio as a function of [**4**]/[lipid] ratio in liposomes made of DLPC (△), POPC/POPG (□), and POPC/POPG with 30 mol % cholesterol (◇). The theoretical curves are nonlinear least-squares fitting of the fluorescence data to the Hill equation.

Conclusions

Classical hydrophobic effect drives the aggregation of hydrophobic molecules in water. By pulling water into lipid bilayers with the amphiphilic cholate macrocycles, we "activated" the water molecules and used them to assemble the macrocycles into transmembrane nanopores.[42] Aggregation and pore-formation seem to be quite efficient for the cyclic tricholate, as it only took 1 macrocycle out of 200 lipid molecules to leak 50% of 300 mM glucose from the LUVs in 30

min. Leakage from the cholesterol-containing LUVs was even more efficient—the same leakage only required 1 macrocycle out of 1000 lipid molecules.

The hydrophobically driven pore-forming mechanism yielded some quite unusual transport properties. Contrary to conventional expectations, permeation of hydrophilic guests occurs more readily as the membrane becomes more hydrophobic and longer sugars passed through the membranes more readily than shorter ones. Transmembrane movement of sugars is accomplished by complex protein transporters in nature,[43] but our oligocholates can be synthesized in a few steps from the cholate monomer.[44] Given the unique pore-forming mechanism, the easy synthesis of the oligocholates, the biocompatibility of cholic acid, and the numerous uses of nanopores,[13–21] these compounds may find many applications in biology and chemistry in the future.

Acknowledgment We thank Dr. Xingang Pan for providing compound **1** and performing some initial leakage experiments. We thank NSF (CHE-0748616 and DMR-1005515) for financial support.

Supporting Information Available: The entire experimental section including the general experimental section, synthesis and characterization of the compounds, leakage assays, and fluorescence experiments. This material is available free of charge via the Internet at http://pubs.acs.org.

References

(1) Kasianowicz, J. J.; Robertson, J. W. F.; Chan, E. R.; Reiner, J. E.; Stanford, V. M. *Annu. Rev. Anal. Chem.* **2008**, *1*, 737-766.

(2) (a) Kasianowicz, J. J.; Brandin, E.; Branton, D.; Deamer, D. W. *Proc. Natl. Acad. Sci. U. S. A.* **1996**, *93*, 13770-13773. (b) Akeson, M.; Branton, D.; Kasianowicz, J. J.; Brandin, E.;

Deamer, D. W. *Biophys. J.* **1999**, *77*, 3227-3233. (c) Meller, A.; Nivon, L.; Brandin, E.; Golovchenko, J.; Branton, D. *Proc. Natl. Acad. Sci. U. S. A.* **2000**, *97*, 1079-1084. (d) Vercoutere, W.; Winters-Hilt, S.; Olsen, H.; Deamer, D.; Haussler, D.; Akeson, M. *Nat. Biotechnol.* **2001**, *19*, 248-252. (e) Howorka, S.; Cheley, S.; Bayley, H. *Nat. Biotechnol.* **2001**, *19*, 636-639. (f) Clarke, J.; Wu, H. C.; Jayasinghe, L.; Patel, A.; Reid, S.; Bayley, H. *Nat. Biotechnol.* **2009**, *4*, 265-270.

(3) (a) Matile, S.; Som, A.; Sorde, N. *Tetrahedron* **2004**, *60*, 6405-6435. (b) Sisson, A. L.; Shah, M. R.; Bhosale, S.; Matile, S. *Chem. Soc. Rev.* **2006**, *35*, 1269-1286.

(4) (a) Granja, J. R.; Ghadiri, M. R. *J. Am. Chem. Soc.* **1994**, *116*, 10785-10786. (b) Sanchez-Quesada, J.; Kim, H. S.; Ghadiri, M. R. *Angew. Chem. Int. Ed.* **2001**, *40*, 2503-2506.

(5) (a) Sakai, N.; Mareda, J.; Matile, S. *Acc. Chem. Res.* **2005**, *38*, 79-87. (b) Das, G.; Talukdar, P.; Matile, S. *Science* **2002**, *298*, 1600-1602. (c) Sakai, N.; Sorde, N.; Matile, S. *J. Am. Chem. Soc.* **2003**, *125*, 7776-7777.

(6) Satake, A.; Yamamura, M.; Oda, M.; Kobuke, Y. *J. Am. Chem. Soc.* **2008**, *130*, 6314-6315.

(7) Helsel, A. J.; Brown, A. L.; Yamato, K.; Feng, W.; Yuan, L. H.; Clements, A. J.; Harding, S. V.; Szabo, G.; Shao, Z. F.; Gong, B. *J. Am. Chem. Soc.* **2008**, *130*, 15784-15785.

(8) Fyles, T. M.; Tong, C. C. *New. J. Chem.* **2007**, *31*, 655-661.

(9) Ma, L.; Melegari, M.; Colombini, M.; Davis, J. T. *J. Am. Chem. Soc.* **2008**, *130*, 2938-2939.

(10) (a) Gokel, G. W.; Mukhopadhyay, A. *Chem. Soc. Rev.* **2001**, *30*, 274-286. (b) Fyles, T. M. *Chem. Soc. Rev.* **2007**, *36*, 335-347. (c) Koert, U.; Al-Momani, L.; Pfeifer, J. R. *Synthesis-Stuttgart* **2004**, 1129-1146. (d) Gokel, G. W.; Murillo, O. *Acc. Chem. Res.* **1996**, *29*, 425-432. (e) Jung, M.; Kim, H.; Baek, K.; Kim, K. *Angew. Chem. Int. Ed.* **2008**, *47*, 5755-5757. (f) Li, X.; Shen, B.; Yao, X. Q.; Yang, D. *J. Am. Chem. Soc.* **2009**, *131*, 13676-13680.

(11) Nezil, F. A.; Bloom, M. *Biophys. J.* **1992**, *61*, 1176-1183.

(12) Holthuis, J. C. M.; van Meer, G.; Huitema, K. *Mol. Membr. Biol.* **2003**, *20*, 231-241.

(13) (a) Bandyopadhyay, P.; Janout, V.; Zhang, L. H.; Sawko, J. A.; Regen, S. L. *J. Am. Chem. Soc.* **2000**, *122*, 12888-12889. (b) Goto, C.; Yamamura, M.; Satake, A.; Kobuke, Y. *J. Am. Chem. Soc.* **2001**, *123*, 12152-12159. (c) Maulucci, N.; De Riccardis, F.; Botta, C. B.; Casapullo, A.; Cressina, E.; Fregonese, M.; Tecilla, P.; Izzo, I. *Chem. Commun.* **2005**, 1354-1356. (d) Wilson, C. P.; Webb, S. J. *Chem. Commun.* **2008**, 4007-4009.

(14) (a) Janout, V.; Di Giorgio, C.; Regen, S. L. *J. Am. Chem. Soc.* **2000**, *122*, 2671-2672. (b) Janout, V.; Staina, I. V.; Bandyopadhyay, P.; Regen, S. L. *J. Am. Chem. Soc.* **2001**, *123*, 9926-9927. (c) Janout, V.; Jing, B. W.; Staina, I. V.; Regen, S. L. *J. Am. Chem. Soc.* **2003**, *125*, 4436-4437. (d) Janout, V.; Regen, S. L. *J. Am. Chem. Soc.* **2005**, *127*, 22-23.

(15) (a) Koulov, A. V.; Lambert, T. N.; Shukla, R.; Jain, M.; Boon, J. M.; Smith, B. D.; Li, H. Y.; Sheppard, D. N.; Joos, J. B.; Clare, J. P.; Davis, A. P. *Angew. Chem. Int. Ed.* **2003**, *42*, 4931-4933. (b) Whitmarsh, S. D.; Redmond, A. P.; Sgarlata, V.; Davis, A. P. *Chem. Commun.* **2008**, 3669-3671.

(16) For several representative reviews, see: (a) Gellman, S. H. *Acc. Chem. Res.* **1998**, *31*, 173-180. (b) Hill, D. J.; Mio, M. J.; Prince, R. B.; Hughes, T. S.; Moore, J. S. *Chem. Rev.* **2001**, *101*, 3893-4012. (c) Hecht, S.; Huc, I. *Foldamers : structure, properties, and applications*; Wiley-VCH: Weinheim, 2007. (d) Cubberley, M. S.; Iverson, B. L. *Curr. Opin. Chem. Biol.* **2001**, *5*, 650-653. (e) Kirshenbaum, K.; Zuckermann, R. N.; Dill, K. A. *Curr. Opin. Struct. Biol.* **1999**, *9*, 530-535. (f) Goodman, C. M.; Choi, S.; Shandler, S.; DeGrado, W. F. *Nat. Chem. Biol.* **2007**, *3*, 252-262. (g) Bautista, A. D.; Craig, C. J.; Harker, E. A.; Schepartz, A. *Curr. Opin. Chem. Biol.* **2007**, *11*, 685-692.

(17) (a) Zhao, Y.; Zhong, Z. *J. Am. Chem. Soc.* **2005**, *127*, 17894-17901. (b) Zhao, Y.; Zhong, Z.; Ryu, E. H. *J. Am. Chem. Soc.* **2007**, *129*, 218-225. (c) Cho, H.; Zhao, Y. *J. Am. Chem. Soc.* **2010**, *132*, 9890-9899. (d) Zhao, Y. *J. Org. Chem.* **2009**, *74*, 834-843. (e) Pan, X.; Zhao, Y. *Org. Lett.* **2009**, *11*, 69-72.

(18) Som, A.; Matile, S. *Chem. Biodiv.* **2005**, *2*, 717-729.

(19) (a) Rostovtsev, V. V.; Green, L. G.; Fokin, V. V.; Sharpless, K. B. *Angew. Chem. Int. Ed.* **2002**, *41*, 2596-2599. (b) Kolb, H. C.; Finn, M. G.; Sharpless, K. B. *Angew. Chem. Int. Ed.* **2001**, *40*, 2004-2021.

(20) Dunitz, J. D. *Science* **1994**, *264*, 670.

(21) (a) Bonarlaw, R. P.; Davis, A. P.; Murray, B. A. *Angew. Chem. Int. Ed. Engl.* **1990**, *29*, 1407-1408. (b) Davis, A. P.; Walsh, J. J. *Chem. Commun.* **1996**, 449-451. (c) Brotherhood, P. R.; Davis, A. P. *Chem. Soc. Rev.* **2010**, *39*, 3633-3647. (d) Brady, P. A.; BonarLaw, R. P.; Rowan, S. J.; Suckling, C. J.; Sanders, J. K. M. *Chem. Commun.* **1996**, 319-320. (e) Ghosh, S.; Choudhury, A. R.; Row, T. N. G.; Maitra, U. *Org. Lett.* **2005**, *7*, 1441-1444.

(22) In our leakage assay, we added **1** to the liposomal solution as a solution of DMSO (10–20 μL). The amount of DMSO was tested and found to have negligible effects on the LUVs.

(23) Kinsky, S. C.; Haxby, J. A.; Zopf, D. A.; Alving, C. R.; Kinsky, C. B. *Biochemistry* **1969**, *8*, 4149-4158.

(24) Struck, D. K.; Hoekstra, D.; Pagano, R. E. *Biochemistry* **1981**, *20*, 4093-4099.

(25) The 100% end point in a fusion assay can be measured either after a surfactant such as Triton X-100 is added to destroy the liposomes or through a "mock" fusion product (i.e., liposomes whose probe density corresponds to that of completely fused liposomes). Because Triton X-100 impacts the quantum yield of NBD, we mainly used the second approach for our fusion

experiments. For a discussion on different lipid-mixing fusion assays, see: Hoesktra, D.; Düzgüneş, N. *Methods Enzymol.* **1993**, *220*, 15-32.

(26) Smith, B. D.; Lambert, T. N. *Chem. Commun.* **2003**, 2261-2268.

(27) (a) Deng, G.; Merritt, M.; Yamashita, K.; Janout, V.; Sadownik, A.; Regen, S. L. *J. Am. Chem. Soc.* **1996**, *118*, 3307-3308. (b) Merritt, M.; Lanier, M.; Deng, G.; Regen, S. L. *J. Am. Chem. Soc.* **1998**, *120*, 8494-8501.

(28) Hille, B. *Ionic channels of excitable membranes*; 2nd ed.; Sinauer Associates: Sunderland, Mass., 1992.

(29) Litvinchuk, S.; Bollot, G.; Mareda, J.; Som, A.; Ronan, D.; Shah, M. R.; Perrottet, P.; Sakai, N.; Matile, S. *J. Am. Chem. Soc.* **2004**, *126*, 10067-10075.

(30) Leakage at 60 min gave similar results, but the curve fitting to the Hill equation was less certain because the data points clustered at either very high ($Y > 90\%$) or very low ($Y < 30\%$) leakage.

(31) Lewis, B. A.; Engelman, D. M. *J. Mol. Biol.* **1983**, *166*, 203-210.

(32) Hydrogen bonds among the amides along the pore axis are unlikely to contribute significantly because the amides are exposed to water molecules inside the pore. Also, the steroid backbone is large on the amino end and small near the carboxy tail. The geometry of the macrocycle thus prohibits close contact of the amide bonds in the *z*-direction.

(33) (a) Demel, R. A.; Bruckdor, K. R.; Vandeene, L. L. *Biochim. Biophys. Acta* **1972**, *255*, 321-330. (b) Demel, R. A.; R., B. K.; L., V. L. *Biochim. Biophys. Acta* **1972**, *255*, 321-330. (c) Papahadjopoulos, D.; Nir, S.; Ohki, S. *Biochim. Biophys. Acta* **1972**, *266*, 561-583.

(34) (a) London, E. *Curr. Opin. Struct. Biol.* **2002**, *12*, 480-486. (b) Edidin, M. *Annu. Rev. Biophys. Biomol. Struct.* **2003**, *32*, 257-283. (c) Silvius, J. R. *Biochim. Biophys. Acta* **2003**,

1610, 174-183. (d) Zhao, J.; Wu, J.; Heberle, F. A.; Mills, T. T.; Klawitter, P.; Huang, G.; Costanza, G.; Feigenson, G. W. *Biochim. Biophys. Acta* **2007**, *1768*, 2764-2776.

(35) (a) Lambert, J. B.; Mark, H. W. *J. Am. Chem. Soc.* **1978**, *100*, 2501-2505. (b) Lambert, J. B.; Larson, E. G. *J. Am. Chem. Soc.* **1985**, *107*, 7546-7550.

(36) (a) Talukdar, P.; Sakai, N.; Sorde, N.; Gerard, D.; Cardona, V. M. F.; Matile, S. *Bioorg. Med. Chem.* **2004**, *12*, 1325-1336. (b) Bhosale, S.; Matile, S. *Chirality* **2006**, *18*, 849-856. (c) Shank, L. P.; Broughman, J. R.; Takeguchi, W.; Cook, G.; Robbins, A. S.; Hahn, L.; Radke, G.; Iwamoto, T.; Schultz, B. D.; Tomich, J. M. *Biophys. J.* **2006**, *90*, 2138-2150. (d) Ferdani, R.; Pajewski, R.; Djedovic, N.; Pajewska, J.; Schlesinger, P. H.; Gokel, G. W. *New J. Chem.* **2005**, *29*, 673-680. (e) Chen, W. H.; Shao, X. B.; Regen, S. L. *J. Am. Chem. Soc.* **2005**, *127*, 12727-12735.

(37) Weiss, J. N. *FASEB J.* **1997**, *11*, 835-841.

(38) Birks, J. B.; Munro, I. H.; Dyson, D. J. *Proc. R. Soc. London Ser. A* **1963**, *275*, 575-588.

(39) Olson, F.; Hunt, C. A.; Szoka, F. C.; Vail, W. J.; Papahadjopoulos, D. *Biochim. Biophys. Acta* **1979**, *557*, 9-23.

(40) Smith, S. A.; Morrissey, J. H. *J. Thromb. Haemost.* **2004**, *2*, 1155-1162.

(41) Chan, H. S.; Bromberg, S.; Dill, K. A. *Philos. Trans. R. Soc. London B* **1995**, *348*, 61-70.

(42) For an example of water-promoted assembly in the solid state, see: Carrasco, H.; Foces-Foces, C.; Perez, C.; Rodriguez, M. L.; Martin, J. D. *J. Am. Chem. Soc.* **2001**, *123*, 11970-11981.

(43) Saier, M. H., Jr. In *The Structure of biological membranes*; Yeagle, P. Ed; CRC Press: Boca Raton, 1992; Chapter 18.

(44) For boronic acid-based sugar transporters, see: (a) Westmark, P. R.; Smith, B. D. *J. Am. Chem. Soc.* **1994**, *116*, 9343-9344. (b) Westmark, P. R.; Gardiner, S. J.; Smith, B. D. *J. Am. Chem. Soc.* **1996**, *118*, 11093-11100.

CHAPTER 3. AROMATICALLY FUNCTIONALIZED CYCLIC TRICHOLATE MACROCYCLES: AGGREGATION, TRANSMEMBRANE PORE FORMATION, FLEXIBILITY, AND COOPERATIVITY

A paper published in *Journal of Organic Chemistry* **2012**, *77*, 4679−4687.

Lakmini Widanapathirana and Yan Zhao

Abstract

The aggregation of macrocyclic oligocholates with introverted hydrophilic groups and aromatic side chains was studied by fluorescence spectroscopy and liposome leakage assays. Comparison between the solution and the membrane phase afforded insight into the solvophobically driven aggregation. The macrocycles stacked over one another in lipid membranes to form transmembrane nanopores, driven by a strong tendency of the water molecules in the interior of the amphiphilic macrocycles to aggregate in a nonpolar environment. The aromatic side chains provided spectroscopic signatures for stacking, as well as additional driving force for the aggregation. Smaller, more rigid macrocycles stacked better than larger, more flexible ones

because the cholate building blocks in the latter could rotate outward and diminish the conformation needed for the water templated hydrophobic stacking. The acceptor−acceptor interactions among naphthalenediimide (NDI) groups were more effective than the pyrene−NDI donor−acceptor interactions in promoting the transmembrane pore formation of the oligocholate macrocycles.

Introduction

Chemists have long been intrigued by the abilities of biological transporters to move molecules from one side of the membrane to the other by channels or pores.[1] The process is important to not only many key biofunctions but also a number of practical applications including drug delivery,[1] sensing,[2] and catalysis.[3] In recent years, synthetic transmembrane pores with an inner diameter of 1 nm or larger have attracted the attention of many researchers.[4] The research is expected to improve our understanding of the biological pore-forming mechanisms, as well as providing useful materials for practical applications.

Unlike ion channels frequently prepared from flexible structures such as crown ethers,[5] pore-forming materials need to have significant rigidity to withstand the external membrane pressure to keep the internal pore from collapsing.[6] A number of successful synthetic nanopores have been constructed following this principle. Ghadiri, for example, utilized hydrogen-bonding interactions to assemble cyclic D/L-peptides into nanopores large enough for glucose and glutamic acid to pass through.[7] Matile and co-workers developed an extremely versatile class of β-barrel pores from oligo(phenylene) derivatives[3,8] and demonstrated their applications in artificial photosynthesis[9] and catalysis.[3] Other reported examples include the porphyrin-based nanopores by Satake and

Kobuke,[10] the π-stacked aromatic heterocycles by Gong,[11] Fyles's metal-coordinated nanopores,[12] and the guanosine quartet-based giant ion channels by Davis.[13]

We recently reported that amphiphilic macrocyclic oligocholates such as **1** could form transmembrane nanopores.[14] Key evidence for the pore formation includes strong cooperativity among four macrocycles in the transport activity, ineffectiveness of the linear trimer, a counterintuitive increase of glucose transport with increasing hydrophobicity of the membrane, an unusual faster transport of maltotriose over glucose, shutting down of the pore-transport mechanism with guests whose cross-section was larger than the pore diameter, and excimer formation in pyrene-labeled macrocycles.

The pore formation was proposed to be promoted by hydrophobic interactions, which typically work in aqueous instead of hydrocarbon-based media. Macrocycle **1** has an internal hydrophilic cavity nearly 1 nm across. Being overall hydrophobic, compound **1** prefers a membrane over an aqueous environment. Once the molecule enters the membrane, however, the amphiphilic macrocycle needs to solvate its introverted hydrophilic groups by water instead of the lipid hydrocarbon. The conflicting solvation requirements of the introverted hydrophilic groups and the exterior hydrocarbon framework are solved when multiple macrocycles stack over one another to form a transmembrane pore (Figure 1). The arrangement allows the water molecules inside the macrocycles to interact with one another, solvate the polar groups of the cholates, and still exchange readily with the bulk water. The driving force for the stacking is essentially the associative interactions among the "activated" water molecules in the interior of the macrocycles located in a highly hydrophobic environment. The exchange of the water molecules inside the pore with those in the bulk outside the membrane may also be important, as the entropic cost for trapping a single water molecule can be as high as 2 kcal/mol under certain conditions.[15]

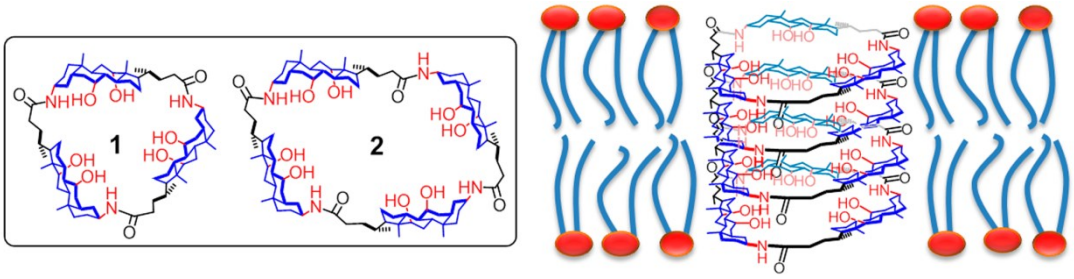

Figure 1. Schematic representation the idealized pore formation of oligocholate macrocycle **1** in a lipid bilayer membrane.

Aromatic interactions are among the most important tools in supramolecular chemistry.[16] The interactions enabled the construction of many interesting materials including foldamers[16,17] and have already been utilized in synthetic pore-forming materials.[3,8–13] The interactions have a number of components including electrostatic, van der Waals, and solvophobic interactions. Depending on the electronic nature of the aromatic systems and the media involved, the interacting partners may adopt edge-to-face, offset stacked, or face-to-face stacked configurations.[16]

In this paper, we report several oligocholate macrocycles with aromatic side chains.[18] A main objective of the research was to design aromatically functionalized oligocholate pore-forming materials in which the aromatic interactions and the above-mentioned hydrophobic interactions could work cooperatively. The oligocholate macrocycles were inspired by our linear oligocholate foldamers whose folding is driven by solvophobic interactions in mixed organic solvents.[19] In fact, the folding of the oligocholate foldamers and the stacking of the cholate macrocycles are driven by essentially the same solvophobic interactions.[14a] Although it is clear that organic solvents and lipid bilayers are very different media, it is often not clear how different environments impact the outcome and especially the mechanism of molecular recognition. When it comes to investigation

of molecular recognition in difficult-to-study environments such as lipid membranes, researchers frequently extrapolate learning from solution studies to the new environment. For these reasons, we are particularly interested in the effects of environments on the intermolecular interactions of the macrocycles. The study revealed a number of important factors in the pore-forming mechanism including the rigidity of the macrocycle, the lipid composition, and the type of π systems most effective in promoting the hydrophobic stacking of the oligocholate macrocycles.

Results and Discussion

Design and Syntheses of Oligocholate Macrocycles. Chart 1 shows the aromatically functionalized oligocholates synthesized in this study. Compound **3** was previously prepared as a fluorescently labeled macrocycle to study the stacking mechanism by fluorescence spectroscopy.[14a] Macrocycle **4** carries a naphthalenediimide (NDI) group instead of pyrene on the side chain. The NDI group is an electron-deficient π system, known to interact strongly with π donors.[16,17] Its ability to quench the pyrene fluorescence allows us to study its interaction with pyrene-labeled macrocycles such as **3** and **5** by fluorescence spectroscopy.

Both **3** and **5** have the pyrenyl group on the side chain; their difference is in the number of atoms in between the oligocholate macrocycle and the aromatic group. Whereas **3** and **4** are matched nearly perfectly regarding the length of the tether in between the macrocycle and the aromatic side chain, **5** and **4** are mismatched. If the cholate macrocycles stack up to engage in the aforementioned hydrophobic interactions, the aromatic side chains would have difficulty achieving the face-to-face configuration for the aromatic donor−acceptor inter¬actions.[16] The molecules thus were designed to test whether the electron donor-acceptor interactions would work cooperatively with the hydrophobic, water-templated stacking of the oligocholate macrocycles.

Chart 1. Aromatically Functionalized Oligocholate Macrocycle (**2**–**8**) Used in the Current Study.

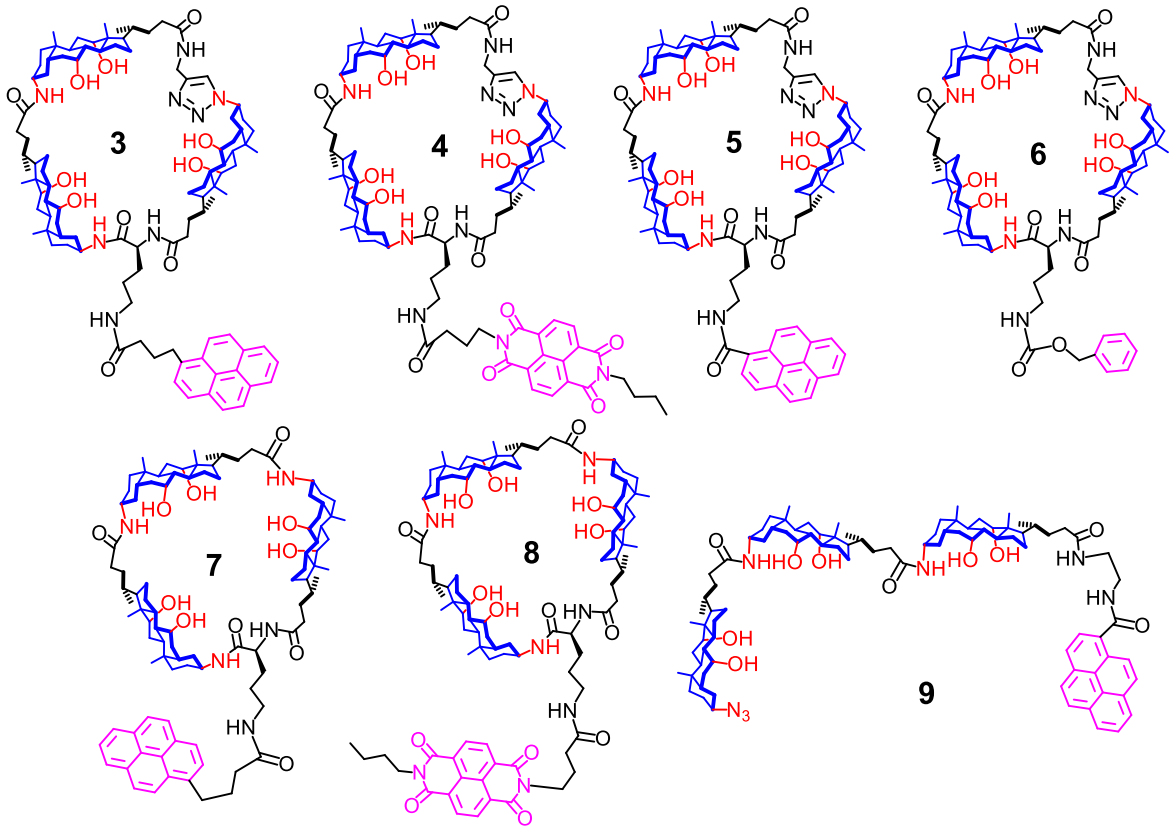

Compounds **3**–**5** were all synthesized from the previously reported **6**,[14a] which has a Cbz-protected L-ornithine. All the macrocycles were cyclized by the highly efficient alkyne–azide click reaction.[20] The cyclization was employed partly because the synthesis of linear, amide-linked oligocholates always leaves behind an azide and an ester at the chain ends.[21] The most efficient way to synthesize an oligocholate macrocycle, therefore, is to hydrolyze the ester, couple it to an alkyne-terminated amine such as propargyl amine, and cyclize through the click reaction.

Another way of macrocyclization is to couple an amine–carboxyl-terminated linear oligocholate by amide coupling. Scheme 1 shows the syntheses of macrocycles **7** and **8** using this method. First, the amine-terminated dimer **10** and a cholate monomer with a Cbz-protected L-ornithine (**11**) were coupled to afford linear trimer **12** using benzotriazole-1-yl-oxy-tris(dimethylamino)phosphonium

hexafluorophosphate (BOP) as the coupling reagent. The azido group of **12** was reduced by triphenylphosphine to afford amine–ester terminated **13**, which was hydrolyzed into the carboxylate and cyclized using BOP. After deprotection of the Cbz group, the amine derivative **15** was allowed to react with activated esters **16** and **17** to afford the all-amide-linked oligocholate macrocycles **7** and **8**, respectively.

Scheme 1. Syntheses of Macrocycles **7** and **8**.

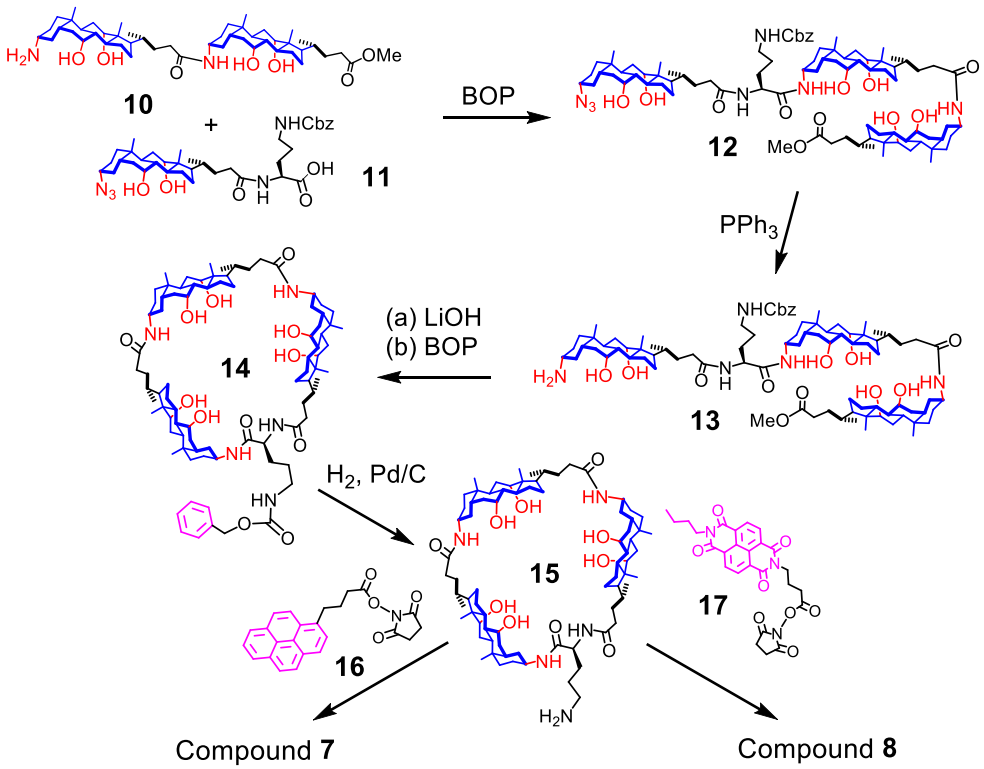

Aggregation of Oligocholate Macrocycles in Solution. The oligocholate macrocycles were inspired by our linear oligocholate foldamers. Both the folding of linear oligocholates and the aggregation of the oligocholate macrocycles are driven by the same form of solvophobic interactions.[14a] In a nonpolar solvent containing a few percent of a polar solvent, the extended conformer of a linear oligocholate is disfavored because of its exposed polar faces to the nonpolar

solvent, the major component of the solvent mixture. By folding into a helix with introverted hydrophilic groups, the oligocholate creates a hydrophilic internal cavity filled disproportionally with the polar solvent (Figure 2, left panel). The arrangement satisfies the needs of the cholate polar groups to be solvated by polar instead of nonpolar solvent. Meanwhile, the nonpolar surface of the oligocholate is exposed to the nonpolar solvent and some polar solvent molecules are able to reside in a hydrophilic microenvironment. Since the folded oligocholate prefers a trimeric periodicity,[18a,21] macrocycle **1** essentially is a cross-section of the folded helix. The solvophobic forces that drive the folding of the linear oligocholate will promote the stacking of the macrocycles in the z-direction (Figure 2, right panel).

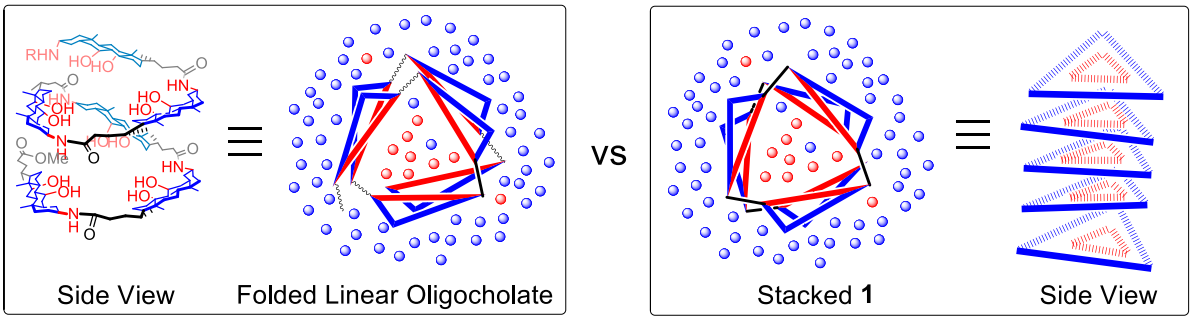

Figure 2. Schematic representation of the solvophobically driven folding of a linear oligocholate and aggregation of macrocyclic oligocholate **1**. The red and blue circles represent polar and nonpolar solvent molecules, respectively. (Reprinted with permission from Ref 25. Copyright 2011, American Chemical Society, Washington, DC.)

The most "folding-friendly" solvents for the oligocholate foldamers are ternary mixtures such as 2:1 hexane/ethyl acetate with a small amount of methanol.[19a] Hexane is immiscible with methanol but miscible with ethyl acetate. A large amount of hexane in the mixture, thus, makes it easy to phase-separate methanol from the bulk and reduces the energetic cost associated with the folding. As the amount of methanol increases, the folded oligocholate typically unfolds, due to the

better solvation of the polar groups by the bulk solvent.[19] When the hydrophilic and hydrophobic faces of the linear oligocholates become both well-solvated, the unfolded conformation is more favorable because of its higher conformational entropy.

To understand the stacking of the aromatically functionalized macrocycles, we first performed fluorescence quenching of the pyrene-labeled oligocholates by the NDI-functionalized ones in 2:1 hexane/ethyl acetate with varying percentage of methanol. A small amount of methanol was needed to dissolve the compounds in nonpolar solvents. As described earlier, the polar solvent also serves to "template" the aggregation of the macrocycles by interacting with one another through hydrogen bonds. Essentially, by interacting with one another and with the polar groups on the internal wall of the stacked nanopore via hydrogen bonds, the methanol molecules within the pore act as a solvophobic "glue" to pull the amphiphilic macrocycles together.

Figure 3a shows the normalized emission intensity of pyrene-labeled oligocholates (i.e., **3**, **5**, and **9**) in the presence of 1 equiv NDI-functionalized **4** in the ternary solvents. The emission intensity was normalized to that in 0.5% methanol for all three pairs, allowing us to compare the different fluorophores more accurately.[22] The solvophobic driving force is expected to be the strongest in 0.5% methanol. An increase of methanol lowers the driving force for the aggregation and should reduce the quenching of pyrene by NDI and enhances the pyrene emission.

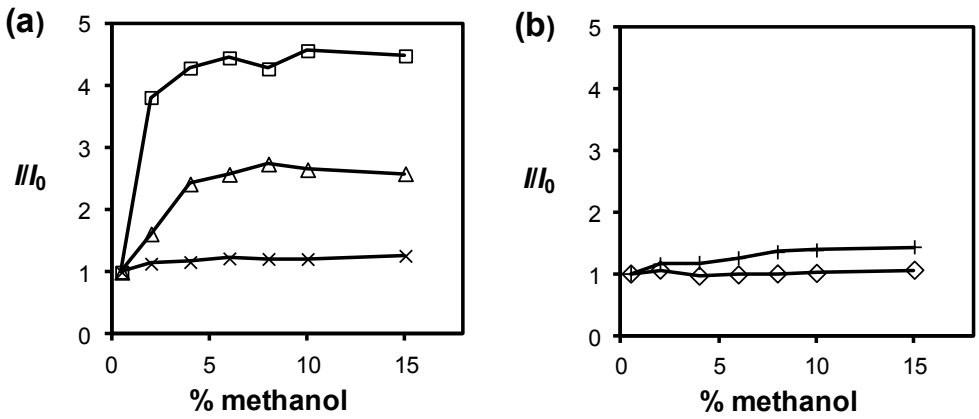

Figure 3. (a) Normalized emission intensity at 397 nm of a 1:1 mixture of **3** and **4** (□), **5** and **4** (△), and **9** and **4** (×) in 2:1 hexane/ethyl acetate with different percentage of methanol. (b) Normalized emission intensity of a 1:1 mixture of **7** and **8** (◇) and **9** and **8** (+) in 2:1 hexane/ethyl acetate with different percentage of methanol. The emission intensity in 0.5% methanol was taken as the I_0. λ_{ex} = 350 nm. [Oligocholate] = 2.0 μM.

Indeed, both the matched pair (**3** and **4**, □) and the mismatched pair (**5** and **4**, △) displayed stronger emission in higher methanol solvents. Thus, aggregation-induced quenching did exist in low methanol solvents. As a control experiment, we studied the quenching of the linear tricholate **9** by the NDI-labeled **4**. Because linear oligocholates can only fold cooperatively with at least five cholate units,[21] trimer **9** cannot adopt the reverse micelle-like conformation with introverted hydrophilic groups. Stacking, thus, should be very difficult, if not impossible, with the 1:1 mixture of **9** and **4**. Consistent with our stacking model, the control pair (×) showed nearly constant pyrene emission over the same solvent change, indicating that the cyclic motif was necessary for the quenching in low methanol solvents and that the change of pyrene emission in the first two mixtures was *not* caused by a generic solvent effect.

Figure 3b shows the same quenching study done with the all-amide-linked macrocycles (**7** and **8**). Likewise, we performed the control experiment with the linear tricholate **9**. In our hands, both

pairs displayed small or negligible changes in fluorescence intensity during the methanol titration. The results were quite surprising to us, as we thought that rigidity of the macrocycles was beneficial to the solvent-induced aggregation.[14a] (We will come back to this point toward the end of the paper.)

Aggregation of Oligocholate Macrocycles in Lipid Membranes. We could not perform solvent titration in membranes as in organic solutions. Instead, we varied the concentration of the oligocholates in the membrane. As demonstrated by our previous study, the oligocholate macrocycles aggregate in membranes only above a critical aggregation concentration (CAC).[14a] Quenching of the pyrene emission, thus, should become significant above the CAC for the pyrene–NDI mixed pairs.

Figure 4a shows the emission intensity of the 1:1 mixture of **3**/**4** (□) and **5**/**4** (△) in 1,2-dilauroyl-*sn*-glycero-3-phosphocholine (DLPC) membranes. The intensity was normalized to that of the same mixture at 10 mol % concentration in the membrane. The 10 mol % concentration is well above the CACs of **1** or **2**,[14a] and should correspond to the fully aggregated form. As expected, both mixtures displayed much higher emission intensity at lower concentrations, suggesting that strong quenching did exist at higher concentrations of the oligocholates in the membrane. Most interestingly, the CAC of the matched pair (**3** and **4**, □, ~0.5 mol %) was noticeably lower than the mismatched pair (**5** and **4**, △, ~1.0 mol %), evident from the earlier inflection point in the quenching curves for the former. The result agreed well with the stronger quenching found for the matched pair in Figure 2a and suggests that the hydrophobic stacking of the oligocholate macrocycles and the pyrene–NDI aromatic interactions did seem to work together (see later sections for further discussion).

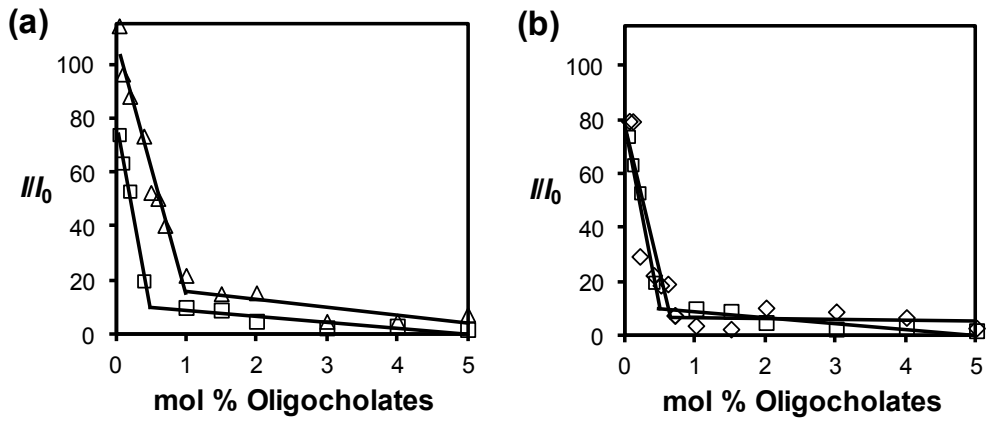

Figure 4. (a) Normalized emission intensity at 398 nm of a 1:1 mixture of **3** and **4** (□) and **5** and **4** (△) as a function of the molar percentage of the total oligocholates in DLPC membranes. (b) Normalized emission intensity at 398 nm of a 1:1 mixture of **3** and **4** (□) and **7** and **8** (◇) as a function of the molar percent of the total oligocholates in DLPC membranes. The data for **3** and **4** (□) were shown in both figures for comparison. The emission intensity with [total oligocholates]/[phospholipids] = 1/10 was taken as the I_0. λ_{ex} = 350 nm. The CACs (in mol % with respect to the phospholipids) were obtained by linear regression of the data points below and above the inflection point in the quenching curves. Because aggregation of two different oligocholate macrocycles involves many different aggregated structures, the CAC is actually the CAC probed by the co-assembly of the NDI- and pyrene-labeled macrocycles. [Oligocholate] = 2.0 μM.

Figure 4b compares the clicked (**3** and **4**,□) and the all-amide pairs (**7** and **8**, ◇), both matched in the length of the tether between the cholate macrocycle and the aromatic side chain. The concentration-dependent aggregation was evident in both cases as shown by the strong emission at lower concentrations and a sharp decrease at ca. 0.5 mol % concentration of the oligocholates. The experiment, however, was not able to distinguish the two types of macrocycles, as both pairs gave similar CACs.

According to the pore-forming mechanism, the aggregation of the macrocyclic oligocholates should occur more easily in more hydrophobic membranes.[14a] We, therefore, performed the similar quenching studies in 1-palmitoyl-2-oleoyl-sn-glycero-3-phosphocholine (POPC) membranes, which were more hydrophobic than the C12 DLPC membranes.[23] Figure 5 shows the normalized emission intensity of the 1:1 mixture of **3**/**4**, **5**/**4**, and **7**/**8** in DLPC (blue) and POPC (red) membranes. One clear trend observed for all three pyrene–NDI pairs was that the emission was stronger in DLPC than in POPC membranes at low concentrations of the oligocholates. Assuming that the difference in pyrene emission intensity was not a generic environmental effect—reasonable given the methanol-insensitive emission of pyrene displayed by **9**/**4** in Figure 3a—the data suggests that significant quenching already existed at low oligocholate concentrations in the POPC membranes. Aggregation thus was indeed easier in the more hydrophobic membranes.

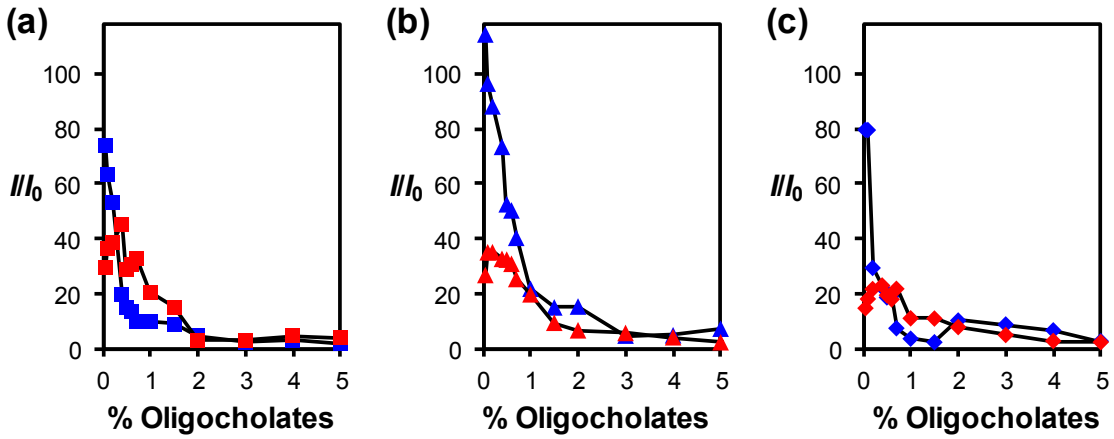

Figure 5. Normalized emission intensity at 398 nm of 1:1 mixture of (a) **3** and **4**, (b) **5** and **4**, and (c) **7** and **8** as a function of [total oligocholates]/[lipid] ratio in POPC/POPG membranes. The blue and red data points were obtained in DLPC and POPC/POPG membranes, respectively. The emission intensity with [total oligocholates]/[phospholipids] = 1/10 was taken as the I_0. λ_{ex} = 350 nm. The large unilamellar vesicles (LUVs) were made by detergent dialysis for the DLPC and POPC/POPG membranes with [total oligocholates] = 2.0 μM. The LUVs ([phospholipids] = 107

μM) were made by membrane extrusion with the cholesterol-containing membranes, due to their incompatibility with the detergent dialysis.[14a]

The hydrophobic aggregation model also predicts that the CACs of the oligocholates should be lower in POPC than in DLPC membranes. The quenching data, nevertheless, did not reveal such a trend. The inflection points of the quenching curves for the POPC membranes in general are difficult to be identified (especially in Figure 5c for the all-amide-linked pair). One complication, as mentioned above, might come from that aggregation already occurred at low concentrations. We believe another complication comes from the different aggregation propensities of the pyrene and NDI groups in the membranes. As will be shown by the glucose leakage assay, the NDI-labeled macrocycles prefer to self-associate instead of aggregating with the pyrene-functionalized macrocycles in lipid membranes (vide infra). Especially in POPC membranes in which the driving force for the aggregation is high, the majority of the NDI-labeled macrocycles (**5** and **8**) should be involved in self-aggregation instead of interacting with the pyrene-functionalized macrocycles. Fluorescent quenching, consequently, only reports a fraction of the entire aggregation process.

Fortunately, pyrene itself could be used as a probe to monitor the aggregation (although no information can be obtained through this method for the NDI-labeled macrocycles). Due to its long fluorescence lifetime, pyrene can form excimers quite readily even at relative low concentrations.[24] Hetero-aggregation is no longer an issue when only one type of cyclic oligocholate exists in the membrane. Figure 6 shows the normalized emission spectra of pyrene-labeled macrocycle **7** in three different lipid membranes. In general, the excimer emission at ca. 470 nm increased relative to that of the monomer at 378 nm with higher concentrations of **7** in the membrane. Aggregation of the macrocycle thus was clearly concentration-induced. In the DLPC membrane, the excimer formation was sluggish until the concentration of **7** reached 10 mol % (Figure 6a). In the more

hydrophobic POPC/POPG membranes, the excimer formed more easily and the emission at 470 nm increased steadily with an increase in the concentration of the macrocycle. The addition of cholesterol enhanced the pyrene excimer even further. Even at the lowest tested concentration (0.02 mol %), significant excimer formation was observed for compound **7** (Figure 6c).

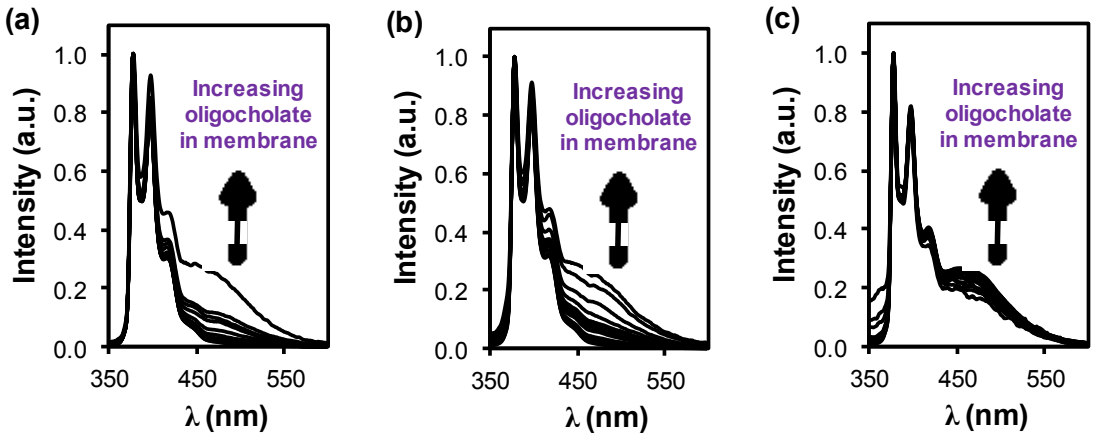

Figure 6. Normalized emission spectrum of **7** in (a) DLPC, (b) POPC/POPG, and (c) POPC/POPG membranes with 30 mol % cholesterol. The molar percentage of **7** in the membrane was from 0.05 to 10% from bottom to top in (a) and (b). The molar percentage of **7** in the membrane was from 0.002 to 10% from bottom to top in (c). λ_{ex} = 350 nm. The large unilamellar vesicles (LUVs) were made by detergent dialysis for the DLPC and POPC/POPG membranes with [oligocholate] = 2.0 μM. The LUVs ([phospholipids] = 107 μM) were made by membrane extrusion with the cholesterol-containing membranes, due to their incompatibility with the detergent dialysis.[14a]

The excimer formation of the clicked macrocycle **3** was studied previously.[14a] Figure 7 compares the excimer/monomer ratio of **3** and **7** as a function of the macrocycle concentration in the membrane. In all three cases, the all-amide-linked **7** showed stronger pyrene excimer than the clicked **3**, as indicated by the former's generally higher excimer/monomer ratio at the same concentration. Although the trend was visible in DLPC and POPC/POPG membranes, it was most clear in the most hydrophobic, cholesterol-containing POPC/POPG membranes. The consistently

high excimer/monomer ratio in **7**, even at low concentrations, suggests that the all-amide-linked oligocholate macrocycle aggregated more easily than the clicked **3** in lipid membranes (Figure 7c).

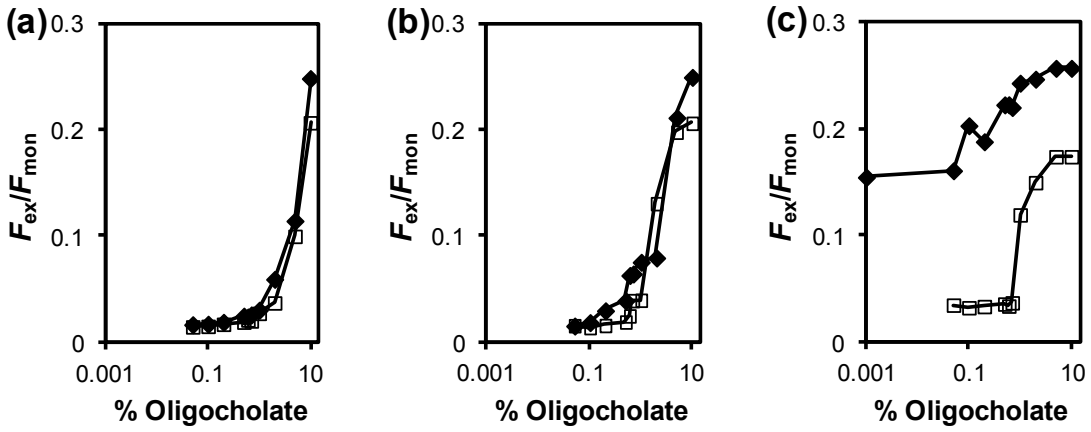

Figure 7. The excimer/monomer ratio (i.e., emission intensity ratio of 470 vs. 378 nm) as a function of [oligocholate]/[lipid] ratio in liposomes made of (a) DLPC, (b) POPC/POPG, and (c) POPC/POPG with 30 mol % cholesterol. The data points shown in filled diamonds (◆) and empty squares (□) are for **3** and **7**, respectively. λ_{ex} = 350 nm. The large unilamellar vesicles (LUVs) were made by detergent dialysis for the DLPC and POPC/POPG membranes with [oligocholate] = 2.0 μM. The LUVs ([phospholipids] = 107 μM) were made by membrane extrusion with the cholesterol-containing membranes, due to their incompatibility with the detergent dialysis.[14a]

Glucose Transport by Aromatically Functionalized Oligocholate Macrocycles. Strong evidence for the stacked nanopores of **1** and **2** was obtained by their transport of sugars across lipid bilayer membranes.[14a] The internal cavity of **1** is triangularly shaped and ca. 1 nm on the side, large enough for glucose to pass through. In the glucose transport assay, a high concentration (300 mM) of glucose was first trapped inside large unilamellar vesicles (LUVs).[25] After the external glucose was removed by gel filtration, hexokinase, glucose-6-phosphate dehydrogenase, NADP, and ATP were added to liposomal solution. In the absence of transporting agents, the glucose stays inside the LUVs and remains intact. If an added reagent causes leakage of the liposomes, the

escaped glucose will be converted by the enzymes to glucose-6-phosphate while NADP reduced to NADPH. Because of the fast enzymatic kinetics, the formation of NADPH at 340 nm normally correlates directly with the rate of glucose efflux.[7a] At the end of the experiments, a nonionic surfactant, Triton X-100, is added to destroy the liposomes and the amount of NADPH formed is used as the reference for 100% leakage.

Figure 8a shows the percent leakage of glucose triggered by the pyrene-labeled clicked macrocycle **3** (△), the NDI-labeled **4** (◇), and a 1:1 mixture of **3** and **4** (□). The total concentration of the oligocholates was kept the same (5 μM) in all the leakage assays. This concentration was able to cause complete leakage of the glucose with the parent cyclic trimer **1**.[14a] As indicated by the leakage data (Figure 8a), however, all three clicked macrocycles were quite incompetent in comparison to the parent macrocycle, with only the NDI-functionalized **4** showing modest activity.

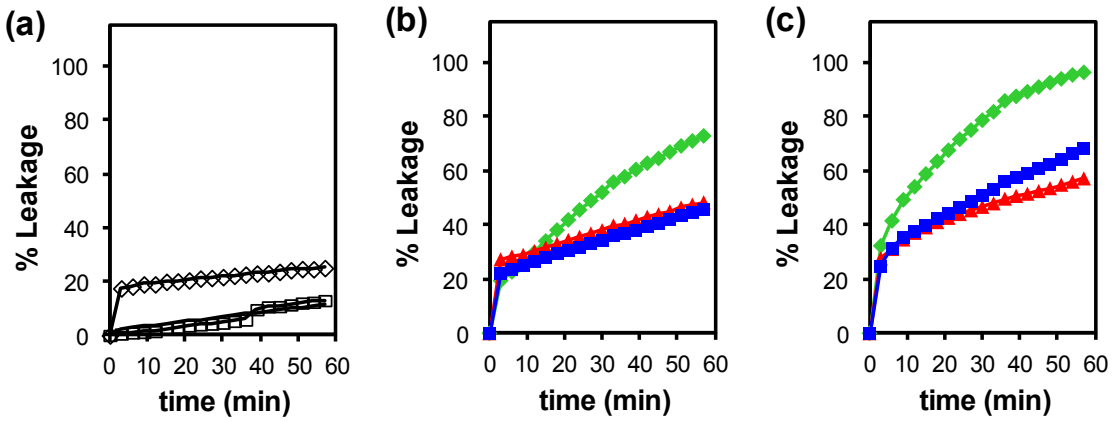

Figure 8. Percent leakage of glucose from (a) POPC/POPG LUVs upon the addition of **3** (△), **4** (◇), and 1:1 mixture of **3** and **4** (□), and from (b) POPC/POPG LUVs and (c) POPC/POPG LUVs with 30% cholesterol upon the addition of **7** (▲), **8** (◆), and 1:1 mixture of **7** and **8** (■). [total

oligocholates] = 5.0 μM. [phospholipids] = 104 μM. The liposomes were lysed at 60 min upon addition of 1% Triton X-100.

The all-amide-linked macrocycles had considerably higher activities than the clicked ones (Figure 8b). The glucose leakage at the end of 60 min reached over 70% with the NDI-functionalized **8**. The NDI-labeled macrocycle was clearly more potent than either the pyrene-functionalized one or the 1:1 mixture, suggesting that the aromatic interactions of the electron-deficient π system were stronger in the membrane than aromatic donor–acceptor interactions.

An important outcome of the hydrophobically driven pore formation for the oligocholate macrocycles was their counterintuitive faster transport of glucose in thicker and more hydrophobic, membranes.[14a] Figure 8c shows the leakage profiles caused by the all-amide-linked macrocycles in POPC/POPG membranes with 30 mol % cholesterol. This level of cholesterol is known to increase the hydrophobic thickness of POPC bilayer from 2.58 to 2.99 nm[26] and decrease its fluidity.[27] Cholesterol-containing bilayers have been shown to be much less permeable to hydrophilic molecules, including glucose.[28] Cholesterol incorporation, however, increased the driving force for the hydrophobic stacking interactions of the oligocholate macrocycles and was found to *accelerate* the glucose leakage induced by **1** and **2**.[14a] The effect was once again observed for the amide-linked macrocyclic oligocholates (compare Figures 8b and 8c). In corroboration with the cholesterol-enhanced pyrene excimer-formation (Figure 6c), the leakage data strongly suggest that the same pore-forming mechanism was involved in these experiments.

Environmental Effects on the Intermolecular Interactions of the Oligocholate Macrocycles. The obvious "inconsistency" so far is between the quenching data in solution (Figure 3) and the pyrene excimer/leakage data in lipid membranes (Figures 7 and 8). The former

suggests that the clicked macrocycles aggregate more strongly than the all-amide-linked ones in mixed organic solvents, whereas the latter indicates the opposite in lipid membranes.

The solvophobic interactions in the oligocholates derive from the need for the introverted hydrophilic groups to be solvated by polar solvent, as well as the tendency of the polar solvent to avoid contact with the nonpolar environment (Figure 2).[14a,19] This model predicts that the solvophobic interactions are the strongest when the polar/nonpolar solvents are least miscible and the polar solvent has a large cohesive energy density (i.e., total intermolecular interactions per unit volume).

The lipid membrane is ideal for the solvophobically driven aggregation.[14a] Water and the lipid hydrocarbon are completely immiscible, meaning that placing water inside the oligocholate macrocycles does not bear the cost of "de-mixing" the polar solvent such as methanol from the nonpolar hexane/ethyl acetate. Water has a much higher cohesive energy density than methanol (2294 vs. 858 MPa),[29] meaning that the tendency for the "activated" water molecules inside the macrocycles to aggregate in membranes is much stronger than that for the methanol in mixed organic solvent. The concentration of the oligocholates in the membrane (i.e., up to 5 mol % with respect to the phospholipids) was much higher than that used in the fluorescence quenching experiments (i.e., 2.0 μM), making aggregation of the oligocholates much easier in the membranes than in the mixed organic solvents.

Both the pyrene-excimer formation and the glucose leakage assay indicate that the all-amide-linked macrocycles were better at stacking than the clicked ones. The results are reasonable considering that the proposed hydrophobic stacking needs the reverse micelle-like configuration of the macrocycles with introverted polar groups. The clicked macrocycles are larger than the amide-linked ones and also have more rotatable bonds—both factors make it easier for the cholate

to twist and turn the introverted hydroxyl groups outward. Such motion not only reduces the solvophobic driving force of the stacking but also makes the interior of the nanopore less hydrophilic even if the pore is formed. Glucose leakage is expected to be difficult and was indeed observed with the clicked macrocycles (Figure 8a).

What then is the reason for the enhanced quenching found for the clicked macrocycles in mixed organic solvents (Figure 3a)? A strong possibility is that the quenching of the pyrene-labeled macrocycle **3** by the NDI-labeled **4** in 0.5% methanol was caused not by the solvophobic stacking of the macrocycles but by the cholate units rotating outward and hydrogen-bonding with one another intermolecularly. Such hydrogen-bonded interactions are more likely for the more flexible clicked macrocycles and should be the strongest in the least methanol-containing solvents. Essentially, two different but related mechanisms were operating in solution and in the lipid membrane, respectively. In solution and only in low methanol (0.5%) solutions, the hydrogen-bond-assisted aggregation occurred with the clicked, flexible oligocholate macrocycles (**3**–**5**). The polar solvent-induced solvophobic stacking of the macrocycles was probably not strong enough to operate in the mixed organic solvents, due to low concentrations of the macrocycles, good miscibility of methanol/ethyl acetate/hexane, and the low cohesive energy density of methanol.

Conclusions

This study yielded additional insight into the hydrophobic stacking of the oligocholate macrocycles in lipid membranes. Mechanistically, the aggregation of the amphiphilic macrocycles is similar to the formation or reverse micelles by a head/tail surfactant in nonpolar solvents in the presence of a small amount of water.[30] Both the stacking of the macrocycles and the aggregation of surfactants to form reverse micelles are driven by the same solvophobic interactions—i.e., the tendency of the polar groups to avoid contact with the bulk, nonpolar solvent and the strong

preference of water molecules to associate with water instead of the nonpolar solvent. The different self-assembled structures (i.e., water-filled nanopores vs. spherical, water-filled reverse micelles) simply result from the different topologies of the amphiphiles.

The effectiveness of the NDI group in lipid membranes is noteworthy. The aromatic donor–acceptor interactions between an NDI and a 1,5-dialkoxynaphthalene derivative were found to be 1–2 orders of magnitude stronger than the acceptor–acceptor interactions in several *polar* solvents.[31] Our leakage data, however, clearly shows that the acceptor–acceptor interactions were more effective at promoting the stacking of the oligocholate macrocycles. Our current explanation for the result was based on the solvation of the NDI group in *nonpolar* environments. In our experience, compounds with the NDI group tend to have much poorer solubility than pyrene derivatives in common organic solvents including hydrocarbons. The poor solubility probably comes from the strong intermolecular interactions of the NDI groups *and* its poor solvation by common organic solvents. When the NDI-functionalized oligocholates enter the lipid membrane, the poor solubility of the NDI group in hydrocarbons translates to a stronger tendency to aggregate in lipid hydrocarbon and was clearly beneficial to the transport ability of macrocycle **8**.

Experimental Section.

The syntheses of compound **3**,[14a] **6**,[14a] **9**,[32] **10**,[21] **11**,[19c] **12**,[14a] **16**,[14a]**17**,[32] and **18**[32] were previously reported. The preparation of LUVs,[32] the procedures for the leakage assays,[32] and the incorporation of oligocholates into liposomes by detergent dialysis and direct addition to preformed LUVs[14a] were reported previously.

General Methods. For spectroscopic purposes, methanol, hexanes, and ethyl acetate were of HPLC grade. All other reagents and solvents were of ACS-certified grade or higher and were used as received from commercial suppliers.

Compound 4. The amine derivative[14a] of compound **6** (50 mg, 0.037 mmol), compound **17** (56 mg, 0.108 mmol), and diisopropylethylamine (DIPEA, 32 μL, 0.184 mmol) were dissolved in anhydrous DMF (0.2 mL). The mixture was stirred at 50 °C overnight and poured into dilute HCl aqueous solution (0.05 M, 50 mL). The precipitate was collected by suction filtration and purified by preparative TLC using 9:1 $CHCl_3/CH_3OH$ as the developing solvent to afford a light brown powder (36 mg, 50%). ^{1}H NMR (400 MHz, $CDCl_3/CD_3OD$ = 1:1, δ): 8.68 (s, 4H), 7.75 (m, 1H), 7.43 (m, 1H), 4.30 (m, 3H), 4.14 (br, 5H), 3.86 (br, 3H), 3.72 (br, 2H), 3.39 (m, 2H), 3.08 (br, 2H), 2.70 (q, 1H), 2.38−1.0 (a series of m), 0.61 (s, 1H). ^{13}C NMR (100 MHz, $CDCl_3/CD_3OD$ = 1:1, δ): 175.3, 174.9, 174.5, 171.9, 164.5, 144.5, 131.0, 127.3, 125.9, 125.1, 125.0, 124.9, 124.8, 124.7, 123.3, 120.7, 72.9, 68.0, 61.5, 53.5, 49.6, 46.4, 45.7, 42.2, 39.5, 36.7, 35.7, 34.6,32.7, 31.8, 29.6,27.5, 27.1, 26.6, 25.9, 23.1, 22.3, 17.0, 12.2. ESI-HRMS (m/z): $[M + Na]^+$ calcd for $C_{102}H_{148}N_{10}NaO_{15}$ 1776.1018, found 1776.1008.

Compound 5. The amine derivative[14a] of compound **6** (92 mg, 0.067 mmol), compound **16** (58 mg, 0.169 mmol), and DIPEA (59 μL, 0.337 mmol) were dissolved in anhydrous DMF (0.3 mL). The mixture was allowed to react in a microwave reactor at 100 °C for 30 min and poured into dilute HCl aqueous solution (0.05 M, 50 mL). The precipitate was collected by suction filtration and purified by preparative TLC using 9:1 $CHCl_3/CH_3OH$ as the developing solvent to afford anoff-white powder (50 mg, 45%). ^{1}H NMR (400 MHz, $CDCl_3/CD_3OD$ = 1:1, δ): 8.60 (br, 1H), 8.42 (br, 1H), 8.26−7.99 (9H), 4.48 (br, 3H), 4.35 (br, 1H), 3.92 (br, 3H), 3.76 (br, 3H), 3.58 (br, 3H), 3.51 (br, 1H), 2.85 (br, 1H), 2.38−1.0 (a series of m), 0.88 (s, 9H), 0.67 (d, 9H). ^{13}C NMR

(100 MHz, $CDCl_3/CD_3OD$ = 1:1, δ): 175.2, 174.8, 173.7, 171.7, 162.8, 144.7, 130.5, 126.8,120.8, 73.1, 67.9, 61.6, 56.7, 53.3, 46.5, 39.7, 34.7, 31.9, 29.4, 26.5, 23.3, 20.4, 16.7, 13.4, 11.9. ESI-HRMS (m/z): $[M + H]^+$ calcd for $C_{97}H_{139}N_8O_{11}$ 1592.0558, found 1592.0570.

Compound 13. Compound **12** (230 mg, 0.156 mmol) and triphenylphosphine (73.7 mg, 0.281 mmol) were dissolved in MeOH (2 mL). The reaction mixture was heated to reflux for overnight. The solvent was removed by rotary evaporation. The residue was purified by column chromatography over silica gel with 15:1 CH_2Cl_2 /CH_3OH and then with 6:1:0.1 $CH_2Cl_2/CH_3OH/Et_3N$ (6/1/0.1) as the eluents to afford an off-white powder (103 mg, 46%). ^1H NMR (400 MHz, $CD_3OD/CDCl_3$ = 1:1, δ): 7.28 (br, 5H), 5.04 (br, 2H), 4.25 (br,1H), 3.93 (br, 3H), 3.78 (br, 3H) 3.62 (s, 3H), 3.49 (br, 2H), 3.13(m, 2H), 2.38−1.0 (a series of m), 0.88(s, 9H), 0.64 (d, 9H). ^{13}C NMR (100 MHz, $CDCl_3/CD_3OD$ = 1:1, δ): 175.6, 175.2, 174.5, 171.8, 157.6, 136.9, 128.5, 128.0, 127.8, 73.0, 68.1, 66.6, 61.6, 53.2, 50.7, 48.8, 46.5, 42.8, 41.8, 39.5, 36.3, 35.4, 35.0, 33.6, 32.8, 31.8, 31.1, 29.9, 28.4, 27.7, 26.6, 23.3, 22.5, 18.2, 17.0, 12.6. ESI-HRMS (m/z): $[M + H]^+$ calcd for $C_{86}H_{138}N_5O_{13}$ 1449.0286, found 1449.0273.

Compound 14. Hydrolyzed compound **13** (50 mg, 0.034 mmol), BOP (75 mg, 0.169 mmol), and HOBT (23 mg, 0.169 mmol) were dissolved in DMF (30 mL), and DIPEA (60 μL, 0.34 mmol) was added. The mixture was allowed to react in a microwave reactor at 100 °C for 1 h and poured into dilute HCl aqueous solution (0.05 M, 50 mL). The precipitate formed was collected by suction filtration, washed with water, dried in air, and purified by column chromatography over silica gel with 10:1 CH_2Cl_2/CH_3OH as the eluent to afford an ivory powder (47 mg, 98%). ^1H NMR (300 MHz, CD_3OD, δ): 7.30 (br, 5H), 5.04 (br, 2H), 4.14 (br,1H), 3.92 (br, 3H), 3.78 (br, 3H), 3.48 (br, 2H), 3.13 (m, 3H), 2.38−1.0 (a series of m), 0.88(s, 9H), 0.67 (d, 9H). ^{13}C NMR (100 MHz, $CDCl_3/CD_3OD$ = 1:1, δ): 176.7, 175.2, 174.9, 172.3, 158.2, 136.9, 128.5, 128.0, 127.8, 73.0, 68.1,

66.6, 61.6, 53.2, 50.7, 48.8, 46.5, 42.8, 41.8, 39.5, 36.3, 35.4, 35.0, 33.6, 32.8, 31.8, 31.1, 29.9, 28.4, 27.7, 26.6, 23.3, 22.2, 19.1, 16.8, 12.8. ESI-HRMS (m/z): $[M + Na]^+$ calcd for $C_{85}H_{133}N_5O_{12}Na$ 1438.9843, found 1438.9833.

Compound 15. Pd/C (240 mg, 10 wt %) was added to a solution of **5** (236 mg, 0.167 mmol) in CH_3OH (20 mL). The mixture was stirred under a H_2 balloon at room temperature for 3 d. Pd/C was removed by filtration through a pad of Celite, and the solvent was removed by rotary evaporation to afford a white power (150 mg, 80%). ^{1}H NMR (300 MHz, CD_3OD, δ): 4.23 (br,1H), 3.93 (br, 3H), 3.78 (br, 3H), 3.47 (br, 3H), 2.74−0.98 (a series of m), 0.89 (s, 9H), 0.67 (d, 9H). ^{13}C NMR (100 MHz, $CDCl_3/CD_3OD$ = 1:1, δ): 176.8, 175.4, 175.1, 172.6, 158.5, 136.9, 73.0, 68.1, 66.6, 53.2, 50.7, 48.8, 46.5, 42.8, 41.8, 39.5, 36.3, 35.4, 35.0, 33.6, 32.8, 31.8, 31.1, 29.9, 28.4, 27.7, 26.6, 23.3, 22.2, 19.3, 16.6, 12.4. ESI-HRMS (m/z): $[M+H]^+$ calcd for $C_{77}H_{128}N_5O_{10}$ 1282.9656, found 1282.9645.

Compound 7. Compound **15** (80 mg, 0.062 mmol), compound **16** (72 mg, 0.187 mmol), and DIPEA (109 μL, 0.624 mmol) were dissolved in anhydrous DMF (0.2 mL). The mixture was stirred at 60 °C overnight and poured into a dilute HCl aqueous solution (0.05 M, 30 mL). The precipitate was collected by suction filtration and purified by preparative TLC using 9:1 $CHCl_3/CH_3OH$ as the developing solvent to afford an off-white powder (40 mg, 42%). ^{1}H NMR (400 MHz, $CDCl_3/CD_3OD$ = 1:1, δ): 8.30 (m, 2H), 8.09 (m, 4H), 7.98 (m, 2H), 7.84 (m, 1H), 4.21(m, 1H), 3.90 (br, 3H), 3.77 (br, 3H), 3.59 (q, 2H), 3.50 (br, 3H), 2.92 (m, 2H), 2.46 (br, 2H), 2.38−1.0 (a series of m), 0.58 (m, 7 H), 0.44 (s, 2H). ^{13}C NMR (100 MHz, $CDCl_3$/ CD_3OD = 1:1, δ): 175.3, 174.9, 174.5, 171.9,144.5, 136.0, 127.3, 125.9, 125.1,125.0,124.9,124.8, 124.7, 123.3, 120.7, 72.9, 68.0, 61.5, 53.5, 49.6, 46.4, 45.7, 42.2, 39.5, 36.7, 35.7, 34.6,32.7, 31.8, 29.6,27.5, 27.1, 26.6, 25.9, 23.1, 22.3, 17.0, 12.2. ESI-HRMS (m/z): $[M +H]^+$ calcd for $C_{97}H_{142}N_5O_{11}$

1553.0700, found 1553.0687.

Compound 8. Compound **15** (55 mg, 0.043 mmol), compound **17** (65 mg, 0.129 mmol), and DIPEA (37 μL, 0.215 mmol) were dissolved in anhydrous DMF (0.2 mL). The mixture was stirred at 60 °C overnight and poured into a dilute HCl aqueous solution (0.05 M, 30 mL). The precipitate was collected by suction filtration and purified by preparative TLC using 9:1 $CHCl_3/CH_3OH$ as the developing solvent to afford an off-white powder (52 mg, 72%). ^{1}H NMR (400 MHz, $CDCl_3/CD_3OD$ = 1:1, δ): 8.73 (s, 4H), 4.24(m, 4H), 3.94 (br, 3H), 3.79 (br, 3H), 3.52 (q, 2H), 3.17 (br, 3H), 2.45−0.73 (a series of m), 0.66 (m, 9 H). ^{13}C NMR (100 MHz, $CDCl_3/CD_3OD$ = 1:1, δ): 177.6, 176.2, 175.2, 163.7, 131.6, 127.3, 73.6, 68.5, 62.6, 52.8, 47.9, 46.7, 42.7, 39.9, 36.9, 36.0, 35.2, 32.4, 31.6, 28.6, 28.4, 27.3, 23.2, 17.7, 14.3, 12.9. ESI-HRMS (m/z): $[M + H_3O]^+$ calcd for $C_{99}H_{148}N_7O_{16}$, 1692.1016 found, 1692.0574.

Fluorescence Titrations. Stock solutions (5×10^{-4} M) of the appropriate oligocholate pyrene−NDI pairs in anhydrous THF were prepared. An aliquot (8.0 μL) of the stock solution was added to 2.00 mL mL of hexane/ethyl acetate (v/v = 2/1) containing varying amounts of methanol (0.5−15%) in a quartz cuvette. The sample was gently vortexed for 30 s after each addition before the fluorescence spectrum was recorded. The excitation wavelength was 350 nm.

Acknowledgment is made to NSF (DMR-1005515) for supporting the research.

Supporting Information Available: NMR data for the key compounds. This material is available free of charge via the Internet at http://pubs.acs.org.

References

(1) (a) Stein, W. D. *Carriers and Pumps: An Introduction to Membrane Transport*; Academic Press: San Diego, CA, 1990. (b) Gokel, G. W.; Carasel, I. A. *Chem. Soc. Rev.* **2007**, *36*, 378-

389. (c) Fyles, T. M. *Chem. Soc. Rev.* **2007**, *36*, 335-347. (d) McNally, B. A.; Leevy, W. M.; Smith, B. D. *Supramol. Chem.* **2007**, *19*, 29-37. (e) Davis, J. T.; Okunola, O.; Quesada, R. *Chem. Soc. Rev.* **2010**, *39*, 3843-3862.

(2) Litvinchuk, S.; Sorde, N.; Matile, S. *J. Am. Chem. Soc.* **2005**, *127*, 9316-9317.

(3) Sakai, N.; Sorde, N.; Matile, S. *J. Am. Chem. Soc.* **2003**, *125*, 7776-7777.

(4) (a) Matile, S.; Som, A.; Sorde, N. *Tetrahedron* **2004**, *60*, 6405-6435. (b) Sisson, A. L.; Shah, M. R.; Bhosale, S.; Matile, S. *Chem. Soc. Rev.* **2006**, *35*, 1269-1286.

(5) (a) Gokel, G. W.; Mukhopadhyay, A. *Chem. Soc. Rev.* **2001**, *30*, 274-286. (b) Koert, U.; Al-Momani, L.; Pfeifer, J. R. *Synthesis* **2004**, 1129-1146. (c) Gokel, G. W.; Murillo, O. *Acc. Chem. Res.* **1996**, *29*, 425-432. (d) Jung, M.; Kim, H.; Baek, K.; Kim, K. *Angew. Chem. Int. Ed.* **2008**, *47*, 5755-5757. (e) Li, X.; Shen, B.; Yao, X. Q.; Yang, D. *J. Am. Chem. Soc.* **2009**, *131*, 13676-13680.

(6) Som, A.; Matile, S. *Chem. Biodiv.* **2005**, *2*, 717-729.

(7) (a) Granja, J. R.; Ghadiri, M. R. *J. Am. Chem. Soc.* **1994**, *116*, 10785-10786. (b) Sanchez-Quesada, J.; Kim, H. S.; Ghadiri, M. R. *Angew. Chem. Int. Ed.* **2001**, *40*, 2503-2506.

(8) (a) Sakai, N.; Mareda, J.; Matile, S. *Acc. Chem. Res.* **2005**, *38*, 79-87. (b) Das, G.; Talukdar, P.; Matile, S. *Science* **2002**, *298*, 1600-1602.

(9) Bhosale, S.; Sisson, A. L.; Talukdar, P.; Furstenberg, A.; Banerji, N.; Vauthey, E.; Bollot, G.; Mareda, J.; Roger, C.; Wurthner, F.; Sakai, N.; Matile, S. *Science* **2006**, *313*, 84-86.

(10) Satake, A.; Yamamura, M.; Oda, M.; Kobuke, Y. *J. Am. Chem. Soc.* **2008**, *130*, 6314-6315.

(11) Helsel, A. J.; Brown, A. L.; Yamato, K.; Feng, W.; Yuan, L. H.; Clements, A. J.; Harding, S. V.; Szabo, G.; Shao, Z. F.; Gong, B. *J. Am. Chem. Soc.* **2008**, *130*, 15784-15785.

(12) Fyles, T. M.; Tong, C. C. *New. J. Chem.* **2007**, *31*, 655-661.

(13) Ma, L.; Melegari, M.; Colombini, M.; Davis, J. T. *J. Am. Chem. Soc.* **2008**, *130*, 2938-2939.

(14) (a) Cho, H.; Widanapathirana, L.; Zhao, Y. *J. Am. Chem. Soc.* **2011**, *133*, 141-147. (b) Cho, H.; Zhao, Y. *Langmuir* **2011**, *27*, 4936-4944.

(15) Dunitz, J. D. *Science* **1994**, *264*, 670.

(16) (a) Hunter, C. A.; Lawson, K. R.; Perkins, J.; Urch, C. J. *J. Chem. Soc. Perkin Trans. 2* **2001**, 651-669. (b) Waters, M. L. *Curr. Opin. Chem. Biol.* **2002**, *6*, 736-741.

(17) (a) Philp, D.; Stoddart, J. F. *Angew. Chem. Int. Ed. Engl.* **1996**, *35*, 1154-1196. (b) Scott Lokey, R.; Iverson, B. L. *Nature* **1995**, *375*, 303-305. (c) Gabriel, G. J.; Sorey, S.; Iverson, B. L. *J. Am. Chem. Soc.* **2005**, *127*, 2637-2640. (d) Nelson, J. C.; Saven, J. G.; Moore, J. S.; Wolynes, P. G. *Science* **1997**, *277*, 1793-1796. (e) Stone, M. T.; Heemstra, J. M.; Moore, J. S. *Acc. Chem. Res.* **2006**, *39*, 11-20. (f) Huc, I. *Eur. J. Org. Chem.* **2004**, 17-29.

(18) For other related cyclic cholate derivatives, see: (a) Brady, P. A.; Bonar-Law, R. P.; Rowan, S. J.; Suckling, C. J.; Sanders, J. K. M. *Chem. Commun.* **1996**, 319-320. (b) Davis, A. P.; Walsh, J. J. *Chem. Commun.* **1996**, 449-451. (c) Whitmarsh, S. D.; Redmond, A. P.; Sgarlata, V.; Davis, A. P. *Chem. Commun.* **2008**, 3669-3671. (d) Ghosh, S.; Choudhury, A. R.; Row, T. N. G.; Maitra, U. *Org. Lett.* **2005**, *7*, 1441-1444. (e) Albert, D.; Feigel, M.; Benet-Buchholz, J.; Boese, R. *Angew. Chem. Int. Ed.* **1998**, *37*, 2727-2729. (f) Feigel, M.; Ladberg, R.; Winter, M.; Blaser, D.; Boese, R. *Eur. J. Org. Chem.* **2006**, 371-377.

(19) (a) Zhao, Y.; Zhong, Z.; Ryu, E.-H. *J. Am. Chem. Soc.* **2007**, *129*, 218-225. (b) Cho, H.; Zhong, Z.; Zhao, Y. *Tetrahedron* **2009**, *65*, 7311-7316. (c) Cho, H.; Zhao, Y. *J. Am. Chem. Soc.* **2010**, *132*, 9890-9899. (d) Zhong, Z.; Li, X.; Zhao, Y. *J. Am. Chem. Soc.* **2011**, *133*, 8862-8865.

(20) Rostovtsev, V. V.; Green, L. G.; Fokin, V. V.; Sharpless, K. B. *Angew. Chem. Int. Ed.* **2002**, *41*, 2596-2599.

(21) Zhao, Y.; Zhong, Z. *J. Am. Chem. Soc.* **2005**, *127*, 17894-17901.

(22) Normalization allowes us to compare the different pyrene-labeled oligocholates more accurately. These compounds have different structures and thus potentially different solvent shells around the fluorophore in the mixed polar/nonpolar solvents. Because fluoresence is often sensitive to the solvent composition around the fluorophore, the different pyrene-labelled oligocholates may not be comparable directly.

(23) Lande, M. B.; Donovan, J. M.; Zeidel, M. L. *J. Gen. Physiol.* **1995**, *106*, 67-84.

(24) Birks, J. B.; Munro, I. H.; Dyson, D. J. *Proc. R. Soc. London Ser. A* **1963**, *275*, 575-588.

(25) Kinsky, S. C.; Haxby, J. A.; Zopf, D. A.; Alving, C. R.; Kinsky, C. B. *Biochemistry-Us* **1969**, *8*, 4149-&.

(26) Nezil, F. A.; Bloom, M. *Biophys. J.* **1992**, *61*, 1176-1183.

(27) Holthuis, J. C. M.; van Meer, G.; Huitema, K. *Mol. Membr. Biol.* **2003**, *20*, 231-241.

(28) (a) Demel, R. A.; Bruckdor.Kr; Vandeene.Ll *Biochim. Biophys. Acta* **1972**, *255*, 321-330. (b) Papahadjopoulos, D.; Nir, S.; Ohki, S. *Biochim. Biophys. Acta* **1972**, *266*, 561-583.

(29) Reichardt, C. In *Solvents and solvent effects in organic chemistry*; 3rd ed.; Wiley-VCH: Weinheim, 2003; p 63.

(30) Pileni, M. P. *Structure and Reactivity in Reverse Micelles*; Elsevier: Amsterdam, 1989.

(31) Cubberley, M. S.; Iverson, B. L. *J. Am. Chem. Soc.* **2001**, *123*, 7560-7563.

(32) Zhang, S.; Zhao, Y. *Chem. -Eur. J.* **2011**, *17*, 12444-12451.

CHAPTER 4. HYDROGEN BOND-ASSISTED MACROCYCLIC OLIGOCHOLATE TRANSPORTERS IN LIPID MEMBRANES

A paper published in *Organic & Biomolecular Chemistry* **2012**, *10*, 5077-5083.

(Reproduced by permission of The Royal Society of Chemistry)

Lakmini Widanapathirana, Xueshu Li and Yan Zhao

Abstract

Three macrocyclic oligocholates containing a carboxyl group, a guanidinium ion, and a Cbz-protected amine, respectively, was studied as membrane transporters for hydrophilic molecules. To permeate glucose across lipid bilayers, the macrocycles stacked over one another to form a transmembrane nanopore, driven by a strong tendency of the water molecules in the internal cavities of the amphiphilic macrocycles to aggregate in a nonpolar environment. To transport larger guests such as carboxyfluorescein (CF), the macrocycles acted as carriers to shuttle the guest across the membrane. Hydrogen-bonds among the side chains of the macrocycles strongly affected the transport properties. Surprisingly, the carboxyl group turned out far more effective at assisting the aggregation of the oligocholate macrocycles in the membrane than the much stronger carboxylate–guanidinium salt bridge, likely due to competition from the phosphate groups of the lipids for the guanidinium.

Introduction

Controlled passage of molecules and ions through protein-based pores and channels is a main method for cells to regulate the traffic across their membranes. The process, taking place both on the plasma membrane that separates the cell from its environment and on the membranes of many organelles within the cell, is vital to many biofunctions.[1] Although developing a detailed understanding of membrane transport is essential to biology, structural characterization of transport proteins is difficult. The challenge comes not only from the difficulty in crystallizing membrane proteins. Many pore-formation mechanisms operate with certain lipid compositions and/or in the presence of other membrane proteins. Static characterization techniques under idealized experimental conditions could easily miss the working structures that exist under the biological settings.

Chemists can contribute to this effort by synthesizing simpler and yet functional transmembrane channels and pores.[2] Synthetic transmembrane pores with an inner diameter of 1 nm or larger, in particular, have attracted much attention in recent years.[3] Knowledge gained through such studies can help us understand biological pore formation, as similar covalent and noncovalent forces are often involved in both types of nanopores. More importantly, synthetic pore-forming materials may have a number of practical applications including sensing,[4] drug delivery,[2] DNA sequencing,[5] and catalysis.[6]

Unlike ion channels constructed frequently from crown ethers and other open chain, flexible structures,[2,7] pore-forming materials need to have significant rigidity to withstand the external membrane pressure to keep the internal pore from collapsing.[8] Despite the significant effort devoted to synthetic nanopores, limited designs are available currently. One of the earliest such

examples was reported by Ghadiri, who assembled cyclic D/L-peptides into peptide nanotubes.[9] Matile and coworkers developed an extremely versatile class of β-barrel pores from oligo(phenylene) derivatives[6,10] and applied them to artificial photosynthesis[11] and catalysis.[6] Other reported examples include the porphyrin-based nanopores by Satake and Kobuke,[12] the π-stacked aromatic heterocycles by Gong *et al.*,[13] Fyles's metal-coordinated nanopores,[14] and the guanosine quartet-based giant ion channels by Davis *et al.*[15]

Two of the most prevalent interactions in synthetic nanopores are hydrogen bonds[3] and metal–ligand complexation.[12,14] We recently reported amphiphilic macrocyclic oligocholates (**1**–**3**) that formed nanopores through *hydrophobic interactions*, a noncovalent force normally expected to operate in water instead of in a hydrophobic environment.[16] Being overall hydrophobic, these macrocycles prefer lipid membranes instead of water. Once entering the membrane, however, they need to solvate their introverted hydrophilic groups by water instead of the lipid hydrocarbon.

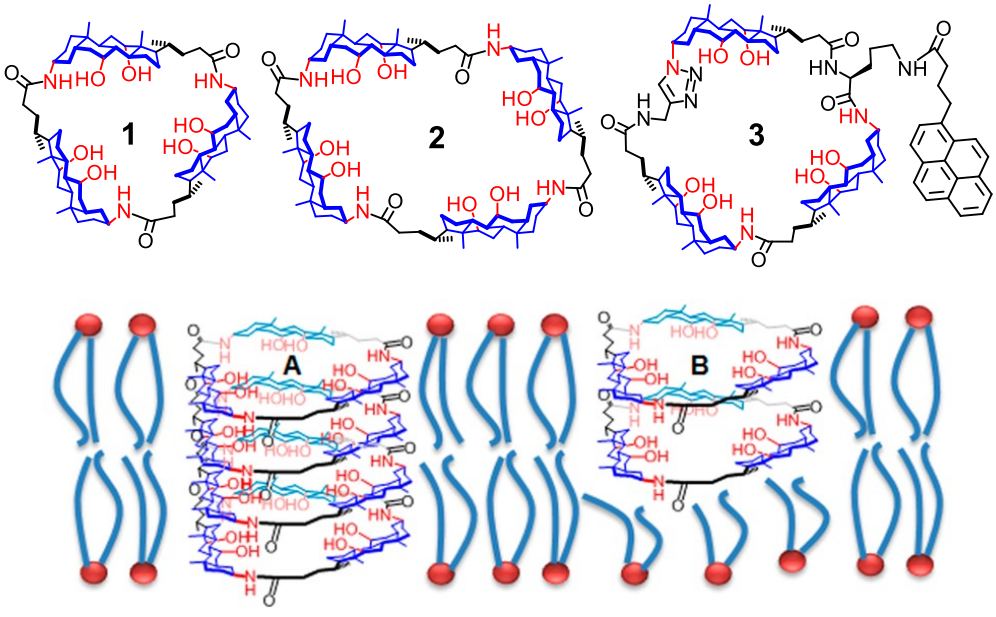

Figure 1. Schematic representation of two ways of aggregation for oligocholate **1** in a lipid bilayer

membrane.

The dilemma is solved when the macrocycles stack over one another to form a transmembrane pore, enabling the water molecules in the interior to interact with one another, solvate the polar groups of the cholates, and still be able to exchange with the bulk water (Fig. 1). The driving force for the stacking is essentially the hydrophobic interactions among the internal, "activated" water molecules that prefer to aggregate instead of facing the lipid hydrocarbon. The exchange of these water molecules with the bulk water could also be important, as the entropic cost for trapping a single water molecule can be as high as 2 kcal mol^{-1} under certain conditions.[17]

To regulate the traffic across the membrane, the nanopore should be tunable, preferably through noncovalent interactions. This paper reports our initial effort toward this goal and aims to control the pore formation through hydrogen-bonds introduced on the side chains of several functionalized cholate macrocycles. A surprising discovery was that the carboxyl group was far more effective than the carboxylate–guanidinium salt bridge in the lipid membrane—the latter is known to have exceptional strength in typical nonpolar environments.[18] The trend was also maintained whether the functionalized oligocholate macrocycles operated through the pore-forming or carrier-based mechanism.

Results and discussion.

Our previous study revealed that it took four molecules of the cholate macrocycles to form the transmembrane pore in POPC/ POPG bilayers (Fig. 1, A).[16a] The molecularity results from the matching between the hydrophobic thickness of the membrane and the stacked macrocycle. Other evidence for the hydrophobically driven pore formation includes the correlation between the

rigidity of the macrocycle and the transport of glucose, the inactivity of the linear tricholate, the unusual increase in the transport rate of glucose with an increase of membrane hydrophobicity, and the counterintuitive faster translocation of maltotriose over glucose. Moreover, when an analogous "clicked" tricholate (**3**) was incorporated into lipid bilayers, the formation of pyrene excimer scaled with the thickness and hydrophobicity of the membrane, providing spectroscopic evidence for the pore formation.

In this paper, we synthesized oligocholates **4**–**6**, which are identical to **3** in the macrocyclic structure but different in the side chain.

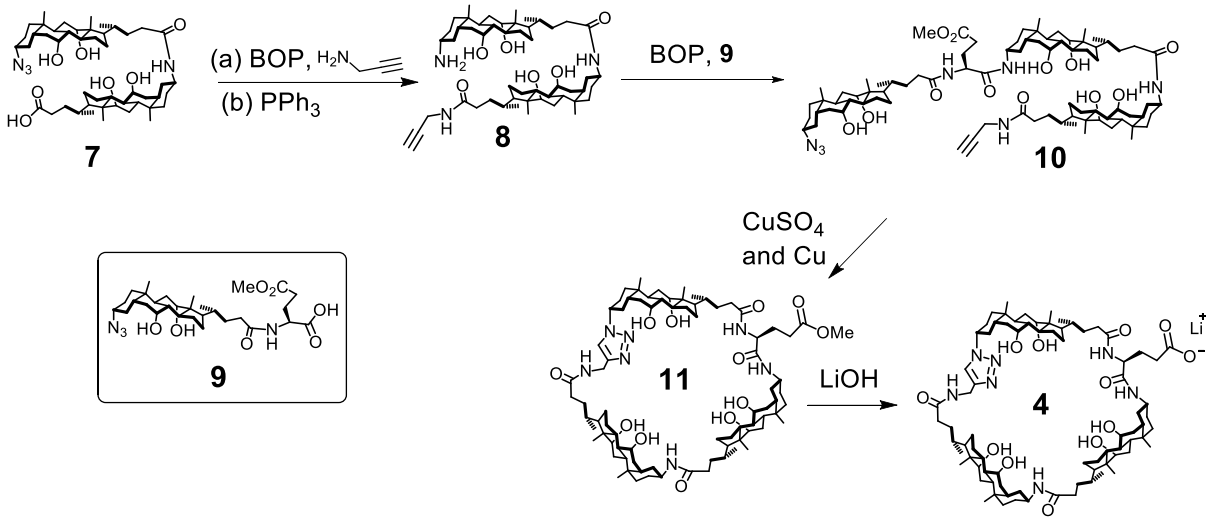

Scheme 1. Synthesis of macrocycle **4**.

Two considerations went into the design of the molecules. First, the iterative synthesis of our oligocholates always leaves behind an azide and an ester at the two chain ends, respectively.[19] The most efficient way to synthesize an oligocholate macrocycle, therefore, is to hydrolyze the ester, couple it to an alkyne-terminated amine (*e.g.*, propargyl amine), and cyclize through the highly efficient click reaction.[20] Second, since the pore formation of the macrocycles occurs in a nonpolar environment, other noncovalent forces such as hydrogen-bonds should have sufficient strength to

be useful. If the pore formation can be tuned by noncovalent interactions introduced through the side chain of the macrocycle, we should have a rational way to control the traffic across the lipid membrane.

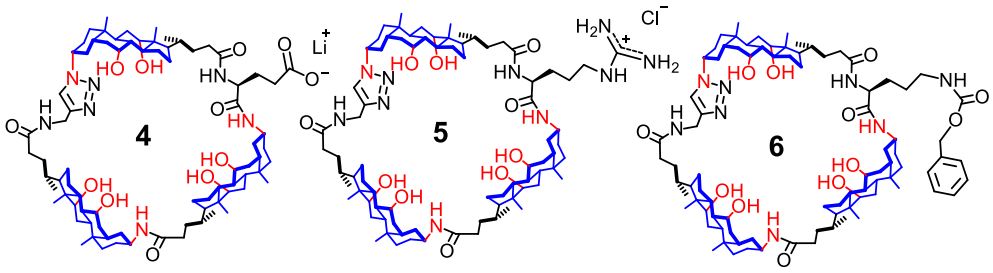

The carboxylate–guanidinium salt bridge is strong in most nonpolar environments[18] and has been reported to work well at the lipid–water interface.[21] Fortunately, the amide linkage in the oligocholates makes it easy to introduce the acid and guanidinium groups by L-ornithine and L-arginine, respectively. Compound **5** was synthesized by deprotecting the Cbz group of **6** and guanidinating the resulting amine derivative with 1-*H*-pyrazole-1-carboxamidine hydrochloride. As shown in Scheme 1, the carboxylated macrocycle (**4**) was synthesized from dimer acid **7**, which was converted to the azide–alkyne-terminated dimer **8** according to a previously reported procedure.[22] The azido group of **8** was reduced by triphenylphosphine. The resulting amine was coupled to glutamic acid-functionalized cholate **9**[23] to afford trimer **10**, followed by the click cyclization and basic hydrolysis to afford **4** .

Tricholate **1** has a triangularly shaped internal cavity approximately 1 nm on the side, large enough for glucose to pass through.[16a] To understand the transport abilities of the functionalized macrocycles, we employed the glucose leakage assay.

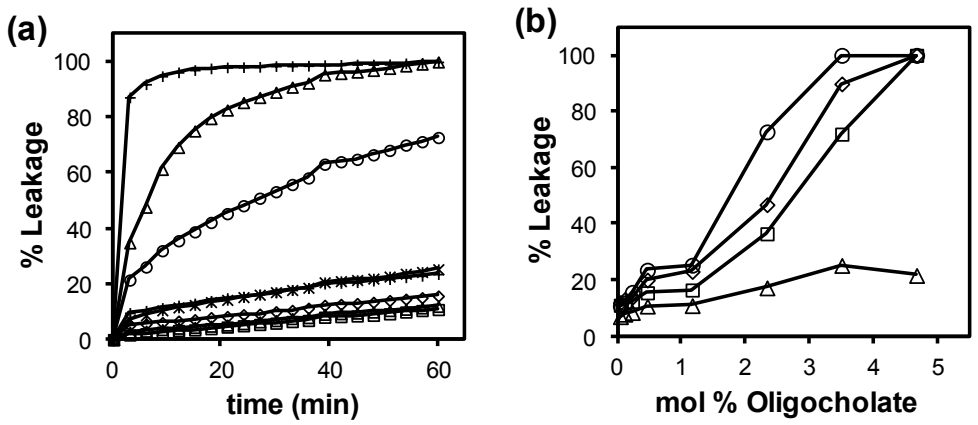

Figure 2. (a) Percent leakage of glucose from POPC/POPG LUVs upon the addition of different concentrations of **4**. The concentrations of the oligocholate added were 0, 0.125, 0.25, 0.5,1.25, 2.5, 3.75, and 5 μM from bottom to top. The concentration of glucose was 300 mM within the LUVs. (b) Percent leakage of glucose at 60 min from POPC/POPG LUVs as a function of oligocholate concentration for **4** (○), **5** (□), **6** (△), and a 1:1 mixture of **4** and **5** (◇) at ambient temperature. [phospholipids] = 107 μM. These leakage experiments were typically done in duplicates, with the error within the two <10%.

Typically, a high concentration (300 mM) of glucose was first trapped inside large unilamellar vesicles (LUVs) prepared by the extrusion method.[24] The liposomes were formulated with a neutral lipid (POPC) and an anionic one (POPG)—the latter was added mainly to enhance the colloidal stability of the liposomes. After the external glucose was removed by gel filtration, hexokinase, glucose-6-phosphate dehydrogenase, NADP, and ATP were added to liposomal solution. In the absence of transporting agents, the glucose stays inside the LUVs and remains intact. If an added reagent causes leakage of the liposomes, the escaped glucose will be converted by the enzymes to glucose-6-phosphate while NADP reduced to NADPH. Because of the fast enzymatic kinetics, the formation of NADPH at 340

nm normally correlates directly with the rate of glucose efflux.[9a] At the end of the experiments, a nonionic surfactant, Triton X-100, is added to destroy the liposomes and the amount of NADPH formed is used as the reference for 100% leakage.

Fig. 2a shows the percent leakage of glucose triggered by the carboxylated tricholate (4) from the LUVs over a period of 60 min. The leakage increased with an increasing concentration of the macrocycle. Fig. 2b compares the induced glucose leakage of the three newly synthesized macrocycles as a function of their concentrations in the membrane.[25]

Cholesterol is known to increase the hydrophobic thickness[26] of POPC bilayer and decrease its fluidity.[27] Cholesterol-containing bilayers have been shown to be much less permeable to hydrophilic molecules, including glucose.[28] A highly unusual observation in the oligocholate-induced glucose leakage was the *faster* leakage in *more hydrophobic* membranes. Although contrary to conventional thinking, the result is fully expected from the hydrophobically driven pore-forming mechanism. As the membrane becomes more hydrophobic, the (hydrophobic) driving force for the pore formation increases, making guests pass through the membrane more easily.[16a]

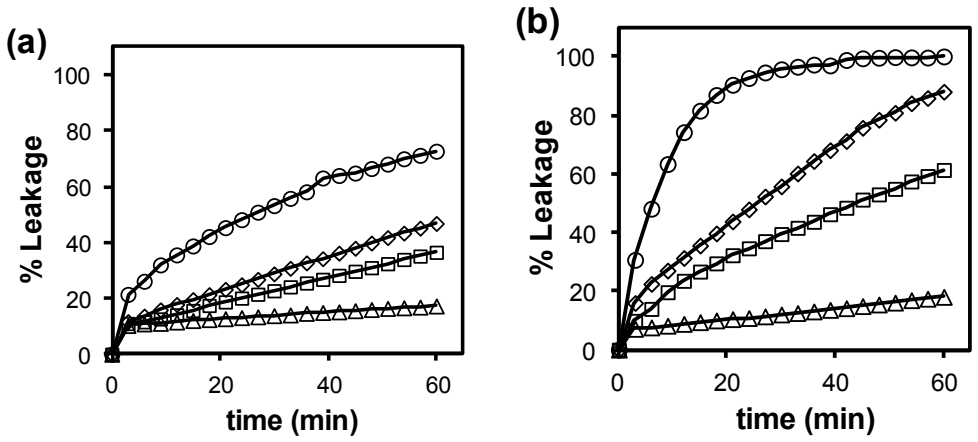

Figure 3. Percent leakage of glucose from (a) POPC/POPG LUVs and (b) POPC/POPG LUVs with 30% cholesterol upon the addition of **4** (○), **5** (□), **6** (△), and a 1:1 mixture of **4** and **5** (◇).

[Oligocholate] = 2.5 μM. [phospholipids] = 104 μM. The liposomes were lysed at 60 min upon addition of 1% Triton X-100.

Fig. 3 compares the glucose leakage induced by **4**–**6** from POPC/POPG LUVs with and without 30 mol% cholesterol in the membrane. A very notable *increase* of glucose leakage was observed for all the active transporters (i.e., **4**, **5**, and the **4**/**5** mixture). The results were opposite to what is expected from other transport mechanisms such as carrier-based transport. In a recent work of ours, the same level of cholesterol *decreased* the activity of carrier-based oligocholate foldamer transporters.[29]

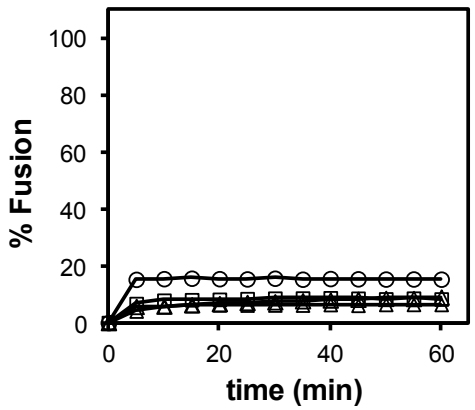

Figure 4. Percent fusion of LUVs as a function of time for **4** (○), **5** (□), and **6** (△).The data points are connected to guide the eye. [Oligocholate] = 2.5 μM. [phospholipids] = 54 μM.

We also performed a lipid-mixing assay to confirm the integrity of the lipid bilayers. In this assay, a batch of unlabelled LUVs is mixed with another batch labeled with 1 mol% NBD-and rhodamine-functionalized lipids. Any processes that destroys the membranes (*e.g.*, disintegration of the lipid bilayer) or causes the liposomes to fuse or aggregate will change the fluorescence resonance energy transfer (FRET) between the fluorescent labels.[30] As shown in Fig. 4, even at 5 mol%, a concentration that caused complete leakage of glucose, all the macrocycles displayed

<15% mixing of the lipids, indicating that none of the above-mentioned membrane-disrupting processes were significant under our experimental conditions.

Although all the leakage data obtained so far were fully consistent with the hydrophobically driven pore-forming mechanism, several trends were quite unexpected. The Cbz-protected macrocycle (**6**), for example, was almost completely incompetent (Fig. 2b and 3), at least within the 5 mol% tested concentrations.[31] The result was somewhat surprising to us because **6** was very similar to the pyrene-labeled macrocycle **3**, which aggregated in lipid membranes by the hydrophobic mechanism.[16a,32]

Because the parent tricholate macrocycle (**1**) was very potent,[16a] the low activity of 6 should *not* be caused by the lack of a charged functionality. There are two possible reasons for the incompetency of this transporter. First, the macrocycle is considerably more flexible in comparison to the parent macrocycle **1**. Both the ornithine and the triazole moiety in the clicked structure introduced rotatable bonds. Since the pore formation relies on the "reverse micelle-like", amphiphilic configuration of the cholate macrocycle, it is important that the hydrophilic groups of the macrocycle point inward to create the hydrophilic microenvironment in the center of the molecule. For the parent macrocycle (**1**), the hydrophilic groups are forced to turn inward by the curvature of the cholate backbone, caused by the cis-fused AB rings. As more rotatable bonds are present in the macrocycle and its size gets larger, it is easier for the polar groups of **6** to rotate outward. The less preorganized the macro-cycle is for the "reverse micelle-like" conformation, the more difficult it is for the hydrophobically driven pore formation to operate.[16a] Second, the Cbz-side chain introduces a carbamate group. If the hydrogen-bonding needs of the carbamate are not properly satisfied in the stacked nanopore, the group may prefer to stay near the surface of the membrane and thus hinder the formation of the transmembrane pore.

(It should be pointed out that the low activity of **6** was not a problem in the current study. The compound simply provided a reference point for the clicked macrocyclic structure in this study.)

All the leakage data indicated that the guanidinated compound (**5**) was much more active than the nonionic **6**. The result might be perplexing, as placing a charged group in a nonpolar environment is unfavorable.[33] For the pore-forming mechanism, the result is particularly disconcerting because it seems very unreasonable to stack multiple charged macrocycles in a nonpolar environment.

The guanidinium group is an unusual functionality. Although highly polar, it can form strong hydrogen-bonded salt bridges with anions such as carboxylate and phosphate.[18] Once hydrogen-bonded with a lipophilic anion, the guanidinium groups is known to migrate easily into nonpolar solvents and lipid membranes.[34] Our liposomes are made of phospholipids and have net negative charges due to the anionic POPG lipid. The guanidinated macrocycle should be electrostatically attracted to the liposomes. It is possible that, once neutralized by the phosphate headgroup of POPG, the guanidinated macrocycle could stack fairly easily inside the membrane.

In a previous work of ours, a carboxylate–guanidiniumbridged oligocholate foldamer (**12**) with an extra, non-engaging guanidinium side chain was found to fold particularly well in nonpolar solvents containing a small amount of a polar solvent.[35] The effect was attributed to the solvation of the guanidinium group. Essentially, the guanidinium group needs to be solvated by the polar solvent (the minor ingredient in the solvent mixture), regardless of the conformational state of the molecule. The folded helix has an internal hydrophilic cavity filled disproportionately with the polar solvent. Because the folded conformer can satisfy the solvation need of the guanidinium group better than the unfolded conformer, the solvation of the guanidinium indirectly favors the former (Scheme 2, left panel).

Our oligocholate macrocycles were inspired by the folded oligocholate conformers. In fact, the folding of the oligocholate foldamers and the stacking of the cholate macrocycles are driven by exactly the same solvophobic force.[16a] Thus, when the guanidinium group is placed inside the polar solvent-filled hydrophilic cavity, the same "self-solvation" that helped the folding of **12** should facilitate the stacking of **5** in the lipid membrane.

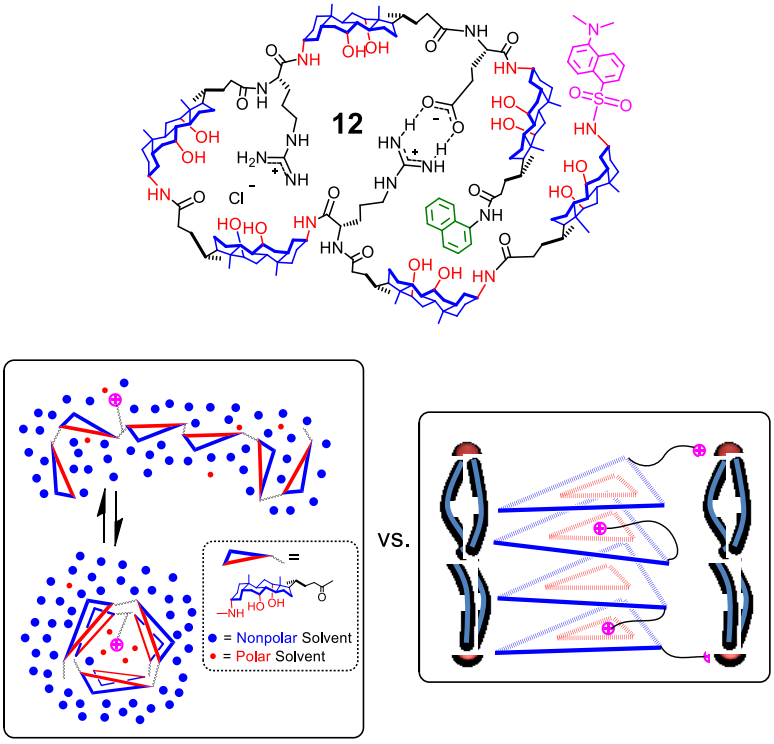

Scheme 2 Enhanced folding of **12** due to the solvation of the guanidinium group and possible stacking of guanidinium-containing macrocycle **5** in a lipid bilayer.

It should be mentioned that, in this model, not all four molecules of **5** needs to place their guanidinium groups in the stacked nanopore. Instead, only the middle two macrocycles have to do so and the two macrocycles near the membrane surface could form salt bridges with the phosphate headgroups (Scheme 2, right panel). Such an arrangement not only avoids lining up four positive charges inside the nanopore but also anchors the two peripheral macrocycles at the membrane–water interface.

Both of the above proposed models for the higher activity of **5** over **6** deal with the "solvation" needs of the guanidinium group in the nonpolar membrane. The difference between the two is how the guanidinium is stabilized in a nonpolar membrane, whether by salt-bridging with the phosphate group or by insertion into the hydrophilic cavity of the macrocycle. It is possible that both mechanisms could be operating simultaneously, depending on where the macrocycle is located in the hydrophobic core of the membrane or near the surface where phosphate groups exist in abundance.

The overall transport activity follows the order of **4** >1:1 **4**/**5** mixture > **5** over a broad range of concentrations (Fig. 2b). Hence, there was no benefit in having the carboxylated and guanidinated macrocycles in the same membrane.[25] The intermediate activity of the **4**/**5** mixture suggests that the two macro-cycles were probably operating independently—a very surprising result given the strength of the salt guanidinium–carboxylate salt bridge in nonpolar media including at the membrane–water interface.[18]

The most likely reason for the noninvolvement of the carboxylate–guanidinium salt bridge is the competition from the phosphate. Both carboxylate and phosphate can form strong salt bridges with guanidinium.[18] In order for **5** to engage in the salt bridge with **4**, it has to do so selectively in the presence of a large excess of phosphate groups on the membrane surface. Unless there are special reasons for **4** and **5** to interact with each other, such selectivity would be difficult.

Another unexpected result—most surprising to us—was the consistently high activity of the carboxylated macrocycle **4**.Over a broad range of concentrations (Fig. 2b) and in the presence or absence of cholesterol (Fig. 3), this compound outperformed other clicked macrocycles in the glucose transport. Provided that the glucose leakage mainly occurs through the nanopore formation of the oligocholates, the carboxyl side chain must have provided special benefit to the stacked

nanopore.

Our rationale for the effectiveness of **4** involves the hydrogen-bonded dimer formed between the carboxyl side chains. Lipophilic acids such as fatty acids have a pKa of ca. 4 in solution and 7.5 when bound to lipid membrane.[36] Under physiological conditions, therefore, a significant amount of the acid is in the protonated, uncharged form in the membrane. Uncharged fatty acids are known to readily partition into lipid membranes and diffuse across the bilayer. In fact, the flip-flop of fatty acids in common phospholipid bilayers has a half life of less than 10 ms without any protein transporters.[37] Macrocycle **4** is essentially a lipophilic acid with an internal hydrophilic cavity. Since bile acids permeate lipid bilayers in a similar fashion as fatty acids,[38] macrocycle **4** should be able to readily partition into the membrane in the protonated form.

Once getting into the hydrophobic membrane, **4** has two potential interactions to assist its stacking: the activated water molecules in its interior promote the pore formation by the afore-mentioned hydrophobic interactions, and the hydrogen-bonded carboxyl dimer between the side chains should also be effective. The dimerization constant of carboxylic acids is reported to be 10^3-10^4 M^{-1} in nonpolar solvents such as CCl_4 and heptane, translating to 4–5 kcal mol^{-1} in binding free energy.[39] Once the dimer is formed through the side-chain interactions, it is much easier for two dimers to stack and form the transmembrane pore. Of course, the carboxyl dimerization is not limited to specific pairs of macrocycles, any neighboring pairs could engage in such interactions, helping the transmembrane pore formation.

Changing the size of the permeant is a useful way to probe the transport mechanism. Guests too large to pass through the pore would have to move across the membrane by alternative mecha-nisms. We thus studied the permeation of carboxyfluorescein (CF) through the POPC/POPG membrane. The fluorescent probe is commonly used in liposome research to study transmembrane

movement due to its self-quenching at relatively high concentrations (*e.g.*, 50 mM).[40] Our previous work indicated that the probe was too large to pass through the pore formed by stacked tricholate 1. Instead, the molecule seemed to move across a membrane as being sandwiched between two cholate macrocycles.[16b]

The functionalized macrocycles (**4**–**6**) were able to permeate CF through POPC/POPG membranes as well.[41] The leakage profile for guanidinated compound (**5**) is shown in Fig. 5a as an example. The other compounds displayed similar profiles.

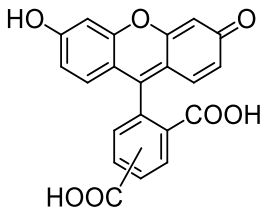

CF

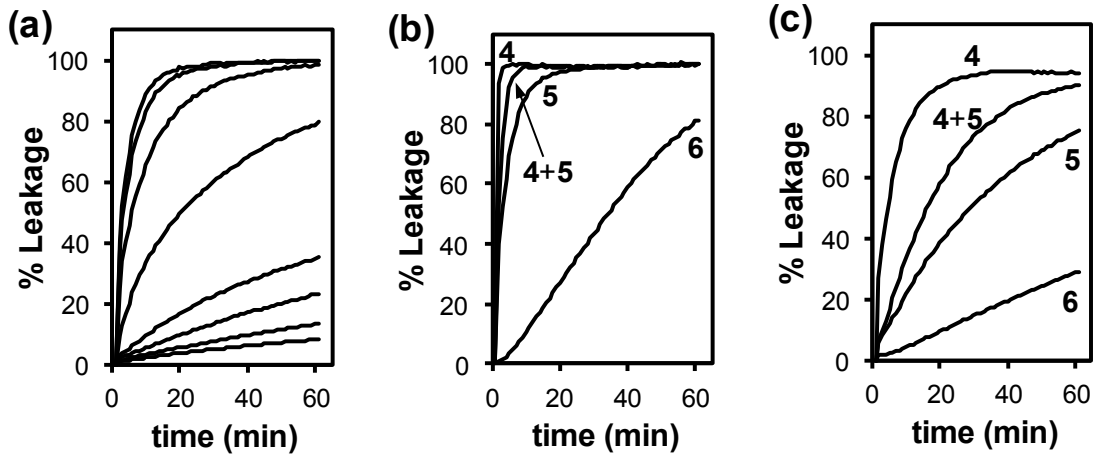

Figure 5. (a) Percent leakage of CF from POPC/POPG LUVs upon the addition of different concentrations of **5**. The concentrations of the oligocholate added were 0, 0.005, 0.0125, 0.025,0.05, 0.125, 0.25, 0.375, and 0.5 μM from bottom to top. The concentration of CF was 50 mM within the LUVs. [phospholipids] = 2.9 μM. The liposomes were lysed at 60 min upon addition of 1% Triton X-100. (b,c) Percent leakage of CF from POPC/POPG LUVs (b) and

POPC/POPG LUVs with 30% cholesterol (c) upon the addition of **4**, **5**, **6**, and a 1:1 mixture of **4** and **5**. [Oligocholate] = 0.25 μM. [phospholipids] = 2.9 μM. The liposomes were lysed at 60 min upon addition of 1% Triton X-100.

Because 30% cholesterol increases the hydrophobic thickness[26] of POPC bilayer from 2.58 to 2.99 nm and decrease its fluidity,[27] carrier-based transport generally slows down upon cholesterol incorporation.[2e] Consistent with the changed transport mechanism, all three oligocholates displayed *lower* CF transport across the cholesterol-containing membranes (Figure 4b,c). The result was exactly opposite to what was observed with glucose as the permeant (Figure 2a,b).

Most interestingly, the activities of the functionalized macrocycles followed the same order in the CF transport, i.e., **4** > 1:1 **4**/**5** mixture > **5** (Figure 4b,c). Unlike glucose, CF has two carboxyl groups and should be able to bind to the guanidinated macrocycle (**5**). It is, therefore, quite significant that the carboxylated macrocycle remained as the most active transporter. Quite likely, the carboxyl dimer interaction assisted the dimerization of **5**, making it better able to sandwich CF and shield it while passing through the membrane. It is also possible that the strong guanidinium–phosphate salt bridge formed between **4** and the phosphate groups on the membrane hindered the transmembrane movement of the macrocycle, interfering with the carrier-based transport.

Conclusions

The lipid membrane is a unique environment due to its amphiphilicity, nanodimension, liquid crystallinity, and possible microphase separation of lipids when multiple components exist. Chemists clearly need to recalibrate their thinking when moving their molecules from homogenous solutions to the lipid membrane.[29,35] The guanidinium–carboxylate salt bridge

finds numerous applications in supramolecular chemistry.[18] In the phospholipid membranes, however, it fails to help the aggregation of the oligocholate macrocycles, whether when the macrocycles engage in transmembrane pore formation or as carriers to shuttle the guest across. The results once again remind us that supramolecular chemistry is a game of competition. Although the carboxylate–guanidinium salt bridge is strong in typical nonpolar environments,[18] the carboxylated macrocycle (**4**) needs to compete with the abundant phosphate groups to engage with the guanidinated compound (**5**). The carboxyl dimer interaction, on the other hand, operates easily in the membrane without major competitors. The cooperativity between the hydrophobic interactions of the entrapped water molecules in the carboxylated macrocycles and the hydrogen-bonds among side chains makes **4** a particularly effective transporter, whether as a pore-forming molecule or a transmembrane carrier. These results should be useful for the design of additional functionalized transporters in the future.

Experimental

General

The syntheses of **6**,[16a] **7**,[22] **8**,[22] and **9**[23] were reported previously. All reagents and solvents were of ACS-certified grade or higher, and were used as received from commercial suppliers. Millipore water was used to prepare buffers and the liposomes. UV-vis spectra were recorded on a Cary 50 Bio UV-visible spectrophotometer. Fluorescence spectra were recorded on a Varian Cary Eclipse Fluorescence spectrophotometer.

Synthesis

Compound 10. Compound **9** (118.6 mg, 0.2 mmol), compound **8** (183.5 mg, 0.22 mmol), 1-hydroxybenzotriazole hydrate (HOBt, 48.6 mg, 0.36 mmol), and benzotrazol-1-yloxy-tris(dimethylamino)phosphonium hexafluorophosphate (BOP, 159 mg, 0.36 mmol) were dissolved

in anhydrous DMF (5 mL). Diisopropylethylamine (DIPEA, 174 μL, 1 mmol) was added. The reaction mixture was stirred at 40 °C under N_2 overnight and was poured into 1 N HCl (100 mL). The precipitate was collected by suction filtration, washed with water (3 × 10 mL), dried in air, and purified by column chromatography over silica gel using 9 : 1 CH_2Cl_2–MeOH (9 : 1) as the eluent to give an off-white powder (205 mg, 73%). ^{1}H NMR (400 MHz, $CDCl_3/CD_3OD$ = 1:1, δ): 4.32 (br, 1H), 4.30–3.92 (m, 5H), 3.83 (s, 3H), 3.69 (s, 3H), 3.53 (br, 2H), 3.17 (br, 1H), 2.40–1.05 (series of m, 80H), 1.02 (d, 9H), 0.94 (s, 9H), 0.71 (s, 9H). ^{13}C NMR (100 MHz, $CDCl_3/CD_3OD$ = 1:1, δ): 174.6, 174.0, 173.3, 170.6, 79.1, 72.4, 72.4, 72.4, 70.50, 67.51, 67.4, 67.4, 61.0, 52.1, 51.1, 49.6, 49.3, 49.1, 48.8, 46.4, 46.3, 45.9, 41.6, 41.6, 41.3, 41.2, 39.1, 39.0, 35.7, 35.7, 35.4, 35.2, 35.1, 35.0, 34.4, 34.3, 34.3, 34.1, 34.0, 33.0, 32.9, 32.5, 32.5, 32.4, 32.4, 31.7, 31.3, 31.3, 29.8, 29.7, 29.1, 28.1, 27.8, 27.7, 27.3, 27.1, 26.8, 26.2, 26.1, 22.7, 22.9, 21.9, 16.5, 16.5, 16.4, 11.8. HRMS (ESI) (m/z): $[M + H]^+$ calcd for $C_{81}H_{130}N_7O_{12}$, 1392.9777; found 1392.9772.

Compound 11. A solution of **10** (129 mg, 91.6 μmol) in 2:1 THF–MeOH (9 mL) was added via a syringe pump to a vigorously stirred solution of $CuSO_4 \cdot 5H_2O$ (0.1 M, 1.83 mL, 183 μmol) and sodium ascorbate (72.5 mg, 366 μmol) in 2:1:1 THF–MeOH–H_2O (31 mL) at 50 °C under N2 for 4 h. After the addition was complete, the reaction mixture was stirred for another 4 h at 50 °C. The solvents were removed by rotary evaporation and the residue was purified by column chromatography over silica gel using 8 : 1 CH_2Cl_2–MeOH as the eluent to give an off-white powder (108 mg, 85%). ^{1}H NMR (400 MHz, $CDCl_3/CD_3OD$ = 1:1, δ): 4.39–4.22 (m, 4H), 4.10 (m, 1H), 3.94–3.90 (m, 3H), 3.80–3.75 (m, 3H), 3.64–3.59 (m, 4H), 3.47 (m, 1H), 2.50–0.73 (series of m, 98H), 0.68–0.65 (m, 9H). ^{13}C NMR (100 MHz, $CDCl_3/CD_3OD$ = 1:1, δ): 176.2, 174.6, 172.2, 145.3, 121.5, 74.0, 68.7, 68.6, 68.4, 62.3, 53.9, 52.2, 43.0, 42.9, 42.78, 42.7, 40.4,

40.3, 37.6, 37.0, 36.8, 36.7, 36.6, 36.5, 35.6, 35.5, 35.4, 35.3, 35.2, 32.7, 32.6, 31.1, 30.4, 29.2, 29.1, 28.6, 28.4, 27.9, 27.8, 27.6, 27.5, 27.4, 23.9, 23.1, 22.9, 17.7, 13.0. HRMS (ESI) (m/z): $[M + H]^+$ calcd for $C_{81}H_{130}N_7O_{12}$, 1392.9777; found 1392.9740.

Compound 4. Compound **11** (60 mg, 43 μmol) was dissolved in 1:1 THF–MeOH (5 mL). A solution of LiOH (2 M, 0.2 mL, 0.4 mmol) was added and the reaction mixture was stirred until the starting material was consumed. After the solvent was removed under reduced pressure, the residue was purified by column chromatography on silica gel using 4 : 1 CH_2Cl_2–MeOH as the eluent to give a white powder (55 mg, 93%). ^{1}H NMR (400 MHz, $CDCl_3/CD_3OD$ = 1:1, δ): 4.53–4.41 (m, 3H), 4.30 (m, 1H), 4.00–3.95 (m, 3H), 3.83 (bs, 3H), 3.52–3.49 (m, 2H), 2.39–0.93 (series m, 95H), 0.74–0.71 (m, 9H). ^{13}C NMR (100 MHz, $CDCl_3/CD_3OD$ = 1:1, δ):175.4, 175.3, 174.7, 171.4, 144.4, 120.6, 72.7, 67.8, 67.7, 67.5, 61.4, 53.2, 49.9, 49.4, 46.6, 46.4, 46.3, 46.2, 46.1, 46.0, 45.3, 42.1, 41.8, 41.7, 39.4, 39.3, 36.0, 35.8, 35.7, 35.6, 34.8, 34.7, 34.6, 34.5, 34.4, 34.3, 34.2, 28.1, 27.4, 26.6, 26.5, 23.0, 22.27, 2.2, 22.1, 16.7, 12.0. HRMS (ESI) (m/z): $[M + H]^+$ calcd for $C_{80}H_{128}N_7O_{12}$, 1378.9621; found 1378.9633.

Compound 5. A mixture of the amino derivative of compound **3**[16a] (15 mg, 0.01 mmol) and 1H-pyrazole-1-carboximidamide (18 mg, 0.12 mmol) was dissolved in anhydrous DMF (0.25 mL). DIPEA (80 μL, 0.5 mmol) was added to the above mixture, which was stirred at 50 °C overnight. The reaction was monitored by ^{1}H NMR spectroscopy. When the reaction was complete, the mixture was poured in brine and the precipitate was collected by suction filtration, dissolved in methanol, and precipitated again in acetonitrile to give an off-white powder (11 mg, 69%). ^{1}H NMR (400 MHz, $CDCl_3/CD_3OD$ = 1:1, δ): 7.82 (br, 1H), 4.37 (m, 3H), 3.92 (br, 3H), 3.79 (br, 1H), 3.50 (br, 2H), 3.17 (br, 2H), 2.74 (br, 1H), 2.39–0.76 (series of m), 0.67 (s, 9H). ^{13}C NMR

(100 MHz, $CDCl_3/CD_3OD$ = 1:1, δ): 175.4, 174.9, 172.0, 157.6, 136.8, 128.5, 128.0, 127.5, 72.8, 66.5, 62.7, 53.7, 53.6, 46.8, 46.8, 46.0, 40.2, 35.2, 33.0, 29.0, 26.9, 22.5,17.1, 12.5, 12.4, 12.3. ESI-MS (m/z): $[M + H]^+$ calcd for $C_{81}H_{134}N_{10}O_{10}$, 1407.0279; found, 1407.0247.

Acknowledgements

We thank NSF (DMR-1005515) for supporting the research.

Notes and references

(1) (a) G. Lee, *Biomembranes: A Multi-Volume Treatise*, JAI Press, Greenwich, Conn., 1995; (b) G. Menestrina, M. Dalla Serra and P. Lazarovici, *Pore-Forming Peptides and Protein Toxins,* Taylor & Francis, London, New York, 2003; (c) F. G. v. d. Goot, *Pore-Forming Toxins*, Springer, Berlin; New York, NY, 2001; (d) L. K. Tamm, *Protein-Lipid Interactions: From Membrane Domains to Cellular Networks*, Wiley-VCH, Weinheim, 2005; (e) R. J. C. Gilbert, *Cell. Mol. Life Sci.*, 2002, **59**, 832.

(2) (a) W. D. Stein, *Carriers and Pumps: An Introduction to Membrane Transport*, Academic Press, San Diego, CA, 1990; (b) G. W. Gokel and I. A. Carasel, *Chem. Soc. Rev*., 2007, **36**, 378; (c) T. M. Fyles, *Chem. Soc. Rev.*, 2007, **36**, 335; (d) B. A. McNally, W. M. Leevy and B. D. Smith, *Supramol. Chem.*, 2007, **19**, 29; (e) J. T. Davis, O. Okunola and R. Quesada, *Chem. Soc. Rev.,* 2010, **39**, 3843.

(3) (a) S. Matile, A. Som and N. Sorde, *Tetrahedron*, 2004, **60**, 6405; (b) A. L. Sisson, M. R. Shah, S. Bhosale and S. Matile, *Chem. Soc. Rev.*, 2006, **35**, 1269.

(4) S. Litvinchuk, N. Sorde and S. Matile, *J. Am. Chem. Soc.*, 2005, **127**, 9316.

(5) (a) J. J. Kasianowicz, E. Brandin, D. Branton and D. W. Deamer, *Proc. Natl. Acad. Sci. U. S. A.*, 1996, **93**, 13770; (b) M. Akeson, D. Branton, J. J. Kasianowicz, E. Brandin and D. W. Deamer, *Biophys. J.*, 1999, **77**, 3227; (c) A. Meller, L. Nivon, E. Brandin, J. Golovchenko

and D. Branton, *Proc. Natl. Acad. Sci. U. S. A.*, 2000, **97**, 1079; (d) W. Vercoutere, S. Winters-Hilt, H. Olsen, D. Deamer, D. Haussler and M. Akeson, *Nat. Biotechnol*., 2001, **19**, 248; (e) S. Howorka, S. Cheley and H. Bayley, *Nat. Biotechnol.,* 2001, **19**, 636; (f) J. Clarke, H. C. Wu, L. Jayasinghe, A. Patel, S. Reid and H. Bayley, *Nat. Biotechnol*., 2009, **4**, 265.

(6) N. Sakai, N. Sorde and S. Matile, *J. Am. Chem. Soc.*, 2003, **125**, 7776.

(7) (a) G. W. Gokel and A. Mukhopadhyay, *Chem. Soc. Rev.*, 2001, **30**, 274; (b) U. Koert, L. Al-Momani and J. R. Pfeifer, *Synthesis*, 2004, 1129; (c) G. W. Gokel and O. Murillo, *Acc. Chem. Res.*, 1996, **29**, 425; (d) M. Jung, H. Kim, K. Baek and K. Kim, *Angew. Chem., Int. Ed*., 2008, **47**, 5755; (e) X. Li, B. Shen, X. Q. Yao and D. Yang, *J. Am. Chem. Soc*., 2009, **131**, 13676.

(8) A. Som and S. Matile, *Chem. Biodiversity*, 2005, **2**, 717.

(9) (a) J. R. Granja and M. R. Ghadiri, *J. Am. Chem. Soc.*, 1994, **116**, 10785; (b) J. Sanchez-Quesada, H. S. Kim and M. R. Ghadiri, *Angew. Chem., Int. Ed.*, 2001, **40**, 2503.

(10) (a) N. Sakai, J. Mareda and S. Matile, *Acc. Chem. Res.*, 2005, **38**, 79; (b) G. Das, P. Talukdar and S. Matile, *Science*, 2002, **298**, 1600.

(11) S. Bhosale, A. L. Sisson, P. Talukdar, A. Furstenberg, N. Banerji, E. Vauthey, G. Bollot, J. Mareda, C. Roger, F. Wurthner, N. Sakai and S. Matile, *Science*, 2006, **313**, 84.

(12) A. Satake, M. Yamamura, M. Oda and Y. Kobuke, *J. Am. Chem. Soc.*, 2008, **130**, 6314.

(13) A. J. Helsel, A. L. Brown, K. Yamato, W. Feng, L. H. Yuan, A. J. Clements, S. V. Harding, G. Szabo, Z. F. Shao and B. Gong, *J. Am. Chem. Soc.*, 2008, **130**, 15784.

(14) T. M. Fyles and C. C. Tong, *New J. Chem.*, 2007, **31**, 655.

(15) L. Ma, M. Melegari, M. Colombini and J. T. Davis, *J. Am. Chem. Soc.*, 2008, **130**, 2938.

(16) (a) H. Cho, L. Widanapathirana and Y. Zhao, *J. Am. Chem. Soc.*, 2011, **133**, 141; (b) H. Cho

and Y. Zhao, *Langmuir*, 2011, **27**, 4936.

(17) J. D. Dunitz, *Science*, 1994, **264**, 670.

(18) (a) F. P. Schmidtchen and M. Berger, *Chem. Rev*., 1997, **97**, 1609; (b) M. D. Best, S. L. Tobey and E. V. Anslyn, *Coord. Chem. Rev*., 2003, 240-243.

(19) Y. Zhao and Z. Zhong, *J. Am. Chem. Soc*., 2005, **127**, 17894.

(20) V. V. Rostovtsev, L. G. Green, V. V. Fokin and K. B. Sharpless, *Angew. Chem., Int. Ed.*, 2002, **41**, 2596.

(21) K. Ariga and T. Kunitake, *Acc. Chem. Res.*, 1998, **31**, 371.

(22) Z. Zhong, X. Li and Y. Zhao, *J. Am. Chem. Soc*., 2011, **133**, 8862.

(23) Z. Zhong and Y. Zhao, *Org. Lett*., 2007, **9**, 2891.

(24) S. C. Kinsky, J. A. Haxby, D. A. Zopf, C. R. Alving and C. B. Kinsky, *Biochemistry*, 1969, **8**, 4149.

(25) None of these compounds have any significant water-solubility due to their dominant hydrophobicity. We expect all the compounds to readily enter the lipid membrane instead of staying in water.

(26) F. A. Nezil and M. Bloom, *Biophys. J*., 1992, **61**, 1176.

(27) J. C. M. Holthuis, G. van Meer and K. Huitema, *Mol. Membr. Biol*., 2003, **20**, 231.

(28) (a) R. A. Demel, K. R. Bruckdor and L. L. van Deene, *Biochim. Biophys. Acta*, 1972, **255**, 321; (b) D. Papahadjopoulos, S. Nir and S. Ohki, *Biochim. Biophys. Acta*, 1972, **266**, 561.

(29) S. Zhang and Y. Zhao, *Chem.–Eur. J*., 2011, **17**, 12444.

(30) D. K. Struck, D. Hoekstra and R. E. Pagano, *Biochemistry*, 1981, **20**, 4093.

(31) The background leakage in these experiments was typically 6–10% over 60 min.

(32) Although **6** and **3** both could aggregate in the membranes by the same hydrophobic

mechanism, the aggregational states required for the formation of the pyrene excimer and for the glucose leakage could be quite different. Because the two processes operate on a very different time scale and have different sensitivity, an aggregational state sufficient for the pyrene excimer may not allow glucose to permeate the membrane.

(33) I. Gitlin, J. D. Carbeck and G. M. Whitesides, *Angew. Chem., Int. Ed*., 2006, **45**, 3022.

(34) N. Sakai and S. Matile, *J. Am. Chem. Soc*., 2003, **125**, 14348.

(35) H. Cho and Y. Zhao, *J. Am. Chem. Soc*., 2010, **132**, 9890.

(36) J. A. Hamilton,in *Carbon-13 NMR Spectroscopy of Biological Systems*, ed. N. Beckmann, Academic Press, San Diego, 1995, p. 117.

(37) (a) F. Kamp and J. A. Hamilton, *Proc. Natl. Acad. Sci. U. S. A*., 1992, **89**, 11367; (b) F. Kamp, D. Zakim, F. Zhang, N. Noy and J. A. Hamilton, *Biochemistry*, 1995, **34**, 11928; (c) J. A. Hamilton, W. Guo and F. Kamp, *Mol. Cell. Biochem*., 2002, **239**, 17.

(38) F. Kamp and J. A. Hamilton, *Biochemistry*, 1993, **32**, 11074.

(39) (a) J. Wenograd and R. A. Spurr, *J. Am. Chem. Soc.*, 1957, **79**, 5844; (b) D. S. Goodman, *J. Am. Chem. Soc*., 1958, **80**, 3887. 40 R. R. C. New, *Liposomes: A Practical Approach*, IRL Press, Oxford, 1990. 41 Although the concentrations of the transporters in the CF leakage (Fig. 5) were much lower than those in the glucose leakage assays (Fig. 1), the data do not mean that these compounds were better transporters for the larger CF. Because the UV-based glucose assay had lower sensitivity than the fluorescence-based CF assay, a much higher concentration of LUVs (107 vs. 2.9 μM) had to be used in the former. Since the oligocholates were essentially insoluble in water, the effective concentration of the transporter in the membrane would increase with a decrease in the phospholipid concentration.

CHAPTER 5. EFFECTS OF AMPHIPHILE TOPOLOGY ON THE AGGREGATION OF OLIGOCHOLATES IN LIPID MEMBRANES: MACROCYCLIC VERSUS LINEAR AMPHIPHILES

A paper published in *Langmuir* **2012**, *28,* 8165−8173.

Lakmini Widanapathirana and Yan Zhao

Abstract

A macrocyclic and a linear trimer of a facially amphiphilic cholate building block were labeled with a fluorescent dansyl group. The environmentally sensitive fluorophore enabled the aggregation of the two oligocholates in lipid membranes to be studied by fluorescence spectroscopy. Concentration-dependent emission wavelength and intensity revealed higher concentration of water for the cyclic compound. Both compounds were shown by the red-edge excitation shift (REES) to be located near the membrane/water interface at low concentrations but the cyclic trimer was better able to migrate into the hydrophobic core of the membrane than the linear trimer. Fluorescent quenching by a water-soluble (NaI) and a lipid-soluble (TEMPO) quencher indicated that the cyclic trimer penetrated into the hydrophobic region of the membrane

more readily than the linear trimer, which preferred to stay close to the membrane surface. The fluorescent data corroborated with the previous leakage assays that suggested the stacking of the macrocyclic cholate trimer into transmembrane nanopores, driven by the strong associative interactions of water molecules inside the macrocycles in a nonpolar environment.

Introduction

Amphiphiles are molecules with segregated hydrophilic and hydrophobic moieties in the structure. Among them are common head/tail surfactants, amphiphilic block copolymers, most proteins, nucleic acids, and some carbohydrates. Even the simplest class of amphiphiles, the head/tail surfactants, can form a wide variety of self-assembled structures, depending on the relative volumes of the hydrophilic and hydrophobic components.[1] The hydrophilic and hydrophobic groups may be arranged in other topologies as well. Facial amphiphiles, for example, have their amphiphilic groups located on opposite faces instead of on opposite ends as in the head/tail surfactants.[2-4] When multiple facial amphiphiles are connected by covalent bonds,[5-7] a rich array of structures can be obtained including molecular umbrellas,[8-10] responsive molecular receptors,[11-15] foldamers,[16-21] and novel dendrimeric hosts.[22-24]

We recently synthesized cholate-derived macrocycles such as **1**,[25,26] inspired by our previously reported oligocholate foldamers that adopt helical structures with nanometer-sized hydrophilic internal cavities.[19-21] Hydrophobic interactions typically work in aqueous solution instead of a nonpolar medium. Macrocycle **1**, however, was found to aggregate in lipid bilayers to form transmembrane nanopores, driven by an unusual form of hydrophobic interactions in the nonpolar membrane environment. Briefly, the rigid steroid backbone and the macrocyclic framework fix the compound into a "reverse micelle-like" configuration in which the polar hydroxyl and amide groups point inward. The large, external hydrophobic surface makes the macrocycle prefer the

nonpolar membrane instead of aqueous environment. Once the macrocycle enters the membrane, its highly polar interior needs to be solvated by water instead of lipid hydrocarbon whereas the water molecules inside strongly prefer to interact with other water molecules instead of the lipid tails. The conflicting solvation requirements for the interior and the exterior of the molecule are resolved if multiple macrocycles stack over one another into a transmembrane pore (Figure 1). The arrangement allows the water molecules inside the macrocycles to solvate the polar groups of the cholates and still exchange with the bulk water readily. The exchange of water may be quite important to the pore formation, as the entropic cost for trapping a single water molecule can be as high as 2 kcal/mol in some cases.[27]

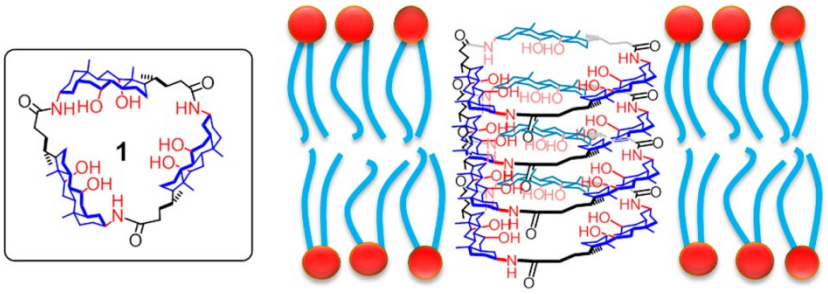

Figure 1. Schematic representation the idealized pore formation of oligocholate macrocycle **1** in a lipid bilayer membrane.

Transmembrane pores with inner diameter of 1 nm or larger allow molecules and ions of significant size to pass through the lipid membrane.[27,28] Synthetic pore-forming agents in recent years have attracted many researchers' attention. Although a number of designs are available, the noncovalent forces utilized in the self-assembling are limited to hydrogen bonds,[29-32] aromatic interactions,[33,34] and metal–ligand coordination.[35,36] To the best of our knowledge, hydrophobic interactions have never been used as the primary driving force in synthetic pore-forming agents in the membrane environment.

The main evidence for the pore formation came from leakage assays and various control experiments.[25,26] Although a pyrene-labeled macrocycle provided spectroscopic support for the pore formation,[25] we were interested in gaining further insight into the aggregational process. The emission of a fluorophore is often highly sensitive to its environment.[37] In this paper, we prepared a cyclic trimer (**2**) and a linear trimer (**3**), both labeled with a dansyl group. The fluorescent labeling allowed us to study the aggregation of the two oligocholates in membranes by a number of techniques including environmentally sensitive emission, red-edge excitation shift (REES), and fluorescence quenching. The study revealed the importance of amphiphile topology on the aggregation of the amphiphiles and provided additional evidence for the hydrophobically driven pore formation.

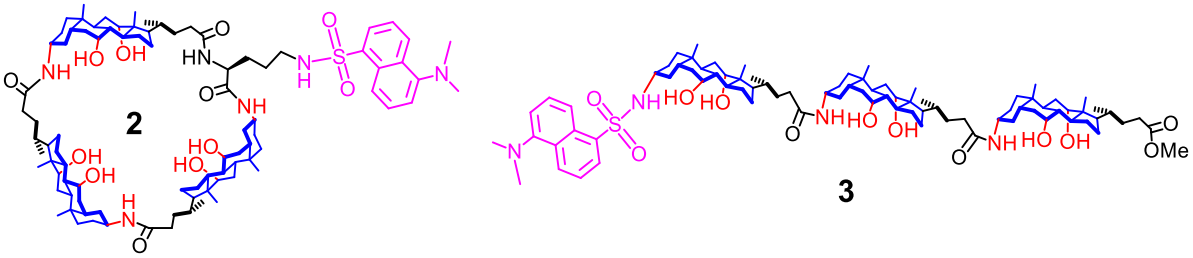

Experimental Section

General. All reagents and solvents were of ACS-certified grade or higher and used as received from commercial suppliers. Millipore water was used to prepare buffers and liposomes. Routine ^{1}H and ^{13}C NMR spectra were recorded on a Varian VXR-400 or on a Varian MR400 spectrometer. Fluorescence spectra were recorded at ambient temperature on a Varian Cary Eclipse fluorescence spectrophotometer. The syntheses of compounds **3**[21] and **4**[25] were reported previously.

Synthesis of Compound 2. Compound **4** (44 mg, 0.034 mmol) and dansyl chloride (10 mg,

0.036 mmol) were dissolved in a mixture of CH_2Cl_2 (0.3 mL) and CH_3OH (0.2 mL). Triethylamine (10 μL, 0.068 mmol) was added, and the mixture was stirred at room temperature overnight. The solvents were removed by rotary evaporation. The residue was purified by preparative TLC using 8:1 CH_2Cl_2/CH_3OH as the developing solvent to give a light yellow powder (21 mg, 40%). ^{1}H NMR (400 MHz, CD_3OD, δ): 8.50 (d, 1H), 8.32 (d, 1H), 8.14 (d, 1H), 7.38 (m, 2H), 7.11 (d, 1H), 4.14 (br,1H), 3.90 (br, 3H), 3.76 (br, 3H), 3.28 (br, 3H), 2.81 (s, 6H), 2.38−1.0 (series of m), 0.88 (s, 9H), 0.65 (s, 9H). ^{13}C NMR (100 MHz, $CDCl_3/CD_3OD$ = 1:1, δ): 176.9, 175.6, 172.4, 170.1, 151.7, 130.5, 128.9, 127.9, 127.3, 126.2, 123.9, 122.3, 115.2, 73.6, 68.7, 59.3, 54.4, 50.1, 45.9, 36.8, 36.3, 32.2, 28.7, 27.2, 22.8, 17.6, 12.7. ESIHRMS (m/z): $[M + H]^+$ calcd for $C_{89}H_{139}N_{65}O_{12}S$, 1516.0170; found, 1516.0166.

Liposome Preparation. Unlabeled POPC/POPG large unilamellar vesicles (LUVs) were prepared according to a literature procedure.[38] A chloroform solution of POPC (25 mg/mL, 198 μL) and POPG (50 mg/mL, 10.0 μL) was placed in a 10 mL test tube and dried under a stream of nitrogen. The residue was dried further under high vacuum overnight. Rehydration of the lipids was done using HEPES buffer (10 mM HEPES, 107 mM NaCl, pH = 7.4) and allowed to continue for 30 min with occasional vortexing. The opaque dispersion was subjected to ten freeze−thaw cycles. The resulting mixture was extruded 29 times through a polycarbonate filter (diameter = 19 mm, pore size = 100 nm) at room temperature using an Avanti Mini-Extruder. A portion (0.3 mL) of the liposome solution was diluted to 5.0 mL with the HEPES (10 mM HEPES, 107 mM NaCl, pH = 7.4) buffer. The concentration of phospholipids in the stock solution was 0.86 mM.

Fluorescence Spectroscopy and REES. Stock solutions (2.0×10^{-4} M) of **2** and **3** in DMSO were prepared. Aliquots of the above LUV solution (250 μL) and HEPES buffer (1750 μL, 10 mM HEPES, 107 mM NaCl, pH = 7.4) were placed in a series of cuvettes. The

concentration of phospholipids in each cuvette was 107 μM. Aliquots of the oligocholate solution were added to the cuvettes via a microsyringe. The amount of DMSO introduced to each sample was ≤20 μL. The sample was vortexed gently for 5 s. The fluorescence spectrum was recorded with the excitation wavelength set at 330 nm. For the REES experiments, the excitation wavelength was varied from 340 to 365 nm while the maximum emission wavelength was monitored.

Fluorescence Quenching. A typical procedure for the quenching experiment is as follows. Stock solutions (5.0×10^{-4} M) of **2** and **3** in DMSO were prepared. An aliquot of the above LUV solution (250 μL) and HEPES buffer (1750 μL, 10 mM HEPES, 107 mM NaCl, pH = 7.4) were placed in a quartz cuvette. The concentration of phospholipids in each cuvette was 107 μM. An aliquot (13.0 μL) of the stock solution was added via a microsyringe and vortexed gently for 5 s before the initial fluorescence spectrum was recorded. In the case of the water-soluble quencher, aliquots (10.0 μL) of NaI (7 M in the above HEPES buffer that contained 0.1 mM $Na_2S_2O_3$) were added with a Hamilton Gastight syringe. In the case of the lipid-soluble quencher, aliquots (2.0 μL) of TEMPO (0.5 M in ethanol) were added. After each addition, the sample was vortexed gently for 5 s. The fluorescence spectrum was recorded over 10 min at 1 min intervals and averaged. The excitation wavelength was set at 330 nm.

Results and Discussion

Environmentally sensitive fluorescence. The main evidence for the pore formation of the oligocholate macrocycles is as follows.[25] First, cyclic trimer **1** triggered highly efficient leakage of glucose and even maltotriose from large unilamellar vesicles (LUVs). Second, lipid-mixing assays and DLS confirmed the integrity of the membranes and ruled out other mechanisms such

as membrane fusion and destruction as the cause of the leakage. Third, strong cooperativity was found among four macrocycles in the glucose transport across POPC/POPG membranes. The hydrophobic matching between the membrane and the height of the macrocycle suggests that it takes approximately four stacked macrocycles to span the hydrophobic core of a POPC/POPG bilayer. Fourth, the addition of 30 % cholesterol to the POPC/POPG membrane caused a counterintuitive *increase* in the glucose transport rate. Cholesterol is known to increase the hydrophobic thickness[39] of POPC bilayer and decrease its fluidity.[40] Cholesterol-containing bilayers have been shown to be much less permeable to hydrophilic molecules, including glucose.[41,42] The result, however, is fully consistent with the hydrophobically driven pore formation—as the membrane becomes more hydrophobic with the addition of cholesterol, the driving force for the stacking is higher and more efficient pore formation is expected to afford faster glucose transport. Fifth, a longer hydrophilic guest should have more difficulty moving across the membrane but maltotriose was found to be transported *faster* across the membrane than glucose, especially by the cyclic cholate tetramer. The result was attributed to the trisaccharide threading through multiple macrocycles to "template" the formation of the nanopore. Sixth, guests whose cross-section is larger than the inner diameter of the macrocycle do not display the signatures of the pore-forming mechanism during leakage assays.[26]

Although convincing, the data from the leakage assays mainly provided *functional* evidence for the nanopores. The pore formation was inferred from performance data that could not be explained easily by alternative mechanisms. Spectroscopic techniques, on the other hand, potentially can afford details such as the location of the molecule of interest, its local environment, and concentration-dependency. Such studies should complement the functional assays and give insights into the pore-forming mechanism difficult to be obtained otherwise.

How do we use the dansyl-labeled compounds to probe the pore formation? Our previous study shows that linear trimer **5** was completely inactive at transporting hydrophilic molecules across lipid membranes.[25,26] Clearly, although having the same number of the facially amphiphilic cholate building blocks, the arrangement of the cholates is critical to the transport activity. Linear oligocholates, hence, should behave differently from cyclic ones in a membrane, making compounds **2** and **3** a perfect pair to compare.

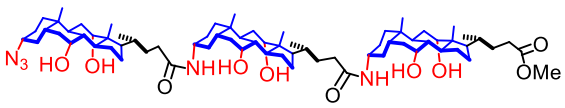

5

Both the emission intensity and wavelength of dansyl are highly sensitive to its local environment.[43] In general, the emission wavelength (λ_{em}) shifts to the red in more polar environments while the emission intensity decreases. The trend is true in both binary solvents[43] and in microphase-separated systems such as micelles.[44]

Figure 1a shows the emission intensity of **2** and **3** in POPC/POPG membranes (data points connected by solid lines). In these experiments, the concentration of the oligocholate was varied while that of the phospholipids was kept the same (107 μM). Because cholate oligomers have negligible solubility in water,[25,45] both **2** and **3** were assumed to be solubilized within the lipid membranes in the aqueous solution. It is clear from that data that the linear trimer (◆) emitted much more strongly than the cyclic trimer (■), indicative of a higher environmental polarity for the dansyl in the latter. The same conclusion could be drawn from the emission wavelength. As shown by Figure 1b, the average λ_{em} for the linear and the cyclic trimer in the POPC/POPG membrane was 493.1 ± 1.3 and 502.2 ± 1.6 nm, respectively. The 9 nm red shift for the cyclic compound indicates that its dansyl was indeed in a more polar microenvironment than that of the linear trimer.

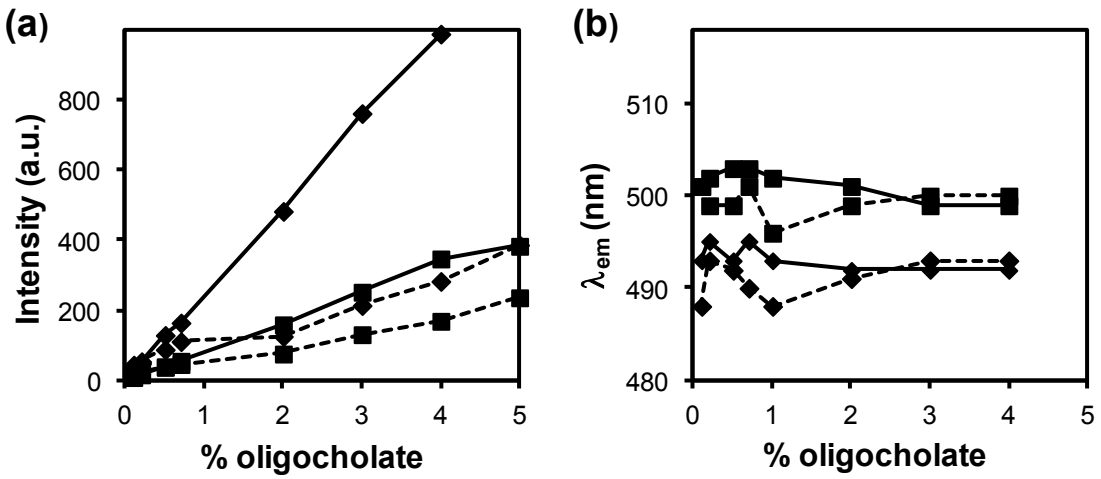

Figure 1. (a) Emission intensity and (b) maximum emission wavelength (λ_{em}) of compounds **2** (■) and **3** (◆) in POPC/POPG membranes (data points connected by solid lines) and 30% cholesterol/POPC/POPG membranes (data points connected by dashed lines). λ_{ex} = 330 nm. [Phospholipids] = 107 μM.

There are at least two possible ways to explain the different environmental polarity for the two compounds. First, the macrocyclic trimer (**2**) has a fixed hydrophilic cavity and thus is expected to be better at retaining water than the linear trimer. If a small water pool exists in the center of the cyclic trimer, the nearby dansyl should sense the local hydrophilicity and display red-shifted and weaker emission as a result. According to the pore-forming mechanism, the cyclic trimer can stack up in the *z*-direction and aggregate into a nanotube (Figure 1). The model suggests that the stacked oligocholate macrocycles have a continuous water pore going through the center. These water molecules should increase the local polarity for the dansyl group on the cyclic trimer, weakening the emission intensity and shifting λ_{em} to the red. Second, the two compounds may penetrate to different degrees into the hydrophobic core of the membrane. If a compound penetrates deeper into the membrane, its dansyl should be less exposed to water and thus emits more strongly at a shorter wavelength. As will be shown later, however, an oil-soluble quencher accessed the cyclic

trimer better than it did the linear trimer (and the opposite was true with a water-soluble quencher). Thus, the cyclic compound was actually deeper into the membrane than the linear trimer. Normally, the dansyl emission should be blue-shifted and stronger for the cyclic trimer under such a condition. Clearly, something other than the membrane penetration was controlling the emission of the dansyl.

As mentioned earlier in the paper, the addition of cholesterol increases the hydrophobic thickness[39] of POPC bilayer and decrease its fluidity.[40] Assuming both the cyclic and the linear oligocholates are embedded in the membranes—due to the dominance of hydrophobic groups in the structure—the addition of cholesterol into the membrane should increase the overall environmental hydrophobicity. As shown by the dashed lines in Figure 1a, however, both compounds displayed weaker emission.

In POPC/POPG membranes, the weaker emission of the cyclic trimer (■) was accompanied by a red shift of λ_{em} (the solid lines in Figures 1a and 1b). The weaker emission in the cholesterol-containing membranes, however, did not display the concomitant red shift. The average emission wavelengths of compound **2** were 499.4 ± 1.6 nm and 502.2 ± 1.6 nm with and without cholesterol, respectively; those of compound **3** were 491.0 ± 2.1 nm and 493.1 ± 1.3 nm, respectively. Statistically, therefore, the addition of cholesterol did not shift the emission wavelength, suggesting that the lower emission intensity of **2** and **3** in the presence of cholesterol did not derive from higher local environmental polarity but may have other origins that are currently not clear to us.

It should be mentioned that the relative difference between the cyclic and the linear compound was maintained in the cholesterol-containing membranes. The emission intensity, for example, was lower for the cyclic trimer (■) than for the linear trimer (◆), as shown by the dashed lines in

Figure 1a. The emission wavelength was about 8 nm red-shifted for the cyclic trimer (Figure 1b). Therefore, regardless of the exact reasons for the overall lower emission intensity of the dansyl in the cholesterol-containing membranes, the environmental polarity for the dansyl was higher for the cyclic than the linear trimer. The observation was consistent with the stronger ability of the cyclic compound to retain water in the membrane and the pore formation as a result of the associative interactions of the entrapped water.

Red-edge excitation shift (REES). The shape of the emission spectrum of a fluorophore in solution is independent of the excitation wavelength because, prior to the emission, fast internal conversion makes the excited fluorophore rapidly relax to the lowest-energy vibrational state of the first singlet excited state (Kasha's rule). Solvent relaxation, however, slows down in motion-restricting environments. In a highly viscous solution, for example, when the fluorophore is excited on the red edge of the absorption band, the subpopulation of the fluorophore with the solvation shell similar to that of the excited state is selectively excited, yielding a lower-energy emission band. This phenomenon, referred to as the red-edge excitation shift or REES, is typically found for polar fluorophores that interact strongly with solvent molecules in a motion-restricting environment.[46,47]

When a fluorophore is in the bulk aqueous phase, although it may interact strongly with the solvent, solvent relaxation is fast due to rapid solvent reorientation. When the fluorophore is located inside the hydrocarbon phase of the membrane, the nondirectional van der Waals interactions do not respond strongly to the increased polarity of the excited fluorophore and the solvation effect is often quite weak. At the membrane/water interface, the water molecules can only form a limited number of favorable interactions with other water molecules at the interface and with the lipid headgroups. Under such a condition, solvent relaxation slows down

dramatically, making the membrane/water interface the most "REES-prone" region of the lipid bilayer.[48,49]

Figure 2a shows the emission wavelengths (λ_{em}) of oligocholates **2** and **3** as a function of the excitation wavelength (λ_{ex}) at [oligocholate]/[phospholipids] = 0.05% (Figure 2a). Glucose transport at this level of the oligocholates (cyclic or linear) was negligible.[25] The cyclic trimer, hence, should be mostly in the nonaggregated or dissociated form at this concentration. Two trends are immediately noticeable when the two compounds are compared. First, the emission wavelength of the cyclic trimer (■) is consistently higher than that of the linear trimer (◆). The observation is consistent with Figure 1b and suggests that the dansyl group of the cyclic compound was in a more polar microenvironment than that of the linear derivative. Second, the linear trimer gives a larger REES (10 nm) than the cyclic trimer (7 nm). The 3 nm difference is significant, indicating that a higher percentage of the linear trimer was residing at the membrane/water interface than the cyclic trimer. In other words, it is easier for the cyclic trimer than for the linear trimer to penetrate deep into the membrane, even at this very low concentration.

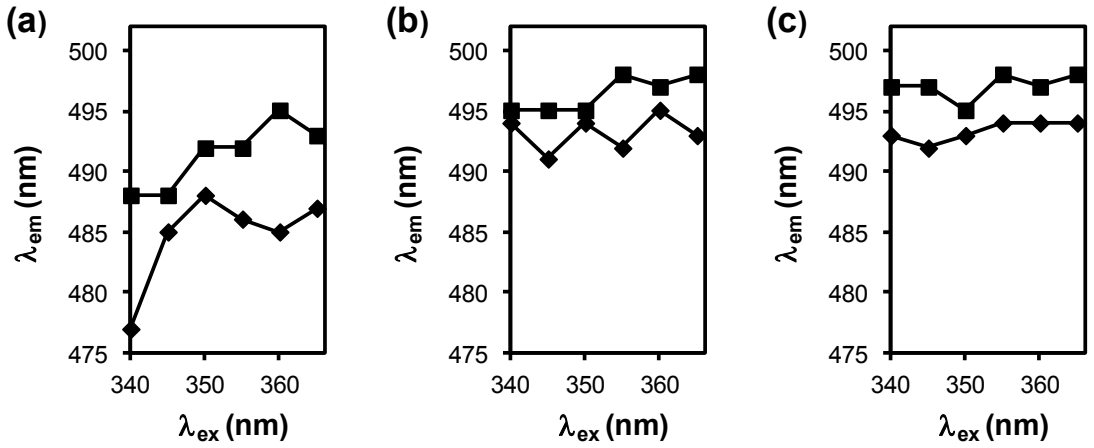

Figure 2. Effect of excitation wavelength on the emission wavelength for compounds **2** (■) and **3** (◆) in POPC/POPG membranes, with [oligocholate]/[phospholipids] = (a) 0.05%, (b) 0.5% (△), and (c) 5% (□). [Phospholipids] = 107 μM.

The conclusion from the REES is reasonable from a structural point of view. With the hydrophilic hydroxyl and amide groups pointing inside and the exterior completely hydrophobic, the cyclic trimer is more compatible with a nonpolar environment than the linear trimer, which has exposed polar groups. In order for the linear trimer to enter the hydrophobic core of the membrane, it has to either fold into the "reverse micelle-like" helix with introverted polar groups or aggregate intermolecularly to bury the polar groups. Our previous study demonstrated that the parent oligocholate foldamers (i.e., oligocholates without other building blocks in the sequence) require at least five cholate units to fold.[45] It is thus unlikely for **3** to adopt the helical conformation. At low concentrations such as 0.05 mol %, it is probably difficult for **3** to aggregate in the membrane. Most likely, the linear trimer is embedded in the membrane, with its hydrophilic faces toward water. Such a configuration satisfies the needs of both hydrophilic and hydrophobic faces of the molecule and is certainly consistent with the incompetency of the linear trimer in transporting hydrophilic guests across lipid membranes.[25,26]

REES in general decreases with increasing concentrations of the oligocholates in the membrane (Figures 2b and 2c). Apparently, when more oligocholates enter the membrane, the membrane/water interface cannot accommodate all of these amphiphilic molecules. As suggested by the leakage data, the cyclic trimer can enter the hydrophobic core of the membrane and begin to stack into the transmembrane pore. The linear trimer is completely incapable of transporting hydrophilic guests including glucose even at 5 mol % concentration in the membrane.[25] Thus, whether in the aggregated or dissociated form, the linear compound does not have pores large enough for glucose to pass through. Longer oligocholate foldamers such as hexamers are known to fold into guest-binding helices and act as carriers to shuttle guests across the membrane.[21,50] The linear trimer could not do so, evident from its lack of activity in the transport.[25,26] Because REES

demonstrates that the majority of the linear timer was *not* at the membrane/water interface above 0.5 mol % concentration, the compound must be at least partly in the hydrophobic region of the membrane. To be compatible with the nonpolar environment, the linear trimer should be in the aggregated form with the polar groups buried inside. Hydrogen bonds among the polar hydroxyl and amide groups should be the primary driving force for the aggregation.

It should be pointed out that a linear cholate trimer with flexible 4-aminobutyroyl spaces in between the cholate groups was found quite active in glucose transport.[51] The transport displayed zero-order kinetics and was attributed to tight intermolecular aggregates that have hydrophilic crevices for the glucose to "squeeze through". Since REES suggests that compound **3** aggregated at ≥0.5 mol % concentration inside the membrane, the aggregates formed by this compound must be different from those formed by the flexible cholate trimer. There is significant evidence in the literature that suggests rigid (linear) oligocholates cannot pack tightly due to the awkward shape of the molecule, the facial amphiphilicity, and the short linkages between the fused steroid rings.[51-54] To reconcile the leakage [25,26] and the REES data, the aggregates of the (rigid) linear trimer **3** must not be able to migrate easily across the bilayer membrane (otherwise they should be able to encapsulate hydrophilic guests and help their translocation). To penetrate into the hydrophobic core of the membrane without migrating to the other side, the aggregates of the linear trimer most likely equilibrate rapidly with the dissociated form, which lies at the membrane/water interface. In this way, the oligocholate never moves far away from the membrane/water interface even when it (in the aggregated form) enters the hydrophobic region of the bilayer membrane.

Notably, even at higher concentrations (Figures 2b and 2c), the emission wavelength of the cyclic trimer (■) was consistently higher than that of the linear trimer (◆). Hence, despite its deeper penetration into the hydrophobic core of the membrane, the cyclic trimer always has a

higher local polarity near its dansyl group, regardless of its aggregation state. The seemingly contradictory results make perfect sense if the cyclic compounds aggregate into the nanopore depicted in Figure 1. Essentially, although better at penetrating the hydrophobic core of the membrane due to its hydrophobic exterior, the cyclic trimer always carries a nanosized water pool with it due to its highly polar interior. These water molecules have strong preferences to interact with other water molecules instead of the lipid hydrocarbon. It is the associative interactions of these "activated" water molecules that drive the oligocholate macrocycles to stack into the transmembrane pore. In other words, it is the template effect of these water molecules that makes the macrocycles stack.

We also examined the REES at the three different concentrations of the oligocholates in cholesterol-containing membranes (Figure 3). The results overall were quite similar to those without cholesterol. Although slightly smaller REES was obtained at 0.05% of the oligocholates, the concentration-dependent aggregation and the stronger environmental polarity were both observed for the cyclic trimer.

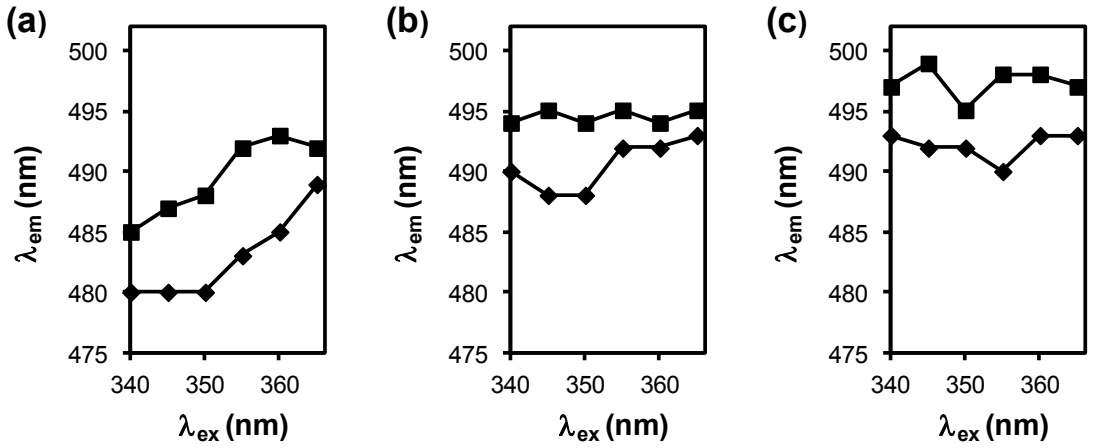

Figure 3. Effect of excitation wavelength on the emission wavelength for compounds **2** (■) and **3** (◆) in 30% cholesterol/POPC/POPG membranes, with [oligocholate]/[phospholipids] = (a) 0.05%, (b) 0.5% (△), and (c) 5% (□). [Phospholipids] = 107 μM.

Fluorescence quenching. Fluorescent quenching is a very useful technique to probe the location of the fluorophore. Depending on the solubility of the quencher, we can easily determine not only the environmental polarity around the fluorophore but also its accessibility. Because of its overall hydrophobicity, an oligocholate prefers the membrane instead of aqueous environment.[25,26] After it enters a membrane, however, it may be deep inside the hydrophobic core of the lipid bilayer or close to the surface, as indicated by the REES. From the structural point of view, to penetrate deep into the membrane, the oligocholate has to bury its polar groups by pore formation,[25,26] folding,[21,50] or intermolecular aggregation.[51] To stay at the membrane/water interface, it needs to turn its hydrophilic faces to water, while keeping its hydrophobic faces in contact with the lipid hydrocarbon.

To understand the behavior of oligocholates **2** and **3** in lipid bilayers, we monitored their fluorescence in the presence of a water-soluble (NaI) and a lipid-soluble quencher (TEMPO), respectively. If the dansyl group is located near the membrane/water interface, its emission should be quenched significantly by NaI. If the dansyl migrates inside the hydrophobic core of the membrane, it should be more accessible to the lipid-soluble TEMPO.

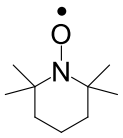

TEMPO

We performed the fluorescence quenching at two different concentrations of the oligocholates, i.e., [oligocholate]/[phospholipids] = 0.2 and 3%. Negligible glucose leakage was observed with 0.2% of macrocycle **1** in POPC/POPG liposomes and complete leakage occurred when the concentration was increased above 2 %.[25] The 0.2 and 3% concentrations, therefore, should correspond to the dissociated and aggregated forms of the cyclic trimer (**2**).

Figure 4 shows the quenching of the oligocholates by the two quenchers with [oligocholate]/[phospholipids] = 0.2%. Quenching by the water-soluble NaI implied that, although solubilized within the lipid bilayers, both compounds were accessible to NaI (Figure 4a). A significant portion of the compounds must be located at the membrane/water interface at this concentration, in agreement with the REES data. The quenching plots for both compounds displayed large downward curvature. The downward deviation from the linear Stern-Volmer plots is frequently observed in proteins in which a portion of the fluorophores is buried and inaccessible to the quencher.[37] The data may be analyzed by the modified Stern-Volmer equation,

$$F_0/(\Delta F) = F_0/(F_0 - F) = 1/(f_a K_a[Q]) + 1/f_a,$$

in which F_0 is the initial fluorescence intensity, F the fluorescence intensity after the addition of the quencher Q, f_a the assessable fraction of the fluorophore to the quencher, and K_a the Stern-Volmer quenching constant for the assessable fluorophores. As shown by Figure 5, the modification indeed afforded linear plots, regardless of the solubility of the quencher.

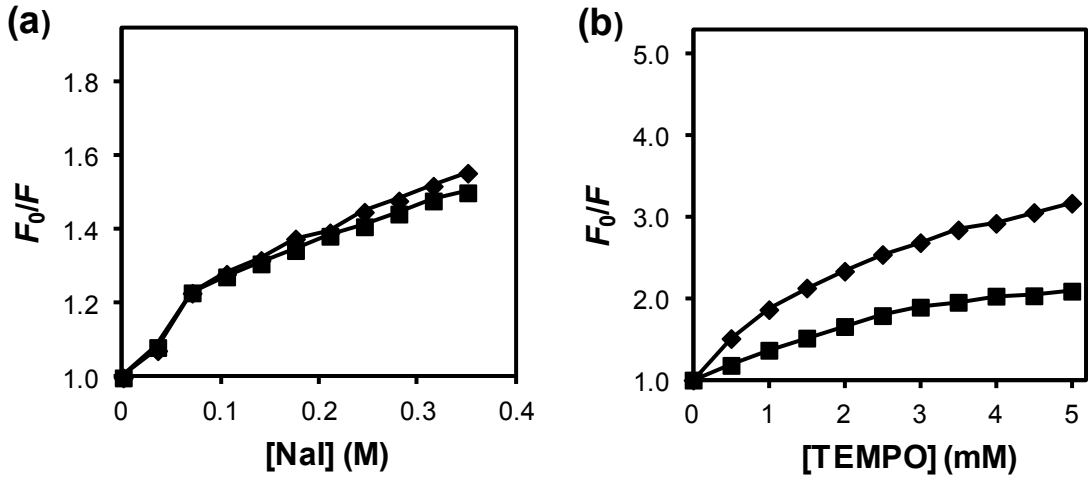

Figure 4. Fluorescence quenching of oligocholates **2** (■) and **3** (◆) using (a) NaI and (b) TEMPO as the quencher. [Oligocholate]/[phospholipids] = 0.2 %. [Phospholipids] = 107 μM.

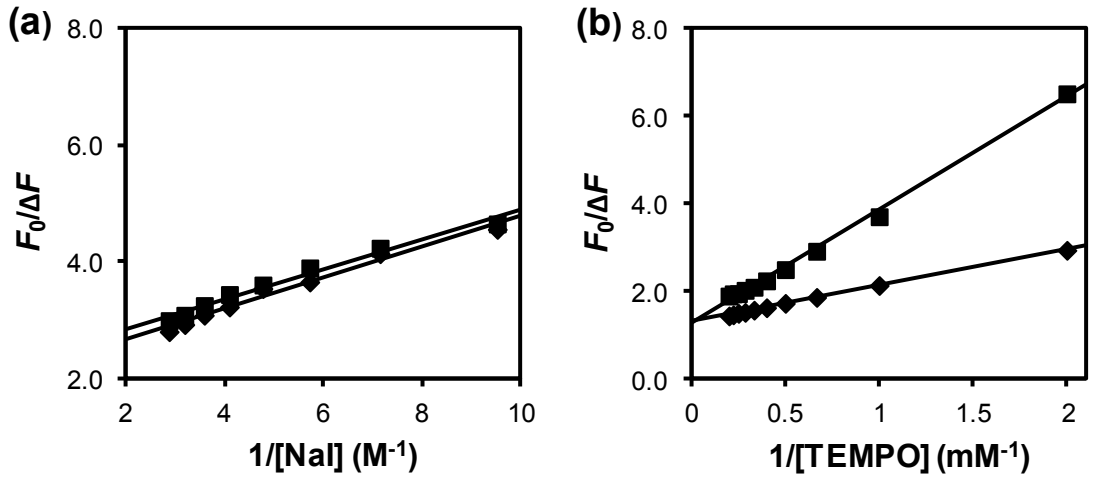

Figure 5. Modified Stern-Volmer plots oligocholates **2** (■) and **3** (◆) using (a) NaI and (b) TEMPO as the quencher. [Oligocholate]/[phospholipids] = 0.2 %. [Phospholipids] = 107 μM.

Figure 6 shows the quenching plots at the higher oligocholate concentration (i.e., 3 mol % in the membrane). The cyclic trimer is supposed to aggregate into the nanopore at this concentration.[25] As shown by Figure 6a, portions of both compounds remained accessible to NaI, although it was clear that the cyclic compound (■) was quenched much less than the linear trimer (◆). Interestingly, the situation became completely different when the lipid-soluble TEMPO was the quencher. The linear Stern-Volmer plots in Figure 6b indicate that the dansyl groups of both oligocholates were fully accessible to the organic quencher.

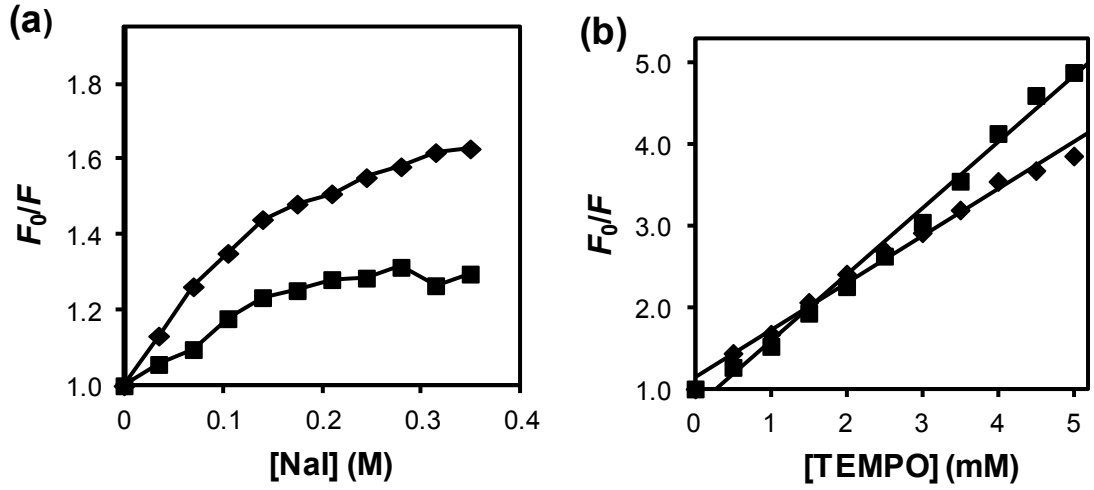

Figure 6. Fluorescence quenching of oligocholates **2** (■) and **3** (◆) using (a) NaI and (b) TEMPO as the quencher. [Oligocholate]/[phospholipids] = 3 %. [Phospholipids] = 107 μM.

Table 1 summarizes the quenching data for the two oligocholates. All the correlation coefficients, whether for the linear Stern-Volmer plots or the modified Stern Volmer plots, were at least 0.99. When the water-soluble NaI was used as the quencher, the accessible fractions (f_a) of the dansyl ranged from 30 to ~50% (entries **1**–**4**). For the oil-soluble TEMPO, the accessible fractions ranged from 76% to 100% (entries **5**–**8**).

Table 1. Quenching data obtained for compounds **2** and **3**.

entry	compound	quencher	f_a	K_a (M^{-1})
1	0.2 mol % **2**	NaI	43%	9.3
2	0.2 mol % **3**	NaI	47%	8.0
3	3 mol % **2**	NaI	30%	10.4
4	3 mol % **3**	NaI	49%	11.3
5	0.2 mol % **2**	TEMPO	77%	501
6	0.2 mol % **3**	TEMPO	76%	1580
7	3 mol % **2**	TEMPO	100%[a]	810
8	3 mol % **3**	TEMPO	100%[a]	580

[a] Linear Stern-Volmer plots were obtained (Figure 6b).

Several conclusions may be drawn from the quenching data. The overall higher f_a values for the oil-soluble quencher confirmed that the oligocholates were in a hydrophobic environment, i.e., they were in the lipid bilayer membrane. Since linear Stern-Volmer plots were obtained when NaI quenching was performed for the oligocholates in a buffer *without* any liposomes (data not shown), the membrane environment must have provided significant "shielding" to the oligocholates,

consistent with the latter's hydrophobicity. Figure 4a shows that NaI could access the two oligocholates (at 0.2 mol % concentration in the membrane) with similar probability. Quantitatively, f_a (43 and 47%) and K_a (9.3 and 8.0 M^{-1}) were both very similar for the two compounds (Table 1, entries 1–2). To the oil-soluble TEMPO quencher, the accessible fractions were experimental identical (77 and 76%, entries 5–6). These results suggest that the oligocholates were in very similar environments at this concentration, most likely at the membrane/water interface while being embedded in the membrane—similar conclusions were drawn earlier from the REES studies. It should be mentioned that the combined accessible fractions for the water- and oil-soluble quencher do not have to add up to 100%, as the fluorophores located at the membrane/water interface should be accessible to both quenchers. It is illuminating to see that both compounds were more accessible to TEMPO than to NaI, suggesting that the compounds were indeed in a hydrophobic environment.

When the concentration of the two oligocholates was increased to 3 mol %, their quenching efficiencies, as suggested by the Stern-Volmer constants (K_a), stayed largely the same (Table 1, entries **3**–**4**). The increasing concentration did not change the accessible fractions of the linear trimer for NaI either—f_a = 47 and 49% with 0.2 and 3 mol % of **3** in the membrane. On the other hand, f_a dropped sharply for the cyclic trimer, from 43 to 30% over the same concentration change. Clearly, the cyclic trimer migrated deeper into the membrane at the higher concentration, exactly as what the REES revealed earlier.

As mentioned previously, the quenching of compounds **2** and **3** by TEMPO afforded linear Stern-Volmer plots at 3 mol % concentration (Figure 6b). Both compounds, hence, became fully accessible to the lipid-soluble quencher. The results agree well with the NaI-quenching data and the REES, suggesting that both compounds migrated into the hydrophobic core of the membrane

at the concentration in the membrane. It is extremely interesting to see that f_a of the linear trimer did *not* change for NaI but increased for TEMPO at the higher concentration of the oligocholate. The data demonstrated that, even though trimer **3** became completely accessible to TEMPO at the higher concentration, the same percentage of the molecule remained close to the surface of the membrane and could be quenched by NaI. The results are in full agreement with the lack of transport activity of the linear trimer[25,26] and once again suggest that the aggregates of the linear trimer never migrated deep inside the membrane and probably equilibrated rapidly with the non-aggregated, surface-occupying form. As discussed earlier, the rapid dissociation is due to the instability of the aggregates, caused by the poor packing of awkwardly shaped oligocholates inside the membrane.[51-54]

The Stern-Volmer constants (K_a) for the cyclic and the linear trimer were quite similar with NaI as the quencher at both concentrations (Table 1, entries 1–4). With TEMPO as the quencher, the concentration effect on K_a was *opposite* for the two compounds (entries 5–8). At 0.2 mol %, K_a was 501 M^{-1} for the cyclic trimer and 1580 M^{-1} for the linear trimer.[55] The number became 810 M^{-1} for the cyclic trimer and 580 M^{-1} for the linear trimer at 3 mol % of the oligocholates. Thus, the increase of the oligocholate concentration caused a large decrease of K_a for the linear trimer (**3**) but a modest increase for the cyclic trimer (**2**). We believe that the opposite concentration effects for the two compounds are additional evidence for their different aggregations in the membrane. For the cyclic compound, aggregation takes place perpendicular to the lipid membrane and affords the transmembrane nanopore. All the dansyl groups in the stacked aggregates should be easily approachable to the lipid-soluble quencher. In fact, because some cyclic trimers will stay in the middle of the lipid bilayer according to the stacking model (Figure 1), the average quenching constant should increase as more cyclic trimers move from the surface to the interior of the

membrane. For the linear trimer, aggregation forms as the molecules hydrogen bond with one another in the nonpolar membrane. Larger aggregates are expected to move slowly in the membrane, which could be one reason for the decreased K_a. In addition, aggregation may partially bury some dansyl groups. Although these (partially buried) dansyl groups may still be accessible to TEMPO, their collision could certainly be hampered by the aggregation.

We also performed the quenching studies with 30 % cholesterol in the membrane. Both compounds became less accessible to the water-soluble NaI quencher (compare the solid and dashed lines in Figure 7a), whereas the quenching by the oil-soluble TEMPO stayed essentially the same (Figure 7b). The results agree well with the earlier data and suggest that the addition of cholesterol makes the membrane more hydrophobic. Such a membrane can better shield the oligocholates from the aqueous solution, reducing their quenching by the water-soluble NaI.

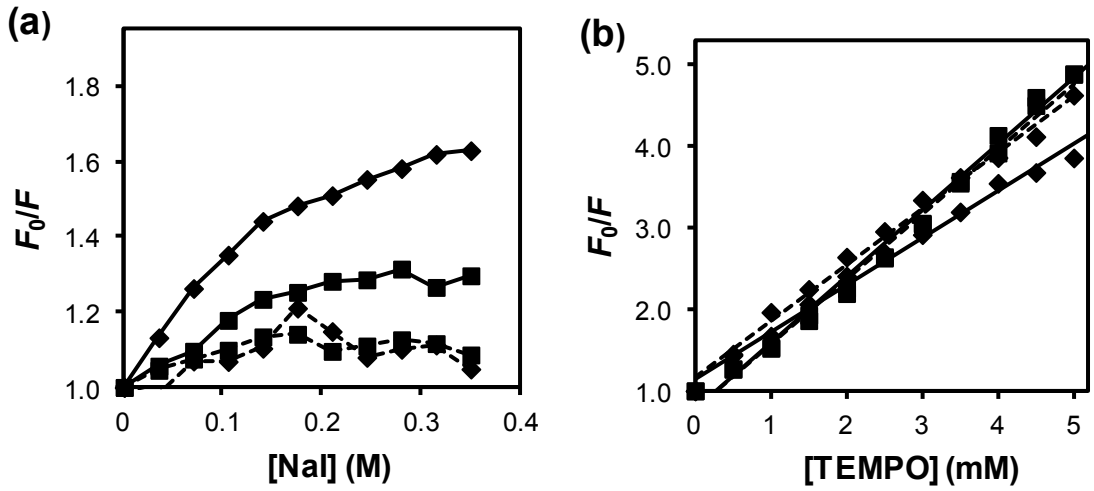

Figure 7. Fluorescence quenching of oligocholates **2** (■) and **3** (◆) using (a) NaI and (b) TEMPO as the quencher. The data points connected by solid lines were from POPC/POPG LUVs and those connected by dashed lines from 30% cholesterol/POPC/POPG LUVs. [Oligocholate]/[phospholipids] = 3 %. [Phospholipids] = 107 μM.

Conclusions

Despite the significant size of the dansyl group, the fluorescently labeled oligocholates (**2** and **3**) provided much insight into how the amphiphile topology may impact the behavior of the amphiphile in the membrane environment. The cyclic cholate trimer (**2**) has an enclosed hydrophilic cavity. The cavity is triangle-shaped with each side about 1 nm in length.[25] Being highly hydrophilic with six hydroxyl groups and three amides, the cavity needs to be filled with water instead of the lipid tails when the molecule enters the membrane. This water pool gives higher environmental polarity to the dansyl of cyclic trimer, reflected by its weaker emission intensity and longer emission wavelength in comparison to those of the linear trimer (**3**). As revealed by REES and the fluorescence quenching, the cyclic trimer can penetrate into the hydrophobic core of the membrane better than the linear trimer, carrying the nanosized water pool into the nonpolar environment. To avoid unfavorable water/hydrocarbon contact, these water molecules cluster together in the membrane, inducing the stacking of cyclic trimers in the *z*-direction and forming the transmembrane nanopore in the meantime.

Our previous leakage assays only revealed the lack of transport activity for the linear trimer.[25,26,51] The current fluorescent study afforded some mechanistic reasons for its incompetency as a membrane transporter. At low concentrations, the linear trimer (**3**) was shown by REES to prefer the membrane/water interface more than the cyclic trimer. The preference is understandable given the ability for the linear trimer to turn its hydrophilic groups to water while being embedded in the membrane. At higher concentrations, the linear trimer still has a stronger preference for the interfacial region of the membrane than the cyclic trimer. Although the TEMPO-quenching experiments demonstrated that the linear oligocholate can aggregate intermolecularly and move toward the interior of the lipid bilayer, the aggregates seem to be close to the membrane

surface and in rapid equilibrium with the dissociated compounds located on the surface. The inability of the linear trimer to move deep into the membrane is the very likely reason for its lack of transport activity and probably related to the poor packing of its intermolecular aggregate. As our previous studies revealed, loosely packed aggregates of rigid oligocholates have low stability in nonpolar environments[51,53,54] and should have difficulty moving across the membrane.

Acknowledgment is made to NSF (DMR-1005515) for supporting the research.

References

(1) Israelachvili, J. N. *Intermolecular and Surface Forces: With Applications to Colloidal and Biological Systems*; Academic Press: London ; Orlando, Fl, 1985.

(2) Cheng, Y.; Ho, D. M.; Gottlieb, C. R.; Kahne, D.; Bruck, M. A. Facial Amphiphiles. *J. Am. Chem. Soc.* **1992**, *114*, 7319-7320.

(3) McQuade, D. T.; Barrett, D. G.; Desper, J. M.; Hayashi, R. K.; Gellman, S. H. Effects of Amphiphilic Topology on Self-Association in Solution, at the Air-Water Interface, and in the Solid State. *J. Am. Chem. Soc.* **1995**, *117*, 4862-4869.

(4) Menger, F. M.; Sorrells, J. L. A Non-Steroidal Facial Amphiphile. *J. Am. Chem. Soc.* **2006**, *128*, 4960-4961.

(5) Virtanen, E.; Kolehmainen, E. Use of Bile Acids in Pharmacological and Supramolecular Applications. *Eur. J. Org. Chem.* **2004**, *2004*, 3385-3399.

(6) Zhu, X. X.; Nichifor, M. Polymeric Materials Containing Bile Acids. *Acc. Chem. Res.* **2002**, *35*, 539-546.

(7) Zhao, Y. Facial Amphiphiles in Molecular Recognition: From Unusual Aggregates to Solvophobically Driven Foldamers. *Curr. Opin. Colloid Interface Sci.* **2007**, *12*, 92-97.

(8) Janout, V.; Lanier, M.; Regen, S. L. Molecular Umbrellas. *J. Am. Chem. Soc.* **1996**, *118*, 1573-1574.

(9) Janout, V.; Jing, B. W.; Staina, I. V.; Regen, S. L. Selective Transport of Atp across a Phospholipid Bilayer by a Molecular Umbrella. *J. Am. Chem. Soc.* **2003**, *125*, 4436-4437.

(10) Janout, V.; Regen, S. L. A Needle-and-Thread Approach to Bilayer Transport: Permeation of a Molecular Umbrella-Oligonucleotide Conjugate across a Phospholipid Membrane. *J. Am. Chem. Soc.* **2005**, *127*, 22-23.

(11) Ryu, E.-H.; Zhao, Y. Environmentally Responsive Molecular Baskets: Unimolecular Mimics of Both Micelles and Reversed Micelles. *Org. Lett.* **2004**, *6*, 3187-3189.

(12) Ryu, E.-H.; Zhao, Y. An Amphiphilic Molecular Basket Sensitive to Both Solvent Changes and Uv Irradiation. *J. Org. Chem.* **2006**, *71*, 9491-9494.

(13) Zhou, Y. B.; Ryu, E.-H.; Zhao, Y.; Woo, L. K. Solvent-Responsive Metalloporphyrins: Binding and Catalysis. *Organometallics* **2007**, *26*, 358-364.

(14) Luo, J. T.; Chen, Y. L.; Zhu, X. X. Invertible Amphiphilic Molecular Pockets Made of Cholic Acid. *Langmuir* **2009**, *25*, 10913-10917.

(15) Zhang, J. W.; Luo, J. T.; Zhu, X. X.; Junk, M. J. N.; Hinderberger, D. Molecular Pockets Derived from Cholic Acid as Chemosensors for Metal Ions. *Langmuir* **2010**, *26*, 2958-2962.

(16) Nelson, J. C.; Saven, J. G.; Moore, J. S.; Wolynes, P. G. Solvophobically Driven Folding of Nonbiological Oligomers. *Science* **1997**, *277*, 1793-1796.

(17) Stone, M. T.; Moore, J. S. A Water-Soluble M-Phenylene Ethynylene Foldamer. *Org. Lett.* **2004**, *6*, 469-472.

(18) Stone, M. T.; Heemstra, J. M.; Moore, J. S. The Chain-Length Dependence Test. *Acc. Chem. Res.* **2006**, *39*, 11-20.

(19) Zhao, Y.; Zhong, Z.; Ryu, E.-H. Preferential Solvation within Hydrophilic Nanocavities and Its Effect on the Folding of Cholate Foldamers. *J. Am. Chem. Soc.* **2007**, *129*, 218-225.

(20) Cho, H.; Zhong, Z.; Zhao, Y. A Dmap-Functionalized Oligocholate Foldamer for Solvent-Responsive Catalysis. *Tetrahedron* **2009**, *65*, 7311-7316.

(21) Cho, H.; Zhao, Y. Environmental Effects Dominate the Folding of Oligocholates in Solution, Surfactant Micelles, and Lipid Membranes. *J. Am. Chem. Soc.* **2010**, *132*, 9890-9899.

(22) Vutukuri, D. R.; Basu, S.; Thayumanavan, S. Dendrimers with Both Polar and Apolar Nanocontainer Characteristics. *J. Am. Chem. Soc.* **2004**, *126*, 15636-15637.

(23) Aathimanikandan, S. V.; Savariar, E. N.; Thayumanavan, S. Temperature-Sensitive Dendritic Micelles. *J. Am. Chem. Soc.* **2005**, *127*, 14922-14929.

(24) R. Ramireddy, R.; Raghupathi, K. R.; Torres, D. A.; Thayumanavan, S. Stimuli Sensitive Amphiphilic Dendrimers. *New J. Chem.* **2012**, *36*.

(25) Cho, H.; Widanapathirana, L.; Zhao, Y. Water-Templated Transmembrane Nanopores from Shape-Persistent Oligocholate Macrocycles. *J. Am. Chem. Soc.* **2011**, *133*, 141-147.

(26) Cho, H.; Zhao, Y. Translocation of Hydrophilic Molecules across Lipid Bilayers by Salt-Bridged Oligocholates. *Langmuir* **2011**, *27*, 4936-4944.

(27) Matile, S.; Som, A.; Sorde, N. Recent Synthetic Ion Channels and Pores. *Tetrahedron* **2004**, *60*, 6405-6435.

(28) Sisson, A. L.; Shah, M. R.; Bhosale, S.; Matile, S. Synthetic Ion Channels and Pores (2004-2005). *Chem. Soc. Rev.* **2006**, *35*, 1269-1286.

(29) Granja, J. R.; Ghadiri, M. R. Channel-Mediated Transport of Glucose across Lipid Bilayers. *J. Am. Chem. Soc.* **1994**, *116*, 10785-10786.

(30) Sakai, N.; Mareda, J.; Matile, S. Rigid-Rod Molecules in Biomembrane Models: From Hydrogen-Bonded Chains to Synthetic Multifunctional Pores. *Acc. Chem. Res.* **2005**, *38*, 79-87.

(31) Das, G.; Talukdar, P.; Matile, S. Fluorometric Detection of Enzyme Activity with Synthetic Supramolecular Pores. *Science* **2002**, *298*, 1600-1602.

(32) Sakai, N.; Sorde, N.; Matile, S. Synthetic Catalytic Pores. *J. Am. Chem. Soc.* **2003**, *125*, 7776-7777.

(33) Helsel, A. J.; Brown, A. L.; Yamato, K.; Feng, W.; Yuan, L. H.; Clements, A. J.; Harding, S. V.; Szabo, G.; Shao, Z. F.; Gong, B. Highly Conducting Transmembrane Pores Formed by Aromatic Oligoamide Macrocycles. *J. Am. Chem. Soc.* **2008**, *130*, 15784-15785.

(34) Ma, L.; Melegari, M.; Colombini, M.; Davis, J. T. Large and Stable Transmembrane Pores from Guanosine-Bile Acid Conjugates. *J. Am. Chem. Soc.* **2008**, *130*, 2938-2939.

(35) Satake, A.; Yamamura, M.; Oda, M.; Kobuke, Y. Transmembrane Nanopores from Porphyrin Supramolecules. *J. Am. Chem. Soc.* **2008**, *130*, 6314-6315.

(36) Fyles, T. M.; Tong, C. C. Long-Lived and Highly Conducting Ion Channels Formed by Lipophilic Ethylenediamine Palladium(Ii) Complexes. *New. J. Chem.* **2007**, *31*, 655-661.

(37) Lakowicz, J. R. *Principles of Fluorescence Spectroscopy*; 2nd ed.; Kluwer Academic/Plenum: New York, 1999.

(38) Westmark, P. R.; Smith, B. D. Boronic Acids Selectively Facilitate Glucose-Transport through a Lipid Bilayer. *J. Am. Chem. Soc.* **1994**, *116*, 9343-9344.

(39) Nezil, F. A.; Bloom, M. Combined Influence of Cholesterol and Synthetic Amphiphillic Peptides Upon Bilayer Thickness in Model Membranes. *Biophys. J.* **1992**, *61*, 1176-1183.

(40) Holthuis, J. C. M.; van Meer, G.; Huitema, K. Lipid Microdomains, Lipid Translocation and the Organization of Intracellular Membrane Transport (Review). *Mol. Membr. Biol.* **2003**, *20*, 231-241.

(41) Demel, R. A.; Bruckdor, K. R.; van Deene, L. L. Effect of Sterol Structure on Permeability of Liposomes to Glucose, Glycerol and Rb^{+}. *Biochim. Biophys. Acta* **1972**, *255*, 321-330.

(42) Papahadjopoulos, D.; Nir, S.; Ohki, S. Permeability Properties of Phospholipid Membranes - Effect of Cholesterol and Temperature. *Biochim. Biophys. Acta* **1972**, *266*, 561-583.

(43) Li, Y. H.; Chan, L. M.; Tyer, L.; Moody, R. T.; Himel, C. M.; Hercules, D. M. Study of Solvent Effects on Fluorescence of 1-(Dimethylamino)-5-Naphthalenesulfonic Acid and Related Compounds. *J. Am. Chem. Soc.* **1975**, *97*, 3118-3126.

(44) Zhao, Y.; Zhong, Z. Detection of Hg^{2+} in Aqueous Solutions with a Foldamer-Based Fluorescent Sensor Modulated by Surfactant Micelles. *Org. Lett.* **2006**, *8*, 4715-4717.

(45) Zhao, Y.; Zhong, Z. Oligomeric Cholates: Amphiphilic Foldamers with Nanometer-Sized Hydrophilic Cavities. *J. Am. Chem. Soc.* **2005**, *127*, 17894-17901.

(46) Mukherjee, S.; Chattopadhyay, A. Wavelength-Selective Fluorescence as a Novel Tool to Study Organization and Dynamics in Complex Biological Systems. *J. Fluorescence* **1995**, *5*, 237-246.

(47) Demchenko, A. P. The Red-Edge Effects: 30 Years of Exploration. *Luminescence* **2002**, *17*, 19-42.

(48) Chattopadhyay, A. Exploring Membrane Organization and Dynamics by the Wavelength-Selective Fluorescence Approach. *Chem. Phys. Lipids* **2003**, *122*, 3-17.

(49) Haldar, S.; Chaudhuri, A.; Chattopadhyay, A. Organization and Dynamics of Membrane Probes and Proteins Utilizing the Red Edge Excitation Shift. *J. Phys. Chem. B* **2011**, *115*, 5693-5706.

(50) Zhang, S.; Zhao, Y. Oligocholate Foldamers as Carriers for Hydrophilic Molecules across Lipid Bilayers. *Chem. -Eur. J.* **2011**, *17*, 12444-12451.

(51) Zhang, S.; Zhao, Y. Flexible Oligocholate Foldamers as Membrane Transporters and Their Guest-Dependent Transport Mechanism. *Org. Biomol. Chem.* **2012**, *10*.

(52) Ryu, E.-H.; Ellern, A.; Zhao, Y. High Guest Inclusion in 3 Beta-Amino-7 Alpha,12 Alpha-Dihydroxycholan-24-Oic Acid Enabled by Charge-Assisted Hydrogen Bonds. *Tetrahedron* **2006**, *62*, 6808-6813.

(53) Zhao, Y. Spacer-Dependent Folding and Aggregation of Oligocholates in Sds Micelles. *J. Org. Chem.* **2009**, *74*, 7470-7480.

(54) Wu, J.; Pan, X.; Zhao, Y. Time-Dependent Shrinkage of Polymeric Micelles of Amphiphilic Block Copolymers Containing Semirigid Oligocholate Hydrophobes. *J. Colloid Interface Sci.* **2011**, *353*, 420-425.

(55) It is unclear to us at this point why the TEMPO quenching constant was higher for the linear than the cyclic trimer. Different lateral mobility, molecular size, and location of the dansyl groups all could have contributed to the difference.

CHAPTER 6. AGGREGATION AND DYNAMICS OF OLIGOCHOLATE TRANSPORTERS IN PHOSPHOLIPID BILAYERS REVEALED BY SOLID-STATE NMR SPECTROSCOPY

A paper published in *Langmuir* **2012**, *28,* 17071−17078.

(Reproduced with permission from *Langmuir* **2012**, *28,* 17071−17078.

Tuo Wang, Lakmini Widanapathirana, Yan Zhao and Mei Hong

Abstract

Macrocycles made of cholate building blocks were previously found to transport glucose readily across lipid bilayers. In this study, a ^{15}N, $^{13}C\alpha$-labeled glycine was inserted into a cyclic cholate trimer and attached at the end of a linear trimer, respectively. The isotopic labeling allowed us to use solid-state NMR spectroscopy to study the dynamics, aggregation, and depth of insertion of these compounds in lipid membranes. The cyclic compound was found to be mostly immobilized in DLPC, POPC/POPG, and POPC/POPG/cholesterol membranes, whereas the linear trimer displayed large-amplitude motion that depended on the membrane thickness and viscosity. ^{13}C-

detected ^{1}H spin diffusion experiments revealed the depth of insertion of the compounds in the membranes, as well as their contact with water molecules. The data support a consistent stacking model for the cholate macrocycles in lipid membranes, driven by the hydrophobic interactions of the water molecules in the interior of the macrocycles. The study also shows a strong preference of the linear trimer for the membrane surface, consistent with its lack of transport activity in earlier liposome leakage assays.

Introduction

Membrane proteins perform vital biological functions including photosynthesis, ion conduction, signal transduction, and immune response and, not surprisingly, account for nearly 50% of all drug targets.[1,2] Protein-based pores and channels are frequently used by cells to control the traffic across their membranes.[3−5] Structural characterization of these proteins is essential to a detailed understanding of molecular transport across lipid membranes but is hampered by the difficulty in expressing and crystallizing membrane proteins in general. The characterization sometimes is difficult also because the structure of the active transporter may vary with lipid composition and the presence of other proteins or ligands.

Chemists can contribute to the understanding of membrane transport from a different perspective. By studying synthetic pore-forming materials, they develop a fundamental understanding of the self-assembling mechanism involved in pore formation.[6−12] Because similar covalent and noncovalent forces are involved in both biological and synthetic nanopores, learning from one can shed light on the other. In addition, structure− activity correlation is more straightforward in simpler synthetic pores, making it easier to extract the fundamental principles that might operate in both systems. Furthermore, synthetic pores, especially those opened and closed (i.e., gated) by chemical or physical stimuli, have practical applications such as delivery of

hydrophilic molecules across cell membranes,[8–12] sensing,[13] DNA sequencing,[14–19] and catalysis.[20]

Recently, we extended the solvophobic folding of linear oligocholate foldamers in organic solution to the membrane environment and created synthetic nanopores formed by oligocholate macrocycles.[21,22] The driving force for these nanopores differs significantly from those in reported synthetic nanopores that typically rely on hydrogen bonds,[20,23–25] aromatic interactions,[26,27] or metal−ligand coordination[28,29] for assembly. Amphiphilic macrocycles such as 1 and 2 have a highly polar interior that tends to carry a pocket of water. When the molecules enter a lipid bilayer, the internal water molecules serve to solvate the polar amide and hydroxyl groups in the nonpolar membrane. For a non-aggregated macrocycle, however, these water molecules are exposed to hydrocarbon on one side of the macrocycle if the molecule lies near the membrane surface and on both sides if it penetrates into the membrane (Figure 1). Such unfavorable hydrophilic−hydrophobic contact can be minimized if multiple macrocycles stack over one another to form a transmembrane (TM) pore. The arrangement allows the water molecules inside the macrocycles to solvate the polar groups of the cholates and still exchange with the bulk water readily. The solvent exchange is entropically favorable to the pore formation. Indeed, it is known that, in some cases, the (entropic) cost for trapping a single water molecule can be as high as 2 kcal/ mol.[30]

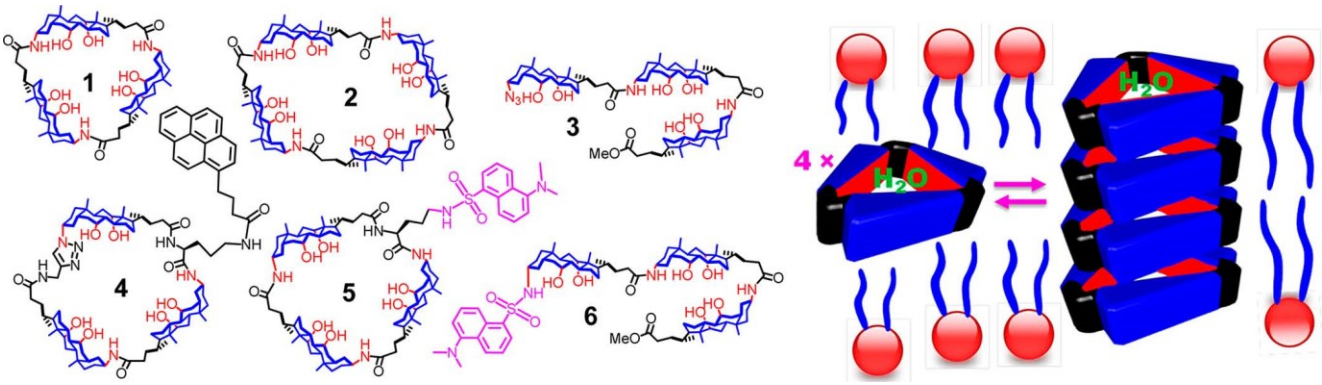

Figure 1. Structures of cyclic and linear oligocholates and the idealized pore formation of oligocholate macrocycles in a lipid bilayer membrane.

The main support for the hydrophobically driven pore formation so far was from leakage assays.[21,22] Spectroscopic evidence was also obtained from the excimer emission of pyrene[21,31] labeled macrocycles such as 4. More recently, we took advantage of the environmental sensitivity of the dansyl group and studied compounds 5 and 6 by a number of fluorescence techniques. The study yielded significant insight into the relationship between the amphiphile topology and its aggregation in the membrane environment.[32]

Solid-state NMR spectroscopy is a powerful technique to study structure, dynamics, and topology of membrane-bound proteins and other macromolecules.[33,34] ^{13}C and ^{15}N chemical shifts give information about the conformation of the membrane-bound species while lipid−protein interactions can be investigated by using various 2D correlation NMR experiments. In particular, ^{1}H spin diffusion from lipid acyl chains or water to the macromolecule of interest can afford semiquantitative information about the depth of insertion and water proximity of the macromolecules, respectively.[35,36]

In this paper, we prepared a cyclic trimer (**7**) and a linear trimer (**8**) containing a ^{15}N, $^{13}C\alpha$-labeled glycine unit. These compounds are referred to as the cyclic trimer (CT) and linear trimer (LT), respectively. The isotope label allowed us to measure the dynamics, aggregation, and depth of insertion of these oligocholates in lipid membranes using solid-state NMR spectroscopy. Previously, incorporation of a single α-amino acid residue in the oligocholate macrocycle was found to be well-tolerated by the pore formation.[31] In comparison to **5** and **6**, the glycine-containing

compounds represent better models for the parent compounds (i.e., 1 and **3**), due to the small size of the label.

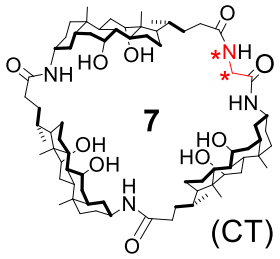

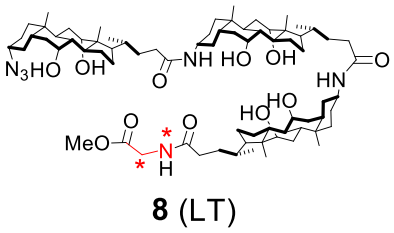

Experimental Section

Synthesis of Compound 8 (LT). The carboxylic acid derivative of **3** (150 mg, 0.122 mmol), glycine methyl ester hydrochloride (31 mg, 0.244 mmol), benzotriazole-1-yl-oxy-tris(dimethylamino)phosphonium hexafluorophosphate (BOP, 135 mg, 0.305 mmol), and 1-hydroxybenzotriazole (HOBt, 42 mg, 0.305 mmol) were dissolved in DMF (0.5 mL), followed by the addition of N,N-diisopropylethylamine (DIPEA, 0.17 mL, 0.976 mmol). The mixture was allowed to react in a microwave reactor at 100 °C for 45 min and poured into dilute HCl aqueous solution (0.05 M, 200 mL). The precipitate formed was collected by suction filtration, washed with water, dried in air, and purified by column chromatography over silica gel with 8:1 CH_2Cl_2/ CH_3OH as the eluent to afford an ivory powder (140 mg, 89%). ^{1}H NMR (400 MHz, $CD_3OD/CDCl_3$ = 1:1, δ) 4.09 (s, 1H), 3.94 (br, 3H), 3.79 (br, 3H), 3.74 (s, 1H), 3.71 (s, 3H), 3.53 (m, 2H), 3.16 (m, 1H), 2.36−0.93 (a series of m), 0.90 (s, 9H), 0.68 (m, 9H). ^{13}C NMR (100 MHz, $CDCl_3/CD_3OD$ = 1:1, δ) 175.8, 174.0, 170.4, 73.0, 68.0, 61.7, 49.8, 47.1, 46.5, 42.3, 41.8, 41.1, 40.9, 39.7, 36.4, 36.1, 35.7, 35.6, 35.0, 34.7, 33.5, 33.0, 23.2, 22.6, 17.1, 12.1. ESI-HRMS (m/z): $[M+H]^+$ calcd for $C_{74}[^{13}C]H_{123}N_5[^{15}N]O_{11}$ 1285.9248, found 1285.9217.

Synthesis of Compound 7 (CT). Compound **8** (100 mg, 0.078 mmol) and triphenylphosphine

(31 mg, 0.117 mmol) were dissolved in MeOH (10 mL). The reaction mixture was heated to reflux overnight. The solvent was removed by rotary evaporation. The residue was purified by column chromatography over silica gel with 15:1 CH_2Cl_2/ CH_3OH and 6:1:0.1 CH_2Cl_2/CH_3OH/Et_3N as the eluents to afford an off-white powder (95 mg, 97%). This product was dissolved in MeOH (3 mL) and a solution of 2 M LiOH (0.4 mL, 0.754 mmol) was added. The reaction was stirred at room temperature and monitored by TLC. After the hydrolysis was complete, the organic solvent was removed by rotary evaporation. After addition of a dilute HCl solution (30 mL, 0.05 M), the precipitate formed was collected by centrifugation, washed with cold water, and dried in vacuo. A portion of the hydrolyzed compound (50 mg, 0.040 mmol), BOP (89 mg, 0.201 mmol), and HOBT (27 mg, 0.201 mmol) were dissolved in DMF (40 mL), followed by the addition of DIPEA (56 μL, 0.321 mmol). The mixture was allowed to react in a microwave reactor at 100 °C for 1 h and poured into dilute HCl aqueous solution (0.05 M, 100 mL). The precipitate formed was collected by suction filtration, washed with water, dried in air, and purified by column chromatography over silica gel with 10:1 CH_2Cl_2/CH_3OH as the eluent to afford an ivory powder (43 mg, 86%). ^{1}H NMR (400 MHz, CD_3OD/ $CDCl_3$ = 1:1, δ) 3.94 (br, 3H), 3.79 (br, 3H), 3.51 (m, 4H), 3.36 (s, 2H), 3.15 (m, 1H), 2.34−0.80 (a series of m), 0.68 (s, 9H). ^{13}C NMR (100 MHz, $CDCl_3$/CD_3OD = 1:1, δ) 174.61, 72.62, 67.72, 45.98, 43.39, 43.27, 43.25, 41.79, 41.48, 40.71, 40.58, 39.25, 35.88, 35.59, 34.63, 34.57, 34.41,34.32, 27.97, 26.61, 26.44, 26.24, 22.86, 22.75, 22.10, 16.83, 16.68, 8.11. ESI-HRMS (m/z): $[M + Na]^+$ calcd for $C_{73}[^{13}C]H_{119}N_3[^{15}N]O_{10}Na$ 1249.8969, found 1249.8799.

Membrane Sample Preparation. Three types of lipid membranes were used to reconstitute the oligocholates: 1,2-didodecanoyl-snglycero-3-phosphocholine (DLPC), 1-palmitoyl-2-oleoyl-sn-glycero-3phosphocholine (POPC) 1-palmitoyl-2-oleoyl-sn-glycero-3-phospho(1′-rac-glycerol) (POPG) (10:1 molar ratio), and POPC/POPG/ cholesterol (10:1:2.5 molar ratio). The trimer/lipid

molar ratio was 1:7.5 for the POPC/POPG membrane, both with and without cholesterol, and 1:9.2 for the DLPC sample. These values corresponded to the same mass ratio of about 1:4.5 between the oligocholates and the lipids. Phospholipids, cholesterol, CT, and LT were dissolved in chloroform, mixed, and dried under a stream of nitrogen gas to form a film. The mixture was suspended in pH 7.5 Tris buffer (10 mM Tris base, 1 mM EDTA, 0.1 mM NaN_3), vortexed, and dialyzed against buffer for one day at room temperature. The dialysis was used to reduce the salt concentration. The suspension was centrifuged at 150 000 g for 4 h to obtain a homogeneous membrane pellet and allowed to equilibrate to 35 wt % hydration. The pellet was then packed into a 4 mm magic-anglespinning (MAS) rotor for solid-state NMR experiments.

Solid-State NMR Experiments. All NMR experiments were conducted at a 9.4 T Bruker DSX-400 spectrometer operating at a Larmor frequency of 400.49 MHz for ^{1}H and 100.72 MHz for ^{13}C. Typical radiofrequency pulse lengths were 4−5 μs for ^{1}H and 5 μs for ^{13}C. ^{13}C chemical shifts were referenced to the ^{13}CO signal of α-Gly at 176.465 ppm on the TMS scale.

$^{13}C-^{1}H$ dipolar couplings were measured with use of the 2D dipolar-chemical-shift (DIPSHIFT) correlation experiments under 3.5 kHz MAS at 298 K.[37,38] ^{1}H homonuclear decoupling was achieved by using the MREV-8 sequence with a ^{1}H 105° pulse length of 4.0 μs.[39] The t1 dimension was fit to give the apparent coupling, which was divided by the theoretical MREV-8 scaling factor of 0.47 to obtain the true dipolar coupling. The order parameter SCH was calculated as the ratio of true couplings to rigid limit value, 22.7 kHz. The model compound formyl-MLF was used to verify the MREV-8 scaling factor.

2D ^{13}C-detected ^{1}H spin diffusion experiments were carried out to determine the depth of insertion and water accessibility of CT and LT. This method has been well-established for

measuring the distances of proteins to the center of the lipid bilayer and to water.[40] The ^{1}H magnetization from mobile lipid chains and water was first selected by using a $^{1}HT_2$ filter and was then transferred to the rigid oligocholates during a mixing period (tm).A $^{1}H180°$ pulse was applied in the middle of the T2 filter to refocus the isotropic chemical shift. Since the intermolecular distances depend on the magnetization transfer rates, semiquantitative distances can be obtained by fitting the $^{1}H-^{13}C$ cross-peak buildup as a function of tm. All samples were measured under 5 kHz MAS above the phase-transition temperature of the lipid membrane. The CT samples were measured at 298 K while the LT sample was measured at 278 K to immobilize the polymer while still retaining the ^{1}H magnetization of water and lipid chains.

Results and Discussion.

Figure 2 shows the 1D ^{13}C cross-polarization (CP) MAS spectra of CT and LT, where the labeled $^{13}C\alpha$ signal is well-resolved from the natural-abundance lipid ^{13}C signals.

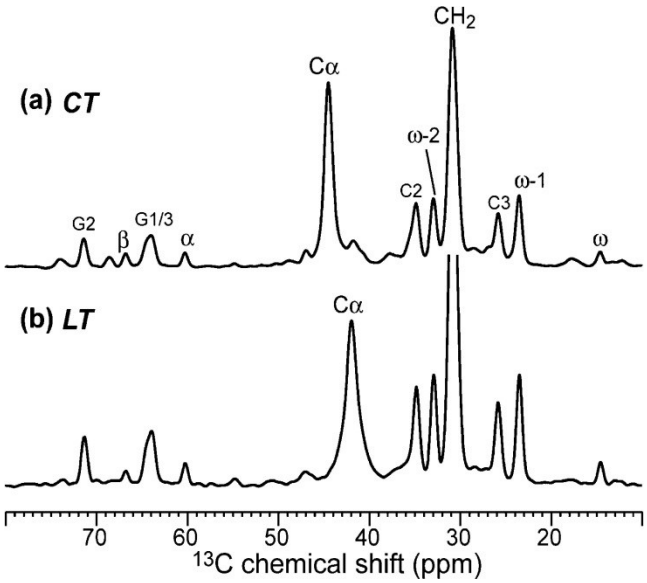

Figure 2. Representative 1D ^{13}C CP-MAS spectra of the cyclic timer (a) and linear trimer (b) in

the DLPC bilayer. The spectra were measured at 298 K under 5 kHz MAS. The single ^{13}C label gives a well-resolved peak at 45 ppm for CT and 42 ppm for LT.

The ^{13}C chemical shifts for the CT (45 ppm) and LT (42 ppm) are different due to the different chemical structures: the Cα is connected to two amide groups in CT while sandwiched between an amide and a methyl ester in LT. The well-resolved signal of the ^{13}C label allowed us to probe the dynamics and depth of insertion of the two oligocholates. Although the effect of the oligocholates on the lipid dynamics is not the focus of this work, the lipid ^{13}C signals in the above spectra, as well as the ^{1}H and ^{31}P spectra of the lipids (data not shown), indicate little change of lipid dynamics in the presence of the oligocholates.

Dynamics of CT and LT in Different Membranes. Among the three membranes used, DLPC is the thinnest and has a low phase-transition temperature of −2 °C. The POPC/POPG membrane is thicker but has a similar phase-transition temperature as DLPC bilayers. The POPC/POPG/cholesterol membrane has the highest membrane viscosity and thickness. The choice of the three lipid systems was the same as in our previous study.[21] The monounsaturated POPC represents the dominant lipids in the plasma membranes of eukaryotic cells.[41] POPG was added to increase the colloidal stability of the liposomes in our leakage assays.[21] Inclusion of cholesterol into the POPC/POPG membrane is known to increase its hydrophobicity and hydrophobic thickness[41] but, counterintuitively, enhanced the transmembrane movement of glucose induced by **1** and **2**.[21] Since hydrophobic interactions are hypothesized to drive the stacking of the oligocholate macrocycles, DLPC was chosen for its lower hydrophobicity.[42] The glucose leakage from POPC/POPG liposomes reached 100% in 30 min with >1 mol % cyclic trimer **1** in the membrane.[21]

Thus, CT is expected to be well above its critical aggregation concentration in the membrane at [oligocholate]/[lipids] = 1:7.5 used for the NMR studies. Since the oligocholates are insoluble in water, we could not add CT and LT to preformed liposomes at such high oligocholate concentrations. Instead, by premixing the lipids and the oligocholates before film formation, we could ensure that the oligocholates were well-dispersed in the membranes.

To determine the mobility of CT and LT in various membranes, we measured the $^{13}C-^{1}H$ dipolar couplings using the DIPSHIFT experiment.[38] These experiments were conducted at 298 K, above the phase-transition temperatures of the membranes. Figures 3 and 4 show the $^{13}C-^{1}H$ dipolar dephasing curves of CT and LT, respectively. In all three membranes, CT exhibited much deeper dephasing than LT, indicating larger dipolar couplings. The order parameters were >0.8 for CT and ~0.5 for LT. Therefore, CT was mostly immobilized in the membranes while LT underwent large-amplitude motions. Notably, the membrane thickness and viscosity had little effect on the order parameters of CT. This is interesting, because both leakage assays and fluorescent studies showed that the stacking of the cholate macrocycles increased in the order of DLPC < POPC/POPG < POPC/POPG/cholesterol.[21,22] Thus, the different aggregational tendency of CT in these membranes was insufficient to cause dynamic differences. Because the mobility of CT was inferred from the labeled glycine, it is possible that the slow motion simply results from the rigid, cyclic structure.

The dynamic nature of LT is in agreement with our previous findings. Fluorescent data suggested that the linear trimer had a stronger preference for the membrane surface than the cyclic analogue.[32] Even though the linear trimer can aggregate intermolecularly at high concentrations and migrate into the hydrophobic core of the membrane, the aggregates seem to be quite unstable and in rapid equilibrium with the surface-bound species, which are expected to be quite mobile.

The dynamics of LT observed in the $^{13}C-^{1}H$ dipolar coupling data is consistent with its surface binding. As long as the aggregation− deaggregation is fast on the NMR time scale and the aggregated LT represents a small population of all the LT molecules, we would expect relatively fast motion for the linear trimer.

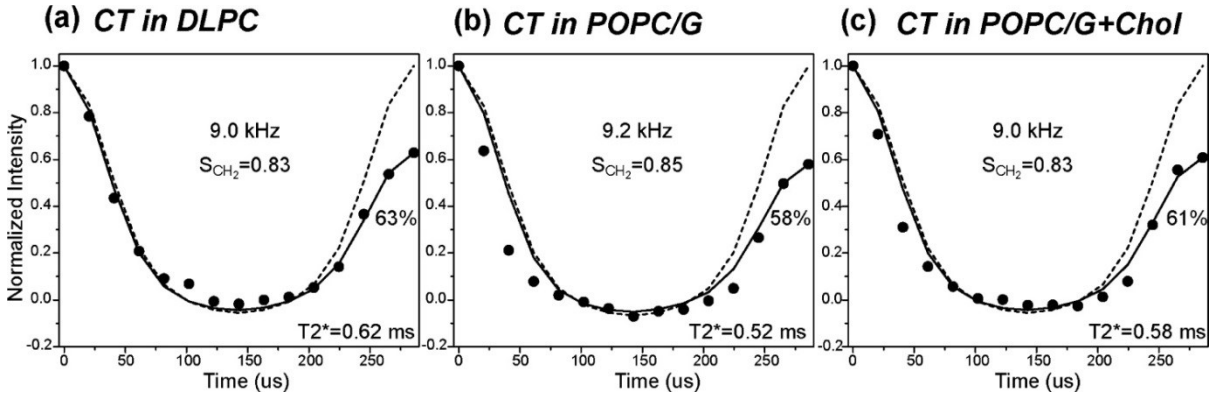

Figure 3. $^{13}C-^{1}H$ dipolar couplings of CT in (a) DLPC, (b) POPC/POPG, and (c) POPC/POPG/cholesterol bilayers to determine CT dynamics in the membrane. All data were measured at 298 K under 3.5 kHz MAS. The solid and dashed lines were best-fit simulations with and without an empirical T_2 decay. The intensity of the last time point relative to the first time point is indicated, along with the apparent T_2. All three CT samples showed dipolar order parameter of ~0.84, indicating small-amplitude motion.

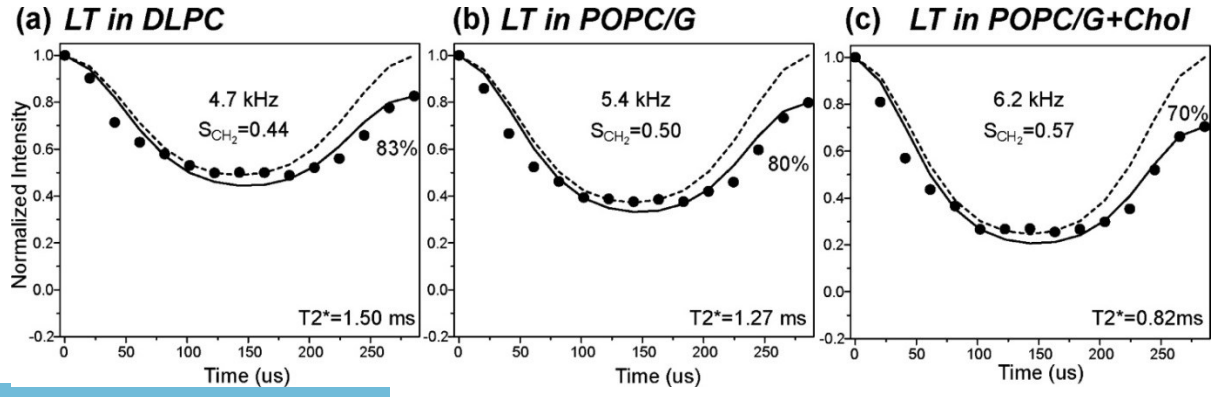

Figure 4. $^{13}C-^{1}H$ dipolar couplings of LT in (a) DLPC, (b) POPC/POPG, and (c) POPC/POPG/cholesterol bilayers. Experimental conditions and symbols were the same as in Figure 3. LT had significantly weaker dipolar couplings and smaller order parameter than CT, indicating large-amplitude motion in all three membranes.

As shown by Figure 4, the LT order parameters increased significantly from DLPC (0.44) to POPC/POPG/cholesterol (0.57). Hence, LT becomes less mobile as the membrane becomes more viscous, thicker, and more hydrophobic. The lower mobility may be caused by the reduced mobility of both the surface-bound LT and the intermolecular aggregates located deeper in the membrane in a more viscous environment. Another contribution might come from the membrane-dependent aggregation of the linear trimer. As the hydrophobicity of the membrane increases from DLPC to POPC/POPG and then to POPC/POPG/cholesterol, the hydrogen bonds among the polar groups of the aggregated oligocholates become stronger. These stronger hydrogen bonds are expected not only to enhance the stability of the aggregates but also to slow down the deaggregation process-both factors should decrease the mobility of LT.

Insertion of CT in DLPC Bilayers. To determine the depth of insertion of the oligocholates in the lipid membrane, we carried out the ^{13}C-detected ^{1}H spin diffusion experiments at 298 K. For the DLPC-bound CT, significant cross peaks from the lipid CH_2 (1.3 ppm) and CH_3 (0.9 ppm) protons to CT ^{13}C were observed already at short mixing times (9 ms), reaching a plateau by 100 ms (Figure 5). The buildup curve was best fit to a 2Å distance, indicating that CT fully inserts into the DLPC bilayer. In comparison, the water cross peak with CT was very slow to develop, reaching a plateau only at 625 ms. The slow intensity buildup was best fit to a distance of 16 Å.

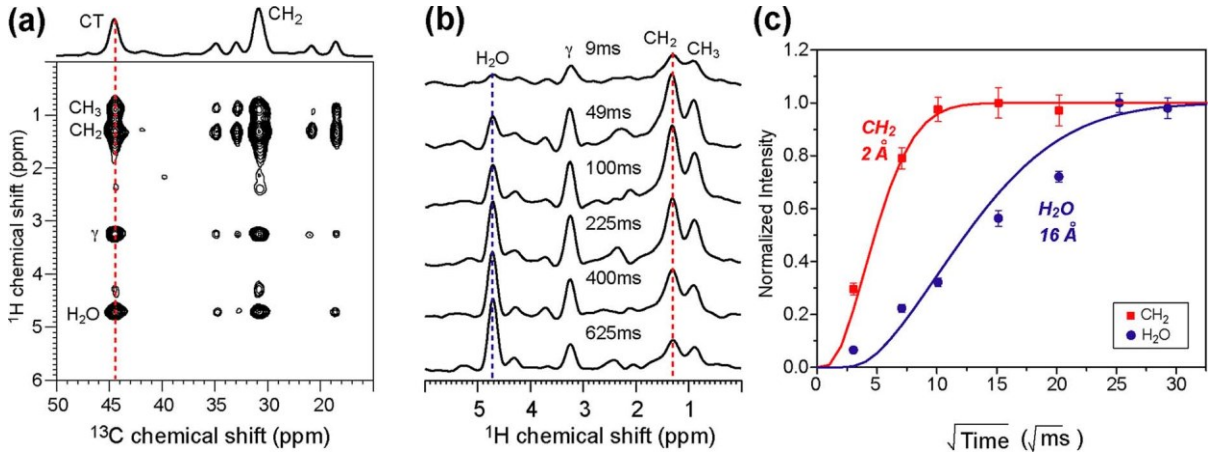

Figure 5. 2D ^{13}C-detected ^{1}H spin diffusion of DLPC-bound CT to determine the depth of insertion. (a) Representative 2D spectrum with 100 ms mixing time. (b) ^{1}H cross sections of the Cα peak as a function of mixing time. (c) Buildup curves of lipid CH_2 (red) and H_2O (blue) cross peaks. The corresponding peaks are marked in panel b by dashed lines. Best fit was obtained with 2 Å for CH_2 and 16 Å for the H_2O cross peak. Fitting parameters are DL = 0.012 nm^2/ms, DW = 0.03 nm^2/ms, DP = 0.3 nm^2/ms, and DI = 0.00125 nm^2/ms for H_2O and 0.0025 nm^2/ms for CH_2.

The short, 2 Å average distance of CT to the lipid CH_2 in the DLPC membrane is reasonable from the viewpoint of molecular dimension. The hydrophobic thickness of the DLPC bilayer is about 2.0 nm.[43] The height of the CT is about 0.6−0.7 nm according to its CPK model. When solubilized in the hydrophobic region of the membrane, the ^{13}C label should be quite close to most carbons on the C-12 chain of DLPC. On the other hand, the 16 Å average distance between CT and water was much longer than expected. We had envisioned that the highly hydrophilic interior of CT would always carry a pocket of water, regardless of the membrane structure, and thus anticipated a rapid buildup of the water cross peaks. For ion channels in lipid membranes, as long as the channel is hydrated, the channel water and membrane-surface water equilibrate rapidly on

the NMR time scale, giving fast intensity buildup for the water−protein cross peaks.[44,45] One possible explanation for the unusually slow buildup of the water cross peaks is that the CT pore may be dehydrated in the DLPC membrane. Filling the interior of CT with lipid chains, however, does not seem favorable from an energetic point of view. An alternative possibility, which is more consistent with the previous fluorescent data,[32] is that water molecules may be present in the interior of the macrocycle in the DLPC bilayer but may not form a continuous conduit to the membrane surface. In comparison to a TM channel with rapidly exchanging water molecules with the surface water, the CT molecules in DLPC bilayers under such a circumstance would experience much fewer water molecules in a given period of time, causing water cross peaks to develop more slowly.

Insertion of CT into POPC/POPG Membranes. Interestingly, in the POPC/POPG membrane, the lipid and water cross peaks to CT reversed trends from the DLPC case (Figure 6): the lipid cross peak intensities increased much more slowly, reaching a plateau only at 625 ms, while the water cross peak equilibrated rapidly, by 100 ms. The lipid chain−CT cross peak buildup was best fit to an average distance of 10 Å, indicating that the cyclic trimer was shallowly inserted in the POPC/POPG membrane, far from the lipid CH_2 groups but with immediate access to water.

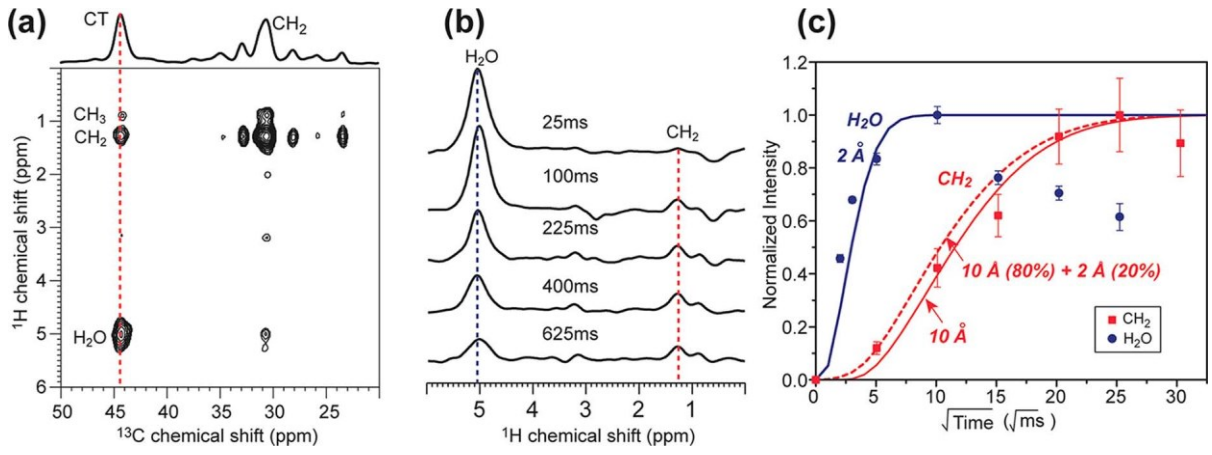

Figure 6. 2D ^{13}C-detected ^{1}H spin diffusion of CT in the POPC/POPG bilayer. (a) Representative 2D spectrum with a 625 ms mixing time. (b) ^{1}H cross sections of the Cα peak as a function of mixing time. (c) Buildup curves of the lipid CH_2 (red) and H_2O (blue) cross peaks. Best fit was obtained with 2 Å for the H_2O buildup and a predominant distance of 10 Å for the lipid CH_2 buildup. Combination of 10 Å (80%) and 2 Å (20%) also has a reasonable fit for experimental data (red dashed line). Diffusion coefficients are DL = 0.012 nm^2/ms, DW = 0.03 nm^2/ms, DP = 0.3 nm^2/ms, and DI= 0.0025 nm^2/ms for H_2O and 0.00125 nm^2/ms for CH_2.

The hydrophobic thickness of POPC is about 2.6 nm.[41] Thus, if CT is close to the membrane surface, its height (0.6−0.7 nm) would not allow it to be in contact with much of the lipid tail. The 10 Å average distance to the lipid CH_2 thus supports partial insertion of the CT. Since CT is effective at transporting glucose above 0.5 mol % of the POPC/POPG membrane,[21] we hypothesize that the depth of 10 Å is an average quantity from a small fraction of fully inserted macrocycles and a dominant fraction of surface-bound species. Indeed, simulations show that the experimental data can be equally well fit to a superposition of a 20% population of a 2-Å distance and an 80% population of a 10-Å distance (Figure 6). Increasing the fraction of the 2-Å component above 20% induces much faster buildup than observed. Thus, only a small fraction of the macrocycles might be responsible for the glucose transport, while the majority of CT is surface-bound and inactive. In this scenario, the high water cross peak in this membrane should result predominantly from the surface-bound CT.

Insertion of CT and LT into POPC/POPG/Cholesterol Membranes. CT displayed the most interesting behavior in the POPC/POPG/cholesterol membrane (Figure 7). The lipid− chain cross peaks rose similarly rapidly as in the DLPC bilayer, with an average distance of 2 Å to the lipid

CH_2. Hence, as the hydrophobic thickness of POPC membranes increased from 2.6 to 3.0 nm,[41] the macrocycle actually became closer to the lipid tails. This result provides the strongest evidence for the TM stacking model for the cyclic oligocholates. As supported by the glucose leakage assays[21] and fluorescence studies,[31,32] by increasing the hydrophobicity of the membrane, cholesterol affords a stronger driving force to the pore formation (Figure 1).

The addition of cholesterol thus favors stacking, transferring more of the surface-bound CT to the hydrophobic core of the membrane. Another interesting observation is the water cross peak buildup: it is intermediate between the DLPC and POPC/POPG cases and fits to a distance of 7 Å. We believe this result supports our explanation for the seemingly "dehydrated" CT in the DLPC membranes. When solubilized in a thicker, more hydrophobic membrane, CT should have more difficulty contacting the surface water molecules. Yet, despite its deep penetration into the membrane (evident from its 2 Å average distance to the lipid CH_2), CT showed a shorter distance to water in the thicker POPC/POPG/cholesterol membrane than in the thinner DLPC membrane. These unusual results are readily explained by our TM stacking model (Figure 1): the more hydrophobic the membrane, the better can the CT molecules stack into the TM pore. Once a nanopore is formed to span the entire thickness of the bilayer, the water molecules inside the pore can exchange with those on the surface readily, giving rise to faster buildup curves than those observed for the DLPC membrane.[46]

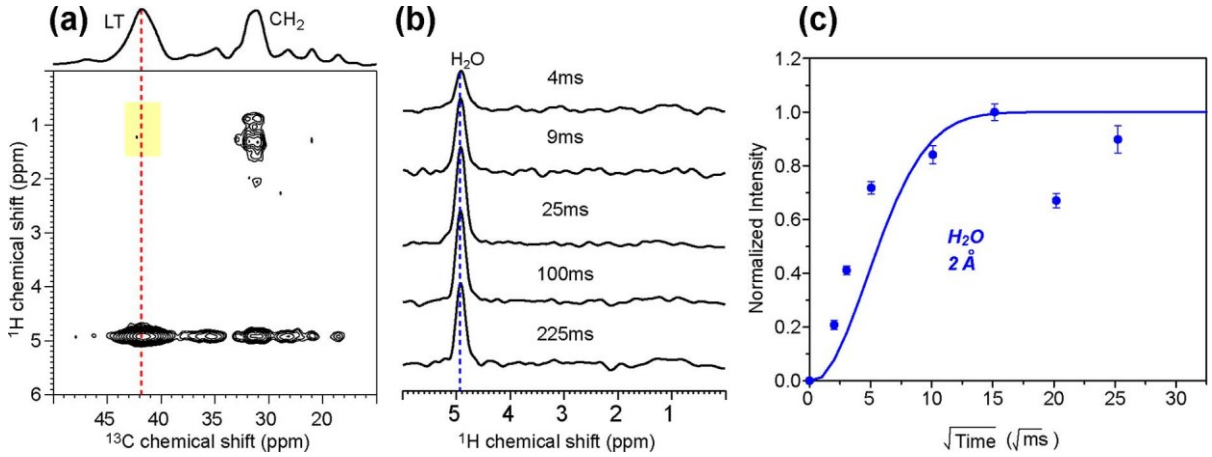

Figure 8. 2D ^{13}C-detected ^{1}H spin diffusion of LT in the POPC/POPG/cholesterol membrane at 278 K under 5 kHz MAS. (a) Representative 2D spectrum with a 225 ms mixing time. The lipid CH_2 cross peak is absent (yellow highlight), indicating that LT resides on the membrane surface. (b) ^{1}H cross sections of the LT Cα peak as a function of mixing time. (c) The water buildup curve is best fit to 2 Å using DL = 0.012 nm^2/ms, DW = 0.03 nm^2/ms, DP = 0.3 nm^2/ms, and DWP = 0.0025 nm^2/ms.

For comparison, we also measured the depth of insertion of LT in the POPC/POPG/cholesterol membrane. Since LT undergoes significant motion at ambient temperature, its ^{13}C signal cannot be distinguished from the lipid signals with the ^{1}H T_2 filter. We, therefore, carried out the spin diffusion experiment at a lower temperature, 278 K, which permitted the complete suppression of the ^{1}H magnetization of LT while maintaining the ^{1}H magnetization of lipids and water. Importantly, both lipids and water remain in the fluid phase at this temperature. Figure 8 shows a strong cross peak between water and LT Cα, which reached equilibrium rapidly, indicating that LT was in close contact with the aqueous environment. Meanwhile, no lipid cross peaks were identified until 625 ms, suggesting that the linear trimer cannot move easily into the hydrophobic core of the membrane.

Conclusions

The above ^{1}H spin diffusion NMR data depict a striking contrast in the behaviors of CT and LT in phospholipid bilayers. CT can either insert into a membrane or stay near the surface, depending on the membrane thickness and the presence of cholesterol. In contrast, LT strongly prefers the membrane surface, in close contact with the membrane-surface water. The surface preference of LT explains the poor transport activity of the linear tricholate.[21,22,47] ^{13}C–^{1}H dipolar couplings show that LT is much more dynamic than CT. It is known that rigid oligocholates (i.e., those without any additional tethering units between the cholates) can only form loose, unstable aggregates in nonpolar environments.[47,48] Thus, even if LT aggregates in the membrane, these aggregates must represent a minor fraction of all the LT molecules and/or be in rapid equilibrium with the highly dynamic, surface-bound species.

This study demonstrates the power of solid-state NMR spectroscopy in characterizing self-assembled structures in phospholipid bilayers on a molecular level.[49] Even though solid-state NMR has been employed extensively to study membrane peptides and proteins, the method is rarely used to characterize synthetic nanopores. Synthetic pore-forming compounds are structural and functional mimics of biological pore-forming proteins but the lipid membrane represents an extremely challenging medium for mechanistic studies of molecular self-assembly. Fluorescence spectroscopy is popular in membrane chemistry because of its high sensitivity. Nevertheless, bulky fluorescent labels are required, which may affect the self-assembly and typically afford low-resolution structural information at the end. Solid-state NMR spectroscopy, on the other hand, utilizes stable isotopes with minimal perturbation to the parent structure and, most importantly, can reveal atomic-scale information as shown in this study.

Acknowledgments We thank NSF (DMR-1005515) for supporting the research.

References

(1) Hopkins, A. L.; Groom, C. R. The druggable genome. *Nat. Rev. Drug Discovery* **2002**, *1*, 727−730.

(2) Lundstrom, K. Latest development in drug discovery on g protein-coupled receptors. *Curr. Protein Pept. Sci.* **2006**, *7*, 465−470.

(3) Lee, A. G. Biomembranes: A multi-volume treatise; JAI Press: Greenwich, CT, **1995**.

(4) Menestrina, G.; Dalla Serra, M.; Lazarovici, P. Pore-forming peptides and protein toxins; Taylor & Francis: London, UK, **2003**.

(5) Tamm, L. K. Protein-lipid interactions: From membrane domains to cellular networks; Wiley-VCH: Weinheim, Germany, **2005.**

(6) Matile, S.; Som, A.; Sorde, N. Recent synthetic ion channels and pores. *Tetrahedron* **2004**, *60*, 6405−6435.

(7) Sisson, A. L.; Shah, M. R.; Bhosale, S.; Matile, S. Synthetic ion channels and pores (2004−2005). *Chem. Soc. Rev.* **2006**, *35*, 1269− 1286.

(8) Stein, W. D. Carriers and pumps: An introduction to membrane transport; Academic Press: San Diego, CA, **1990**.

(9) Gokel, G. W.; Carasel, I. A. Biologically active, synthetic ion transporters. *Chem. Soc. Rev.* **2007**, *36*, 378−389.

(10) Fyles, T. M. Synthetic ion channels in bilayer membranes. *Chem. Soc. Rev.* **2007**, *36*, 335−347.

(11) McNally, B. A.; Leevy, W. M.; Smith, B. D. Recent advances in synthetic membrane transporters. *Supramol. Chem.* **2007**, *19*, 29−37.

(12) Davis, J. T.; Okunola, O.; Quesada, R. Recent advances in the transmembrane transport of anions. *Chem. Soc. Rev.* **2010**, 3*9*, 3843− 3862.

(13) Litvinchuk, S.; Sorde, N.; Matile, S. Sugar sensing with synthetic multifunctional pores. *J. Am. Chem. Soc.* **2005**, *127*, 9316−9317.

(14) Kasianowicz, J. J.; Brandin, E.; Branton, D.; Deamer, D. W. Characterization of individual polynucleotide molecules using a membrane channel. *Proc. Natl. Acad. Sci. U.S.A.* **1996**, *93*, 13770−13773.

(15) Akeson, M.; Branton, D.; Kasianowicz, J. J.; Brandin, E.; Deamer, D. W. Microsecond time-scale discrimination among polycytidylic acid, polyadenylic acid, and polyuridylic acid as homopolymers or as segments within single RNA molecules. *Biophys. J.* **1999**, *77*, 3227−3233.

(16) Meller, A.; Nivon, L.; Brandin, E.; Golovchenko, J.; Branton, D. Rapid nanopore discrimination between single polynucleotide molecules. *Proc. Natl. Acad. Sci. U.S.A.* **2000**, *97*, 1079−1084.

(17) Vercoutere, W.; Winters-Hilt, S.; Olsen, H.; Deamer, D.; Haussler, D.; Akeson, M. Rapid discrimination among individual DNA hairpin molecules at single-nucleotide resolution using an ion channel. *Nat. Biotechnol.* **2001**, *19*, 248−252.

(18) Howorka, S.; Cheley, S.; Bayley, H. Sequence-specific detection of individual DNA strands using engineered nanopores. *Nat. Biotechnol.* **2001**, *19*, 636−639.

(19) Clarke, J.; Wu, H. C.; Jayasinghe, L.; Patel, A.; Reid, S.; Bayley, H. Continuous base identification for single-molecule nanopore DNA sequencing. *Nat. Biotechnol.* **2009**, *4*, 265−270.

(20) Sakai, N.; Sorde, N.; Matile, S. Synthetic catalytic pores. *J. Am. Chem. Soc.* **2003**, *125*,

7776−7777.

(21) Cho, H.; Widanapathirana, L.; Zhao, Y. Water-templated transmembrane nanopores from shape-persistent oligocholate macro-cycles. *J. Am. Chem. Soc.* **2011**, *133*, 141−147.

(22) Cho, H.; Zhao, Y. Translocation of hydrophilic molecules across lipid bilayers by salt-bridged oligocholates. *Langmuir* **2011**, *27*, 4936− 4944.

(23) Granja, J. R.; Ghadiri, M. R. Channel-mediated transport of glucose across lipid bilayers. *J. Am. Chem. Soc.* **1994**, *116*, 10785−10786.

(24) Sakai, N.; Mareda, J.; Matile, S. Rigid-rod molecules in biomembrane models: From hydrogen-bonded chains to synthetic multifunctional pores. *Acc. Chem. Res.* **2005**, *38*, 79−87.

(25) Das, G.; Talukdar, P.; Matile, S. Fluorometric detection of enzyme activity with synthetic supramolecular pores. *Science* **2002**, *298*, 1600− 1602.

(26) Helsel, A. J.; Brown, A. L.; Yamato, K.; Feng, W.; Yuan, L. H.; Clements, A. J.; Harding, S. V.; Szabo, G.; Shao, Z. F.; Gong, B. Highly conducting transmembrane pores formed by aromatic oligoamide macrocycles. *J. Am. Chem. Soc.* **2008**, *130*, 15784−15785.

(27) Ma, L.; Melegari, M.; Colombini, M.; Davis, J. T. Large and stable transmembrane pores from guanosine-bile acid conjugates. *J. Am. Chem. Soc.* **2008**, *130*, 2938−2939.

(28) Satake, A.; Yamamura, M.; Oda, M.; Kobuke, Y. Transmembrane nanopores from porphyrin supramolecules. *J. Am. Chem. Soc.* **2008**, *130*, 6314−6315.

(29) Fyles, T. M.; Tong, C. C. Long-lived and highly conducting ion channels formed by lipophilic ethylenediamine palladium(II) complexes. *New J. Chem.* **2007**, *31*, 655−661.

(30) Dunitz, J. D. The entropic cost of bound water in crystals and biomolecules. *Science* **1994**, *264*, 670.

(31) Widanapathirana, L.; Zhao, Y. Aromatically functionalized cyclic tricholate macrocycles: Aggregation, transmembrane pore formation, flexibility, and cooperativity. *J. Org. Chem.* **2012**, *77*, 4679−4687.

(32) Widanapathirana, L.; Zhao, Y. Effects of amphiphile topology on the aggregation of oligocholates in lipid membranes: Macrocyclic versus linear amphiphiles. *Langmuir* **2012**, *28*, 8165−8173.

(33) Hong, M.; Zhang, Y.; Hu, F. Membrane protein structure and dynamics from NMR spectroscopy. *Annu. Rev. Phys. Chem.* **2012**, *63*,1− 24.

(34) Luca, S.; Heise, H.; Baldus, M. High-resolution solid-state NMR applied to polypeptides and membrane proteins. *Acc. Chem. Res.* **2003**, *36*, 858−865.

(35) Huster, D.; Yao, X. L.; Hong, M. Membrane protein topology probed by ^{1}H spin diffusion from lipids using solid-state NMR spectroscopy. *J. Am. Chem. Soc.* **2002**, *124*, 874−883.

CHAPTER 7. TUNING NANOPORE FORMATION OF OLIGOCHOLATE MACROCYCLES BY CARBOXYLIC ACID DIMERIZATION IN LIPID MEMBRANES

A paper published in *Journal of Organic Chemistry*, **2013**, *78,* 4610–4614.

Lakmini Widanapathirana and Yan Zhao

Abstract

Oligocholate macrocycles self-assemble into trans-membrane nanopores by the associative interactions of water molecules inside the amphiphilic macrocycles. Macrocycles functionalized with a terephthalic acid "side chain" displayed significantly higher transport activity for glucose across lipid bilayers than the corresponding methyl ester derivative. Changing the 1,4-substitution of the dicarboxylic acid to 1,3-substitution lowered the activity. Combining the hydrophobic interactions and the hydrogen-bond-based carboxylic acid dimerization was an effective strategy to tune the structure and activity of self-assembled nanopores in lipid membranes.

Lipid membranes are the barriers that separate the inside of a cell from its environment and the various compartments within the cell from the cytosol. Numerous biological functions occur at

these interfaces,[1] and not surprisingly, membrane proteins account for nearly 50% of all drug targets.[2] For these reasons, understanding how molecules recognize one another in a lipid membrane is of great importance to both biology and chemistry. In the past decades, chemists have gained significant understanding of how molecular recognition occurs in solution. However, when molecules move from a homogeneous solution into an amphiphilic, nanodimensioned, and liquid crystalline membrane, their intermolecular interactions (including those with the environment) change enormously and the relative importance of different noncovalent forces often needs recalibration.

Our group has reported amphiphilic (oligocholate) foldamers prepared from cholic acid.[3] Their steroid-derived backbone and controlled conformations make them excellent mimics of membrane protein transporters.[4] More recently, we prepared oligocholate macrocycles (e.g., **1**−**2**) as novel pore-forming agents.[5] The numerous inward-facing hydroxyl and amide groups make the molecule carry a pool of water in the interior when it enters a membrane. Because these water molecules have a strong tendency to interact with other water molecules instead of the lipid hydrocarbon, the macrocycles prefer to stack over one another to form a transmembrane nanopore. The pore formation was confirmed by the macrocycle-induced leakage of glucose from liposomes[5] and further by fluorescently (e.g., **3**−**4**) and isotopically labeled analogues using fluorescence[6] and solid-state NMR spectroscopy, respectively.[7]

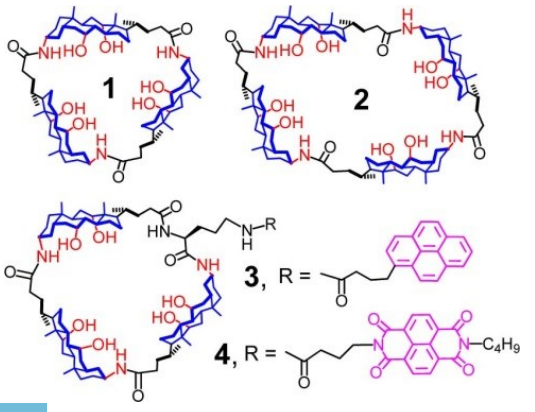

Nanopore-forming agents have numerous applications in drug delivery, separation, sensing, and catalysis.[8] For many of these applications, it is highly desirable that the pore formation be controlled rationally. Compound 5 contains a tricholate macrocycle and a terephthalic acid side chain. Terephthalic acid is known to have two crystalline forms and, in both forms, the molecules are linked together by hydrogen-bonded carboxylic aciddimersintoinfinite chains.[9] Our idea was that a combination of the hydrophobic interactions (among the entrapped water molecules inside the cholate macrocycles) and a tunable, directional polar interactions (among the carboxylic acids on the side chain) would allow us to control the pore formation.[10] Since the height of the cholate macrocycle is similar to the width of a cyclohexane, the hydrogen-bonding interactions of the terephthalic acid and the stacking of the cholate macrocycle should be compatible geometrically.

Scheme 1. Synthesis of Terephthalic Acid-Functionalized Macrocycle **5**

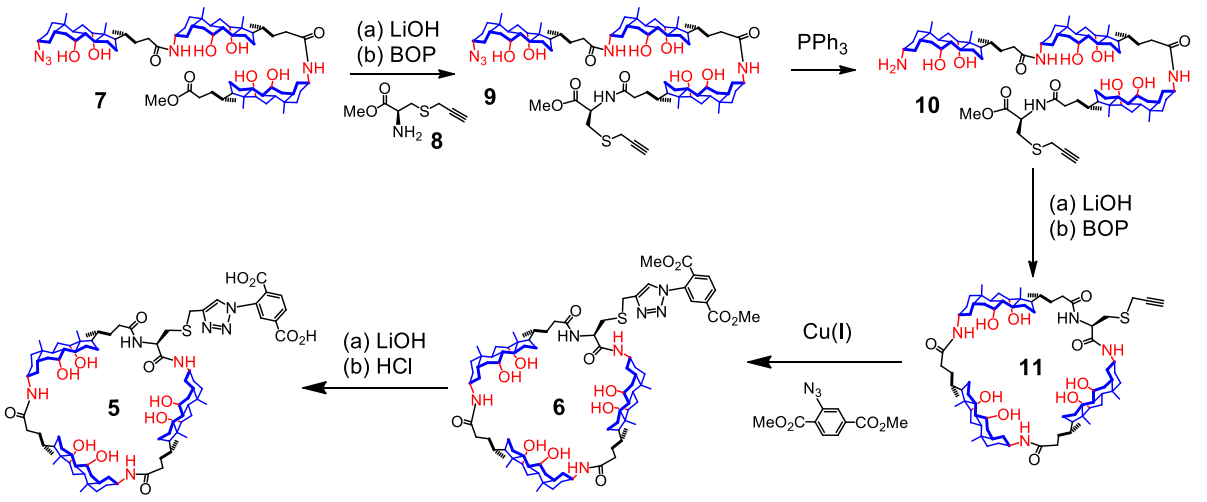

Compound **5** was obtained by the hydrolysis of ester **6**, which was synthesized from the linear tricholate **7** by standard transformations (Scheme 1). The key design of the molecule involves the incorporation of a natural L-cysteine functionalized with a propargyl group. The terminal alkyne allowed a late-stage installation of the terephthalic acid moiety via a convenient click reaction. It also enables us to change the carboxylic side chain of the macrocycle readily (vide infra).

The tricholate macrocycle has a triangularly shaped internal cavity approximately 1 nm on the side, large enough for glucose to pass through.[5] Figure 1 compares the leakage profiles of glucose-filled large unilamellar vesicles (LUVs) induced by the terephthalic acid-functionalized macrocycle (**5**), its methyl ester derivative (**6**), and the linear trimer (**7**). The leakage assay was based on the reactions between the escaped glucose and extravesicular enzymes that released UV-active NADPH.[11] Whereas the linear trimer showed little activity over the background leakage (averaging 6−10% at 60 min), the macrocycles displayed higher activity. The acid derivative was by far the most effective transporter among the three, with all 300 mM of glucose leaking out of the liposomes in <20 min in the presence of 5 μMof 5.

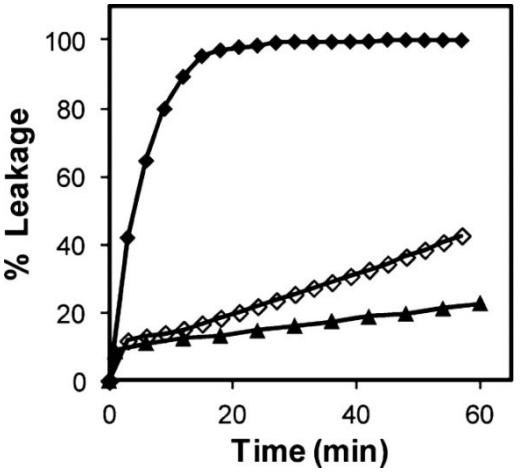

Figure 1. Percent leakage of glucose from POPC/POPG LUVs as a function of time for macrocycle **5** (◆), macrocycle **6** (◇), and linear trimer **7** (▲) at 25 °C. [Oligocholate] = 5.0 μM. [Phospholipids] = 104 μM. The liposomes were lysed at 60 min upon addition of 0.1% Triton X-100.

Most membrane transporters function as either a carrier or a channel/pore.[12] A carrier binds and accompanies its cargo to diffuse across the membrane. A channel or pore, on the other hand, is relatively stationary within the membrane. One way to distinguish pore-based transport from a

carrier-based mechanism is to study the effect of lipid composition on the transport rate. Addition of 30% cholesterol to the POPC/POPG membrane is known to increase the hydrophobic thickness of the membrane from 2.6 to 3.0 nm[13] and decrease its fluidity.[14] Although cholesterol reduces the membrane permeability of hydrophilic molecules in general,[15] cholesterol incorporation was found to *speed up* the glucose transport by macrocycles **1** and **2** across POPC/POPG membranes.[5] The result was counterintuitive according to conventional reasoning but fully consistent with the hydrophobically driven pore formation.

To our surprise, the addition of 30 mol % of cholesterol to the POPC/POPG membranes did not enhance significantly the glucose leakage induced by **5** (Figure 2a). Although the leakage overall was still slightly higher for the cholesterol-containing liposomes, the effect was far smaller than that observed for **1** and **2** (upto 5−7 times faster with the same level of cholesterol, depending on the concentration of the macrocycle).[5] Figure 1 shows that the carboxylic acids were clearly beneficial to the glucose transport across the POPC/POPG membranes. Could it be possible that other mechanisms (than nanopore formation) was responsible for the faster leakage of 5 over 6? To better understand the transport mechanism, we switched the permeant to carboxyfluorescein (CF), a molecule too large to permeate the cyclic tricholate nanopore. CF displays strong self-quenching above 50 mM and, thus, emits more strongly once escaping from a liposome.[16] Our previous study suggests that CF needs to be sandwiched by two cyclic tricholates to move across a membrane via a carrier mechanism.[17] As shown in Figure 2b, the CF leakage induced by 5 slowed down greatly upon the inclusion of cholesterol in the LUVs. At 60 min, the cholesterol-containing liposomes (×) only showed less than half of the leakage found in the cholesterol-free ones (Δ).

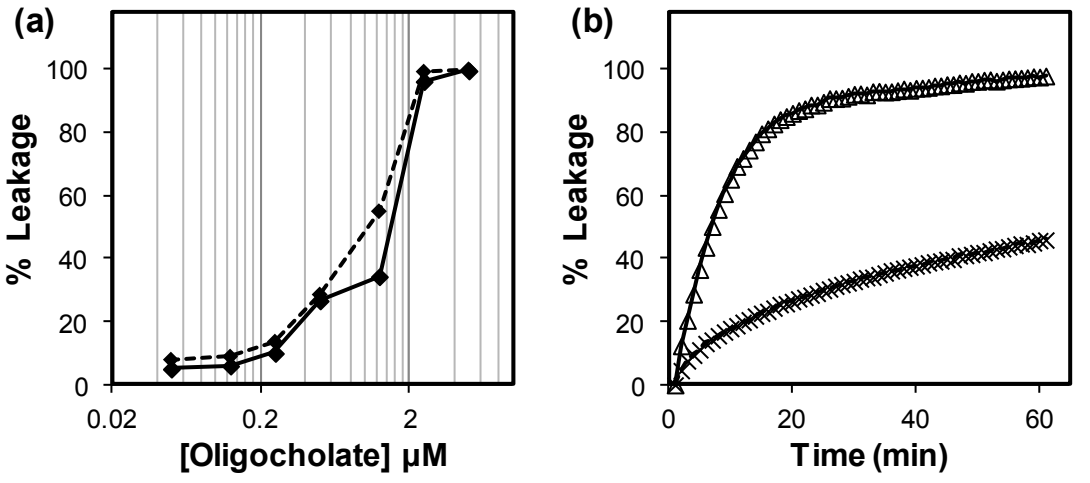

Figure 2. (a) Percent leakage of glucose at 30 min induced by 5 from POPC/POPG LUVs with (dashed line) and without 30% cholesterol (solidline). [Phospholipids]=104μM. (b) Percent leakage of CF induced by 5 from POPC/POPG LUVs with (×) and without 30% cholesterol (Δ). [Oligocholate]= 0.5 μM. [Phospholipids]= 2.9 μM. The leakage experiments were typically run in duplicate.

The above experiments demonstrated that cholesterol was indeed detrimental to carrier-based transport, in agreement with other literature work.[18] The study also assured us that, despite the small enhancement in the glucose leakage caused by cholesterol incorporation, macrocycle 5 did NOT function as a carrier for glucose. If we "normalize" the cholesterol effect on the glucose transport over its (negative) impact on the CF transport, we could still conclude that the glucose leakage induced by 5 from the cholesterol-containing liposomes in Figure 2a was unusually high.

After ruling out the carrier mechanism, we performed the lipid-mixing assay to verify the integrity of the lipid bilayers. In the lipid-mixing assay, a batch of unlabeled LUVs is mixed with another batch labeled with 1 mol % of NBD-and rhodaminefunctionalized lipids. If the carboxylic acid-functionalized 5 destabilized the liposomes by other mechanisms (e.g., membrane fusion or destruction), the fluorescence resonance energy transfer (FRET) between the fluorescent labels would be affected.[19] In our hands, even at the highest concentration studied (5 mol %), the

liposomes showed <16% mixing (Figure 3a), indicating that none of the above-mentioned membrane- disrupting processes was significant in the presence of 5. The conclusion was also supported by dynamic light scattering (DLS) showing nearly constant size of the liposomes after the addition of 5 (Figure 3a).

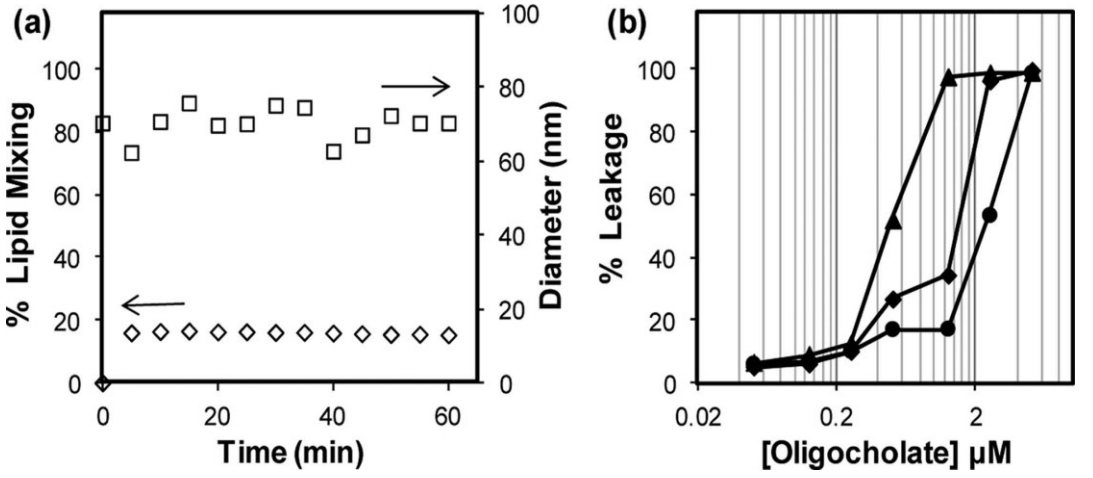

Figure 3. (a) Percent lipid-mixing and the size of the POPC/POPG LUVs upon the addition of **5**. [**5**] = 2.5 μM, [lipids] = 54.0 μM. (b) Percent leakage of glucose at 30 min induced by 1 (▲), 5 (◆), and 12 (●) from POPC/POPG LUVs. [Phospholipids]= 104 μM.

At this point, it seems reasonable to conclude that (a) the carboxylic acids in macrocycle **5** were beneficial to the glucose transport across the membrane and (b) the transport bore essentially all the important hallmarks of the hydrophobically driven pore-forming mechanism. The only "abnormality" was the smaller enhancement of glucose transport upon cholesterol inclusion in the membrane. The observation, however, is not difficult to understand from the viewpoint of polarity. Cholesterol increases the hydrophobicity of the membrane.[13] Although the stronger environmental hydrophobicity facilitates the stacking of cholate macrocycles,[5] it probably lowers the solubility of polar compounds including the terephthalic acid-containing **5**. Even if the carboxylic acid dimer may be stronger in the more hydrophobic, cholesterol-containing

membrane, the overall lower concentration of **5** within the membrane would represent a counterbalancing effect for the pore formation. This could also be one reason why **5** was still less effective in the glucose transport than the parent macrocycle 1 (Figure 3b).[20]

If indeed the carboxylic acid dimerization from the terephthalic acid side chains and the hydrophobically driven stacking of the cholate macrocycles were collectively responsible for the high activity of **5**, altering the dicarboxylic acids should allow one to tune the transport activity. We thus prepared a corresponding "carboxylic acid isomer", i.e., **12**, following a similar click coupling. Unlike terephthalic acid that forms a chain-like structure commensurate with the stacked nanopore, 5-substituted isophthalic acid derivatives tend to adopt cyclic hexameric structures through the carboxylic acid dimerization.[21] Since the stacked cholate macrocycles prefer a linear alignment of the functionalized side chains, isophthalic acid should be less than ideal.

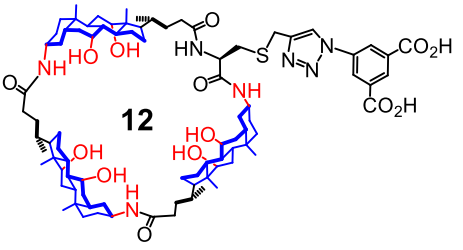

The above postulation was confirmed in our glucose leakage assay. The isophthalic acid-functionalized macrocycle consistently underperformed its *para* isomer as a glucose transporter (Figure 3b), indicating that the orientation of the carboxylic acids was critical to the transport. The result further ruled out "generic" effects of carboxylic acids on the membrane. If compound **5**, for example, simply causes glucose leakage by its amphiphilicity, with the terephthalic acid acting as a hydrophilic moiety, it is difficult to imagine that switching the 1,4 substitution to 1,3 would have a large effect on the transport, especially when there are numerous rotatable bonds between acid-containing phenyl group and the cholate macrocycle.

The importance of carboxylic acid dimerization in membrane is also supported by the literature. When bound to lipid membranes, fatty acids shift their pKa from ca. 4 in solution to 7.5. [22] In the protonated, uncharged form, a fatty acid can migrate into a lipid membrane and rapidly diffuse to the other side. The half-life of the flip-flop of fatty acids in common lipid bilayers is <10 ms.[23] Thus, these acids have no difficulty traversing the membrane, most likely because their dimerization lowers the polarity of the carboxylic acids and make them compatible with nonpolar environments. In summary, carboxylic acid dimerization could be used to rationally tune the hydrophobically driven pore formation of cholate macrocycles. Our previous experience tells us that molecular recognition in membrane could differ enormously from that in solution. The aromatic donor−acceptor interactions between 1,5-dialkoxynaphthalene and NDI, for example, were found to be 1−2 orders of magnitude stronger than the acceptor−acceptor interactions in polar solvents.[24] For the cholate macrocycles, however, 4 transported glucose more efficiently than either **3** or the 1:1 **3**/**4** mixture.[25] The result suggested the acceptor−acceptor interactions were more effective at promoting the stacking of the cholate macrocycles in lipid membranes. Another work of ours indicates that the strong guanidinium−carboxylate salt bridge was rather ineffective at promoting stacking of the cholate macrocycles, due to the strong preference of these polar groups for membrane surface.[10] This work shows that carboxylic acid side chains can be used to regulate the stacking of cholate macrocycles effectively. As chemists become interested in creating functional structures in lipid membranes, the carboxylic acid dimer[26] may be a particularly useful motif for supramolecular construction.[27]

Experimental Section

The preparation of LUVs, the procedures for the leakage assays, and the lipid mixing assay were reported previously.[5] Compound **7**,[28] compound **8**,[29] methyl 2-azidoterephthlate,[30] and 5-

azidoisophthalic acid[30] were synthesized according to literature procedures.

Compound 9. The carboxylic acid of **7**[28] (450 mg, 0.37 mmol), **8** (83 mg, 0.48 mmol), 1-hydroxybenzotriazole (HOBt, 89 mg, 0.66 mmol), and (benzotriazol-1-yloxy)tris(dimethylamino)phosphonium hexafluorophosphate (BOP, 292 mg, 0.66 mmol) were dissolved in anhydrous DMF (2 mL). N,N-Diisopropylethylamine (DIPEA, 0.51 mL, 2.93 mmol) was added. The mixture was allowed to react in a microwave reactor at 100 °C for 1 h and monitored by TLC. When the reaction was complete, the mixture was cooled to room temperature and poured into a dilute HCl solution (0.05 M, 250 mL). The precipitate was collected, dried, and purified by column chromatography over silica gel, using 12:1 CHCl3/CH3OH as the eluent to give a light brown powder (272 mg, 55%). ^{1}H NMR (400 MHz, $CDCl_3/CD_3OD$ = 1:1, δ): 4.70 (br, 1H), 3.93 (br, 3H), 3.79 (br, 3H), 3.73 (s, 3H), 3.50 (br, 2H), 3.25 (s, 1H), 3.17 (m, 2H), 2.95 (m, 1H), 2.93 (m, 1H), 2.43 (t, 1H), 2.38−1.0 (a series of m), 0.66 (s, 9H). ^{13}C NMR (100 MHz, $CDCl_3/CD_3OD$ = 1:1, δ): 176.0, 174.8, 172.2, 79.7, 73.3, 72.4, 68.5, 62.0, 52.7, 52.3, 47.6, 46.7, 42.4, 39.9, 36.5, 36.2, 35.2, 34.0, 33.4, 32.4, 28.8, 27.1, 23.6, 23.0, 19.7, 17.6, 12.9. ESI MS (m/z): $[M + Na]^+$ calcd for $C_{79}H_{126}N_6NaO_{11}S$ 1389.9098, found 1390.9079.

Compound 10. A solution of compound **9** (155 mg, 0.110 mmol) and triphenylphosphine (60 mg, 0.230 mmol) in methanol (4 mL) was heated to reflux overnight. After the solvent was removed by rotary evaporation, the residue was purified by column chromatography over silica gel using 10:1 CH_2Cl_2/MeOH and then 8:1:0.1 CH_2Cl_2/MeOH/Et_3N as the eluents to give an off-white powder (109 mg, 72%). ^{1}H NMR (400 MHz, $CDCl_3/CD_3OD$ = 1:1, δ): 3.95 (br, 3H), 3.79 (br, 3H), 3.74(s, 3H), 3.50 (br, 2H), 3.17 (m, 2H), 2.88 (m, 2H), 2.44 (t, 1H), 2.40−0.77 (a series of m), 0.66 (s, 9H). ^{13}C NMR (100 MHz, $CDCl_3/CD_3OD$ = 1:1, δ): 176.0, 175.0, 172.4, 79.9, 73.4, 72.6, 68.4, 63.0, 59.4, 53.2, 51.5, 47.7, 46.9, 46.5, 42.7, 40.2, 36.9, 35.6, 34.0, 32.6, 28.8, 28.3, 27.3, 23.9, 23.0, 17.6, 12.9, 9.3,7.7. ESI MS (m/ z): $[M + H]^+$ calcd for $C_{79}H_{129}N_4O_{11}S$

1341.9499, found 1341.9411.

Compound 11. Compound **10** was hydrolyzed by standard procedures using 10 equiv of LiOH.[28] The hydrolyzed product (50 mg, 0.038 mmol), BOP (84 mg, 0.190 mmol), and HOBT (26 mg, 0.190 mmol) were dissolved in DMF (30 mL), followed by the addition of DIPEA (66 μL, 0.381 mmol). The mixture was allowed to react in a microwave reactor at 100 °C for 1 h, cooled to room temperature, and poured into a dilute HCl solution (0.05 M, 100 mL). The precipitate was collected, dried, and purified by purified by column chromatography over silica gel using 8:1 CH_2Cl_2/CH_3OH as the eluent to give an ivory powder (30 mg, 60%). ^{1}H NMR (400 MHz, $CDCl_3/CD_3OD$ = 1:1, δ): 4.48 (br, 1H), 3.93 (br, 3H), 3.79 (br, 3H), 3.52 (br, 3H), 3.09 (m, 1H), 2.88 (m, 1H), 2.440 (t, 1H), 2.34−0.74 (a series of m), 0.69 (s, 9H). ^{13}C NMR (100 MHz, $CDCl_3/CD_3OD$ = 1:1, δ): 176.1, 74.3, 73.1, 69.4, 48.1, 47.8, 47.5, 43.2,43.0, 40.9, 37.5, 36.6, 36.2, 35.9, 34.5, 33.7, 33.3, 32.7, 31.0, 29.6, 28.8, 25.5,28.2, 28.1,27.9, 24.5, 23.9, 20.6, 18.3,13.8, 13.6, 9.9. ESI MS (m/z): $[M + Na]^+$ calcd for $C_{78}H_{124}N_4O_{10}SNa$ 1331.8936, found 1331.8909.

Compound 6. Compound **11** (62 mg, 0.047 mmol), methyl-2-azidoterephthlate (13 mg, 0.062 mmol), $CuSO_4 \cdot 5H_2O$ (24 mg, 0.095 mmol), and sodium ascorbate (38 mg, 0.189 mmol) were dissolved in a 2:1:1 mixture of THF/methanol/water (0.8 mL) and stirred at 40 °C overnight. The reaction mixture was concentrated by rotary evaporation and poured into water (50 mL). The precipitate was collected, dried, and purified by purified by column chromatography over silica gel, using 12:1 CH_2Cl_2/CH_3OH as the eluent to give an ivory powder (51 mg, 70%). ^{1}H NMR (400 MHz, $CDCl_3/CD_3OD$ = 1:1, δ): 8.24−8.07 (br, 4 H), 4.53 (br, 1H), 3.97 (s, 3H), 3.93 (br, 3H), 3.79 (br, 3H), 3.73 (s, 3H), 3.43 (br 3H), 2.35−0.78 (a series of m), 0.66 (m, 9H). ^{13}C NMR (100 MHz, $CDCl_3/CD_3OD$ = 1:1, δ): 176.6, 175.4, 170.5, 165.7, 136.7, 134.9, 131.9, 128.0, 88.1, 76.8, 73.5, 68.7, 63.2, 53.5, 42.9, 42.8, 42.6, 42.4, 40.2, 40.0, 36.9, 36.5, 36.3, 35.9, 35.5, 35.2, 32.0, 28.1, 27.6, 27.2, 26.3, 23.7, 23.1, 17.7, 12.9. ESI MS (m/z): $[M + H]^+$ calcd for

$C_{88}H_{134}N_7O_{14}S$ 1544.9704, found 1544.9699.

Compound 5. Compound **6** (37 mg, 0.024 mmol) was dissolved in MeOH (1 mL), and a solution of 2 M LiOH (0.2 mL, 0.40 mmol) was added. The reaction was stirred at room temperature and monitored by TLC. After the hydrolysis was complete, the organic solvent was removed by rotary evaporation. After the addition of a dilute HCl solution (50 mL, 0.05 M), the precipitate formed was collected by centrifugation, washed with water, and dried in vacuo to give a white powder (22 mg, 61%). ^{1}H NMR (400 MHz, $CDCl_3$/ CD_3OD = 1:1, δ): 8.24−8.05 (br, 4 H), 4.47 (br, 1H), 3.93 (br, 3H), 3.79 (br, 3H), 3.50 (br, 3H), 2.32−0.77 (a series of m), 0.67 (m, 9H). ^{13}C NMR (100 MHz, $CDCl_3$/CD_3OD = 1:1, δ): 177.3, 176.1, 171.6, 166.7, 166.4, 137.4, 135.6, 132.8,132.6,132.2, 128.7, 89.1, 77.4, 74.7,74.2,69.5, 54.2, 47.7, 47.6, 47.5, 47.4, 43.4, 43.2, 43.0, 41.0, 40.8, 40.7, 37.5, 37.2, 37.0,36.2,36.0,36.2, 35.9, 34.4,33.7, 33.3, 32.7,32.6, 31.1, 29.6, 28.3, 28.0, 27.9, 24.4, 23.9, 23.8, 18.4, 13.7, 13.5. ESI MS (m/z): $[M + H]^+$ calcd for $C_{86}H_{130}N_7O_{14}S$ 1516.9391, found 1516.9350.

Compound 12. The same procedure as in the synthesis of compound **5** was followed to give **12** as an off-white powder (66%). ^{1}H NMR (400 MHz, $CDCl_3$/CD_3OD = 1:1, δ): 8.22−8.07 (br, 4 H), 4.45 (br, 1H), 3.95 (br, 3H), 3.79 (br, 3H), 3.49 (br, 3H), 2.31− 0.76(a series of m), 0.68 (m, 9H). ^{13}C NMR (100 MHz, $CDCl_3$/ CD_3OD = 1:1, δ): 177.3, 176.1, 171.6, 166.7, 166.4, 137.4, 135.6, 132.8,132.6,132.2, 128.7, 89.1, 77.4, 74.7,74.2,69.5, 54.2, 47.7, 47.6, 47.5, 47.4, 43.4, 43.2, 43.0, 41.0, 40.8, 40.7, 37.5, 37.2, 37.0,36.2,36.0,36.2, 35.9, 34.4,33.7, 33.3, 32.7,32.6, 31.1, 29.6, 28.3, 28.0, 27.9, 24.4, 23.9, 23.8, 18.4, 13.7, 13.5. ESI MS (m/z): $[M - H]^+$ calcd for $C_{86}H_{128}N_7O_{14}S$ 1514.9245, found 1514.9229.

Associated Content General experimental methods and the NMR data for the key compounds. This material is available free of charge via the Internet at http://pubs.acs.org.

Acknowledgments

We thank NSF (DMR-1005515) for supporting the research.

References

(1) Yeagle, P. The Structure of Biological Membranes, 2nd ed.; CRC Press: Boca Raton, **2005**.

(2) (a) Hopkins, A. L.; Groom, C. R. *Nat. Rev. Drug Discovery* **2002**, *1*, 727. (b) Lundstrom, K. *Curr. Protein Pept. Sci.* **2006**, *7*, 465.

(3) (a) Zhao, Y.; Zhong, Z.; Ryu, E.-H. *J. Am. Chem. Soc.* **2007**, *129,* 218. (b) Cho, H.; Zhong, Z.; Zhao, Y. *Tetrahedron* **2009**, *65*, 7311.

(4) (a) Zhang, S.; Zhao, Y. *Chem. Eur. J.* **2011**, *17*, 12444. (b) Cho, H.; Zhao, Y. *J. Am. Chem. Soc.* **2010,** *132*, 9890.

(5) Cho, H.; Widanapathirana, L.; Zhao, Y. *J. Am. Chem. Soc.* **2011**, *133*, 141.

(6) Widanapathirana, L.; Zhao, Y. *Langmuir* **2012**, *28,* 8165.

(7) Wang, T.; Widanapathirana, L.; Zhao, Y.; Hong, M. *Langmuir* **2012**, *28*, 17071.

(8) (a) Granja, J. R.; Ghadiri, M. R. *J. Am. Chem. Soc.* **1994**, *116*, 10785. (b) Sakai, N.; Mareda, J.; Matile, S. *Acc. Chem. Res.* **2005**, *38*, 79. (c) Das, G.; Talukdar, P.; Matile, S. *Science* **2002**, *298*, 1600.

(d) Sakai, N.; Sorde, N.; Matile, S. *J. Am. Chem. Soc.* **2003**, *125*, 7776. (e) Ma, L.; Melegari, M.; Colombini, M.; Davis, J. T. *J. Am. Chem. Soc.* **2008**, *130*, 2938. (f) Chen, L.; Si, W.; Zhang, L.; Tang, G.; Li, Z.-T.; Hou, J.-L. *J. Am. Chem. Soc.* **2013**, *135*, 2152.

(9) (a) Bailey, M.; Brown, C. *J. Acta Crystallogr.* **1967**, *22*, 387. (b) Sledz, M.; Janczak, J.; Kubiak, R. *J. Mol. Struct*. **2001**, *595*, 77.

(10) Widanapathirana, L.; Li, X.; Zhao, Y. *Org. Biomol. Chem.* **2012**, *10*, 5077.

(11) Kinsky, S. C.; Haxby, J. A.; Zopf, D. A.; Alving, C. R.; Kinsky, C. B. *Biochemistry* **1969**, *8*, 4149.

(12) Stein, W. D. Carriers and Pumps: An Introduction to Membrane Transport; Academic Press: San Diego, 1990.

(13) Nezil, F. A.; Bloom, M. *Biophys. J.* **1992**, *61*, 1176.

(14) Holthuis, J. C. M.; van Meer, G.; Huitema, K. *Mol. Membr. Biol.* **2003**, *20*, 231.

(15) (a) Demel, R. A.; Bruckdor, K. R.; van Deene, L. L. *Biochim. Biophys. Acta* **1972**, *255*, 321. (b) Papahadjopoulos, D.; Nir, S.; Ohki, S. *Biochim. Biophys. Acta* **1972**, *266*, 561.

(16) New, R. R. C. Liposomes: A Practical Approach; IRL Press: Oxford, **1990.**

(17) Cho, H.; Zhao, Y. *Langmuir* **2011**, *27,* 4936.

(18) Davis, J. T.; Okunola, O.; Quesada, R. *Chem. Soc. Rev.* **2010**, *39*, 3843.

(19) Struck, D. K.; Hoekstra, D.; Pagano, R. E. *Biochemistry* **1981**, *20*, 4093.

(20) Another reason was the flexibility in the macrocycle introduced by the inserted L-cysteine. Our earlier work indicates that rigidity in the macrocycle facilitates the pore formation: Widanapathirana, L.; Zhao, Y. *J. Org. Chem.* **2012**, *77*, 4679.

(21) (a) Yang, J.; Marendaz, J. L.; Geib, S. J.; Hamilton, A. D. *Tetrahedron Lett.* **1994**, *35*, 3665. (b) Zimmerman, S. C.; Zeng, F. W.; Reichert, D. E. C.; Kolotuchin, S. V. *Science* **1996**, *271*, 1095.

(22) James A, H. In Carbon-13 NMR Spectroscopy of Biological Systems; Academic Press: San Diego, 1995; p 117.

(23) (a) Kamp, F.; Hamilton, J. A. *Proc. Natl. Acad. Sci. U.S.A.* **1992**, *89*, 11367. (b) Kamp, F.; Zakim, D.; Zhang, F.; Noy, N.; Hamilton, J. A. *Biochemistry* **1995**, *34*, 11928. (c) Hamilton, J. A.; Guo, W.; Kamp, F. *Mol. Cell. Biochem*. **2002**, *239*, 17.

(24) Cubberley, M. S.; Iverson, B. L. *J. Am. Chem. Soc.* **2001**, *123*, 7560.

(25) Widanapathirana, L.; Zhao, Y. *J. Org. Chem.* **2012**, *77*, 4679.

(26) In CCl4 and heptane, the dimerization constant of carboxylic acids is $10^{3}-10^{4}$ M^{-1}, equivalent to 4−5 kcal/mol in binding free energy. See: Wenograd, J.; Spurr, R. A. *J. Am.*

Chem. Soc. **1957**, *79*, 5844. Goodman, D. S. *J. Am. Chem. Soc.* **1958**, *80*, 3887. Since the hydrophobic core of the membrane essentially comprises hydrocarbon, a similar binding free energy is expected.

(27) Boccalon, M.; Iengo, E.; Tecilla, P. *J. Am. Chem. Soc.* **2012**, *134*, 20310.

(28) Zhao, Y.; Zhong, Z. *J. Am. Chem. Soc.* **2005**, *127*, 17894.

(29) Struthers, H.; Spingler, B.; Mindt, T. L.; Schibli, R. *Chem. Eur. J.* **2008**, *14*, 6173.

(30) (a) Morris, W.; Taylor, R. E.; Dybowski, C.; Yaghi, O. M.; Garcia-Garibay, M. A. *J. Mol. Struct.* **2011**, *1004*, 94. (b) Pokhodylo, N. T.; Matiychuk, V. S. J. *Heterocycl. Chem.* **2010**, *47*, 415.

APPENDIX. SUPPORTING INFORMATION

I. Water-Templated Transmembrane Nanopores from Shape-Persistent Oligocholate Macrocycles (Chapter 2, pg. 13-34)

General Method

For spectroscopic purpose, methanol, hexanes, and ethyl acetate were of HPLC grade and were purchased from Fisher Scientific. All other reagents and solvents were of ACS-certified grade or higher, and were used as received from commercial suppliers. Routine ^{1}H and ^{13}C NMR spectra were recorded on a Bruker DRX-400 or on a Varian VXR-400 spectrometer. MALDI-TOF mass was recorded on a Thermobioanalysis Dynamo mass spectrometer. UV-vis spectra were recorded at ambient temperature on a Cary 100 Bio UV-visible spectrophotometer. Fluorescence spectra were recorded at ambient temperature on a Varian Cary Eclipse Fluorescence spectrophotometer.

Abbreviation

ATP: adenosine 5′-triphosphoate; HEPES: 4-(2-hydroxyethyl)-1-piperazineethanesulfonic acid; NADP: Nicotinamide adenine dinucleotide phosphate; NBD-DPPE: N-(7-nitro-2-1,3-benzoxadiazol4-yl)-1,2-dipalmitoyl-*sn*-glycero-3-phosphoethanolamine ammonium salt; POPC: 1-palmitoyl-2oleoyl-*sn*-glycero-3-phosphocholine; POPG: 1-palmitoyl-2-oleoyl-*sn*-glycero-3-[phospho-*rac*-(1glycerol)] sodium salt; Rh-DPPE: N-(lissamine rhodamine B sulfonyl) -1,2-dipalmitoyl-*sn*-glycero3-phosphoethanolamine ammonium salt; Tris: tris (hydroxymethyl) aminomethane.

Scheme 1S

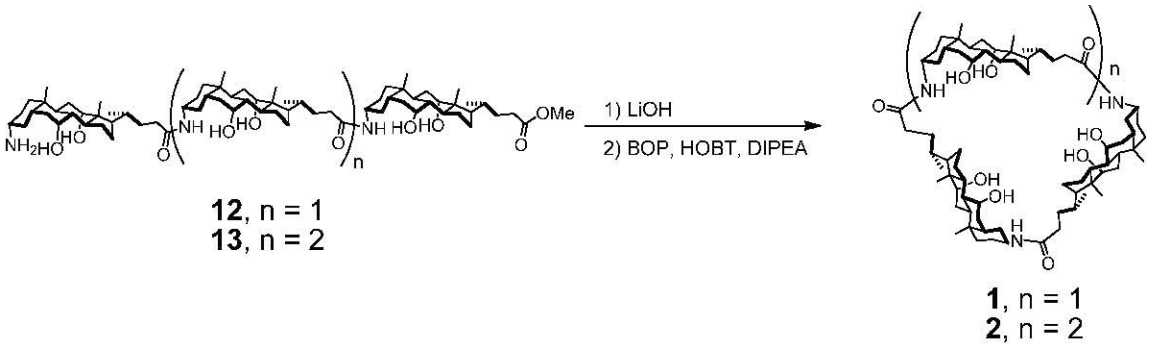

12, n = 1
13, n = 2

1, n = 1
2, n = 2

Synthesis

The syntheses of compounds **3**,[1] **5**,[2] **6**,[1] and **13**[1] were previously reported.

Compound 12. Compound **3** (124 mg, 0.101 mmol) and triphenyl phosphine (40.0 mg, 0.153 mmol) were dissolved in MeOH (2 mL). The reaction mixture was heated to reflux for 4 h. The solvent was removed by rotary evaporation. The residue was purified by column chromatography over silica gel with CH_2Cl_2/MeOH (5:1) and CH_2Cl_2/MeOH/Et_3N (5:1:0.1) as the eluents to give an off-white powder (107 mg, 88%). ^{1}H NMR (400 MHz, CD_3OD, δ): 3.96 (br, 3H), 3.79 (br, 3H), 3.64 (s, CO_2CH_3, 3H), 3.48 (m, 2H), 2.76 (m, 1H), 2.42–0.83 (series of m, 87H), 0.71 (s, 9H). ^{13}C NMR (100 MHz, CD_3OD, δ): 176.6, 176.0, 74.1, 74.0, 69.1, 68.9, 52.8, 52.2, 51.2, 49.8, 49.6, 49.4, 49.1, 48.9, 48.7, 48.5, 48.2, 48.1, 47.7, 47.6, 43.8, 43.4, 43.2, 41.1, 37.5, 37.3, 37.1, 36.9, 36.6, 36.0, 35.9, 35.8, 34.5, 33.6, 32.4, 32.0, 29.8, 29.7, 28.9, 28.6, 28.4, 28.1, 24.4, 24.3, 23.5, 23.3, 17.9, 17.7, 13.2, 13.1. MALDI-TOFMS (*m/z*): $[M + H]^+$ calcd for $C_{73}H_{122}N_3O_{10}$: 1201.8; found, 1200.8.

General procedure for the hydrolysis of methyl ester. The methyl ester of an oligocholate (0.10 mmol) was dissolved in a mixture of THF (1 mL) and MeOH (1 mL). A solution of 2 M LiOH (0.5 mL, 1 mmol) was added. The reaction was monitored by TLC and was complete in 10–24 h. The organic solvents were removed by rotary evaporation. After addition of a dilute HCl solution (30 mL, 0.05 M), the precipitate formed was collected by suction filtration or

centrifugation, washed with cold water, and dried in vacuo. The product was generally used in the next step without further purification.

Compound 1. Hydrolyzed **12** (122 mg, 0.103 mmol), 1-hydroxybenzotriazole hydrate (HOBt, 42 mg, 0.308 mmol), and benzotrazol-1-yloxytris (dimethylamino) phosphonium hexafluorophosphate (BOP, 136 mg, 0.308 mmol) were dissolved in anhydrous DMF (2 mL). *N,N*-Diisopropylethylamine (DIPEA, 0.10 mL, 0.618 mmol) was added. The reaction mixture was stirred at room temperature under N_2 for 2 d and was poured into a dilute HCl aqueous solution (100 mL, 0.05 M). The precipitate formed was collected by suction filtration, washed with water (3 x10 mL), dried in air, and purified by column chromatography over silica gel with CH_2Cl_2/MeOH (8:1) as the eluent to give an off-white powder (91 mg, 76%). ^{1}H NMR (400 MHz, $CDCl_3/CD_3OD$ = 1:1, δ): 3.99 (br, 3H), 3.86 (br, 3H), 3.59 (m, 3H), 2.29~1.04 (series of m, 81H), 0.95 (s, 9H), 0.73 (s, 9H). ^{13}C NMR (100 MHz, CD_3OD, δ): 174.5, 72.9, 67.9, 46.3, 46.0, 45.4, 42.0, 42.0, 41.7, 39.2, 36.1, 36.0, 35.9, 35.8, 35.7, 35.6, 35.5, 35.3, 34.8, 34.7, 34.7, 34.6, 34.5, 34.4, 34.4, 31.2, 31.1, 28.1, 28.0, 28.0, 27.5, 27.0, 27.0, 27.0, 26.6, 26.4, 23.1, 22.9, 22.4, 22.4, 17.0, 16.7, 12.1. MALDI-TOFMS (*m/z*): $[M + Na]^+$ calcd for $C_{72}H_{117}N_3O_9Na$: 1191.7; found, 1192.3.

Compound 2. Hydrolyzed **13** (136 mg, 0.0866 mmol), HOBt (24 mg, 0.173 mmol), and BOP (153 mg, 0.346 mmol) were dissolved in anhydrous DMF (9 mL). DIPEA (0.091 mL, 0.519 mmol) was added. The reaction mixture was stirred at 40 ºC under N_2 for 5 d and was poured into a dilute HCl aqueous solution (50 mL, 0.05 M). The precipitate formed was collected by suction filtration, washed with water (3 x10 mL), dried in air, and purified by column chromatography over silica gel with CH_2Cl_2/MeOH (20:1 to 15:1) as the eluent to give an off-white powder (48 mg, 36%). ^{1}H NMR (400 MHz, CD_3OD, δ): 3.96 (s, 4H), 3.80 (s, 4H), 3.50 (br, 4H), 2.33–0.82 (series of m, 120H), 0.72 (s, 12H). ^{13}C NMR (100 MHz, CD_3OD, δ): 175.5, 74.0, 68.9, 50.7, 47.3,

47.2, 43.1, 42.8, 40.5, 37.2, 36.9, 36.5, 35.7, 33.6, 32.9, 30.5, 29.3, 28.5, 28.1, 27.6, 24.2, 23.3, 17.9, 13.0. MALDI TOFMS (*m/z*): $[M + Na]^+$ calcd for $C_{96}H_{156}N_4NaO_{12}$, 1581.3; found, 1582.9, $[M + H]^+$ calcd for $C_{96}H_{157}N_4O_{12}$, 1559.3; found, 1560.9.

Compound 7. Hydrolyzed **5** (451 mg, 0.660 mmole), compound **6** (644 mg, 0.792 mmole), BOP (525 mg, 1.19 mmol), and HOBt (161 mg, 1.19 mmol) were dissolved in DMF (3 mL) and DIPEA (0.6 mL, 3.23 mmol) was added. The reaction mixture was stirred at 60 ^{0}C overnight, cooled down to room temperature, and poured into a dilute HCl aqueous solution (0.05 M, 100 mL). The precipitate formed was collected by suction filtration, washed with water, dried in air, and purified by column chromatography over silica gel with CH_2Cl_2/MeOH (10:1) as the eluent to give an off-white powder (914 mg, 91%). ^{1}H NMR (400 MHz, $CD_3OD/CDCl_3$ 1:1, δ): 7.30 (br, 5H), 5.04 (br, 2H) ,4.26 (br,1H) ,3.93 (br ,3H), 3.79 (br, 3H) 3.64 (s, 3H), 3.50 (br, 2H), 3.14(m, 3H), 2.18-0.89 (a series of m), 0.67 (d, 9H). ^{13}C NMR (100 MHz, $CDCl_3/CD_3OD$ = 1:1, δ): 175.6, 175.2, 174.5, 171.8, 157.6, 136.9, 128.5, 128.0, 127.8, 73.0, 68.1, 66.6, 61.6, 54.8, 53.2, 50.7, 48.8, 46.5, 42.8, 41.8, 39.5, 36.3, 35.4, 35.0, 33.6, 32.8, 31.8, 31.1, 29.9, 28.4, 27.7, 26.6, 23.3, 22.5, 18.2, 17.0, 12.6. ESI-MS (m/z): $[M + Na]^+$ calcd for $C_{86}H_{135}N_8O_{13}Na$, 1497.0100; found, 1496.9989.

Compound 8. Hydrolyzed **7** (150 mg, 0.201 mmol), BOP (82 mg, 0.184 mmol), and HOBt (25 mg, 0.184 mmol) were dissolved in DMF (0.5 mL). Propargyl amine (10 μL, 0.133 mmol) and DIPEA (0.1 mL, 0.514 mmol) were added. The reaction mixture was stirred at 60 ^{0}C overnight, cooled down to room temperature, and poured into a dilute HCl aqueous solution (0.05 M, 100 mL). The precipitate formed was collected by suction filtration, washed with water, dried in air, was used in the next step without further purification.

Compound 9. A solution of **8** (132 mg, 0.090 mmol) in 2:1 $CHCl_3/CH_3OH$ (2 mL) was

added via a syringe pump at 0.06 mL/hr to a vigorously stirred suspension of Cu powder (55 mg, 0.009 mmol) and $CuSO_4 \cdot 5H_2O$ (0.01 M, 0.9 mL, 0.872 mmol) in 2:1 $CHCl_3/CH_3OH$ (8 mL). The reaction was monitored by TLC. Upon disappearance of the starting material, the solvents were removed by rotary evaporation and the residue purified by column chromatography over silica gel with CH_2Cl_2: MeOH (10:1) as the eluent to give an off-white powder (93 mg, 71%). ^{1}H NMR (400 MHz, $CDCl_3/CD_3OD$ 1:1, δ): 7.69 (br, 1H), 7.36 (br, 1H),7.29 (br, 5H), 5.01 (br, 2H), 4.35 (br, 1H), 4.23 (br, 1H) ,3.93 (br ,3H), 3.79 (br, 3H), 3.47 (br, 2H), 3.12 (m, 2H), 2.75 (br, 1H), 2.34-0.77 (series of m), 0.67 (d, 9H). ^{13}C NMR (100 MHz, $CDCl_3/CD_3OD$ = 1:1, δ): 175.4, 174.9, 172.0, 157.6, 136.8, 128.5, 128.0, 127.5, 72.8, 66.5, 62.7, 53.7, 53.6, 46.8, 46.8, 46.0, 40.2, 35.2, 33.0, 29.0, 26.9, 22.5,17.1, 12.5, 12.4, 12.3. ESI-MS (m/z): $[M + H]^+$ calcd for $C_{88}H_{137}N_8O_{12}$, 1499.0429; found, 1499.0421.

Compound 10. Pd/C (160 mg, 10% wt) was added to a solution of **10** (132 mg, 0.088 mmol) in CH_3OH (30 mL). The mixture was stirred under a H2 balloon at room temperature for 3 d. Pd/C was removed by filtration through a pad of silica gel and the solvent was removed by rotary evaporation to give a white power (96 mg, 80%). ^{1}H NMR (400 MHz, $CDCl_3/CD_3OD$ = 1:1, δ): 8.02 (m, 1H), 7.84 (m, 1H), 7.42 (m, 1H), 4.26 (m, 3H), 3.92 (br, 1H), 3.80 (br, 1H), 3.64 (s, 3H), 3.50 (br, 2H), 2.97 (br, 2H), 2.74 (br, 1H), 2.42–0.77 (series of m), 0.67 (s, 9H). ^{13}C NMR (100 MHz, $CDCl_3/CD_3OD$ = 1:1, δ): 176.2, 175.6, 172.0, 145.32], 130.3, 129.2, 126.5, 121.6, 73.7, 68.8, 67.6, 62.4, 53.8, 47.1, 42.8, 37.6, 35.5, 32.7, 30.1, 28.7, 27.4, 23.2, 21.3, 17.8, 16.8, 14.5, 13.0, 11.6, 11.4, 9.2. ESI-MS (m/z): $[M + H]^+$ calcd for $C_{80}H_{131}N_8O_{10}$, 1363.9983; found, 1363.9966.

Compound 4. Compound **10** (100 mg, 0.073 mmol), **11** (57 mg, 0.146 mmol), and DIPEA (0.064 mL, 0.366 mmol) were dissolved in anhydrous DMF (0.5 mL). The mixture was allowed

to react in a microwave reactor at 100 °C for 30 min. The reaction mixture was poured into a dilute HCl aqueous solution (0.05 M, 50 mL). The precipitate formed was collected by suction filtration, washed with water, dried in air, and purified by preparative TLC with $CHCl_3/CH_3OH$ (9:1) as the developing solvent to give an off-white power (50 mg, 42%). ^{1}H NMR (400 MHz, $CDCl_3/CD_3OD$ = 1:1, δ): 8.29 (d, 1H), 8.00 (m, 2H), 7.97 (m, 2H), 7.79 (m, 2H), 4.30 (m, 3H), 3.92 (br ,3H), 3.78 (br, 3H), 3.48 (br, 2H), 3.19 (m, 2H), 2.72 (br, 1H), 2.38-1.0 (a series of m), 0.67 (m, 7H), 0.57 (s, 1H), 0.52 (s, 1H). ^{13}C NMR (100 MHz, $CDCl_3/CD_3OD$ = 1:1, δ): 175.3, 174.9, 174.5, 171.9,144.5, 136.0, 127.3, 125.9, 125.1,125.0,124.9,124.8, 124.7, 123.3, 120.7, 72.9, 68.0, 61.5, 53.5, 49.6, 46.4, 45.7, 42.2, 39.5, 36.7, 35.7, 34.6,32.7, 31.8, 29.6,27.5, 27.1, 26.6, 25.9, 23.1, 22.3, 17.0, 12.2. ESI-MS (m/z): $[M + H]^+$ calcd for $C_{100}H_{145}N_8O_{11}$, 1634.1027; found, 1634.1036.

Liposome preparation

Glucose-loaded LUVs were prepared according to a slightly modified literature procedure.[3] A chloroform solution of POPC (25 mg/mL, 198 μL) and POPG (50 mg/mL, 10.0 μL) was placed in a 10 mL test tube and dried under a stream of nitrogen. The residue was dried further under high vacuum overnight. A solution of D-(+)-glucose (300 mM) in 50 mM Tris buffer (0.5 mL, pH = 7.5) was added. Rehydration of the lipids was allowed to continue for 30 min with occasional vortexing. The opaque dispersion was subjected to ten freeze–thaw cycles. The resulting mixture was extruded twenty-nine times through a polycarbonate filter (diameter = 19 mm, pore size = 100 nm) at room temperature using an Avanti Mini-Extruder. A portion (0.3 mL) of the liposome solution was passed through a column of Shepadex G-50 using Tris buffer (50 mM Tris, 150 mM NaCl, pH=7.5) as the eluent to remove the extravesicular glucose. The liposome fractions were combined and diluted to 5.0 mL with the Tris buffer. The concentration of phospholipids in the stock solution was 0.86 mM. Maltotriose-loaded LUVs were prepared

in the similar fashion of preparation of glucose-loaded LUVs. A chloroform solution of POPC (25 mg/mL, 198 μL) and POPG (50 mg/mL, 10.0 μL) was placed in a 10 mL test tube and dried under a stream of nitrogen. The residue was dried further under high vacuum overnight. A solution of maltotriose (200 mM, 0.5 mL) in Milipore water was added. Rehydration of the lipids, freeze-thaw cycles, and extrusions were followed in the same way as glucose-loaded LUVs. A portion (0.3 mL) of the liposome solution was passed through a column of Shepadex G-50 using HEPES buffer (50 mM HEPES, 100 mM NaCl, pH=7.0) as the eluent to remove the extravesicular maltotriose. The liposome fractions were combined and diluted to 5.0 mL with the HEPES buffer. The concentration of phospholipids in the stock solution was 0.86 mM.

Glucose leakage assay

Glucose released from the liposomes was measured enzymatically by a slightly modified literature procedure.[4] Aliquots of the above LUV solution (250 μL), Tris buffer (750 μL, 50 mM Tris, pH = 7.5, 145 mM NaCl, 3.5 mM $MgCl_2$, and 0.15 mM $CaCl_2$), the enzyme solution (500 μL, 10 units/mL of hexokinase/glucose-6-phosphoate dehydrogenase and 2 mM ATP dissolved in the above Tris buffer), and NADP solution (500 μL, 1 mM dissolved in the above Tris buffer) were placed in a series of cuvettes. The concentration of phospholipids in each cuvette was 107 μM. Aliquots of the oligocholate solution in DMSO were added to different cuvettes via a microsyringe. The amount of DMSO introduced to each sample was ≤20 μL. The absorbance of NADPH at 340 nm was monitored. To measure the nonspecific glucose leakage from the liposomes, the sample was prepared in an identical fashion and DMSO instead of the oligocholate solution was added. After 1 h, the liposomes were lysed by the addition of 100 μL of Triton X-100 (1% v/v) and the absorbance at 340 nm (A_∞) was used to calculate the percent leakage [= $(A_t - A_0)/(A_\infty - A_0) \times 100$]. A_0 and A_t are the initial and intermediate absorbance, respectively.

Maltotriose leakage assay

Maltotriose released from the liposomes was measured enzymatically by a modified literature procedure.[5] Aliquots of the LUV solution (250 µL, [maltotriose] = 200 mM), HEPES buffer (350 µL, 50 mM HEPES, pH = 7.0, 95 mM NaCl, 3.5 mM $MgCl_2$, and 0.15 mM $CaCl_2$), the enzyme I solution (400 µL, 100 units/mL of α-glucosidase in the above HEPES buffer), the enzyme II solution (500 µL, 10 units/mL of hexokinase/glucose-6-phosphoate dehydrogenase and 2 mM ATP dissolved in the above HEPES buffer), and NADP solution (500 µL, 1 mM dissolved in the above HEPES buffer) were placed in a series of cuvettes. The concentration of phospholipids in each cuvette was 107 µM. Aliquots of the oligocholate solution in DMSO were added to different cuvettes via a microsyringe. The amount of DMSO introduced to each sample was ≤20 µL. The absorbance of NADPH at 340 nm was measured by the same procedure as the glucose leakage assay. After 1 h, the liposomes were lysed by the addition of 10 µL of Triton X-100 (10% v/v) and the absorbance at 340 nm (A_∞) was used to calculate the percent leakage as glucose leakage assay.

Lipid mixing assay[6]

Unlabeled POPC/POPG LUVs were prepared with a mixture of POPC (25 mg/mL, 198 µL) and POPG (50 mg/mL, 10 µL) using HEPES buffer (10 mM HEPES, 107 mM NaCl, pH=7.4), following the procedure described above. Gel filtration was not needed in this experiment. Labeled POPC/POPG LUVs containing 1 mol % of NBD-DPPE and Rh-DPPE were prepared in the same manner. The labeled and the unlabeled LUVs were mixed in a 1:4 ratio. An aliquot of the mixed LUVs (15 µL) was placed in a cuvette and diluted with the HEPES buffer to 2.0 mL. The concentration of lipids was 54 µM in the final mixture. The change of NBD fluorescence (λ_{ex} = 450 nm and λ_{em} = 530 nm) was measured upon injection of the oligocholate solution (0.5 mM in DMSO, 10 µL). An increase of NBD emission indicates dilution of membrane bound

probes caused by membrane fusion. The percentage of fusion was determined using equation,

$$\% \text{ Fusion} = (F_t - F_0)/(F_{max} - F_0) \times 100\%$$

in which F_t is the emission intensity of NBD during the assay, F_0 the initial intensity, and F_{max} the maximum intensity (measured for LUVs containing 0.2 mol % each of NBD-DPPE and Rh-DPPE).

Incorporation of oligocholates into liposomes by detergent dialysis

A typical procedure is as follows. Dilauroylphosphatidylcholine (DLPC) lipid was purchased from Avanti Polar Lipids and stored at -20 ^{0}C. Bio-Beads® SM-2 adsorbent was from BioRad Laboratories. Oligocholate-containing liposomes were prepared according to a literature procedure.[7] A stock solution of Brij 35 (50 mM) was prepared in HEPES buffer (10 mM HEPES, pH 7.4, 100 mM NaCl). Aliquots (20 μL) of **4** (2×10^{-4} M in $CHCl_3/CH_3OH$) were added to 10 glass test tubes. Aliquots of DLPC (25 mg/mL) were added to the test tubes so that the [oligocholate]/[phospholipids] ratios were 0.0005, 0.001, 0.002, 0.005, 0.006, 0.007, 0.01, 0.02, 0.05, and 0.10, respectively. The solvents were removed under a stream of nitrogen gas. The samples were then placed under high vacuum overnight to form a film of lipids on the bottom of the test tubes. The film was rehydrated by the Brij 35 stock solution diluted to 66 mM by HEPES buffer (10 mM HEPES, pH 7.4, 100 mM NaCl). Bio-Beads SM-2 washed according to the literature procedure[4] and stored in HEPES buffer (10 mM HEPES, pH 7.4, 100 mM NaCl) (50 mg) was added and the mixture was stirred at room temperature for 2 h to remove the detergent. Another batch of the Bio-Beads (300 mg) was added and the mixture was stirred for 0.5 h and allowed to sit at room temperature overnight. The supernatant was separated from the beads and the fluorescence spectra were recorded. The excitation wavelength was 350 nm.

Addition of oligocholates to pre-formed LUVs

Cholesterol-containing POPC/POPG LUVs were prepared following the liposome preparation method. Aliquots of the LUV solution (250 μL) were added to 10 separate cuvettes containing HEPES buffer (1.75 mL, 10 mM HEPES, 107 mM NaCl, pH 7.4). The final concentration of lipids was 107 μM in each cuvette. Different amounts of **4** in DMSO were added to the cuvettes via a microsyringe and the final concentration of **4** ranged from 50 nM to 2.0 μM. The amount of DMSO introduced to each sample was ≤20 μL. The samples were allowed to sit at room temperature for 10 min before the fluorescence spectra were recorded. The excitation wavelength was 350 nm.

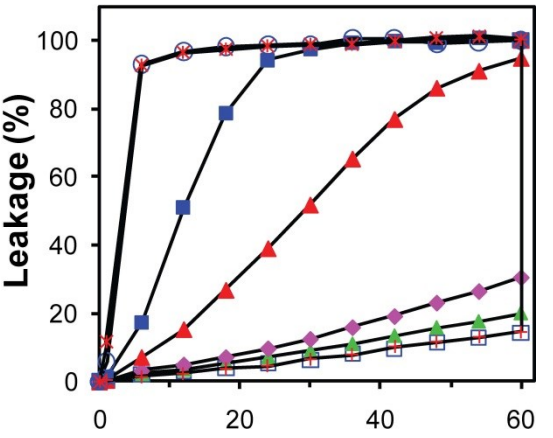

Figure 1S. Percent leakage of glucose from POPC/POPG large unilamellar vesicles (LUVs) upon addition of different concentrations of cyclic tricholate **1**: 0 (+), 0.05 (□), 0.125 (▲), 0.25 (◆), 0.5 (▲), (■) 1.25, 2.5 (○), and 5 μM (✳). Total concentration of phospholipids was 107 μM. The average diameter of the LUVs was about 100–120 nm. The concentration of glucose was 300 mM within the LUVs. The liposomes were lysed at 60 min upon addition of 0.1% Triton X-100.

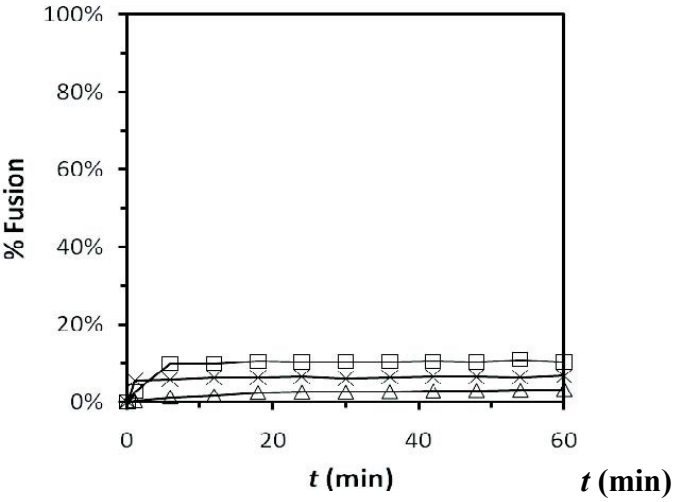

Figure 2S. Percent fusion of LUVs as a function of time for **1** (□), **2** (△), and **3** (×). The data points are connected to guide the eye. [oligocholate] = 2.5 μM, [lipid] = 54 μM.

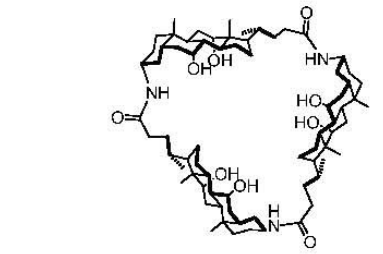

1

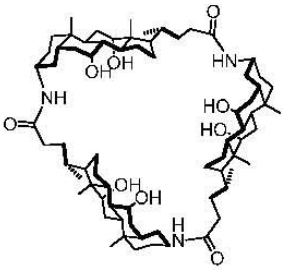

1

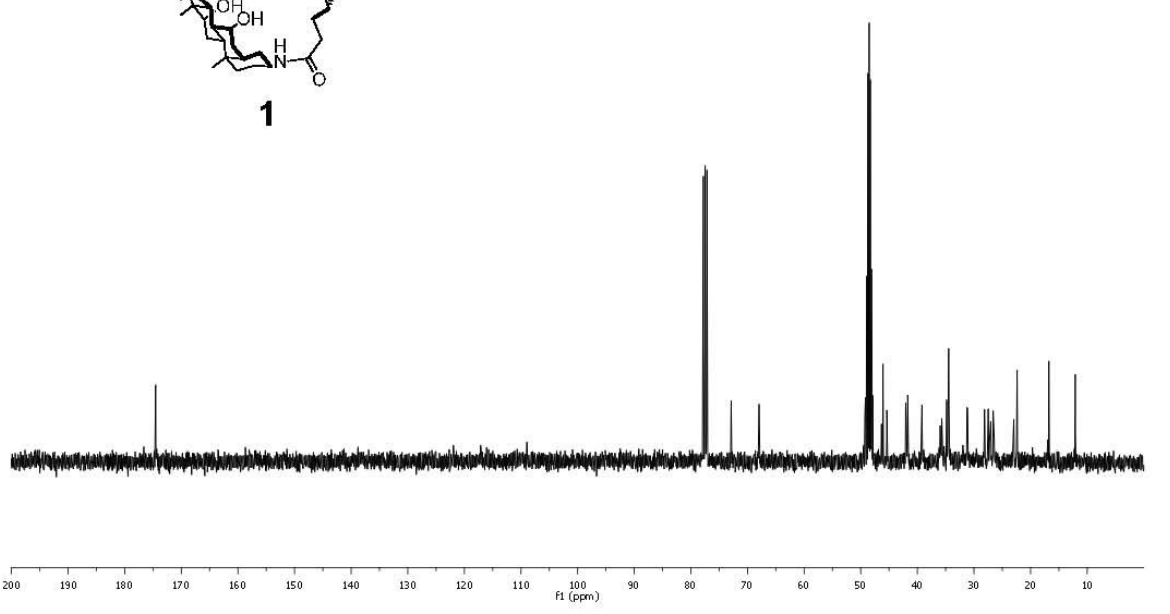

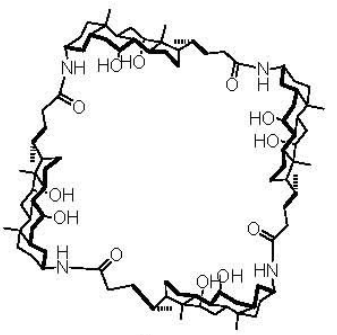

2

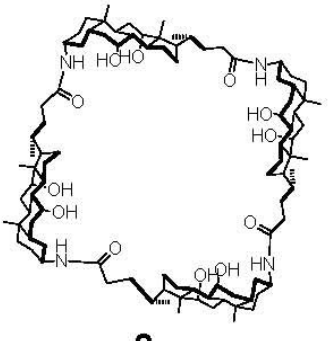

2

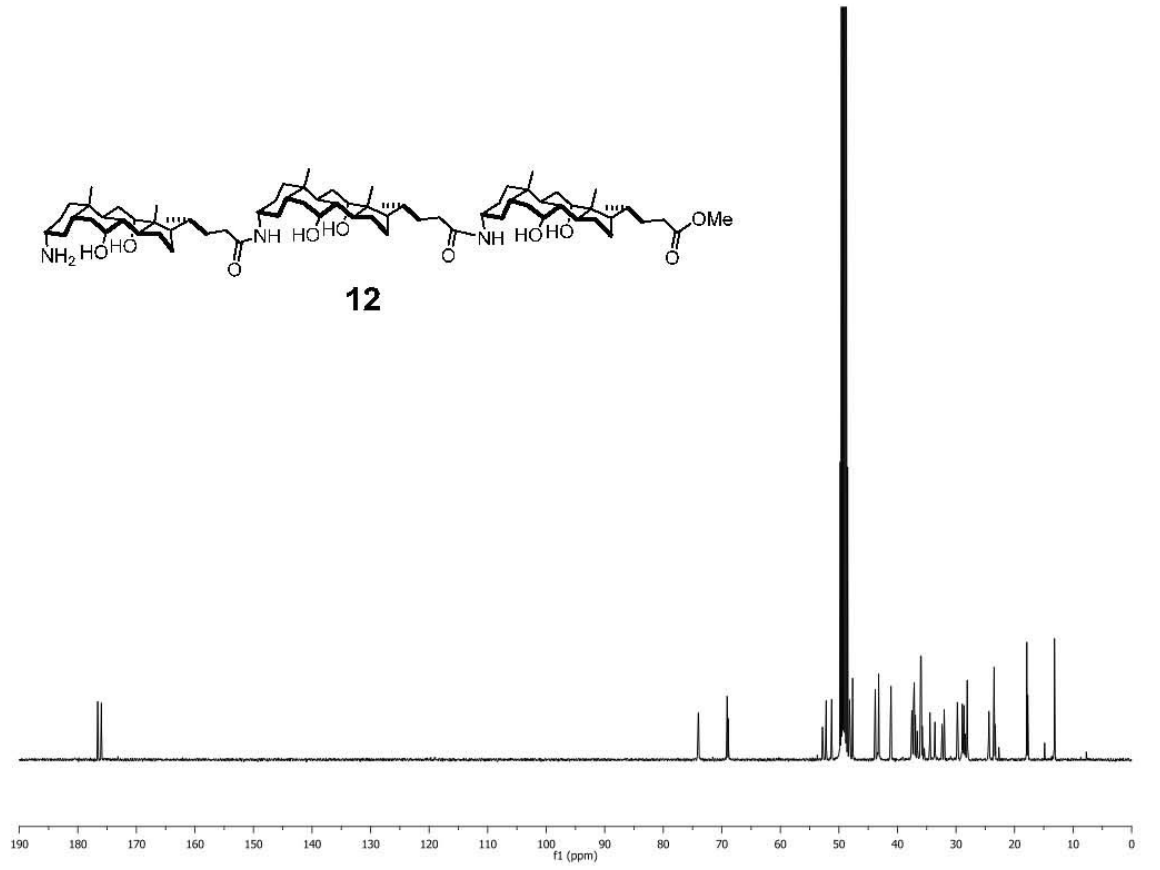

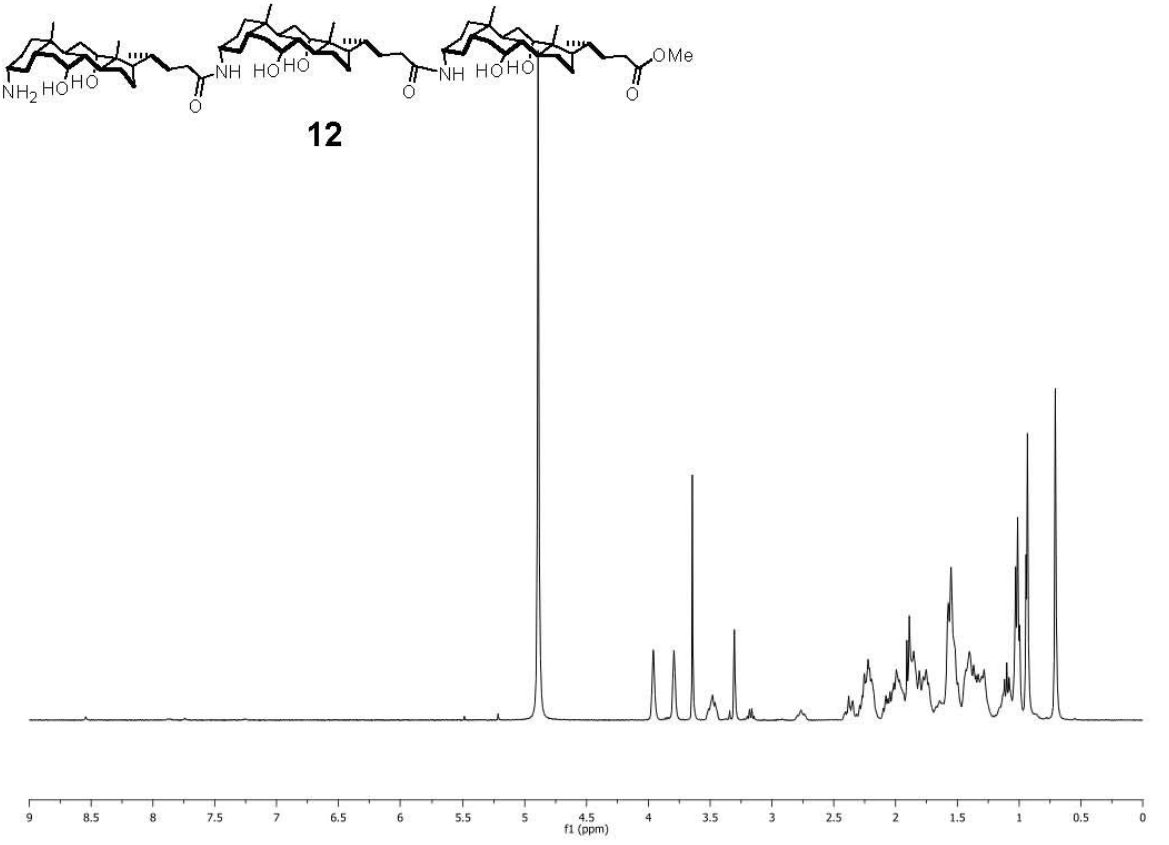

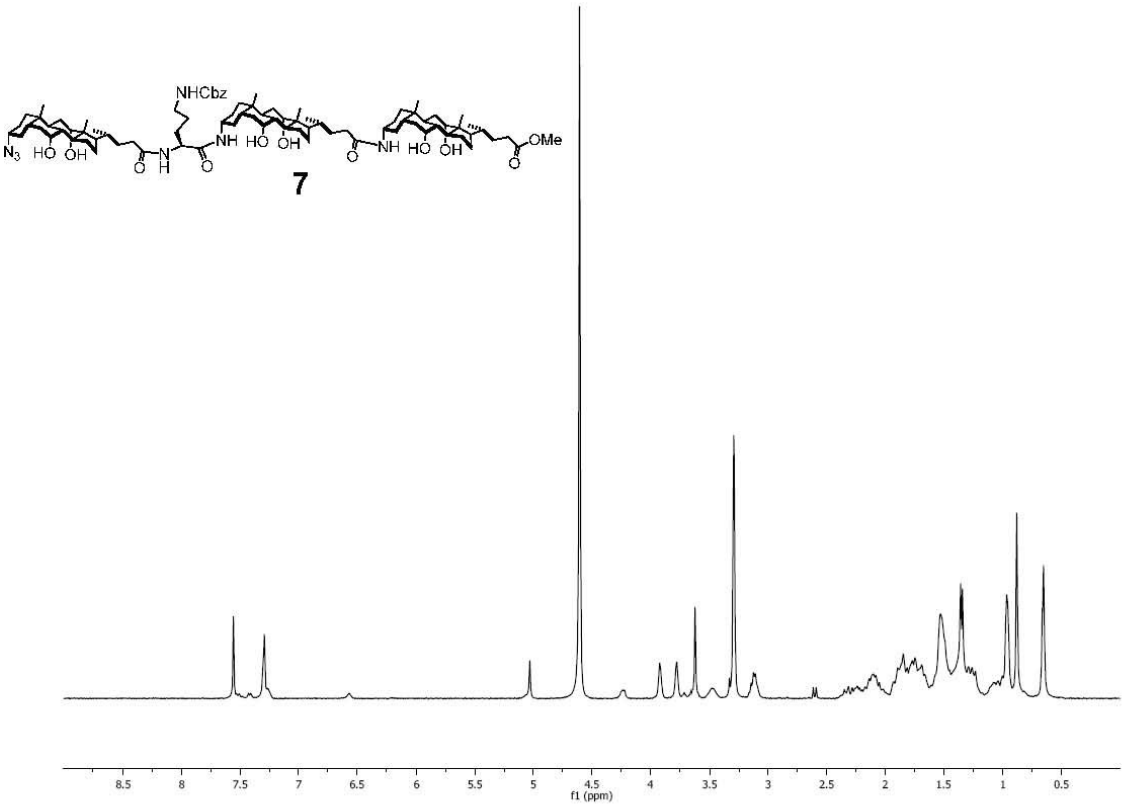

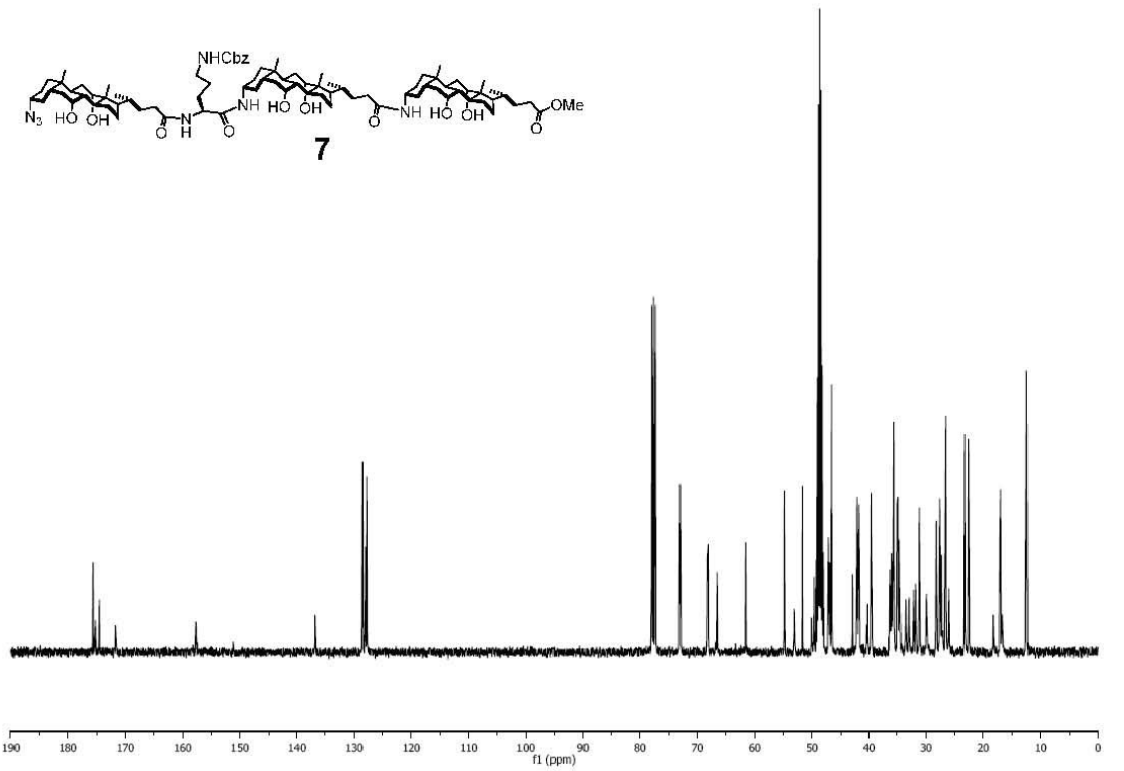

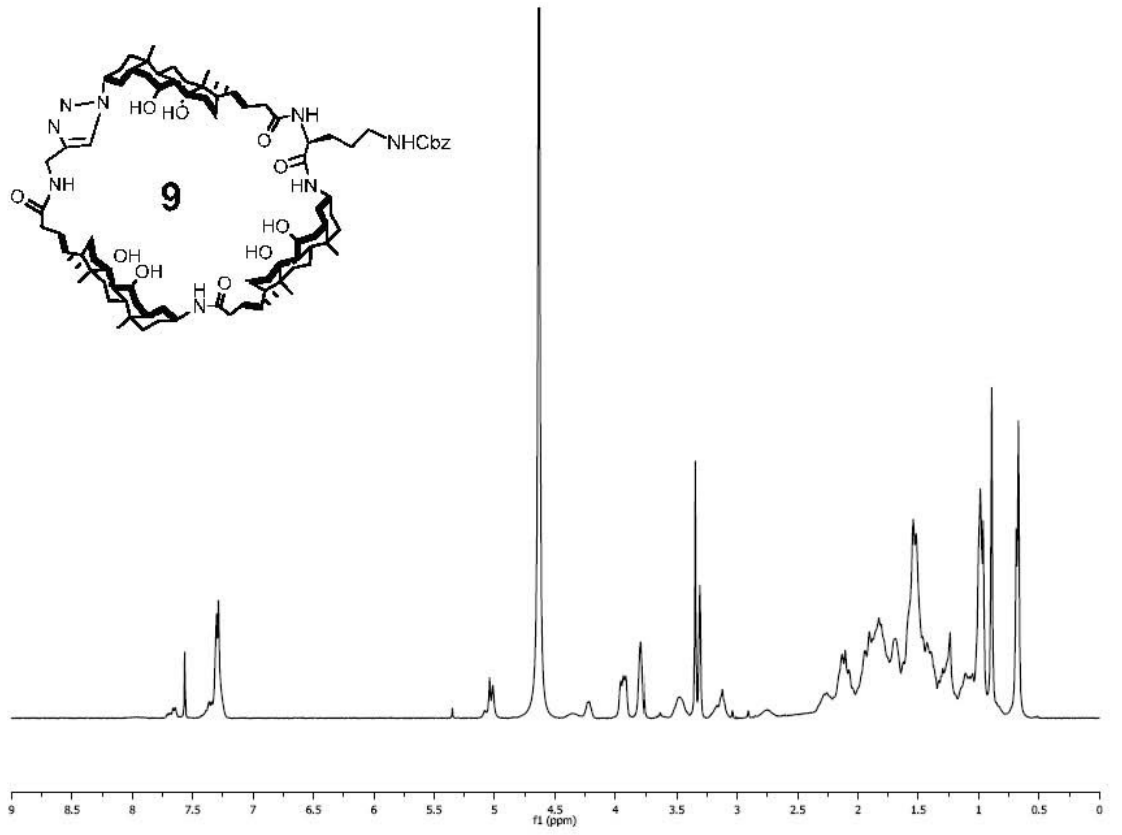

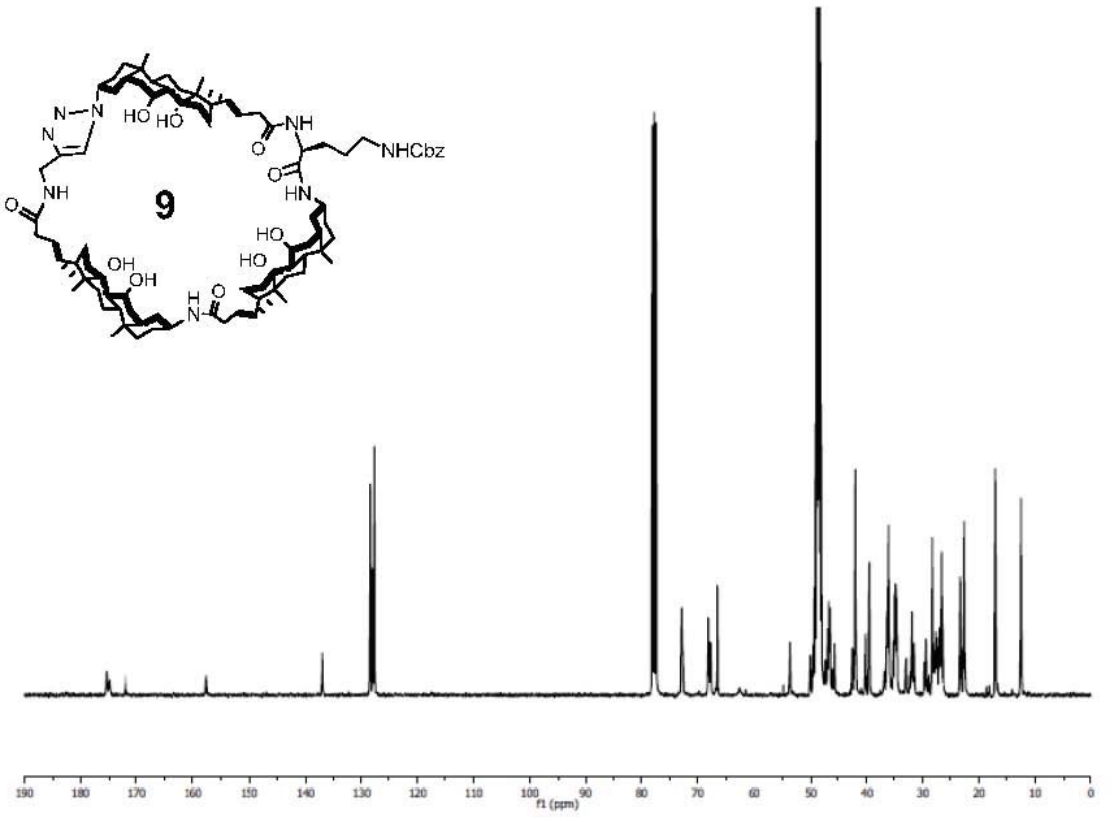

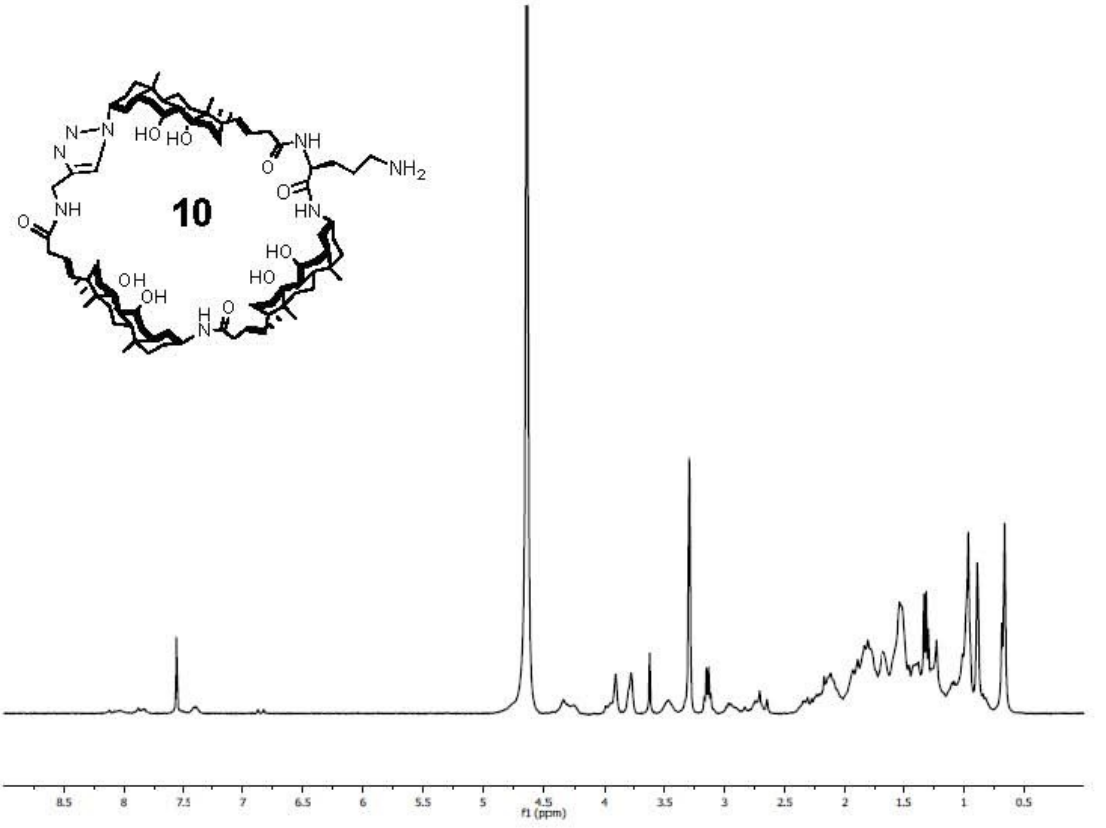

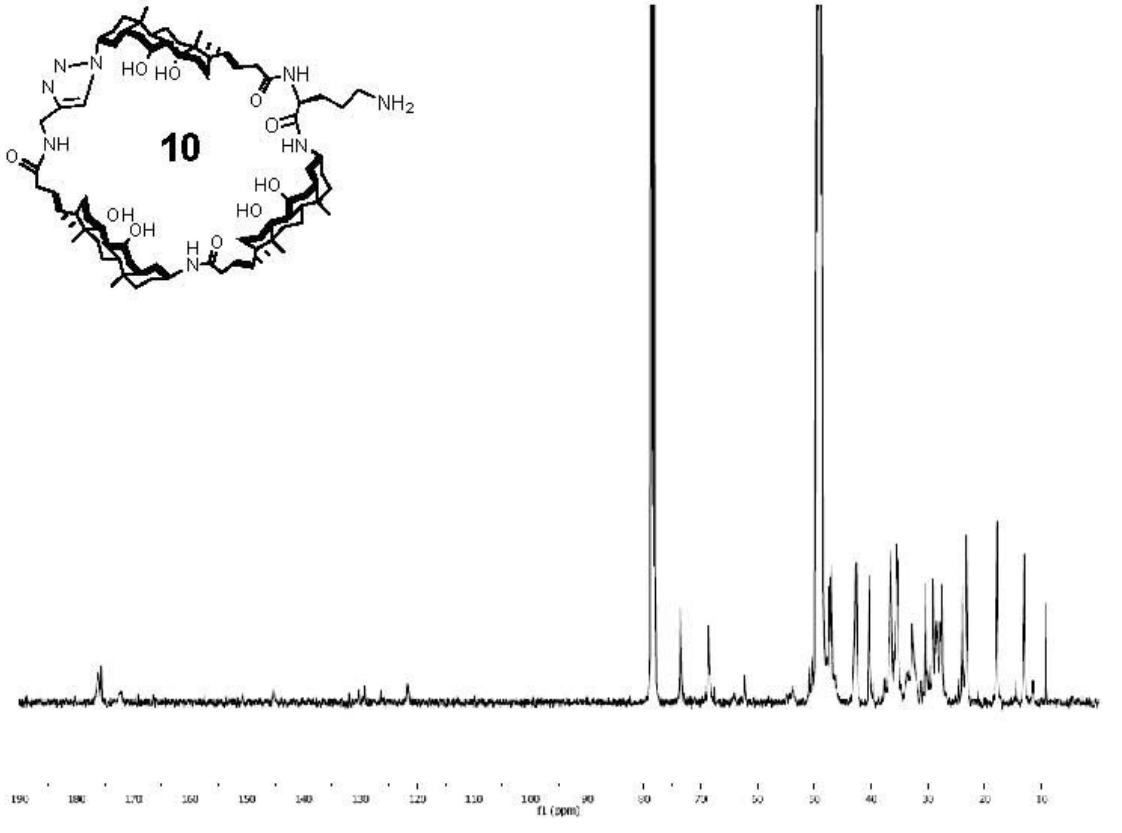

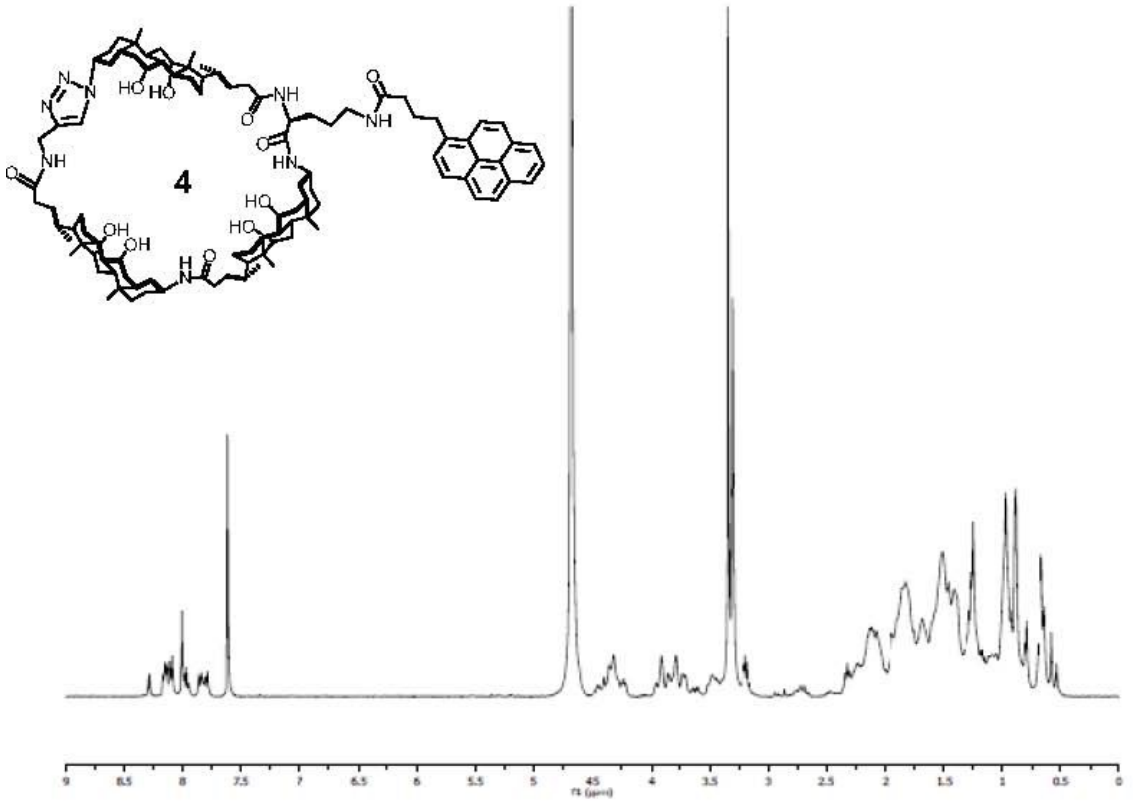

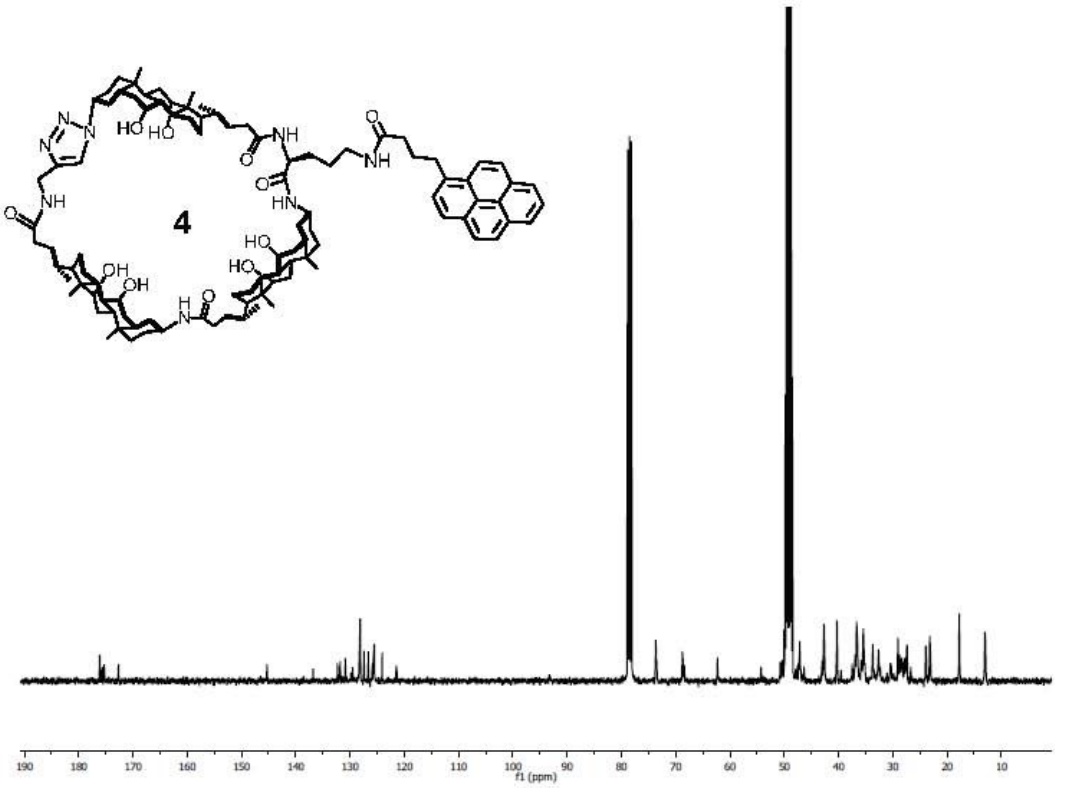

References

(1) Zhao, Y.; Zhong, Z. *J. Am. Chem. Soc.* **2005**, *127*, 17894–17901.

(2) Cho, H.; Zhao, Y. *J. Am. Chem. Soc.* **2010**, *132*, 9890–9899.

(3) Westmark, P. R.; Gardiner, S. J.; Smith, B. D. *J. Am. Chem. Soc.* **1996**, *118*, 11093-11100.

(4) Kinsky, S. C.; Haxby, J. A.; Zopf, D. A.; Alving, C. R.; Kinsky, C. B. *Biochemistry* **1969**, *10*, 4149–4158.

(5) Beutler, H.-O. In *Methods of Enzymatic Analysis, 3rd Ed.,* Vol. 4**;** Bergmeyer, H. U., Ed.; Verlag Chemie: Weinheim, 1984; pp 119-126.

(6) Struck, D. K.; Hoekstra, D.; Pagano, R. E. *Biochemistry* **1981**, *20*, 4093–4099.

(7) Smith, S. A.; Morrissey, J. H. *J. Thromb. Haemost.* **2004**, 2, 1155-1162.

II. Aromatically Functionalized Cyclic Tricholate Macrocycles: Aggregation, Transmembrane Pore Formation, Flexibility, and Cooperativity (Chapter 3, pg. 35-64)

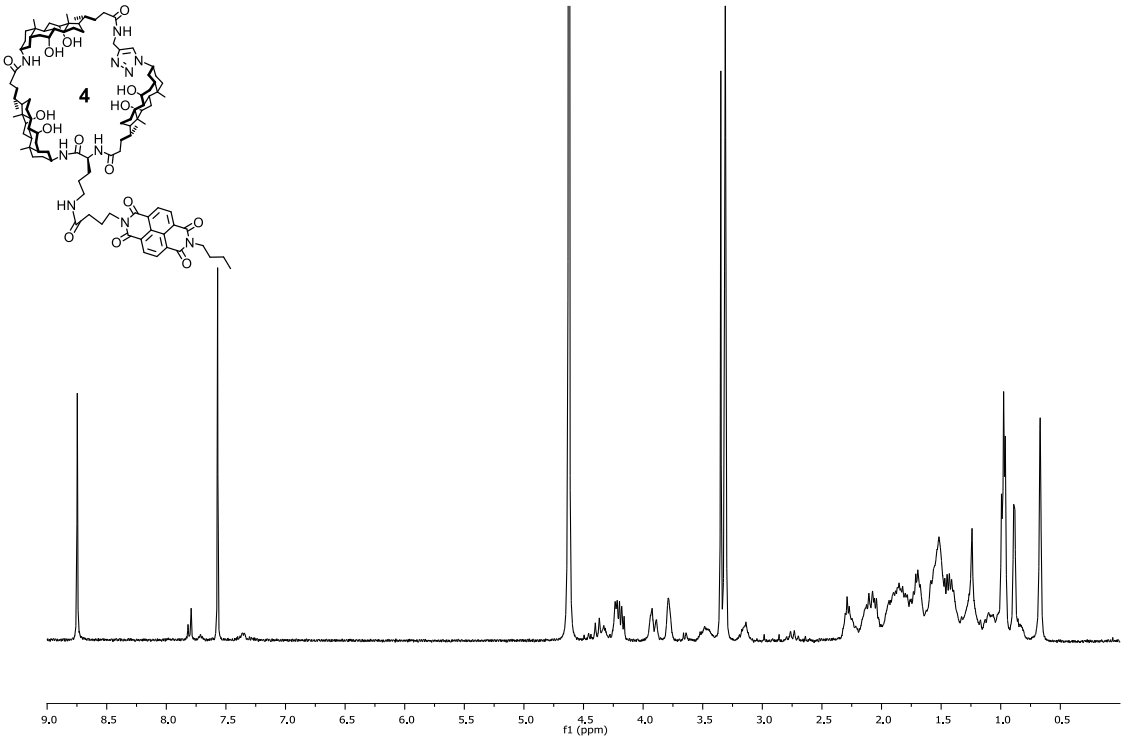

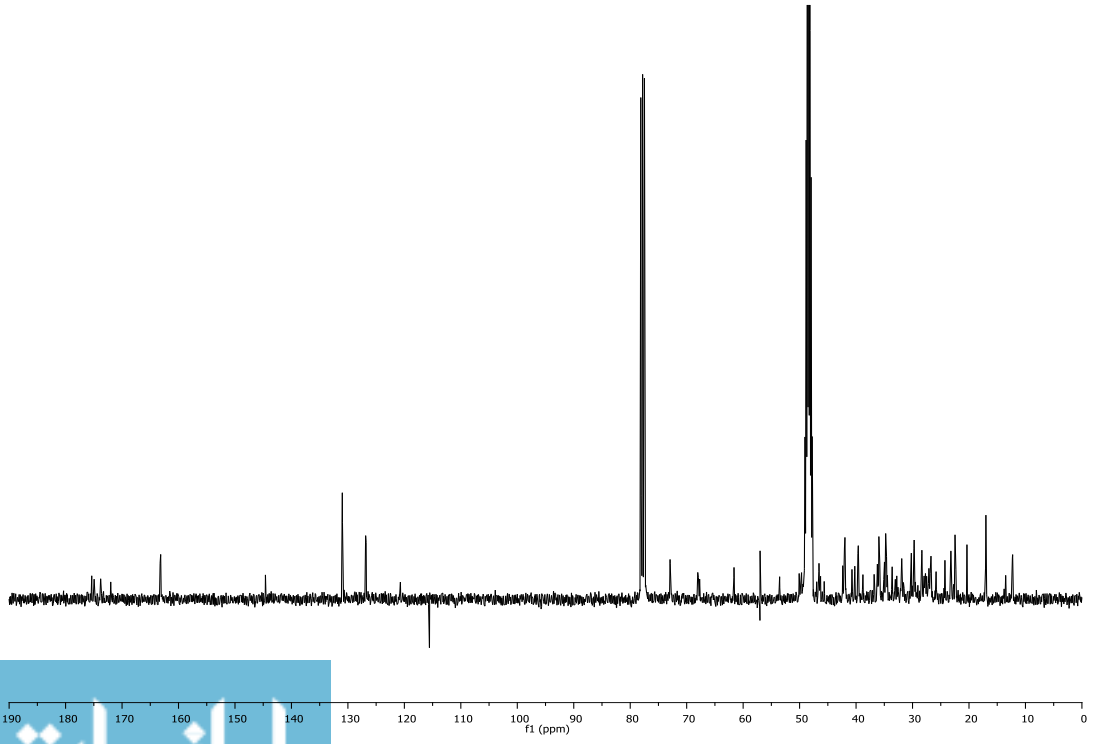

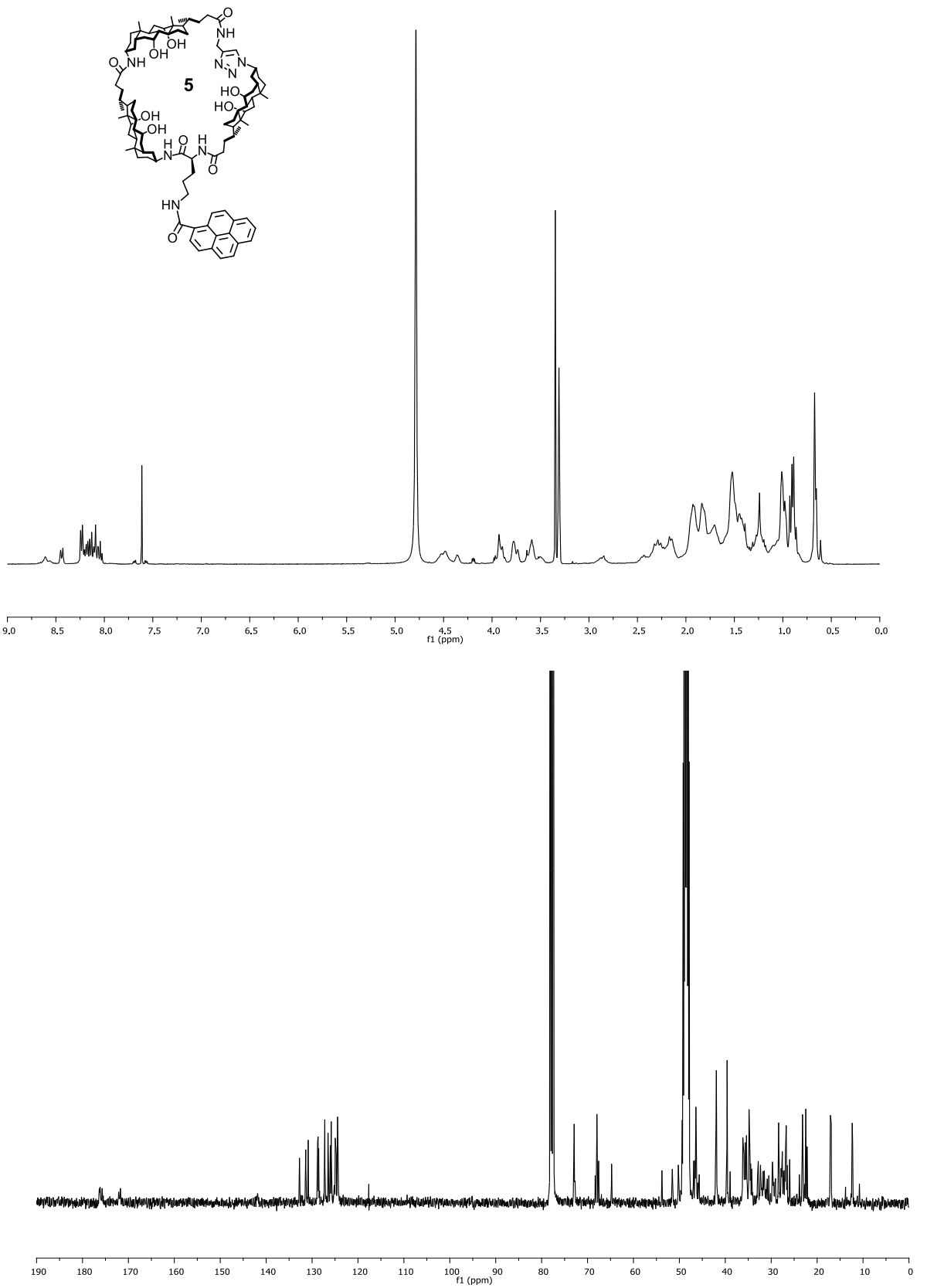

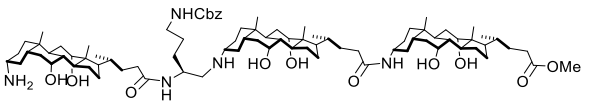

13

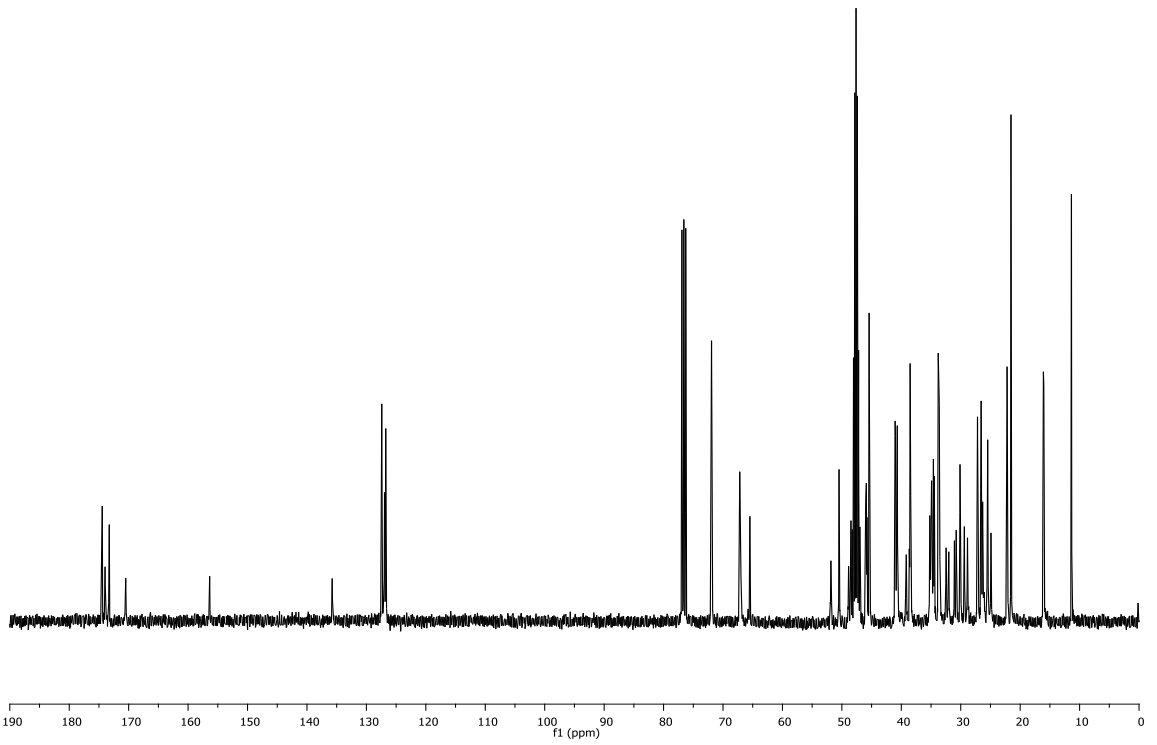

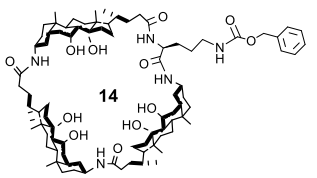

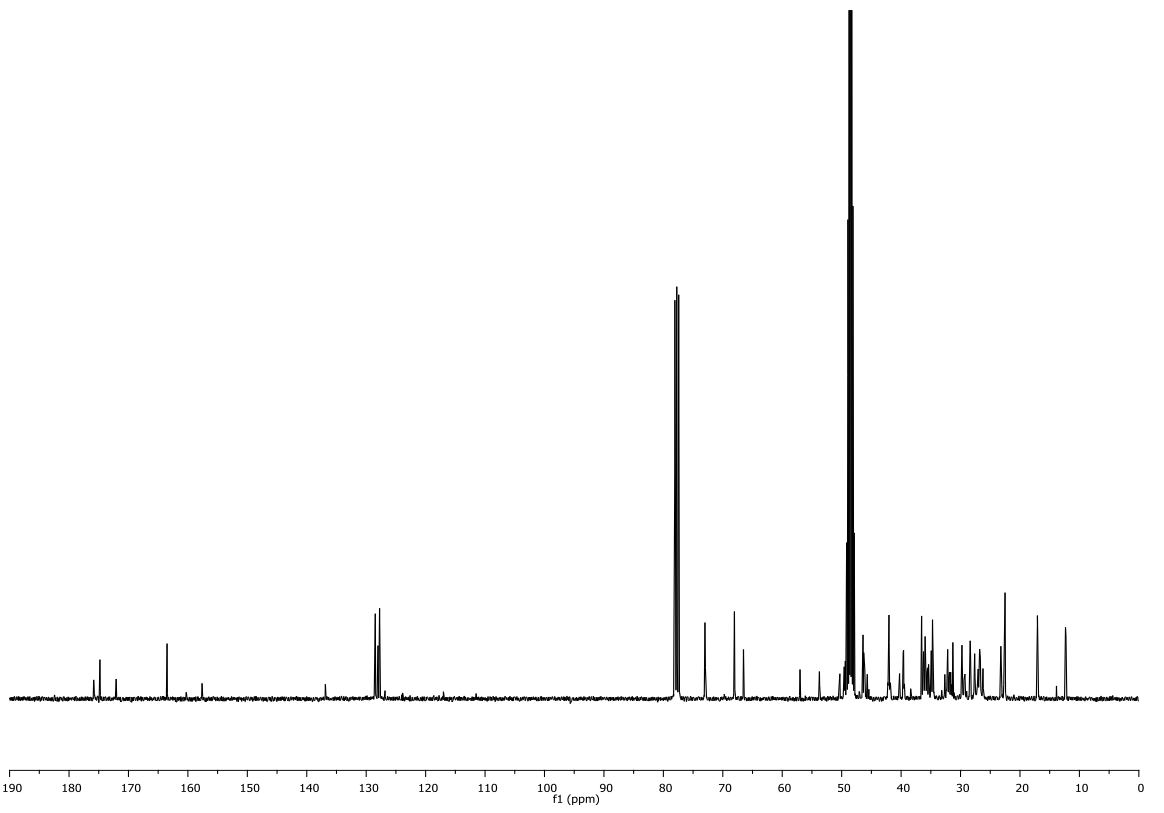

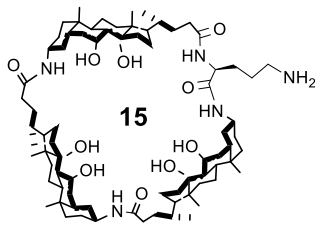

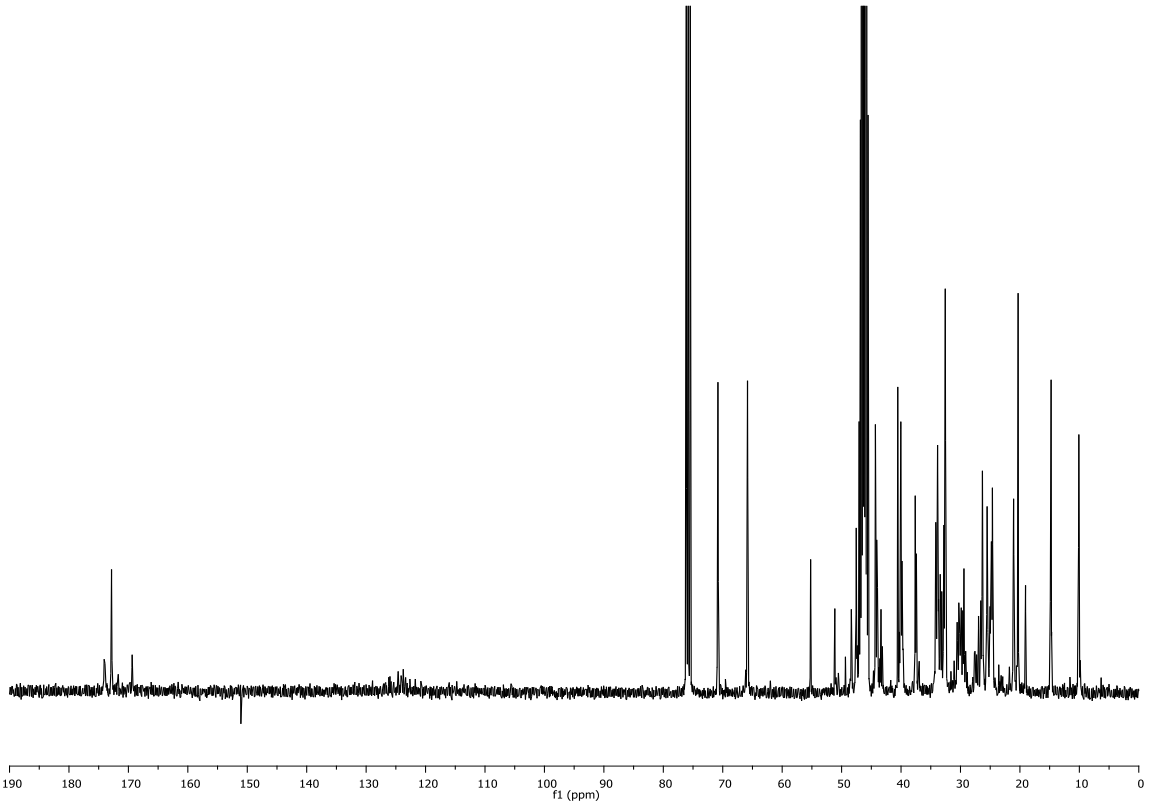

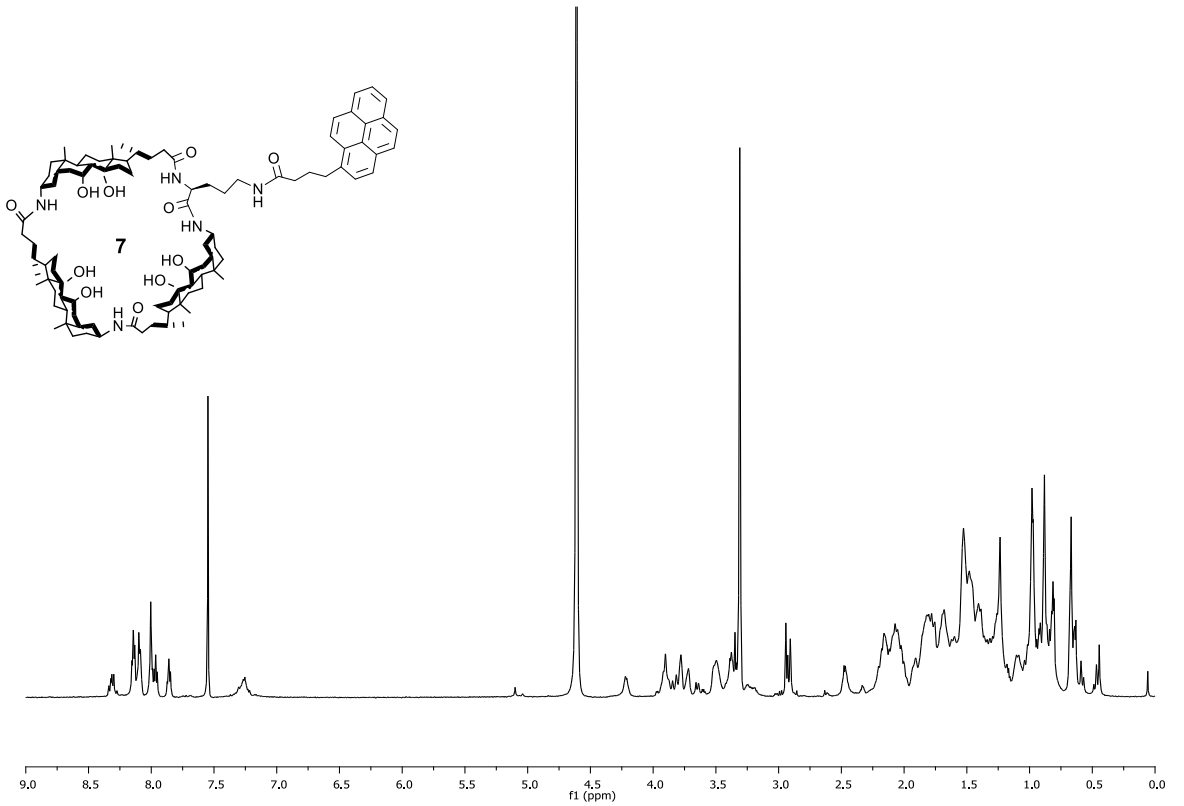

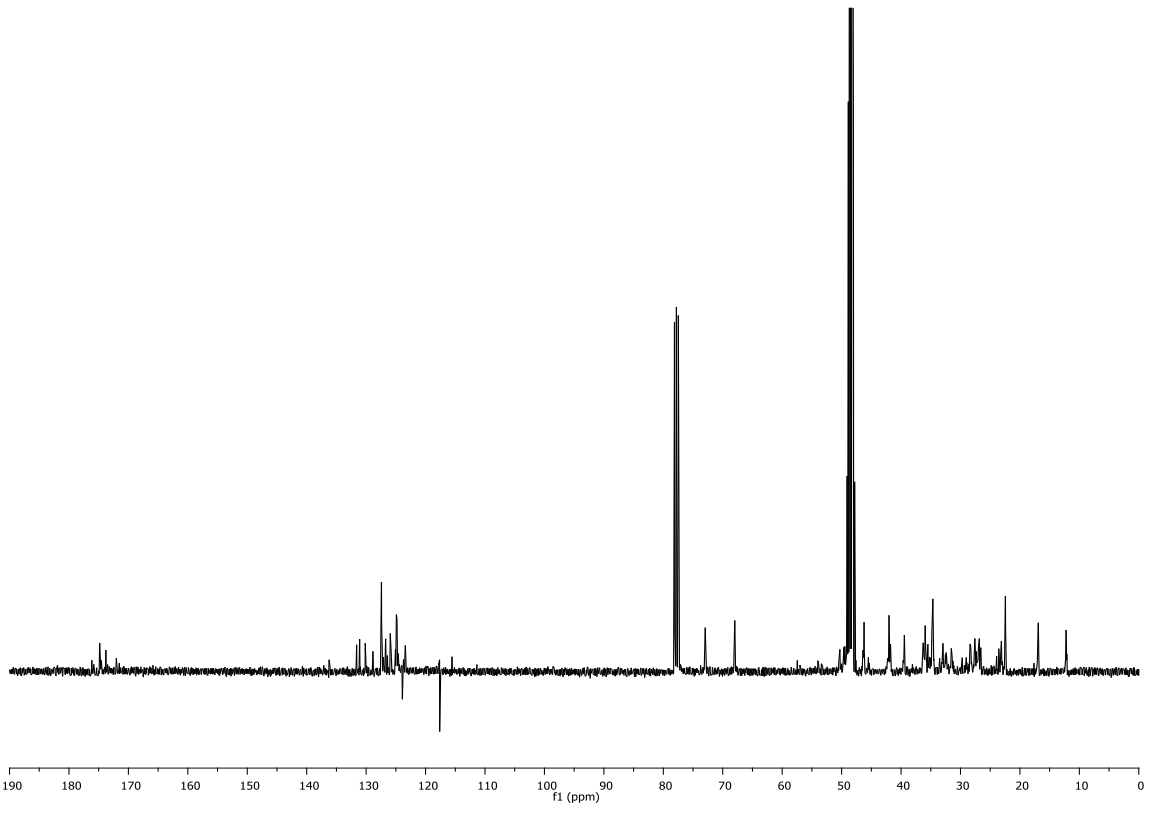

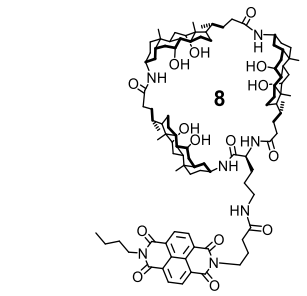

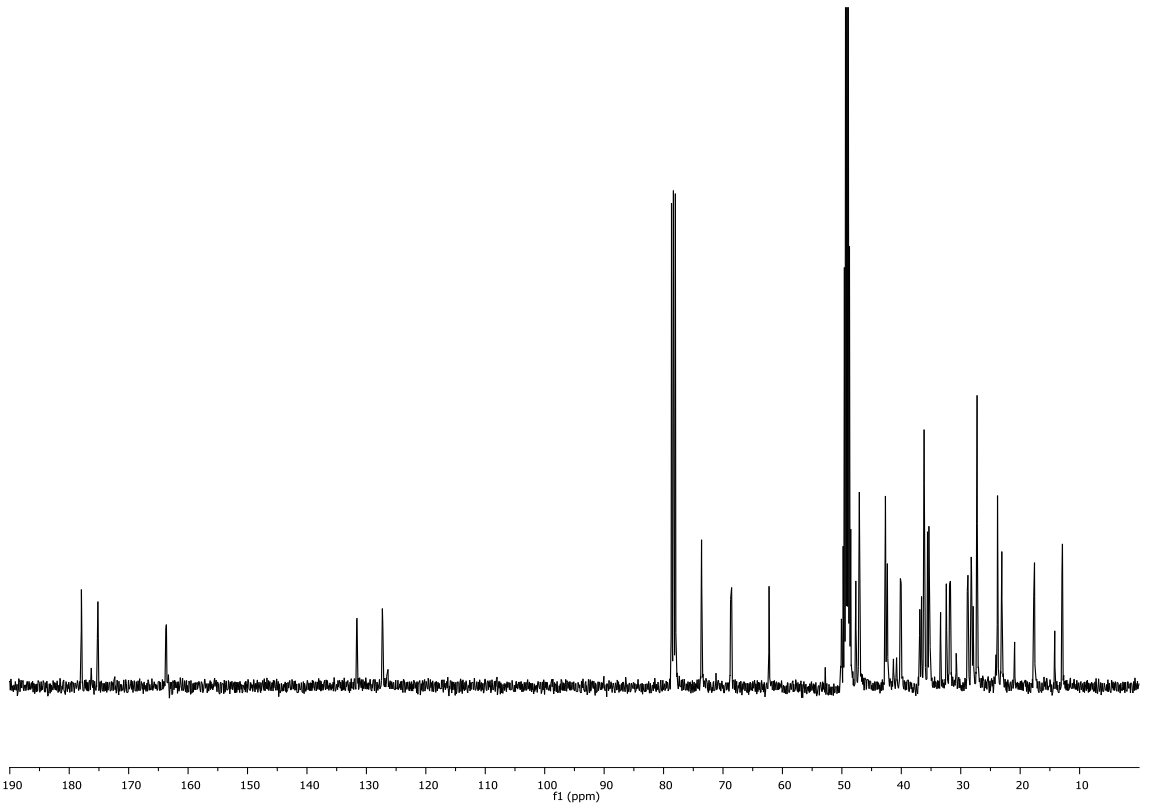

III. Hydrogen Bond-Assisted Macrocyclic Oligocholate Transporters in Lipid Membranes (Chapter 4, pg. 65-88)

Abbreviation

ATP: adenosine 5´-triphosphoate; CF: carboxyfluorescein; HEPES: 4-(2-hydroxyethyl)-1-piperazineethanesulfonic acid; NADP: Nicotinamide adenine dinucleotide phosphate; NBD-DPPE:N-(7-nitro-2-1,3-benzoxadiazol-4-yl)-1,2-dipalmitoyl-sn-glycero-3-phosphoethanolamine ammonium salt; POPC: 1-palmitoyl-2-oleoyl-sn-glycero-3-phosphocholine; POPG: 1-palmitoyl-2-oleoyl-sn-glycero-3-[phospho-rac-(1-glycerol)] sodium salt; Rh-DPPE: N-(lissamine rhodamine B sulfonyl) -1,2-dipalmitoyl-sn-glycero-3-phosphoethanolamine ammonium salt; Tris: tris(hydroxymethyl)aminomethane.

Preparation of the LUVs

CF-containing LUVs were prepared according to a slightly modified literature procedure.[1] A chloroform solution of POPC (25 mg/mL, 198 μL) and POPG (50 mg/mL, 10.0 μL) was placed in a 10 mL test tube and dried under a stream of nitrogen. The residue was dried further under high vacuum overnight. A solution of CF-HEPES buffer (0.5 mL, 50 mM CF, 10 mM HEPES, 10 mM NaCl, pH=7.4) was added. Rehydration of the lipids was allowed to continue for 30 min with occasional vortexing. The opaque dispersion was subjected to ten freeze–thaw cycles. The resulting mixture was extruded twenty-nine times through a polycarbonate filter (diameter = 19 mm, pore size = 100 nm) at room temperature using an Avanti Mini-Extruder. A portion (0.1 mL) of the liposome solution was passed through a column of Sephadex G-50 using HEPES buffer (10 mM HEPES, 107 mM NaCl, pH=7.4) as the eluent to remove the extravesicular CF. The liposome fractions were combined and diluted to

10.0 mL with the HEPES buffer. The concentration of phospholipids in the stock solution was 0.14 mM.

Glucose-leakage assay

Glucose-loaded LUVs were prepared according to a slightly modified literature procedure with 300 mM of D-(+)-glucose in 50 mM Tris buffer (0.5 mL, pH = 7.5).[2] The concentration of phospholipids in the stock solution was 0.86 mM. Glucose released from the liposomes was measured enzymatically by a slightly modified literature procedure.3Aliquots of the above LUV solution (250 μL), Tris buffer (750 μL, 50 mM Tris, pH = 7.5, 145 mM NaCl, 3.5 mM $MgCl_2$, and 0.15 mM $CaCl_2$), the enzyme solution (500 μL, 10 units/mL of hexokinase/glucose-6-phosphoate dehydrogenase and 2 mM ATP dissolved in the above Tris buffer), and NADP solution (500 μL, 1 mM dissolved in the above Tris buffer) were placed in a series of cuvettes. The concentration of phospholipids in each cuvette was 107 μM. Aliquots of the oligocholate solution in DMSO were added to different cuvettes via a microsyringe. The amount of DMSO introduced to each sample was ≤ 20 μL. The absorbance of NADPH at 340 nm was monitored. To measure the nonspecific glucose leakage from the liposomes, the sample was prepared in an identical fashion and DMSO instead of the oligocholate solution was added. After 2 h, the liposomes were lysed by the addition of 100 μL of Triton X-100 (1% v/v) and the absorbance at 340 nm (A_{max}) was used to calculate the percent leakage [= $(A_t - A_0)/ (A_{max} - A_0) \times 100$]. A_0 and A_t are the initial and intermediate absorbance, respectively.

Lipid-mixing assay

Unlabeled POPC/POPG LUVs were prepared with a mixture of POPC (25 mg/mL, 198 μL) and POPG (50 mg/mL, 10 μL) using HEPES buffer (10 mM HEPES, 107 mM NaCl, pH=7.4), following the procedure described above. Gel filtration was not needed in this experiment.

Labeled POPC/POPG LUVs containing 1 mol % of NBD-DPPE and Rh-DPPE were prepared in the same manner. The labeled and the unlabeled LUVs were mixed in 1:4. An aliquot of the mixed LUVs (15 μL) was placed in a cuvette and diluted with the HEPES buffer to 2.0 mL. The concentration of lipids was 54 μM in the final mixture. The change of NBD fluorescence (λ_{ex} = 450 nm and λ_{em} = 530 nm) was measured upon injection of the oligocholate solution (0.5 mM in DMSO, 10 μL). An increase of NBD emission indicates dilution of membrane bound probes caused by membrane fusion. The percentage of fusion was determined using equation % Fusion = $(F_t - F_0)/(F_{max} - F_0) \times 100\%$, in which Ft is the emission intensity of NBD during the assay, F_0 the initial intensity, and F_{max} the maximum intensity (measured for LUVs containing 0.2 mol % each of NBD-DPPE and Rh-DPPE).

CF leakage assay

For fluorescence measurements, aliquots of the above LUV solution (40 μL) were diluted with the HEPES buffer (1.96 mL, 10 mM HEPES, 107 mM NaCl, pH=7.4) in separate cuvettes, resulting in a lipid concentration of 2.9 μM in each cuvette. Aliquots of the appropriate oligocholate in DMSO were added to different cuvettes via a microsyringe. The amount of DMSO introduced to each sample was ≤ 20 μL. The change of emission intensity at 520 nm (λ_{ex}= 492 nm) was monitored over time. After 2 h, 40 μL of Triton X-100 (1% v/v) was added, disrupting the vesicles and releasing the remaining CF (100% release). The percent leakage was defined as % leakage = $(F_t - F_0)/(F_{max} - F_0) \times 100$, in which F_0 and F_t are the initial and intermediate emission intensity, respectively, and F_{max} was taken as the fluorescence intensity after lysis of the LUVs by Triton X-100.

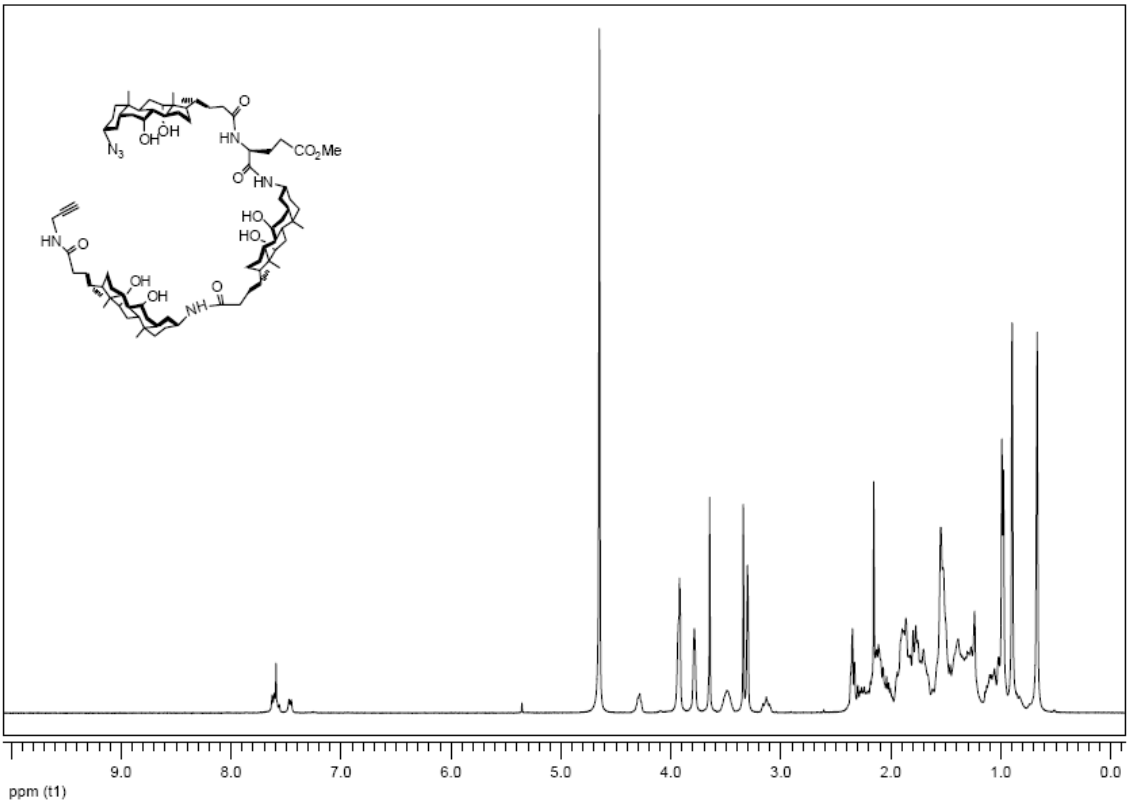

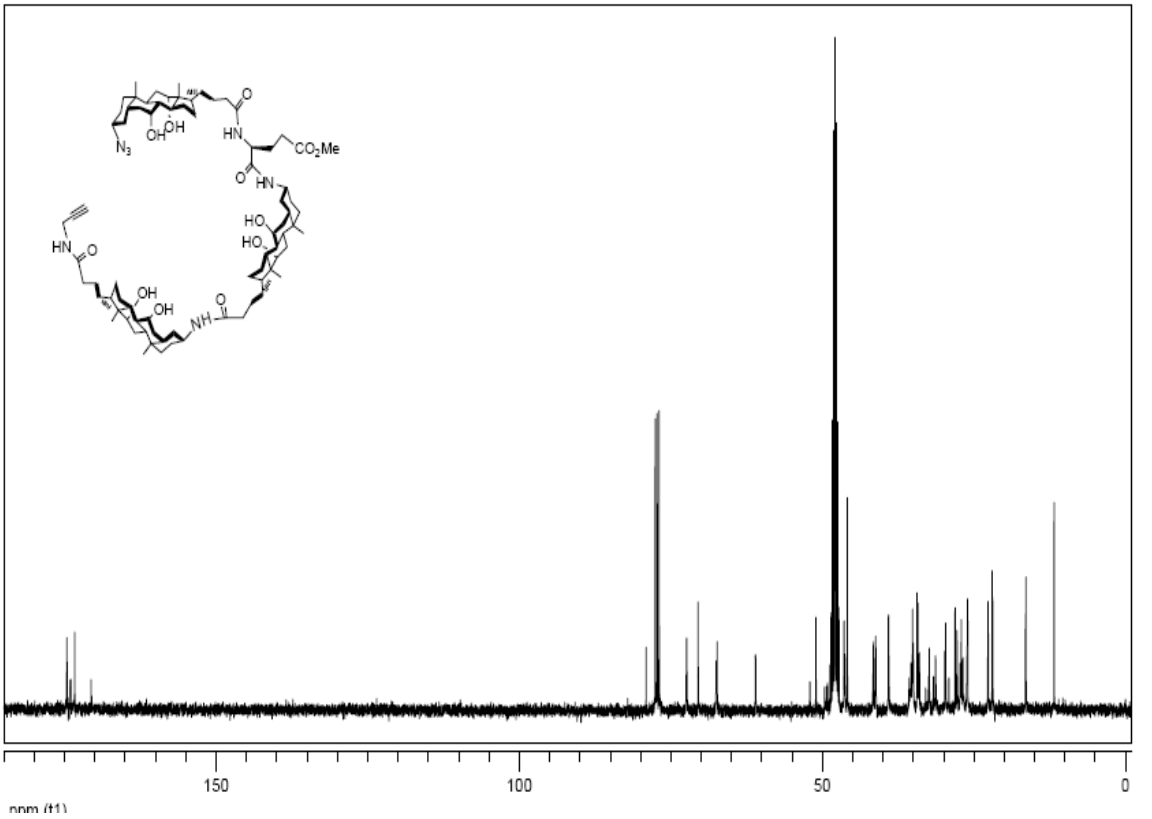

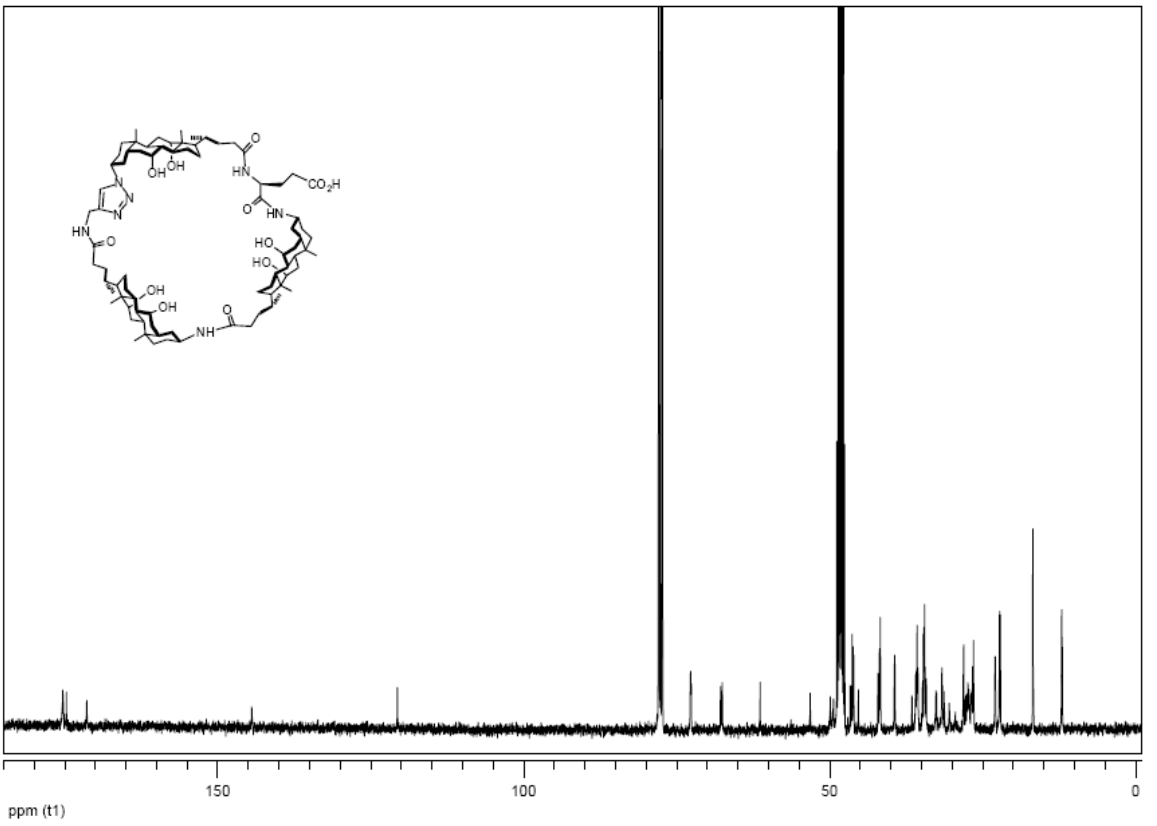

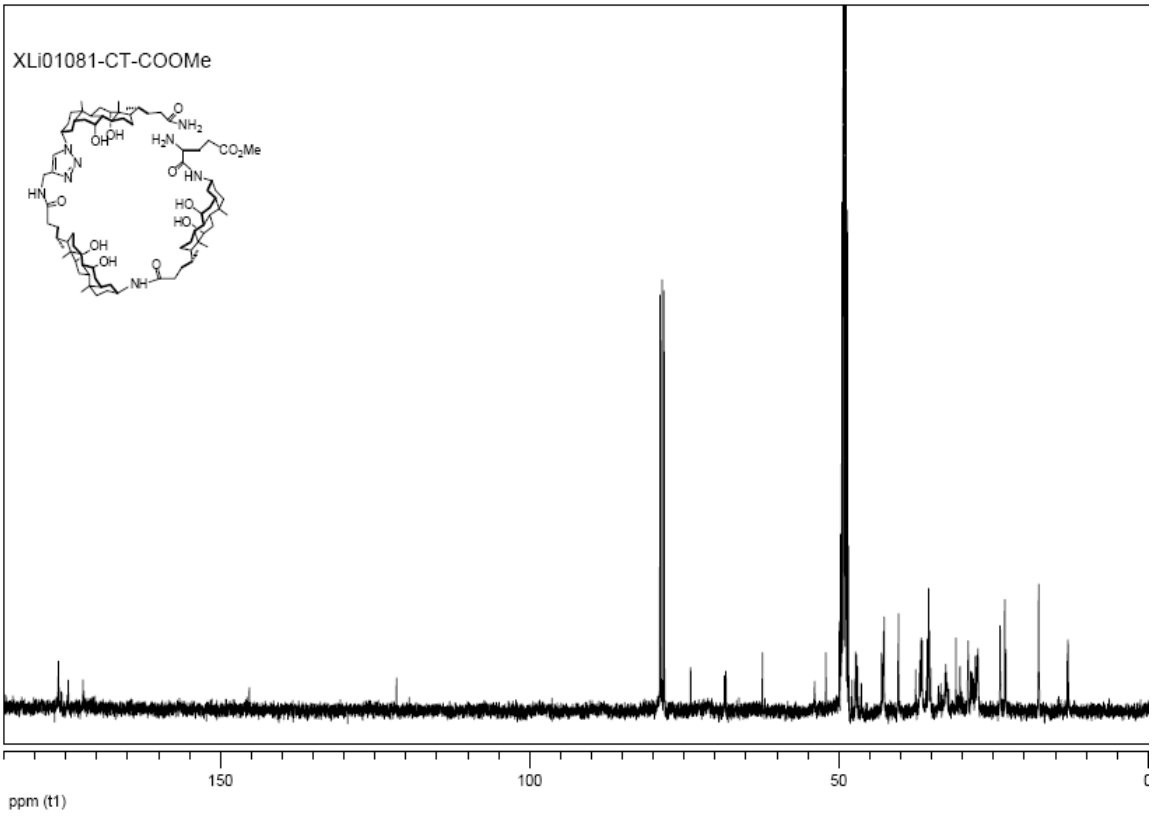

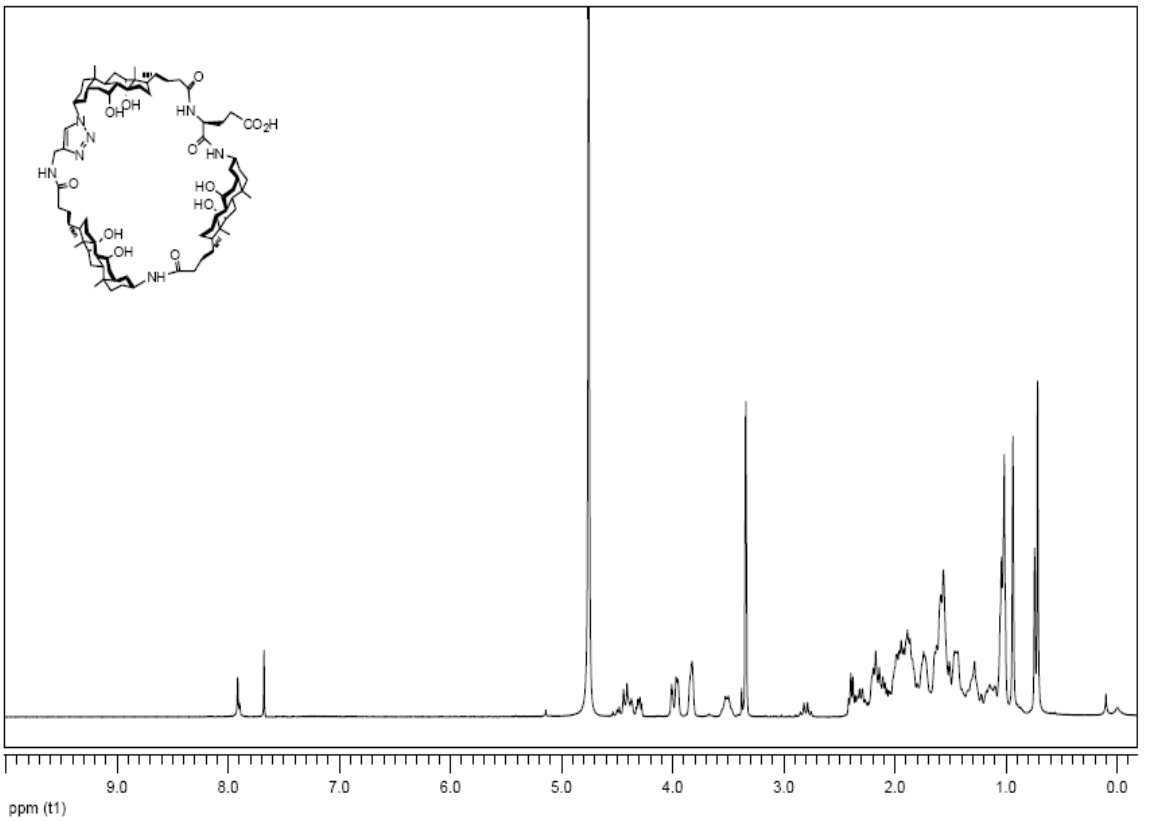

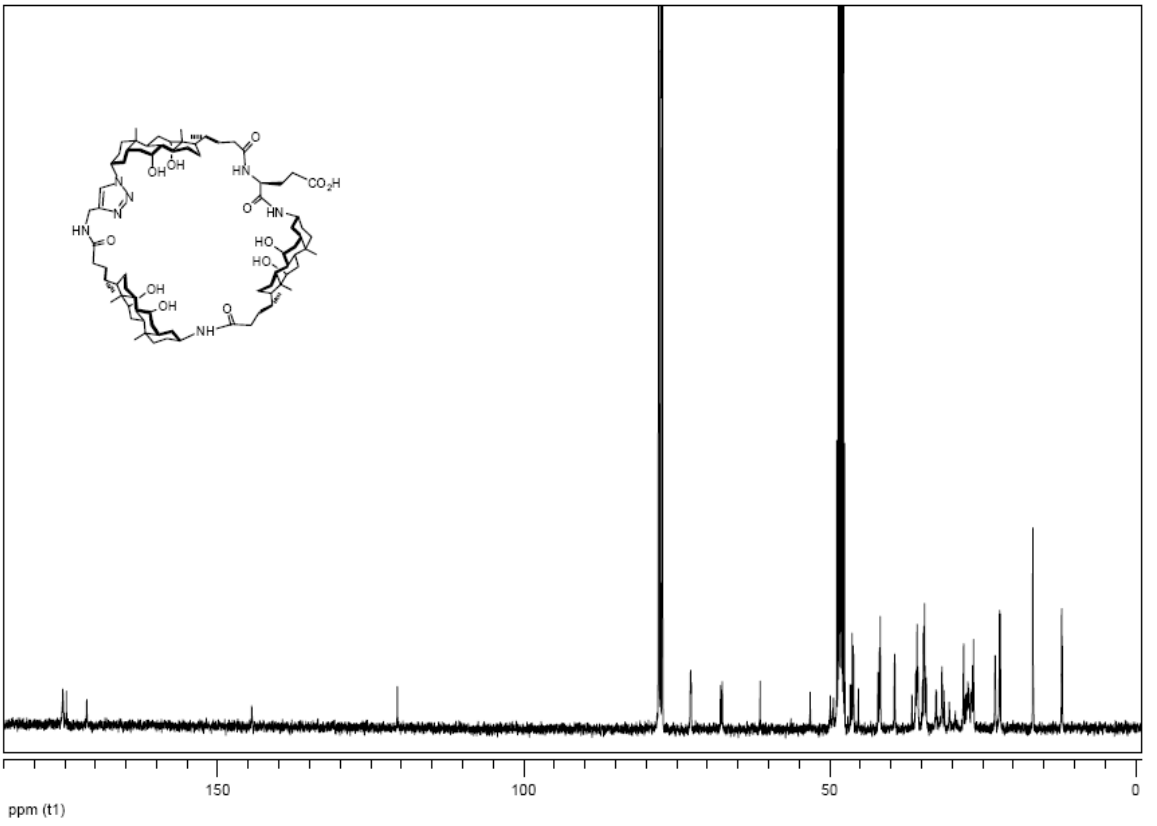

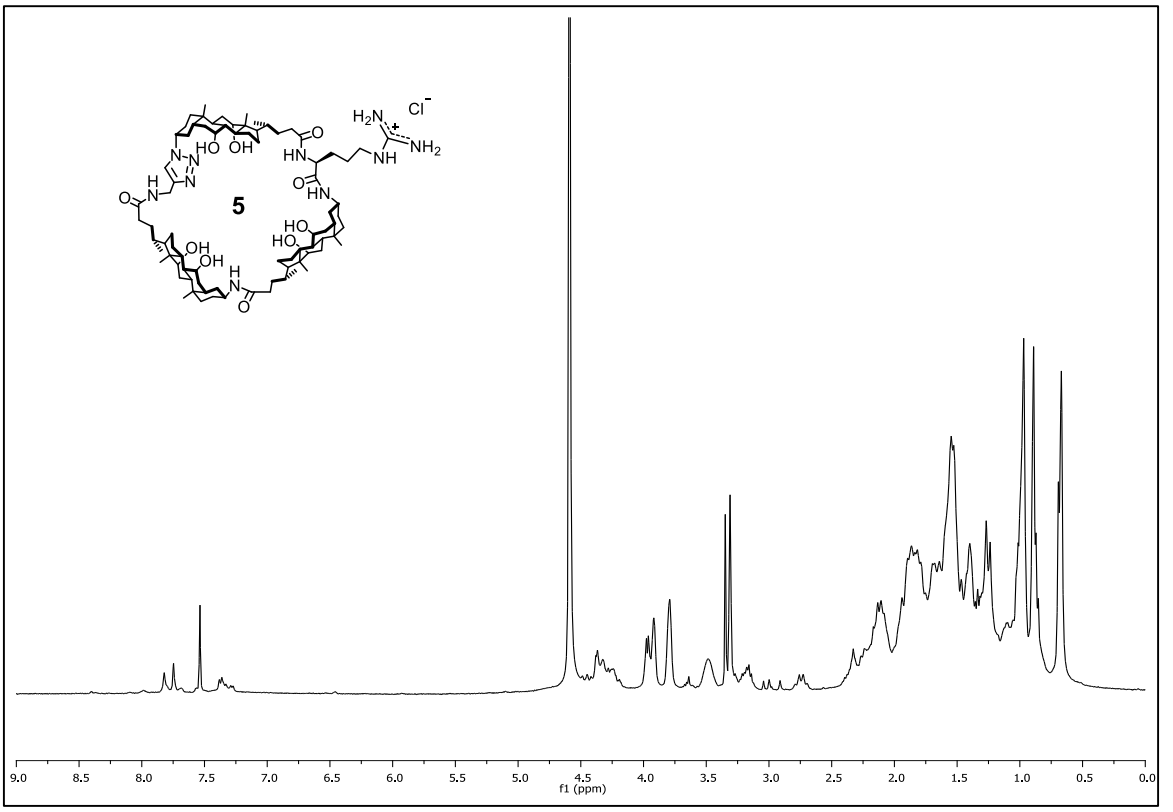

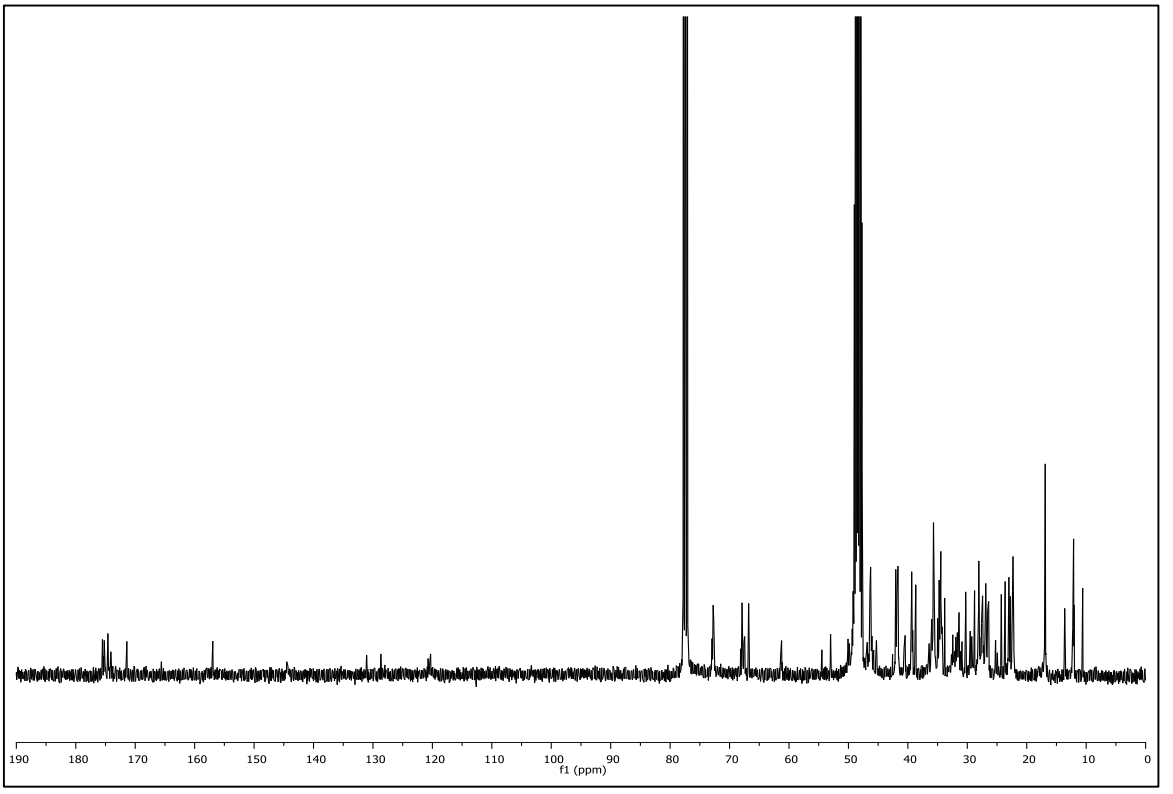

References

(1) Tanaka, H.; Litvinchuk, S.; Tran, D.-H.; Bollot, G.; Mareda, J.; Sakai, N.; Matile, S. *J. Am. Chem. Soc.* **2006**, *128*, 16000-16001.

(2) Westmark, P. R.; Gardiner, S. J.; Smith, B. D. *J. Am. Chem. Soc.* **1996**, *118*, 11093-11100.

(3) Kinsky, S. C.; Haxby, J. A.; Zopf, D. A.; Alving, C. R.; Kinsky, C. B. *Biochemistry* **1969**, *8*, 4149-4158.

IV. Effects of Amphiphile Topology on the Aggregation of Oligocholates in Lipid Membranes: Macrocyclic versus Linear Amphiphiles (Chapter 5, pg. 89-118)

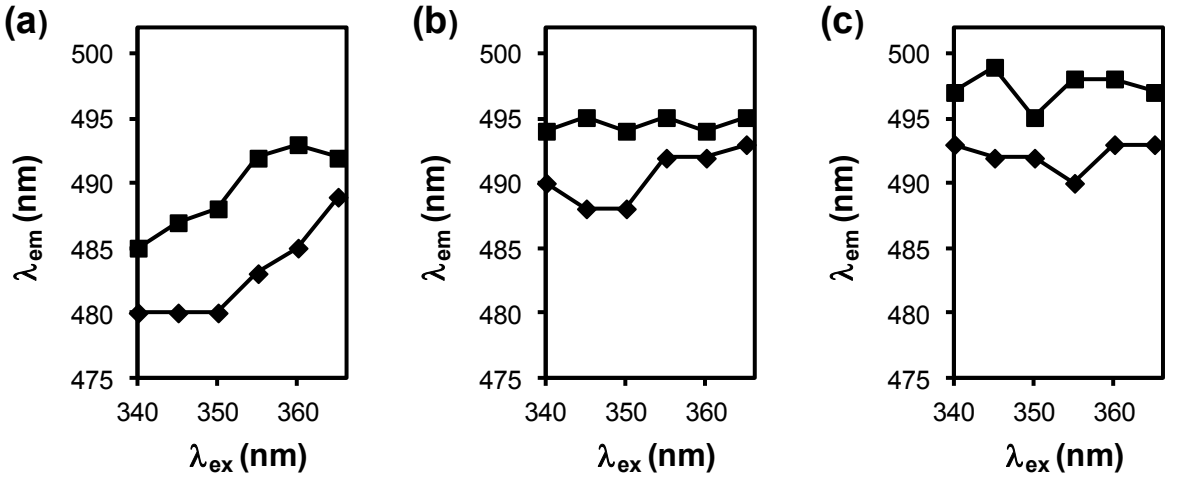

Figure 1S. Effect of excitation wavelength on the emission wavelength for compounds **2** (■) and **3** (◆) in 30% cholesterol/POPC/POPG membranes, with [oligocholate]/[phospholipids] = (a) 0.05%, (b) 0.5% (△), and (c) 5% (□). [Phospholipids] = 107 μM.

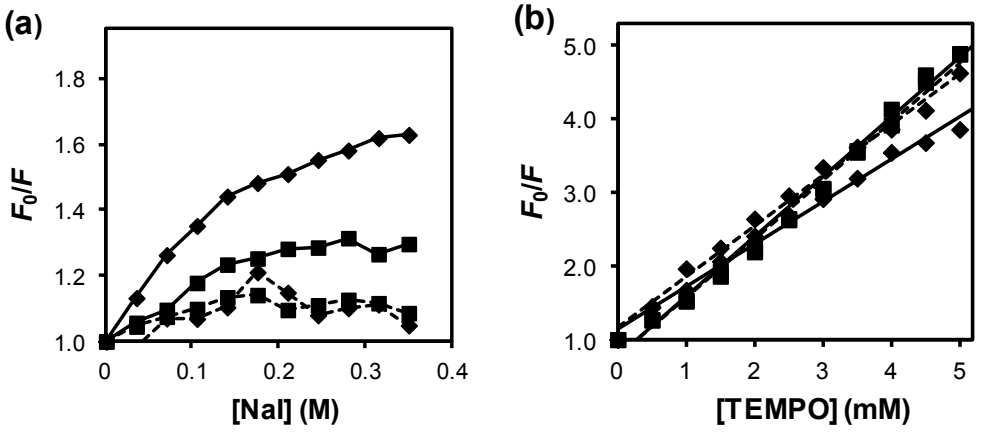

Figure 2S. Fluorescence quenching of oligocholates **2** (■) and **3** (◆) using (a) NaI and (b) TEMPO as the quencher. The data points connected by solid lines were from POPC/POPG LUVs and those connected by dashed lines from 30% cholesterol/POPC/POPG LUVs. [Oligocholate]/[phospholipids] = 3 %. [Phospholipids] = 107 μM.

V. *Tuning Nanopore Formation of Oligocholate Macrocycles by Carboxylic Acid Dimerization in Lipid Membranes* (Chapter 7, pg. 142-156)

General Method

For spectroscopic purpose, methanol, hexanes, and ethyl acetate were of HPLC grade. All other reagents and solvents were of ACS-certified grade or higher, and were used as received from commercial suppliers. All the lipids were purchased from Avanti Polar Lipids and stored at -20 °C. Bio-Beads® SM-2 adsorbent was from BioRad Laboratories. Mass spectrometry was performed on a quadrupole TOF mass spectrometer.